AD NUMBER

ADB029583

LIMITATION CHANGES

TO:

Approved for public release; distribution is unlimited.

FROM:

Distribution authorized to U.S. Gov't. agencies only; Test and Evaluation; JAN 1978. Other requests shall be referred to Air Force Flight Dynamics Laboratory, Attn: AFFDL/FER, Wright-Patterson Air AFB, OH 45433.

AUTHORITY

AFWAL ltr, 6 Nov 1980

AFFDL-TR-78-75

PERFORMANCE CHARACTERISTICS OF 5 FT DIAMETER NYLON AND KEVLAR HEMISFLO RIBBON PARACHUTES AT DYNAMIC PRESSURES UP TO 6000 PSF

CHARLES A. BABISH III

RECOVERY AND CREW STATION BRANCH
VEHICLE EQUIPMENT DIVISION

JUNE 1978

TECHNICAL REPORT AFFDL-TR-78-75
Final Report for Period 1 June 1967 – 30 June 1977

AIR FORCE FLIGHT DYNAMICS LABORATORY
AIR FORCE WRIGHT AERONAUTICAL LABORATORIES
AIR FORCE SYSTEMS COMMAND
WRIGHT-PATTERSON AIR FORCE BASE, OHIO 45433

NOTICES

When Government drawings, specifications, or other data are used for any purpose other than in connection with a definitely related Government procurement operation, the United States Government thereby incurs no responsibility nor any obligation whatsoever; and the fact that the Government may have formulated, furnished, or in any way supplied the said drawings, specifications, or other data, is not to be regarded by implication or otherwise as in any manner licensing the holder or any other person or corporation, or conveying any rights or permission to manufacture, use, or sell any patented invention that may in any way be related thereto.

References to named commercial products in this report are not to be considered in any sense as an endorsement of the product by the United States Air Force or the Government.

This technical report has been reviewed and is approved for publication.

CHARLES A. BABISH III
Project Engineer/Scientist

RICHARD J. DOBBEK
Group Leader, Recovery
Systems Dynamic Analysis
Group

FOR THE COMMANDER

SOLOMON R. METRES
Acting Director
Vehicle Equipment Division

Copies of this report should not be returned unless return is required by security considerations, contractual obligations, or notice on a specific document.

AIR FORCE/56780/3 August 1978 — 250

UNCLASSIFIED

SECURITY CLASSIFICATION OF THIS PAGE *(When Data Entered)*

REPORT DOCUMENTATION PAGE

READ INSTRUCTIONS BEFORE COMPLETING FORM

1. REPORT NUMBER	2. GOVT ACCESSION NO.	3. RECIPIENT'S CATALOG NUMBER
AFFDL-TR-78-75.		

4. TITLE *(and Subtitle)* PERFORMANCE CHARACTERISTICS OF 5 FT DIAMETER NYLON AND KEVLAR HEMISFLO RIBBON PARACHUTES AT DYNAMIC PRESSURES UP TO 6,000 PSF.

5. TYPE OF REPORT & PERIOD COVERED
Final Report, 1 June 1967 to 30 June 1977

6. PERFORMING ORG. REPORT NUMBER

7. AUTHOR(s)
CHARLES A. BABISH, III

8. CONTRACT OR GRANT NUMBER(s)

9. PERFORMING ORGANIZATION NAME AND ADDRESS
Air Force Flight Dynamics Laboratory (FER)
AF Wright Aeronautical Laboratories, AFSC
Wright-Patterson Air Force Base, Ohio 45433

10. PROGRAM ELEMENT, PROJECT, TASK AREA & WORK UNIT NUMBERS
Program Element 62201F
Project 2402, Task 240203
Work Unit 24020313

11. CONTROLLING OFFICE NAME AND ADDRESS

12. REPORT DATE
June 1978

13. NUMBER OF PAGES
232

14. MONITORING AGENCY NAME & ADDRESS *(if different from Controlling Office)*

15. SECURITY CLASS. *(of this report)*
Unclassified

15a. DECLASSIFICATION/DOWNGRADING SCHEDULE
N/A

16. DISTRIBUTION STATEMENT *(of this Report)*
Distribution limited to U.S. Government agencies only; this report contains information on test and evaluation of military hardware; January 1978; other requests for this document must be referred to Air Force Flight Dynamics Laboratory (AFFDL/FER), Wright-Patterson Air Force Base, Ohio 45433 through DDC.

17. DISTRIBUTION STATEMENT *(of the abstract entered in Block 20, if different from Report)*

18. SUPPLEMENTARY NOTES
Available in DDC.

19. KEY WORDS *(Continue on reverse side if necessary and identify by block number)*

Parachutes	Aerodynamic Characteristics	Material Strengths
Drag Force	Supersonic Aerodynamics	Opening Shock
Nylon	Parachute Deployment	Hemisflo-Parachutes
Kevlar	Supersonic-X Parachutes	Deployment Dynamics
Track Tests	Arrowhead Rocket Sled	Decelerators

20. ABSTRACT *(Continue on reverse side if necessary and identify by block number)*
This report describes, and documents the results of a long term, experimental track test program conducted to advance those technologies associated with parachute operation at high Mach numbers and low altitudes; that is, at high dynamic pressures. The objective of the program was to determine deployment techniques, performance characteristics, and structural design criteria for nylon and Kevlar hemisflo parachutes operating

DD FORM 1 JAN 73 1473 EDITION OF 1 NOV 65 IS OBSOLETE

UNCLASSIFIED

SECURITY CLASSIFICATION OF THIS PAGE *(When Data Entered)*

012 070

20. (Continued)

CONT'

at dynamic pressures up to 6000 psf. A total of 20 sled test runs were made; three tests provided no parachute performance data because of deployment system malfunctions, three tests were made with the Tomahawk sled at Mach 1.2 to establish a deployment technique, and 14 tests were made with the Arrowhead sled at Mach numbers of 1.5, 1.8, and 2.2 to obtain the comparative performance and structural integrity data. The filling times, opening shock factors, stability angles, and projected areas of the nylon and Kevlar parachutes were approximately equal for all test conditions. The Kevlar parachutes generated approximately 50 percent higher deployment forces, 22 percent lower opening forces, and 18 percent lower steady state drag forces than the nylon parachutes. Linear relationships were established between parachute opening forces and the ultimate loads in nylon suspension lines and nylon and Kevlar horizontal ribbons. For approximately equal strength hemisflo parachutes, the weights of the Kevlar canopies were between 38 and 55 percent of the weights of the nylon canopies. There were no significant difficulties associated with the fabrication of the parachutes made from the new high strength, low modulus Kevlar materials. The deployment control break tie design calculation technique presented in this report has been shown to be a satisfactory method which can be used to determine the number, locations, and strengths of parachute break ties that will control the deployment of nylon and Kevlar hemisflo parachutes at supersonic speeds and high dynamic pressures.

FOREWORD

This report describes an in-house program conducted by the Recovery and Crew Station Branch (FER), Vehicle Equipment Division (FE), Air Force Flight Dynamics Laboratory, Air Force Wright Aeronautical Laboratories, Wright-Patterson Air Force Base, Ohio, under Project 2402, "Vehicle Equipment Technology," Task 240203, "Aerospace Vehicle Recovery and Escape Subsystems," Work Unit 24020313, "Development and Evaluation of Kevlar-29 Material for Weapon System Parachute Recovery Applications."

The work reported herein was performed during the period 1 June 1967 to 30 June 1977, under the direction of the author, Mr. Charles A. Babish III (AFFDL/FER), project engineer. The report was released by the author in November 1977.

The author wishes to express his appreciation to Mr. J. Pat Brown and Mr. Floyd Amburgey of the 6585th Test Group, Holloman Air Force Base, New Mexico, for their successful management of all aspects of the track tests performed under this program. Special acknowledgment is made to Mr. Philip A. Graf and other personnel at the University of Dayton Research Institute, Dayton, Ohio, for their assistance in data reduction and report preparation. Parachute fabrication, preparation, and packing were performed at the Air Force Aeronautical Systems Division Parachute Shop, WPAFB, Ohio, under the direction of Mr. George Zelinskas and at the M. Steinthal and Co., Inc., Roxboro, North Carolina, under the direction of Messrs. Normand Levesque, Kenneth Smith, and Richard Warren. The support given by all personnel at these facilities is especially appreciated.

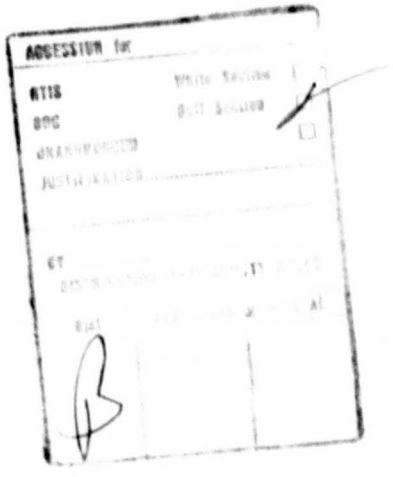

TABLE OF CONTENTS

SECTION		PAGE
I	INTRODUCTION	1
II	DESCRIPTION OF THE TEST PROGRAM	3
	1. Test Facility	
	a. The Holloman Track	3
	b. The Test Vehicles	3
	(1) The Arrowhead Sled	4
	(2) The Tomahawk Sled	4
	2. Parachute Models	10
	a. Configuration Selection	10
	(1) Parachute Type	10
	(2) Canopy Size	10
	(3) Canopy Porosity	12
	(4) Riser Length	12
	b. Hemisflo Design	12
	c. Parachute Construction	13
	d. Physical Characteristics	16
	(1) Component Strengths	16
	(2) Material Characteristics	16
	(3) Parachute Weights	16
	3. Test Technique	22
	a. Track Preparation	22
	b. Parachute Installation	23
	c. Sled Preparation	23
	d. Parachute Deployment	23
	e. Parachute Release	25
	f. Sled Recovery	25
	4. Instrumentation and Data Gathered	29
	a. Meteorological Readings	29
	b. Electronic Instrumentation	29
	(1) On-Board Telemetry	29
	(2) Sled Performance	29
	(3) Parachute Forces	30

TABLE OF CONTENTS (Continued)

SECTION			PAGE
	c.	Optical Instrumentation	31
		(1) Metric Optical Instrumentation	31
		(2) Engineering Optical Instrumentation	31
		(3) Documentary Photography	33
	d.	Timing	33
	5.	Data Reduction and Precision	35
	a.	Time	35
	b.	Meteorological Data	35
	c.	Sled Performance Data	38
		(1) Primary Velocity Measuring System	38
		(2) Backup Velocity Measuring System	40
		(3) Metric Optical Instrumentation System	41
	d.	Relative Wind Data	42
		(1) True Airspeed	42
		(2) Mach Number	43
		(3) Dynamic Pressure	43
	e.	Parachute Performance Data	44
		(1) Event Times	44
		(2) Cone and Bag Separation Distances	45
		(3) Drag Forces	45
		(4) Drag Coefficient	46
		(5) Projected Area	47
		(6) Oscillation Angles	47
	6.	Run Summary	48
III		RESULTS AND DISCUSSION	50
	1.	Sled Test Run Results	50
	a.	Deployment Problems on Early Tests	50
	b.	Deployment Method Selection Runs; $M_\infty = 1.3$	50

TABLE OF CONTENTS (Continued)

SECTION			PAGE
		(1) Test 6P-F1	52
		(2) Test 6P-F2	55
		(3) Test 6P-F3	55
	c.	Runs at Mach 1.5; Q = 2900 psf	59
		(1) Test 6P-E3; Nylon Parachute	59
		(2) Test 6P-E6; Nylon Parachute	63
		(3) Test 6P-E9; Kevlar Parachute	63
		(4) Test 6P-E10; Kevlar Parachute	63
	d.	Runs at Mach 1.8; Q = 4000 psf	72
		(1) Test 6P-G1; Nylon Parachute	72
		(2) Test 6P-G2; Nylon Parachute	80
		(3) Test 6P-G3; Nylon Parachute	80
		(4) Test 6P-G4; Kevlar Parachute	86
		(5) Test 6P-G5; Kevlar Parachute	86
	e.	Runs at Mach 2.2; Q = 6500 psf	86
		(1) Test 6P-H1; Nylon Parachute	96
		(2) Test 6P-H2; Nylon Parachute	96
		(3) Test 6P-H3; Nylon Parachute	102
		(4) Test 6P-H6; Kevlar Parachute	107
		(5) Test 6P-H7; Kevlar Parachute	107
	2.	Performance of the Deployment System Components	115
	3.	Performance of the Test Parachutes	116
		a. Deployment Forces	116
		b. Canopy Inflation Characteristics	116
		(1) Filling Time	116
		(2) Opening Force	118
		(3) Opening Shock Factor	121
		c. Steady State Performance	121
		(1) Drag Coefficient	121
		(2) Stability Angle	122
		(3) Projected Area	122

TABLE OF CONTENTS (Continued)

SECTION			PAGE
	d.	Material Structural Integrity	125
		(1) Suspension Lines	125
		(2) Horizontal Ribbons	127
		(3) Vertical Ribbons	127
		(4) Other Components	129
IV	CONCLUSIONS		130
APPENDIX A -	DESCRIPTION OF THE ARROWHEAD SLED		133
	1.	Preliminary Design	133
		a. Basic Requirements for a Mach 3 Sled	133
		b. Basic Configuration	134
		c. Wind Tunnel Tests	135
	2.	Intermediate Design	139
		a. Design Requirements for the Arrowhead Sled	139
		b. Candidate Configurations	139
		c. Wind Tunnel Tests	140
	3.	Final Design	143
	4.	Sled Fabrication	149
	5.	Sled Checkout Runs	149
APPENDIX B -	DESCRIPTION AND DESIGN OF THE 5 FT NOMINAL DIAMETER HEMISFLO PARACHUTES		153
	1.	General Description	153
	2.	Major Components	153
		a. Canopy	153
		b. Suspension Lines	154
		c. Riser Lines	154
		d. Confluence and Riser Keepers	155
		e. Attachment Loops	155

TABLE OF CONTENTS (Continued)

SECTION		PAGE
3.	Canopy Components	155
	a. Horizontal Ribbons	155
	b. Vertical Ribbon	155
	c. Radials and Radial Tapes	158
	d. Skirt Band	158
	e. Vent Band	159
	f. Vent Lines	159
4.	Canopy Porosity	159
5.	Parachute Materials	160
	a. Strength Requirements	160
	(1) Parachute Opening Force	160
	(2) Suspension Lines, Riser Lines, Vent Lines, and Radials	161
	(3) Horizontal Ribbons	162
	(4) Skirt Band	165
	(5) Vent Band	165
	(6) Confluence Keeper	166
	(7) Other Components	166
	b. Material Characteristics	166
	(1) Nylon Materials	166
	(2) Kevlar Materials	166
6.	Parachute Fabrication	167
	a. Manufacturing Technique	167
	b. Major Seams and Joints	169
7.	Parachute Weights	169
APPENDIX C -	DESCRIPTION AND DESIGN OF PARACHUTE ATTACHMENT, DEPLOYMENT, AND RELEASE COMPONENTS	173
1.	Parachute Attachment/Deployment/ Release Mechanisms	173

TABLE OF CONTENTS (Continued)

SECTION		PAGE
2.	Deployment Cone, Cone Riser, and Release Cables	179
3.	Pilot Chutes	179
a.	Early Sled Tests	179
b.	Supersonic X-3 Pilot Chute Design	182
c.	Pilot Chute Bags	183
4.	Deployment Control Break Ties	183
a.	Deployment Problems at High Dynamic Pressures	183
b.	Break Tie Design Criteria	186
c.	Analytical Simulation of Deployment Dynamics	187
(1)	Calculation Method	187
(2)	Physical System	187
(3)	Dynamic Model	187
(4)	Equations of Motion	188
(5)	Initial Conditions	188
(6)	Maximum Allowable Tie Strength	190
(7)	Minimum Allowable Tie Strength	191
(8)	Other Functional Relationships	192
(9)	Computer Program	193
(10)	Band of Allowable Break Tie Strengths	194
(11)	Trajectories of the Deployment System Components	196
d.	Selection of Break Tie Locations and Strengths	196
e.	Design of the Break Ties	198
f.	Vent Break Cords	205
5.	Parachute Packing	205
a.	Test Parachute Preparation	206
b.	Parachute Bags	206

TABLE OF CONTENTS (Concluded)

SECTION		PAGE
	c. Packing Procedure	207
6.	Parachute Installation on the Sleds	210
REFERENCES		231

LIST OF ILLUSTRATIONS

FIGURE		PAGE
1	Photographs of the Arrowhead Sled with Pusher Sleds	5
2	Basic Dimensions (3 View) of the Arrowhead Sled	6
3	Photographs of the Tomahawk Sled With Pusher Sled	8
4	Basic Dimensions (3 View) of the Tomahawk Sled	9
5	Sketches of the General Arrangement of the Hemisflo Parachutes	11
6	Gore Coordinates of the Nylon and Kevlar Hemisflo Parachute Canopies	15
7	Graphical Comparison of the Weights of Nylon and Kevlar 5 ft Diameter Hemisflo Parachutes	21
8	Photograph of the Test Parachute Installed on the Arrowhead Sled - Test 6P-H1	24
9	Sketch Showing Major Components of a Typical Deployment Sequence	26
10	Photographs of the Deployment Sequence from Test 6P-G1	27
11	Typical Sled Performance and Relative Wind Curves for the Mach 1.3 Test Runs	51
12	Trajectories of Deployment System Components - Test 6P-F1	53
13	Parachute Performance Curves - Test 6P-F1	54
14	Trajectories of Deployment System Components - Test 6P-F2	56
15	Parachute Performance Curves - Test 6P-F2	57
16	Trajectories of Deployment System Components - Test 6P-F3	58

LIST OF ILLUSTRATIONS (Continued)

FIGURE		PAGE
17	Parachute Performance Curves - Test 6P-F3	60
18	Typical Sled Performance and Relative Wind Curves for the Mach 1.5 Test Runs	61
19	Parachute Performance Curves - Test 6P-E3	62
20	Post Test Photograph of the Test Parachute - Test 6P-E3	64
21	Trajectories of Deployment System Components - Test 6P-E6	65
22	Parachute Performance Curves - Test 6P-E6	66
23	Post Test Photograph of the Test Parachute - Test 6P-E6	67
24	Trajectories of Deployment System Components - Test 6P-E9	68
25	Parachute Performance Curves - Test 6P-E9	69
26	Post Test Photograph of the Test Parachute - Test 6P-E9	70
27	Trajectories of Deployment System Components - Test 6P-E10	71
28	Parachute Performance Curves - Test 6P-E10	73
29	Post Test Photograph of the Test Parachute - Test 6P-E10	74
30	Typical Sled Performance and Relative Wind Curves for the Mach 1.8 Test Runs	75
31	Trajectories of Deployment System Components - Test 6P-G1	76
32	Parachute Performance Curves - Test 6P-G1	77
33	Photographs of the Sequence of Parachute Failure - Test 6P-G1 (Photos retouched for clarity.)	78
34	Post Test Photograph of the Test Parachute - Test 6P-G1	79

LIST OF ILLUSTRATIONS (Continued)

FIGURE		PAGE
35	Parachute Performance Curves - Test 6P-G2	81
36	Post Test Photograph of the Test Parachute - Test 6P-G2	82
37	Trajectories of Deployment System Components - Test 6P-G3	83
38	Parachute Performance Curves - Test 6P-G3	84
39	Photographs Showing the Damaged Confluence Keeper on Test 6P-G3 (Photo retouched for clarity.)	85
40	Post Test Photograph of the Test Parachute - Test 6P-G3	87
41	Trajectories of Deployment System Components - Test 6P-G4	88
42	Parachute Performance Curves - Test 6P-G4	89
43	Photograph Showing Partial Inflation of the Test Parachute - Test 6P-G4 (Photo retouched for clarity.)	90
44	Post Test Photograph of the Test Parachute - Test 6P-G4	91
45	Trajectories of Deployment System Components - Test 6P-G5	92
46	Parachute Performance Curves - Test 6P-G5	93
47	Photograph Showing Full Inflation of the Test Parachute - Test 6P-G5	94
48	Post Test Photograph of the Test Parachute - Test 6P-G5	95
49	Typical Sled Performance and Relative Wind Curves for the Mach 2.2 Test Runs	97
50	Parachute Performance Curves - Test 6P-H1	98

LIST OF ILLUSTRATIONS (Continued)

FIGURE		PAGE
51	Post Test Photograph of the Test Parachute-Test 6P-H1	99
52	Trajectories of Deployment System Components-Test 6P-H2	100
53	Parachute Performance Curves - Test 6P-H2	101
54	Post Test Photograph of the Test Parachute-Test 6P-H2	103
55	Trajectories of Deployment System Components-Test 6P-H3	104
56	Parachute Performance Curves -Test 6P-H3	105
57	Post Test Photograph of the Test Parachute-Test 6P-H3	106
58	Trajectories of Deployment System Components-Test 6P-H6	108
59	Parachute Performance Curves -Test 6P-H6	109
60	Post Test Photograph of the Test Parachute-Test 6P-H6	110
61	Trajectories of Deployment System Components-Test 6P-H7	111
62	Parachute Performance Curves -Test 6P-H7	113
63	Post Test Photograph of the Test Parachute-Test 6P-H7	114
64	Variation of Deployment Force with Dynamic Pressure for Nylon and Kevlar Parachutes	119
65	Variation of Opening Force with Dynamic Pressure for Nylon and Kevlar Parachutes	120
66	Variation of Drag Coefficient with Mach Number for Nylon and Kevlar Parachutes	123
67	Variation of Drag Coefficient with Dynamic Pressure for Nylon and Kevlar Parachutes	124

LIST OF ILLUSTRATIONS (Continued)

FIGURE		PAGE
68	Suspension Line Damage as a Function of Line Strength and Opening Force	126
69	Horizontal Ribbon Damage as a Function of Ribbon Strength and Opening Force	128
A-1	Sketch of the Preliminary Mach 3 Sled Configuration	136
A-2	Wind Tunnel Models of the Preliminary Mach 3 Sled Configuration	137
A-3	Measured and Predicted Shock Wave Patterns for the Preliminary Mach 3 Sled	138
A-4	Regular and Schlieren Photographs of the Intermediate Design Arrowhead Sled Wind Tunnel Model During a Mach 1.5 Test (From Reference 10)	142
	a. Regular Photograph; V-Bottom Model with Genie Boosters and Hyperflo Parachute	
	b. Schliern Photograph; V-Bottom Model with Genie Boosters and Hyperflo Parachute	
A-5	Final Design Arrowhead Sled Wind Tunnel Model (From Reference 12)	144
	a. Details of the Foresled	
	b. Details of the Booster Package	
A-6	Schlieren Photograph of the Final Design Arrowhead Sled Wind Tunnel Model; V-Bottom Model with Nike Boosters at Mach 1.5 (From Reference 12)	145
A-7	Final Assembly Drawing of the Arrowhead Sled	146
A-8	Photographs of the IDS 6328 Arrowhead Sled Taken Just Prior to Its First Launch	150
A-9	Photograph of the Arrowhead Sled After Its First Launch Showing the Area of Damage	151

LIST OF ILLUSTRATIONS (Continued)

FIGURE		PAGE
B-1	Confluence and Riser Keeper Design Details	156
B-2	Design Details of the Riser Line Attachment Loops	157
B-3	Suspension Line Strengths as Functions of Opening Force and Freestream Mach Number	163
B-4	Horizontal Ribbon Strengths as Functions of Opening Force and Freestream Mach Number	164
B-5	Design Details for a Typical Horizontal Ribbon Splice	170
B-6	Design Details for a Typical Skirt Band Splice and Suspension Line to Skirt Reinforcement Joint	171
C-1	Photographs Showing the Major Parachute Attachment, Deployment, and Release Components	174
	a. Top of Sled	
	b. Parachute Compartment	
C-2	Major Attachment, Deployment, and Release Components in Their Sequence of Operation	176
C-3	Parachute Attachment/Deployment/Release Mechanism - Used on Tests 1 Through 11 (Those Prior to 1974)	177
C-4	Parachute Attachment/Deployment/Release Mechanism - Used on Tests 12 Through 20 (Those after 1973)	178
C-5	Sketch of the Cone Riser	180
C-6	Design Details of the Supersonic-X-3 Pilot Chutes	184
	a. Parachute Profile	
	b. Construction and Materials	

LIST OF ILLUSTRATIONS (Continued)

FIGURE		PAGE
C-7	Translations and Forces Used in the Model of Deployment Dynamics	189
C-8	Band of Allowable Tie Strengths -Test 6P-H7	195
C-9	Band of Separation Distance Histories for Deployment System Components - Test 6P-H7	197
C-10	Design of the Deployment Control Break Ties	199
	a. Step 1 - Break Tie Tied to First Loop	
	b. Step 2 - Break Tie Passed Through Second Loop	
	c. Step 3 - Break Tie Passed Back Through First Loop	
	d. Step 4 - Break Tie Passed Through Bag Loop	
	e. Step 5 - Break Tie Tied Tightly to Bag Loop	
	f. Sketch of a Break Tie Just Prior to Break	
C-11	Photographs Taken During the Packing of the Parachute for Test 6P-G1	213
	a. Packing Step 1	
	b. Packing Step 2	
	c. Packing Step 3	
	d. Packing Step 4	
	e. Packing Step 5	
	f. Packing Step 6	
	g. Packing Step 7 - Pilot Chute Vent Break Cords	
	h. Packing Step 7 - Pilot Chute Break Ties	
	i. Packing Step 7 - Bridle Connections	
	j. Packing Step 7 - Pilot Chute Compartment Closure	
	k. Packing Step 8	

LIST OF ILLUSTRATIONS (Concluded)

FIGURE		PAGE
C-12	Photographs Taken During Parachute Installation on the Arrowhead Sled	224
	a. Installation Step 1	
	b. Installation Step 2	
	c. Installation Step 3	
	d. Installation Step 4	
	e. Installation Step 5	
	f. Installation Step 6	
	g. Installation Step 7	

LIST OF TABLES

TABLE		PAGE
1	Physical Details and Dimensions of the Nylon and Kevlar Hemisflo Parachutes	14
2	Physical Characteristics of the Nylon Parachutes	17
3	Physical Characteristics of the Kevlar Parachutes	18
4	Nylon and Kevlar Parachute Weights	19
5	Cameras Used During the Test Program	32
6	Precision of the Data	36
7	Run Summary	49
8	5 ft D_o Hemisflo Ribbon Parachute Performance Characteristics	117
B-1	Construction and Characteristics of the Kevlar 29 Materials	168
C-1	Pilot Chutes Used for the Test Program	181
C-2	Breaking Strengths(lb) of Vent Break Cords and Break Ties	212

LIST OF SYMBOLS

C_D	=	Drag coefficient
C_{D_o}	=	Parachute drag coefficient
D	=	Parachute drag force (average of two force records - when more than one), lb
D	=	Drag force of the pilot chute (or cone) and the parachute bag (or pilot chute bag), lb
D	=	Diameter (design projected) of Supersonic X-3 pilot chute, in.
DF1	=	Design factor, defined by Equation (C-5)
DF2	=	Design factor, defined by Equation (C-9)
D_o	=	Hemisflo parachute canopy nominal diameter, ft
D_p	=	Projected diameter of Hyperflo pilot chute, in.
E	=	Horizontal gore coordinate of hemisflo parachute canopies, in.
F	=	Parachute drag force (average of two force records - when more than one), lb
FS	=	Force resisting sled motion, lb
F_{LS}	=	Snatch force (parachute force at line stretch), lb
F_o	=	Parachute opening force (that peak force which occurred during canopy inflation or just after canopy first full-open), lb
H	=	Vertical gore coordinate of hemisflo parachute canopies, in.
HRS	=	Nominal rated breaking strengths of the parachute canopy horizontal ribbons - also the ultimate load in the horizontal ribbons, lb
KEF	=	Knot efficiency factor, 0.75
M	=	Mach number
M_∞	=	Freestream Mach number
M_{LS}	=	Mach number at line stretch

m_p = Parachute mass (used to represent either: (1) the instantaneous mass of the pilot chute and test parachute bag and its contents, or (2) the instantaneous mass of the deployment cone, cone riser, and the pilot chute bag and its contents), slug

m_s = Sled mass (used to represent the mass of the track sled), slug

m_t = Mass that the break tie is holding, slug

n = Number of parachute suspension lines and canopy gores, 12

OF = Overload factor, 1.5

P = Air pressure at the Track, in. Hg

P_{SL} = Standard air pressure at sea level, 29.92 in.Hg

Q = Dynamic pressure, psf

Q_{LS} = Dynamic pressure at line stretch, psf

R = Resisting force of the parachute ties, lb

RHO = Air density at the track, slug/cu ft

$r_{C_{D_o}}$ = Maximum variation in drag coefficient

r_D = Maximum variation in drag force, lb

R_V = Maximum relative variation in sled velocity, percent

S = Reference area, sq ft

SBS = Nominal rated strength of the parachute canopy skirt band, lb

sd = Separation distance between the sled mass, m_s, and the parachute mass, m_p, ft

SF = Safety factor, 1.5

SLS = Nominal rated breaking strengths of the parachute suspension lines -also the ultimate suspension line load, lb.

SS	=	Nominal rated breaking strength of a snubber, lb
S_o	=	Design nominal area of the hemisflo parachute canopy, 19.635 sq ft
S_P, S_{P_l}	=	Projected area of the parachute canopy (largest projected area of the spheroid normal to the centerline of the suspension line -canopy system), sq ft
T	=	Air temperature at the Track, °R
$(TS)_{max}$	=	Maximum allowable nominal rated breaking strength of a break tie, lb
$(TS)_{min}$	=	Minimum allowable nominal rated breaking strength of a break tie, lb
t_f	=	Parachute canopy filling time; the difference between the time of line stretch, t_{LS}, and the time of canopy first full-open, t_{FO} , sec
t_{FO}	=	The time of parachute canopy first full-open (where first full-open is that event where the value of the canopy projected area during inflation first equals the steady state projected area), sec
t_{LS}	=	The time of parachute line stretch, sec.
T_{SL}	=	Standard air temperature at sea level, 518.69°R
VBCS	=	Nominal rated breaking strength of a vent break cord, lb
VBS	=	Nominal rated breaking strength of the parachute canopy vent band, lb
V_S	=	Velocity (speed) of the sled, ft/sec
V_{TAS}	=	True airspeed, ft/sec
V_W	=	Velocity (speed) of the wind, ft/sec
X	=	Parachute opening shock factor, defined by $X = F_O/(C_{D_o} S_o Q_{LS})$

X	=	Axial coordinate of Supersonic - X-3 pilot chute canopy profile, in.
X_b, X_B	=	Separation distance between the leading edge of the parachute bag and the parachute sled attachment point, ft
X_c, X_C	=	Separation distance between the leading edge of the cone and the parachute sled attachment point, ft
x_p	=	Translation of the parachute mass, ft
x_s	=	Translation of the sled mass, ft
x_t	=	Translation of the mass that the break tie is holding, ft
Y	=	Radial coordinate of Supersonic - X-3 pilot chute canopy profile, in.
α	=	Angle between the headings of the sled and the wind, rad
θ, ϕ	=	Parachute stability or oscillation angle; the angle between a ray constructed from the focal point of the lens of one of the on-board cameras to the center of the parachute vent and the optical axis of the camera, deg
θ_q	=	Parachute quadrant angle; the counterclockwise angular displacement of the image of the center of the parachute vent from the positive axis of the on-board camera film plane, deg
λ_g	=	Hemisflo parachute canopy geometric porosity, percent
ρ	=	Air density at the Track, slug/cu ft
ρ_{SL}	=	Standard air density at sea level, 0.002378 slug/cu ft
$\frac{d^2}{dt^2}$	=	Indicates the second derivative of a function with respect to time

SECTION I
INTRODUCTION

This report describes, and documents the results of a long-term track test program conducted to advance those technologies associated with parachute operation at very high dynamic pressures.

First stage type ribbon parachutes, which are used for the recovery of advanced Air Force weapon systems, are required to be deployed, and to operate at high Mach numbers and low altitudes; that is, at high dynamic pressures. The use of rocket powered, track sleds is a valuable and accepted method of obtaining parachute deployment, structural, and operational performance characteristics at high dynamic pressures. When the Arrowhead sled became operational in 1967, it provided the platform necessary to extend the dynamic pressure limit of parachute track testing from 2900 to 8000 psf.

The initial objective of the test program was to determine deployment techniques, performance characteristics, and structural design criteria for nylon hemisflo parachutes operating at dynamic pressures up to 6000 psf. With the advent of the new high-strength, high-modulus Kevlar* parachute materials, which offer the potential for a 50 percent reduction in parachute weight, the objective was expanded to include comparative analyses of the performance and structural characteristics of nylon and Kevlar hemisflo parachutes.

Determination of satisfactory parachute deployment techniques required some departures from accepted practices. The early tests experienced deployment problems and the

---

*Registered trademark of E.I. DuPont de Nemours and Company, Inc. for their aramid fiber.

program was interrupted to establish a reliable technique. An analytical method established a new deployment control break tie design and the Tomahawk sled was used to check-out deployment system improvements at Mach 1.2.

Parachute performance characteristics were determined for nominal deployment Mach numbers of 1.5, 1.8, and 2.2 using the Arrowhead sled. These conditions produced nominal line stretch dynamic pressures of 2500, 3500, and 6000 psf, respectively. A 16.5 percent porosity, 5 ft nominal diameter hemisflo parachute was selected as the test model.

Structural design criteria of the hemisflo parachutes were determined by subjecting various strength parachute components to successively greater parachute opening forces until the material failure thresholds could be established.

To provide the data for the comparative analyses of the performance and structural characteristics of nylon and Kevlar hemisflo parachutes, tests at each nominal deployment Mach number were made first using nylon parachutes and then using equal strength (component for component) Kevlar parachutes.

In this report: the test program is described in Section II and in the Appendices, and includes a description of the Arrowhead sled and an estimation of the uncertainty of the track test data; the results are presented and discussed in Section III; and in Appendix C, a deployment control break tie design calculation technique is introduced which can be used to determine the number, locations, and strengths of parachute break ties that will control the deployment of nylon and Kevlar hemisflo ribbon parachutes at supersonic speeds and high dynamic pressures.

SECTION II

DESCRIPTION OF THE TEST PROGRAM

1. TEST FACILITY

a. The Holloman Track

All parachute tests for this program were conducted at the High Speed Test Track Facility at Holloman Air Force Base, New Mexico. The Holloman Track, which is organized as a division under the 6585th Test Group of the Air Force Systems Command, is an aerospace ground test facility. Its function is to simulate selected portions of flight trajectories under accurately programmed, closely controlled and rigorously monitored conditions. In track testing at Holloman, the payload and instrumentation are moved along a straight line path by means of rocket sleds which operate on a set of heavy duty crane rails. These rails span a total linear distance of 50,788 ft. A detailed description of the Holloman Track, its facilities, its capabilities, and a discussion of all technical and management aspects of testing at the track are given in Reference 1.

b. The Test Vehicles

The vehicles operating at the Holloman Track are referred to as sleds because their interface with the rails consists of steel shoes ("slippers") which are in sliding contact with the rails. Two dual rail sleds were used for this parachute test program, the Arrowhead sled and the Tomahawk sled.

---

(1) Anon: The Holloman Track, Facilities and Capabilities, Air Force Special Weapon Center, 6585th Test Group, Track Test Division, Holloman Air Force Base, New Mexico, Booklet, 1974.

(1) The Arrowhead Sled

The Arrowhead sled is a solid fuel rocket motor powered test vehicle specifically designed for parachute testing at high dynamic pressures. The Arrowhead sled is designated as IDS 6328 by the Holloman Track and operates either as a single stage vehicle or, with a noncaptive pusher sled, as a two-stage test vehicle. Carrying up to five Nike rocket motors on its captive PDS 6328-1 pusher sled, the Arrowhead sled is capable of developing a total of approximately 245,000 lb of thrust. In this configuration, the initial weight of 11,700 lb can be accelerated to a speed of Mach 1.89 at rocket motor burnout. Burnout weight is approximately 7,900 lb and the empty weight of the Arrowhead sled is approximately 4,100 lb. With the addition of the PDS 6328-2 first-stage noncaptive pusher sled containing five Nike rocket motors, the Arrowhead sled can be accelerated to Mach 2.55 at motor burnout. A more detailed description of the Arrowhead sled is given in Appendix A. Figure 1 shows two views of the Arrowhead sled with both pusher sleds on the track prior to test. A three-view sketch giving basic overall dimensions of the Arrowhead sled is shown in Figure 2.

(2) The Tomahawk Sled

The Tomahawk sled is also a solid fuel rocket powered parachute test vehicle which operates either as a single-stage or as a two-stage vehicle. It is designated as IDS 6301 by the Holloman Track. For this test program, eight 2.2 KS 11,000 rocket motors, which develop approximately 90,000 lb of thrust for 2.2 sec, were carried on the Tomahawk sled and four 2.2 KS 11,000 rocket motors were carried on the noncaptive IDS 5802-1 pusher sled. In this configuration, the initial weight of 7,800 lb can be accelerated to approximately Mach 1.3 at rocket motor burnout. The burnout weight is about 6,200 lb and the empty weight of the Tomahawk sled is

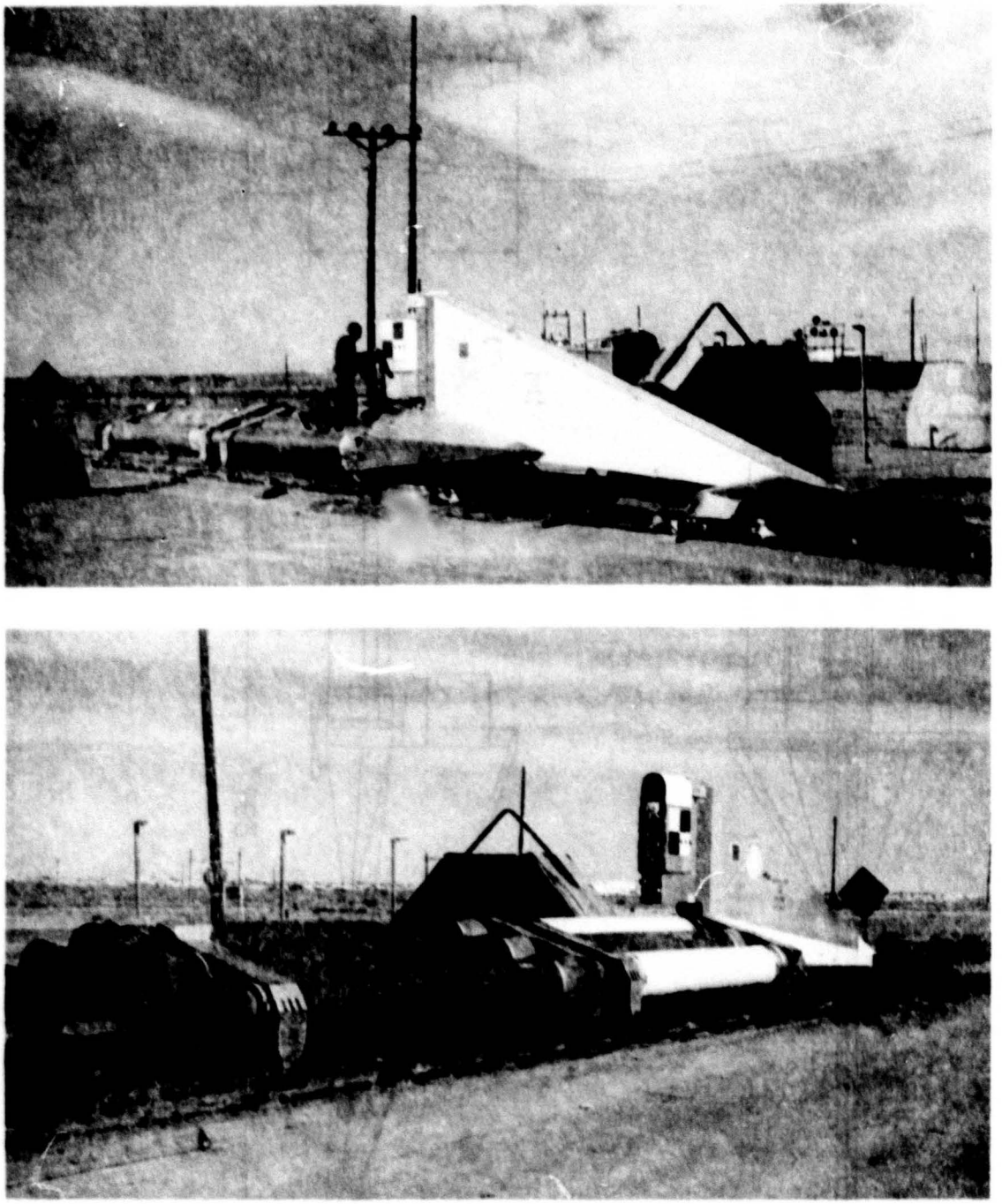

Figure 1. Photographs of the Arrowhead Sled with Pusher Sleds.

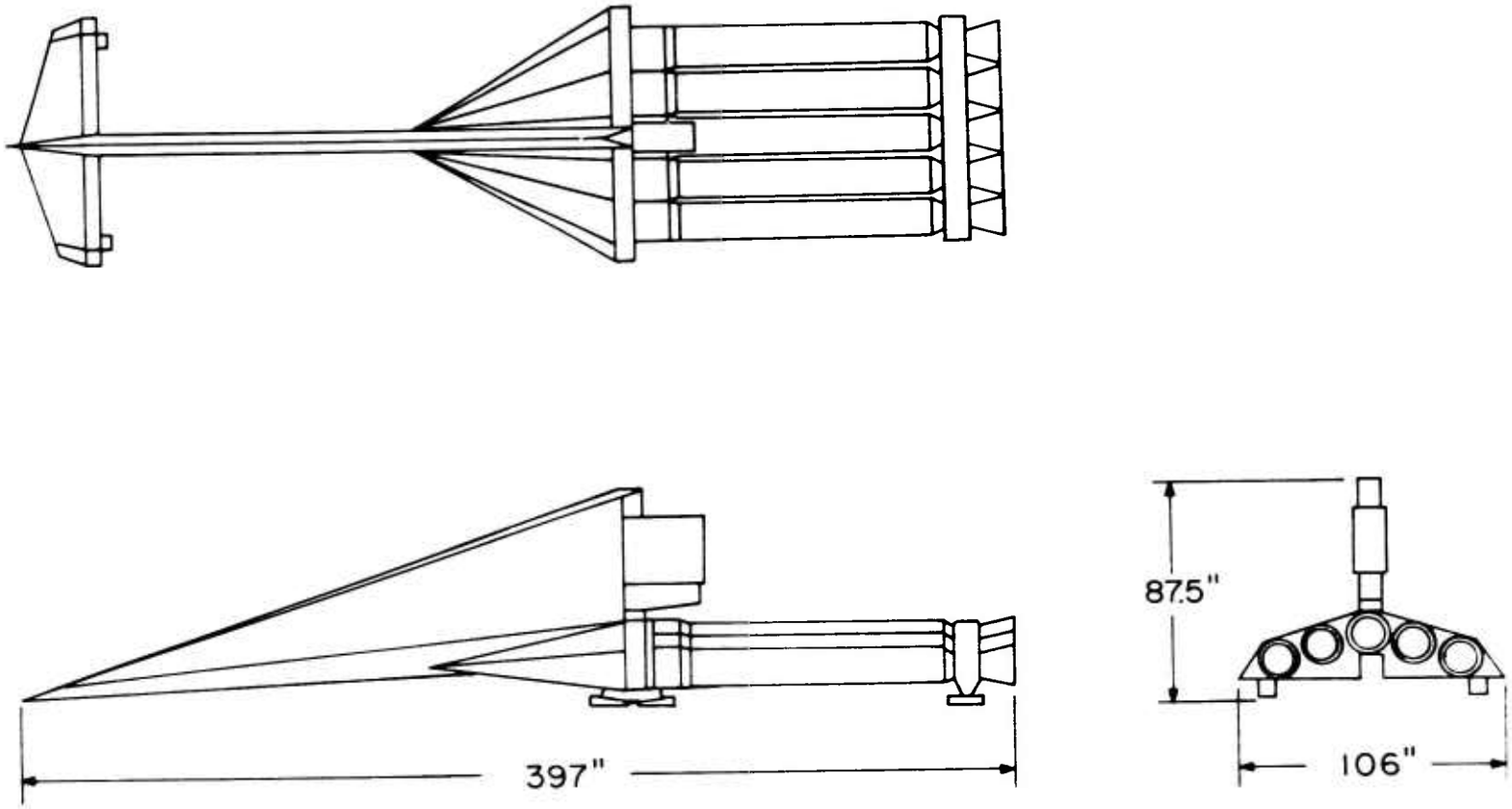

Figure 2. Basic Dimensions (3 View) of the Arrowhead Sled.

about 5,300 lb. More detailed descriptions of the Tomahawk sled are found in References 2 and 3. Figure 3 shows two views of the Tomahawk and pushers sleds on the track prior to test and a three-view sketch giving basic overall dimensions of the Tomahawk sled is shown in Figure 4.

(2) Pederson, Paul E.: Study of Parachute Performance at Low Supersonic Deployment Speeds; Effects of Changing Scale and Clustering, Air Force Aeronautical Systems Division Technical Report 61-186, (AD 267 502), July 1961.

(3) Pederson, P.E.: Study of Parachute Performance and Design Parameters for High Dynamic Pressure Operation, Air Force Flight Dynamics Laboratory Report AFFDL-TDR-64-66, (AD 607 036), May 1964.

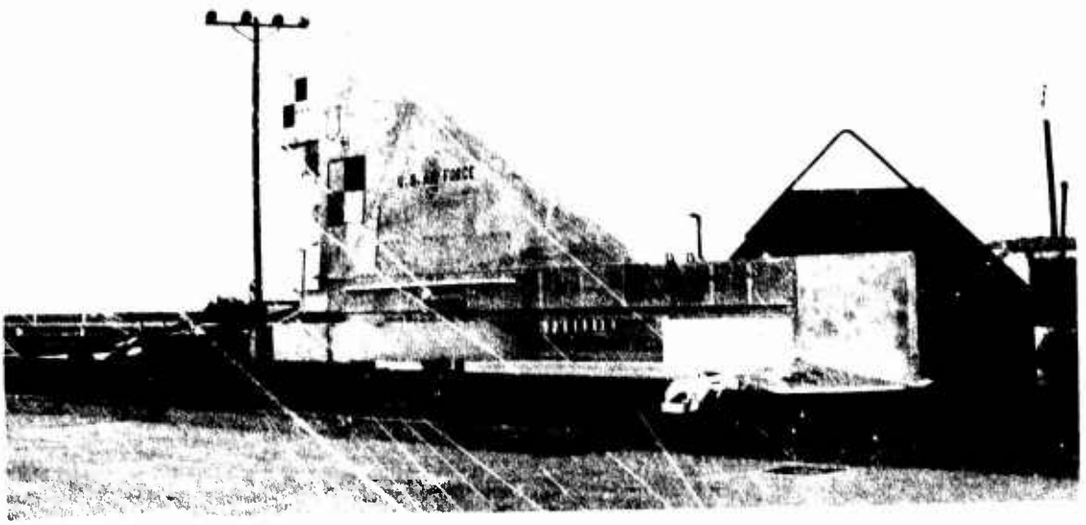

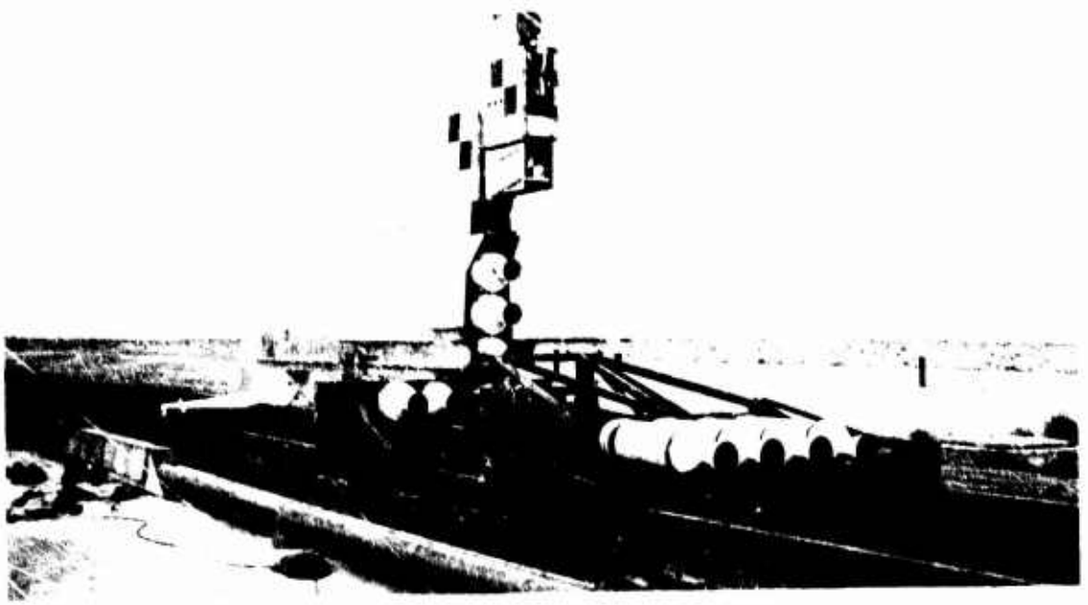

Figure 3. Photographs of the Tomahawk Sled with Pusher Sled.

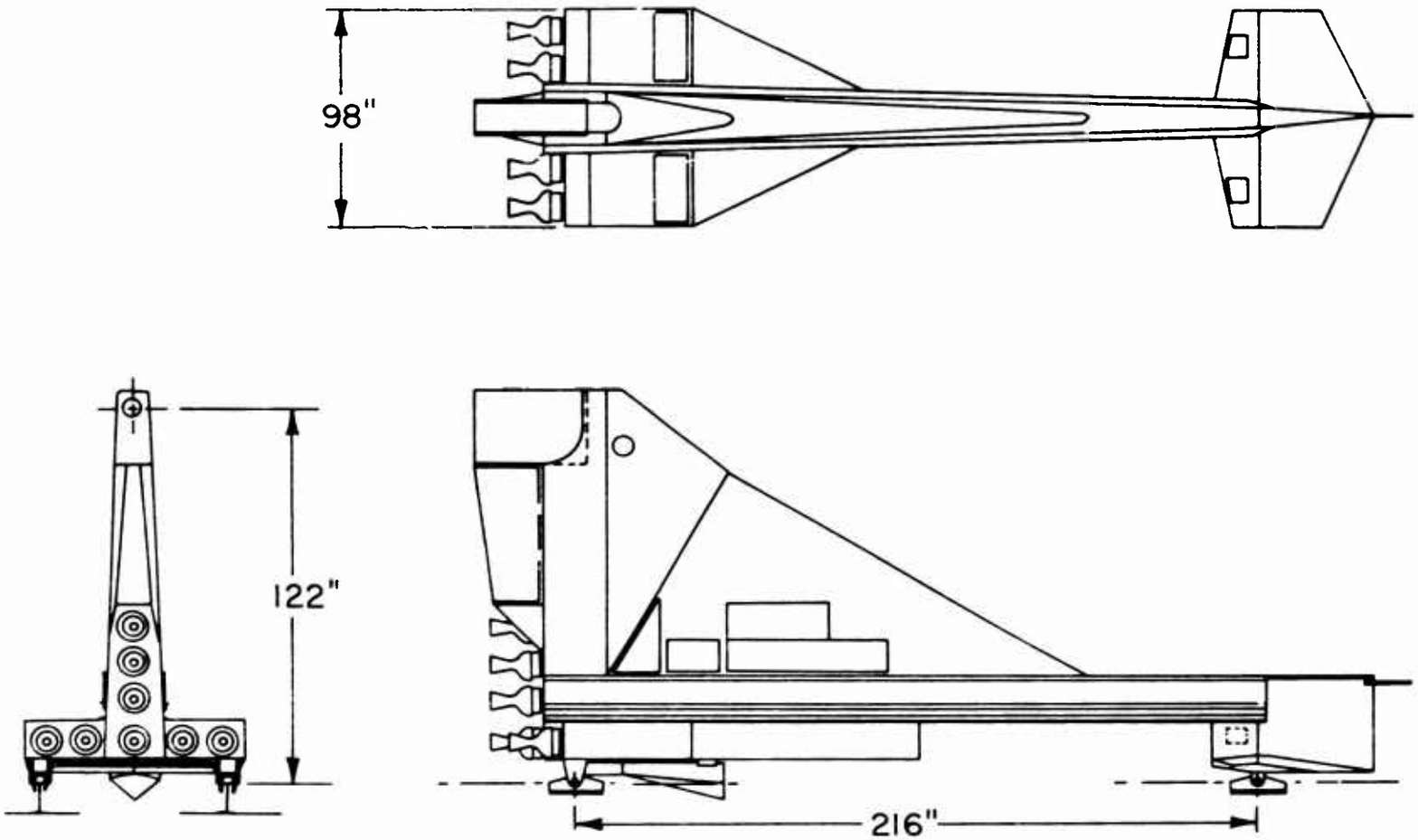

Figure 4. Basic Dimensions (3 View) of the Tomahawk Sled.

2. PARACHUTE MODELS

One parachute type was used for all tests conducted in support of this program, a 5 ft nominal diameter hemisflo ribbon type parachute. The basic differences among the parachute models were the material strengths and material type-nylon and Kevlar. Sketches of the general arrangement of the hemisflo parachutes are given in Figure 5. Detailed descriptions and design of the test parachutes are given in Appendix B.

a. Configuration Selection

(1) Parachute Type

The hemisflo parachute was selected for study under this program to provide an extension of the studies with hemisflo parachutes at lower dynamic pressures (Reference 3) and to provide supersonic, high-dynamic pressure data on a nonreefed model of the reefed hemisflo parachute which was undergoing flight tests for the Air Force Flight Dynamics Laboratory (Reference 4).

The hemisflo parachute has exhibited satisfactory performance characteristics at supersonic speeds and its ribbon construction provides a weight efficient canopy surface that will withstand the large canopy stresses generated at high dynamic pressures.

(2) Canopy Size

Selection of the hemisflo canopy size was based upon estimated parachute performance, maximun sled

---

(4) Bloetscher, F.: Aerodynamic Deployable Decelerator Performance Evaluation Program, Phase II, Air Force Flight Dynamics Laboratory Report, AFFDL-TR-67-25, (AD 819 915), April 1967.

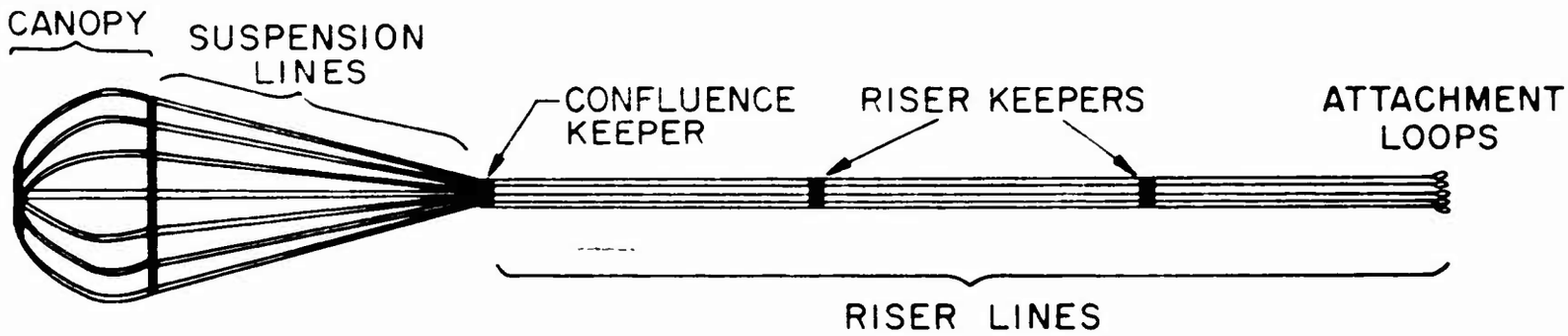

a. MAJOR PARACHUTE COMPONENTS

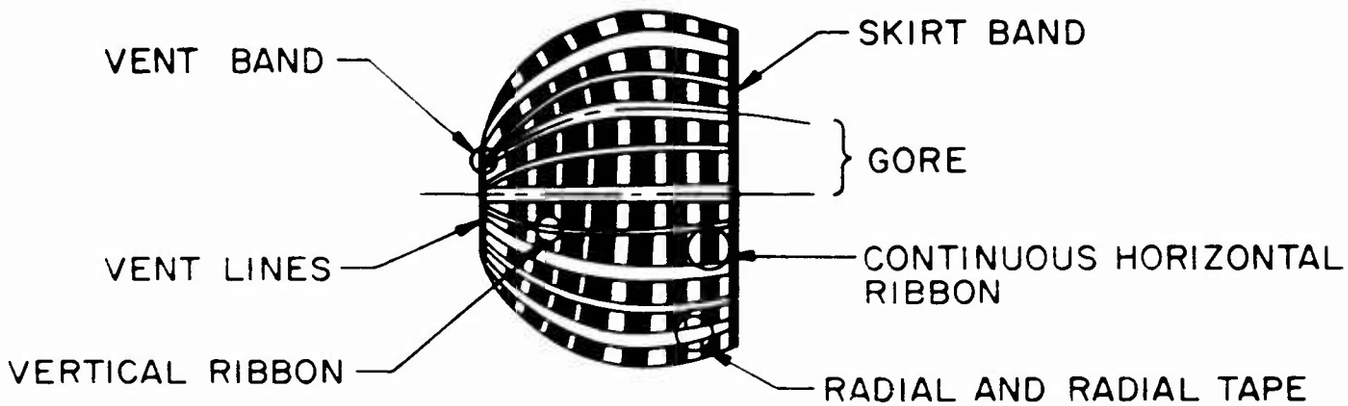

b. MAJOR CANOPY COMPONENTS

Figure 5. Sketches of the General Arrangement of the Hemisflo Parachutes.

velocity (M_∞ = 2.55), maximum parachute load allowed to be applied to the sled (150,000 lb), and a safety factor of 1.5). The 5 ft nominal diameter hemisflo parachute canopy chosen in this manner for the test program gave a slightly positive margin of safety.

(3) Canopy Porosity

A hemisflo canopy porosity in the range from 14 to 18 percent was considered desirable for use on this test program. A 14 percent porosity hemisflo parachute was chosen for the supersonic flight test program documented in Reference 4 and an 18 percent porosity hemisflo parachute performed satisfactorily during wind tunnel tests at Mach numbers of 1.8, 2.0, and 2.2 (Reference 5).

A 5 ft diameter hemisflo parachute canopy with a geometric porosity of 16.5 percent porosity was designed for this test program; see Appendix B.

(4) Riser Length

Riser lines were used to position the canopy downstream of the strong shock waves generated by the Arrowhead sled. These shock waves for Mach numbers 2.0 and 3.0 are shown in Figure A-3 of Appendix A. Riser lines 20 ft long were required for tests at Mach 1.5 and riser lines 30 ft long were used for tests at Mach 1.8 and 2.2.

b. Hemisflo Design

The designs of all hemisflo parachutes were the same and were in accordance with the method outlined on pages

---

(5) Reichenau, D.E.A.: Aerodynamic Performance of Various Hyperflo and Hemisflo Parachutes at Mach Numbers from 1.8 to 3.0, Arnold Engineering Development Center Report, AEDC-TR-65-57, (AD 358 325), March 1965.

517 through 522 of the "Parachute Handbook" (Reference 6), which gives sample calculations and design equations for hemispherical canopies.

Physical details and dimensions of the hemisflo parachutes are given in Table 1 and the gore coordinates are given in Figure 6. Measurements were taken on the canopy under nominal (less than 40 lb) tension within 15 sec after application of the nominal tension.

c. Parachute Construction

The parachute canopy gores were assembled using the continuous ribbon technique. Each ribbon and vent and skirt band was continuous around the canopy, passing between the radials of each gore with a single splice between the radials. The locations of the splices were staggered around the canopy. Ribbon spacing was maintained by one vertical ribbon on the centerline of each gore.

An integral suspension line/riser arrangement with restraining keepers was used. The suspension lines also passed over the canopy and served as the radials and the vent lines. Attachment loops were sewn at the end of each of the twelve riser lines.

Although significant difficulties were expected during the fabrication of the parachutes made from the new high strength, low modulus Kevlar materials, none were experienced.

---

(6) Anon. (American Power Jet Co.): Performance of and Design Criteria for Deployable Aerodynamic Decelerators, Air Force Flight Dynamics Laboratory, Technical Report ASD-TR-61-579, (AD 429 971), December 1963.

TABLE 1

PHYSICAL DETAILS AND DIMENSIONS OF THE
NYLON AND KEVLAR HEMISFLO PARACHUTES

Nominal diameter, D_o (ft)	5.0
Canopy area, S_o (sq ft)	19.635
Geometric porosity, λg (percent)	16.5
Number of gores	12
Number of suspension lines	12
Suspension line length (in.)	100
Number of horizontal ribbons	11
Number of vertical ribbons per gore	1
Separate vent band	Yes
Separate skirt band	Yes
Number of vent lines	6
Finished vent line length (in.)	5.0
Gore width at vent (in.)	1.62
Finished gore width at vent (in.)	1.43
Finished gore height (in.)	31.9
Finished gore width at skirt (in.)	9.3
Finished skirt circumference (in.)	112

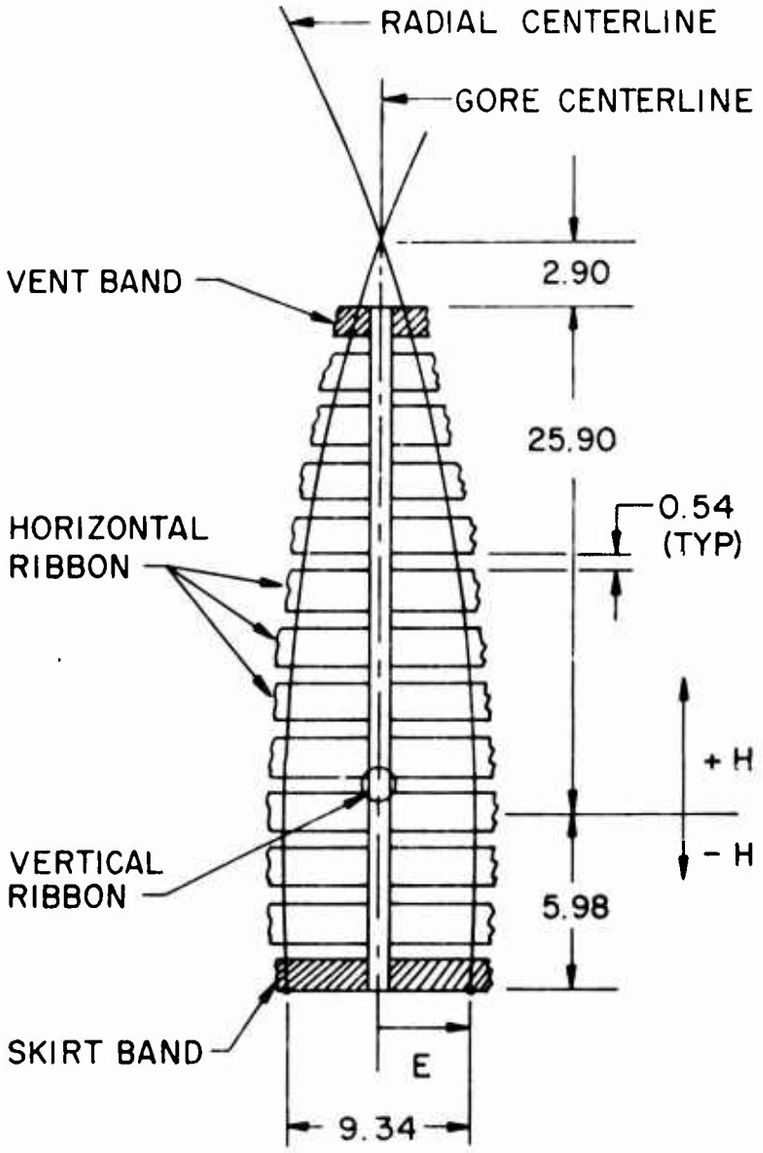

H	± E
-5.98	4.67
0	4.90
3.19	4.83
6.40	4.62
9.60	4.28
12.80	3.80
16.00	3.21
19.20	2.47
22.30	1.75
25.80	0.95
28.80	0

NOTE: ALL DIMENSIONS IN INCHES

Figure 6. Gore Coordinates of the Nylon and Kevlar Hemisflo Parachute Canopies.

d. Physical Characteristics

The physical characteristics of the nylon and Kevlar parachutes are listed in Tables 2 and 3, respectively.

(1) Component Strengths

The major structural components were analyzed to estimate strength requirements and select materials. The overall strength requirements for the suspension lines, horizontal ribbons, and skirt and vent bands were estimated by applying design factors to the expected maximum parachute opening forces. It was expected that the range of material strengths chosen for these components (listed in Tables 2 and 3) would be sufficiently large such that the ultimate loads in these components could be determined from the tests. That is, the material strengths were selected such that, for a given opening force, a material of one strength might be expected to fail while the next higher strength material would be undamaged.

(2) Material Characteristics

The general characteristics of the materials selected for the various components of each test parachute used on this test program are summarized in Tables 2 and 3. The detailed characteristics of the nylon materials can be found in the applicable Military Specifications. The construction and characteristics of the Kevlar materials are summarized in Table B-1 of Appendix B.

(3) Parachute Weights

Since Kevlar materials weigh considerably less than nylon materials of comparable strength, the weights of all parachutes were recorded to document the weight savings for constructed parachutes. These weights are included in Tables 2 and 3 and are also listed in Table 4.

TABLE 2

PHYSICAL CHARACTERISTICS OF THE NYLON PARACHUTES

CHARACTERISTICS	PARACHUTE DESIGNATIONS								
	FDFRA-1	FDFRA-2	FDFRA-3-2	FDFRA-4-1	FDFRA-4-2	FERR-1-1	FERR-1-2	FERR-1-3-1	FERR-1-1-2
RISER LINES, SUSPENSION LINES, RADIALS, VENT LINES									
Number of plies	2	2	2	2	2	2	2	2	2
Width (in.)	3/4	3/4	1	1	1	1	1	1	1
Strength (lb)	3000	3000	4000	6000	6000	6000	6000&9000	9000	9000
Spec. MIL-W-	27657	27657	27657	27657	27657	27657	27657	27657	27657
Spec. Type	I	I	II	III	III	III	III&V	V	V
HORIZONTAL RIBBONS									
Number of plies	1	1	1	1	2	1	2	2	2
Width (in.)	2	2	2	2	2	2	2	1 7/8	2
Strength (lb)	2000	3000	3000	4000	2000	4000	2000&3000	3000	3000
Spec. MIL-T-	5608	5608	5608	5608	5608	5608	5608	5608	5608
Spec. Type	IV	V	V	VI	IV	VI	IV&V	V	V
RADIAL TAPE -PLY MIL-W-4088, 1-in., 600 lb, Type II	1	1	None	None	None	None	None	None	None
VERTICAL RIBBON -Ply MIL-T-5038, 5/8-in. 625 lb, Type IV	2	2	2	2	2	2	4	4	4
SKIRT BAND									
Number of plies	1	1	1	1	1	1	2	2	2
Width (in.)	1 23/32	1 23/32	1 23/32	1 23/32	1 23/32	1 23/32	1 23/32	1 23/32	1 23/32
Strength (lb)	4500	6500	6500	8700	8700	8700	4500&6500	6500	6500
Spec. MIL-W-	4088	4088	4088	4088	4088	4088	4088	4088	4088
Spec. Type	XVI	XIII	XIII	X	X	X	XVI&XIII	XIII	XIII
VENT BAND									
Number of plies	2	2	2	2	2	2	2	3	3
Width (in.)	1 23/32	1 23/32	1 23/32	1 23/32	1 23/32	1 23/32	1 23/32	1 23/32	1 23/32
Strength (lb)	3600	3600	4500	6500	6500	6500	9500&8700	6500	6500
Spec. MIL-W-	4088	4088	4088	4088	4088	4088	4088	4088	4088
Spec. Type	XVI	XIII	XIII	X	X	X	XVI&XIII	XIII	XIII
CONFLUENCE KEEPER									
Number of plies	2	2	2	2	2	2	2	3	3
Width (in.)	1 23/32	1 23/32	1 23/32	1 23/32	1 23/32	1 23/32	1 23/32	1 23/32	1 23/32
Strength (lb.)	3600	3600	3600	3600	3600	3600	9500	10,000	10,000
Spec. MIL-W-	4088	4088	4088	4088	4088	4088	4088	27657	27657
Spec. Type	VIII	VIII	VIII	VIII	VIII	VIII	XXII	VI	VI
RISER, KEEPERS -Ply MIL-W-4088, 1 23/32 in., 3600 lb. Type VIII	2	2	2	2	2	2	2	2	2
RISER LENGTH (ft)	20	20	30	30	30	30	30	30	30
CANOPY WEIGHT (lb)	5.5	6.0	6.5	8.0	9.0	8.0	11.0	14.0	14.0
TOTAL WEIGHT (lb)	20.0	20.5	33.5	38.5	42.0	39.5	49.5	62.0	62.0
USED ON TEST NUMBER 6P-	E3	E2,P1, F2,& P6	G1	E4&P1	G2	G3	H1	H2	H3

TABLE 3

PHYSICAL CHARACTERISTICS OF THE KEVLAR PARACHUTES

CHARACTERISTICS	PARACHUTE DESIGNATION						
	FERA-1-K	FERA-2-K	FERA-3-K	FERR-1-1-K1	FERR-1-2-K	FERR-1-3-K	FERR-1-4-K
RISER LINES, SUSPENSION LINES, RADIALS, VENT LINES							
Number of Plies	2	2	2	2	2	2	2
Width (in.)	3/4	3/4	3/4	1	1	1	1
Strength (lb)	3000	3000	4000	6000	6000&9000	9000	12000
Spec. Type	II	II	IIa	V	V & VI	VI	VII
HORIZONTAL RIBBONS							
Number of Plies	1	1	1	1	2	2	2
Width (in.)	2	2	2	2	2	2	2
Strength (lb)	2000	3000	3000	4000	2000&3000	3000	4000
Spec. Type	XII	XIII	XIII	XIV	XII & XIII	XIII	XIV
RADIAL TAPE							
Number of Plies	1	1	1	None	None	None	None
Width (in.)	1	1	1				
Strength (lb)	1000	1000	2500				
Spec. Type	VI	VI	IV				
VERTICAL RIBBON-PLY 5/8 in.,625 lb, Spec. Type V	2	2	2	2	4	4	4
SKIRT BAND							
Number of Plies	1	1	1	1	2	2	2
Width (in.)	1 3/4	1 3/4	1 3/4	1 3/4	1 3/4	1 3/4	1 3/4
Strength (lb)	4500	6500	6500	8700	4500&6500	6500	8700
Spec. Type	XV	XVI	XVI	XVIII	XV&XVI	XVI	XVIII
VENT BAND							
Number of Plies	2	2	2	2	2	3	3
Width (in.)	1 3/4	1 3/4	1 3/4	1 3/4	1 3/4	1 3/4	1 3/4
Strength (lb)	3600	3600	3600	3600	8700	6500	6500
Spec. Type	XIV	XIV	XIV	XIV	XVIII	XVI	XVI
RISER KEEPERS-PLY 1 3/4 in.,3600lb, Spec. Type XIV	2	2	2	2	2	2	2
RISER LENGTH (ft)	20	20	30	30	30	30	30
CANOPY WEIGHT (lb)	2.1	2.5	3.0	4.0	6.0	6.5	7.0
TOTAL WEIGHT (lb)	8.2	9.5	14.5	24.1	31.0	35.6	36.0
USED ON TEST 6P -	E9	E10	G4	G5	H5	H6	H7

TABLE 4

NYLON AND KEVLAR PARACHUTE WEIGHTS

Total Nominal Strength of Horizontal Ribbons (lb)	Nominal Strength of Two Ply Suspension Lines (lb)	Nylon Canopy Weight (lb)	Kevlar Canopy Weight (lb)	Kevlar Canopy Weight (Percent of Nylon)	Nylon Parachute Total Weight (lb)	Kevlar Parachute Total Weight (lb)	Kevlar Parachute Total Weight (Percent of Nylon)
2000	6000	5.5	2.1	38	20.0	8.2	41
3000	6000	6.0	2.5	42	20.5	9.5	46
3000	8000	6.5	3.0	46	33.5	14.5	43
4000	12,000	8.3 *	4.0	48*	40.0*	24.1	60*
5000	15,000	11.1	6.0	55	49.5	31.0	63
6000	18,000	14.0	6.5	46	62.0	35.6	57

*Average values for three nylon parachutes.

Table 4 also presents a tabular comparison of the weights of nylon and Kevlar parachutes as functions of canopy ribbon and parachute suspension line strengths. This comparison is also graphically illustrated in Figure 7. All Kevlar parachute canopies weighed less than 56 percent of comparable strength nylon canopies. For the three stronger parachutes the weight savings of the overall Kevlar parachutes were less than the weight savings of the Kevlar canopies. This indicates that the Kevlar horizontal and vertical ribbons contribute more to the weight savings than do the Kevlar suspension and riser lines, for these three stronger parachutes.

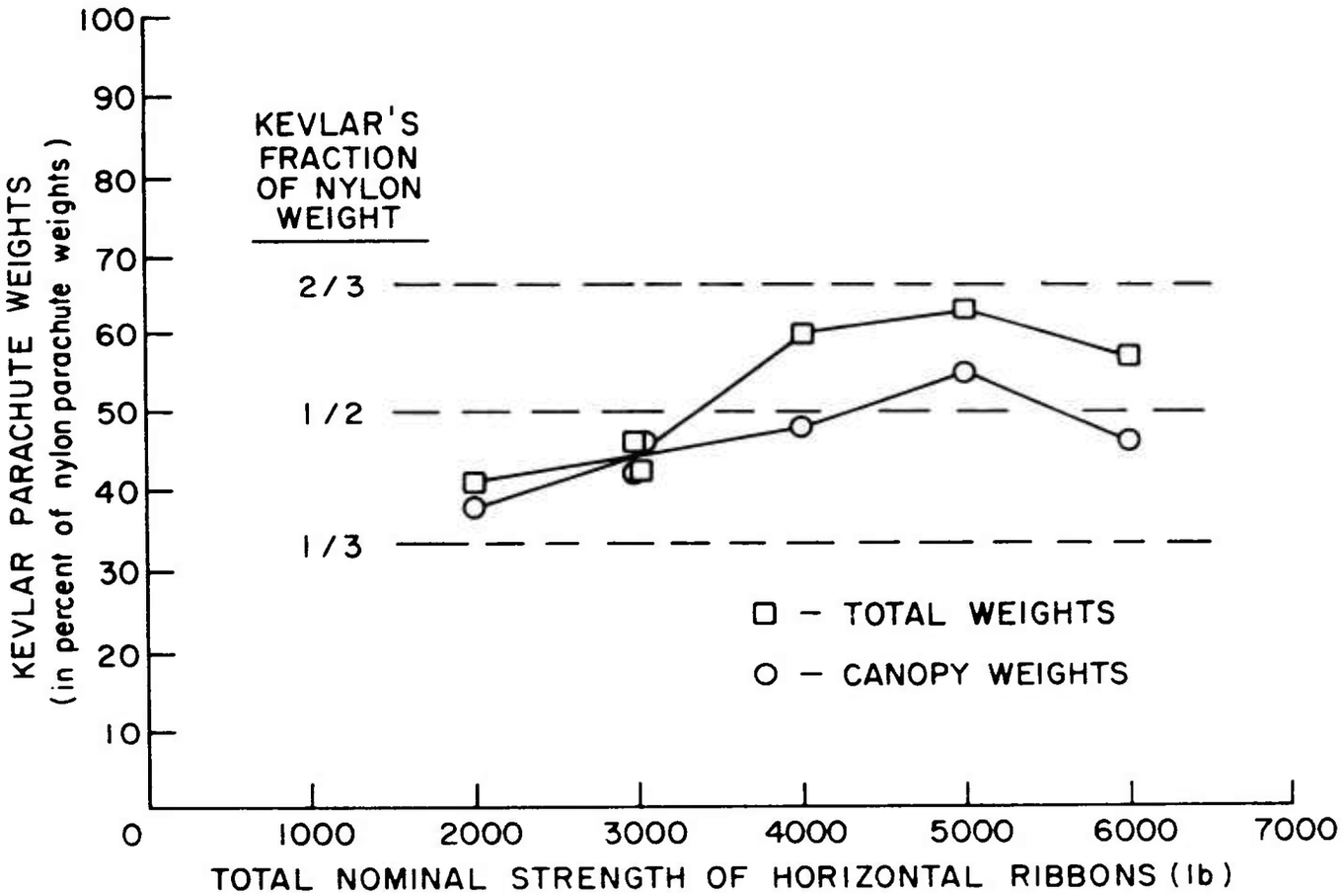

Figure 7. Graphical Comparison of the Weights of Nylon and Kevlar 5 ft Diameter Hemisfio Parachutes.

3. TEST TECHNIQUE

The Holloman Track prepared an Operations Plan (OPLAN) for each test run series; that is, one OPLAN for each sled configuration and desired parachute deployment Mach number. The OPLAN included: (1) test administrative information, (2) track station locations for events, (3) electronic instrumentation support requirements, (4) electronic data reduction requirements, (5) photographic instrumentation support requirements, (6) sled and track preparation instructions, (7) run profile data, and (8) a master countdown checklist.

On the day before a test, the track and sled were prepared as specified in the OPLAN and the test parachute was installed on the sled. On the day of the test, the countdown proceeded in accordance with the master countdown checklist. The sled was fired and moved down the track; the required test data was gathered throughout its run. The test parachute was deployed and released at prescribed track locations. After the run, the sled and test parachute were recovered.

a. Track Preparation

Track preparation included: (1) the installation of full slippers on the sled, (2) the installation of the required number of water dams for braking the sled, (3) the erection of a synchronization light stand which provided an event-time correlation for the on-board cameras, and (4) the installation of screenboxes which are intercepted by sled-borne knife blades, and which conduct an electric current from the ground to the sled as long as the knife blades are in contact with the screen. Currents from the screenboxes were used to stage the rocket motors, turn off the on-board cameras, fire the parachute deployment and release mechanism squibs, and flash the camera syncronization light.

b. Parachute Installation

The packed test parachute was inserted into the parachute storage compartment of the sled and the riser lines and cone riser were attached to the parachute attachment/deployment/release mechanism. The parachute attachment cover was then fastened in place on top of the storage compartment. Detailed descriptions of the parachute attachment, deployment, and release components including parachute packing and installation instructions and photographs are given in Appendix C. A photograph of a test parachute installed on the Arrowhead sled is presented in Figure 8.

c. Sled Preparation

The sled, with the parachute and camera box installed, was positioned on the track and attached to the slippers. Then the cameras, rocket motors, ignitors, and pyrotechnic actuators were installed. All wiring from the knife blades to the actuators and ignitors, and all other internal sled instrumentation wiring, was connected. Finally, all sled access doors were closed and the sled was armed.

d. Parachute Deployment

After ignition of the rocket motors, the sled accelerated down the track. Shortly after burnout of the last stage of rocket motors, the knife blades on the sled intercepted the parachute deployment screenbox. This screenbox was located at that track station where it was predicted that the sled would have the speed desired for parachute deployment initiation. Electrical current from the screenbox fired the drogue gun squibs in the parachute deployment mechanism. The resulting gas pressure sheared the drogue gun mortar pin and propelled the deployment cone downstream from the sled. Cone drag and momentum were transferred as tension forces through the cone riser to the test parachute restraining strap release cables

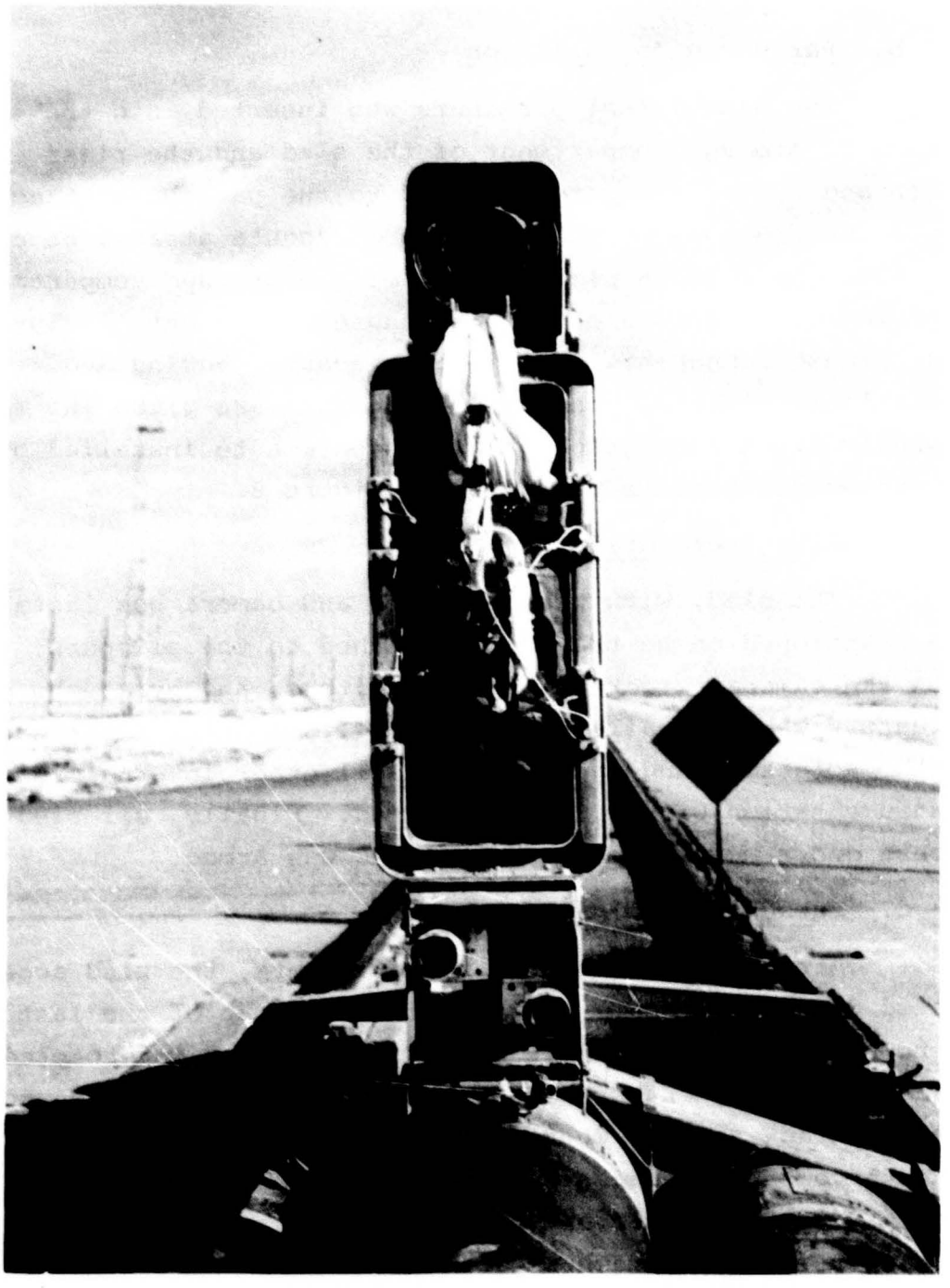

Figure 8. Photograph of the Test Parachute Installed on the Arrowhead Sled - Test 6P-H1.

and to the pilot chute bag. After the restraining strap was released, the cone pulled the pilot chute and bag about six feet downstream from the sled, at which point the pilot chute exited the bag and inflated. The pilot chute then pulled the test parachute and bag to line stretch of the parachute, at which point the canopy exited the bag and inflated. Pilot chute and test parachute were prevented from prematurely exiting their deployment bags by line and canopy ties of appropriate strengths. Detailed descriptions of the deployment system components used for each test and the calculation method used for determining the strengths of the ties are given in Appendix C. A sketch of a typical deployment sequence showing the major components is presented in Figure 9 and photographs of an actual deployment sequence are presented in Figure 10.

e. Parachute Release

After all parachute performance data had been gathered and before the sled entered the water dams, knife blades on the sled intercepted the parachute release screenbox. Electric current from the screenbox fired the parachute release mechanism squibs. The parachute was released from the sled to prevent it from being damaged during sled recovery.

f. Sled Recovery

After parachute release, sled-borne knives intercepted a screenbox which turned off the on-board cameras. The sled then entered the water dams. Sled deceleration resulting from its aerodynamic drag and frictional resistance with the rails then became augmented by water braking. The braking force was generated by momentum transfer from the moving sled to water, which was scooped up from the dams and ejected into the air. The braking force was controlled by adjusting the number and height of the frangible dams.

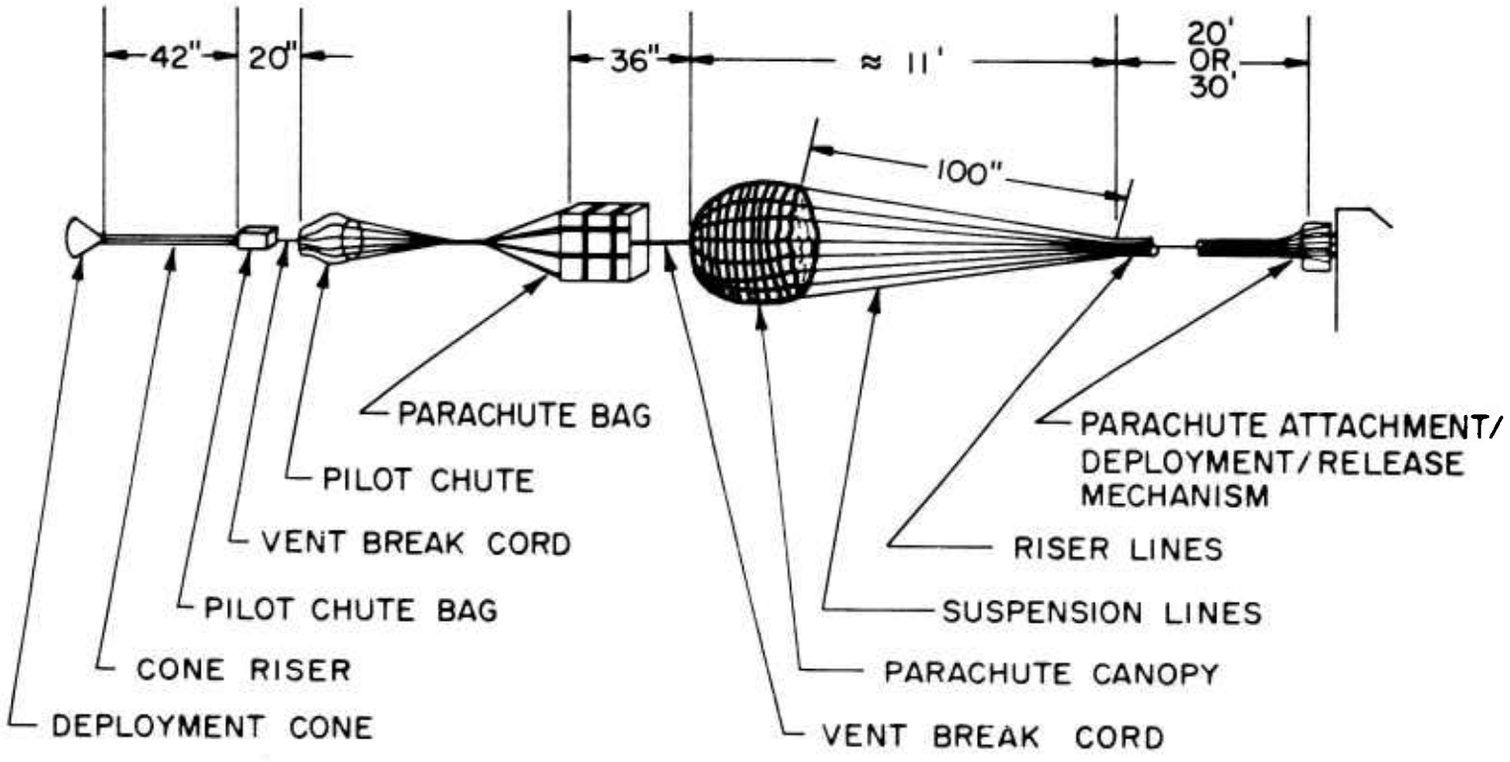

Figure 9. Sketch Showing Major Components of a Typical Deployment Sequence.

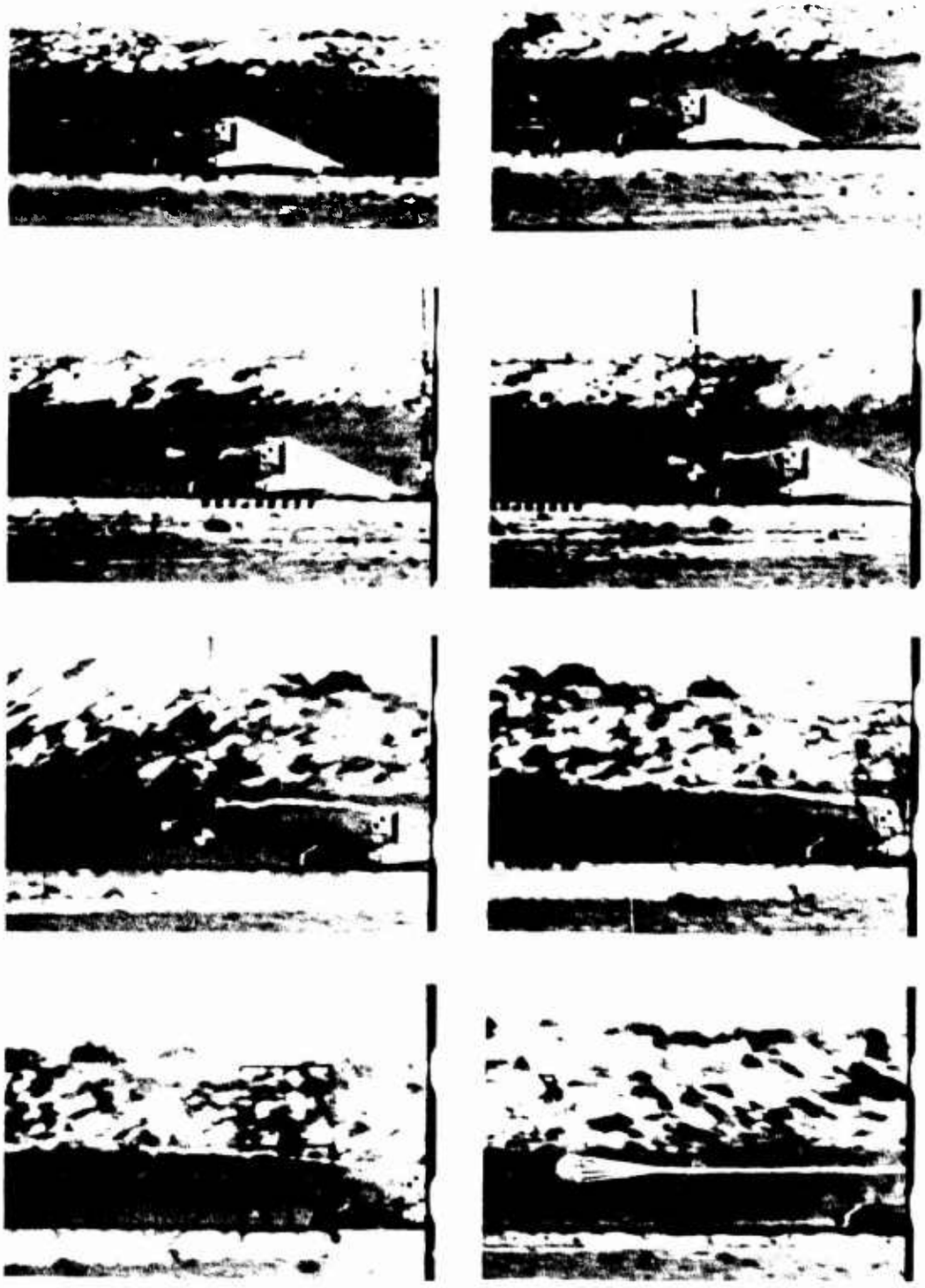

Figure 10. Photographs of the Deployment Sequence From Test 6P-G1.

After the sled came to a stop, the screenboxes were disarmed and the sled, pusher, slippers, screenboxes, and all parachute components were removed from the track.

4. INSTRUMENTATION AND DATA GATHERED

a. Meteorological Readings

The Holloman Track is located at elevations above mean sea level that gradually increase from 4,058 ft at track station zero to 4,099 ft at track station 50,770. The atmospheric conditons which existed just prior to a test run were obtained from the Holloman Air Force Base weather station which is at an elevation of 4,092 ft above mean sea level.

The meteorological readings recorded for each test were wind direction, wind speed, temperature, (absolute) barometric pressure, and relative humidity.

b. Electronic Instrumentation

(1) On-Board Telemetry

Radio frequency telemetry, of the FM/FM type, was used to transmit sled and parachute performance data. Two channels were used for the sled Velocity Measuring System (VMS), two were used for the parachute tensiometer, and one channel was used to monitor the on-board telemetry battery.

Track-side decommutation, data recording, reproduction, and duplicating was done on magnetic tape, direct writing oscillographs, and stylus recorders at the Midway data acquisition and recording building.

(2) Sled Performance

An electro-optical VMS determined sled position as a function of time by means of track-fixed light beam interrupters. The interrupters consisted of metal plates which were positioned at 13 ft intervals along the track. Real time measurements were obtained from a sledborne sensing head which provided a light beam between a light source and a photo-transistor. The beam was interrupted each time the sensing head passed an interrupter. The output was a series of pulses

which was transmitted to Midway by telemetry. The time versus position data obtained this way was processed by computer to yield smoothed and unsmoothed sled position, velocity, and acceleration as functions of time. The smoothed sled velocity data was then combined with the meteorological data to derive relative wind true airspeed, Mach number, and dynamic pressure, also as functions of time.

Two back-up and quick-look type velocity measuring systems were also used to evaluate sled performance. Both systems consisted of a series of sensors positioned in holders along the track and spaced at distances of 208 ft from each other. In one system the sensors were thin balsa wood "breaksticks" which were coated with aluminum paint to provide a conductive surface. Each stick was broken by direct contact with the sled, generating an electric pulse by interrupting the current through the stick. In the other system the sensors were magnetic. After being set, these magnetic sensors provided a single electric pulse when the first steel slipper of the sled passed close by. The signals from these sensors were transmitted to Midway by cables and were recorded as functions of time. This data was also processed to yield sled position, velocity, and acceleration versus time.

(3) Parachute Forces

Forces generated by the test parachute were measured by a tensiometer which formed part of the parachute attachment and release mechanism. Two conventional strain gages, connected in bridge configurations, were employed as the sensing elements on a steel tension link. Outputs from both sensing elements were transmitted to Midway by telemetry and recorded on magnetic tape and by a direct print oscillograph. The rated full-scale range of the tensiometer was 100,000 lb. The approximate full-scale output of each sensing element was 25 millivolts.

During the test program, drag forces were transmitted through various low pass filters whose band widths ranged from 220 to 2100 Hz. However, on each test there was one drag force channel with a filter of at least 660 Hz. The maximum frequency responses of the galvanometers used in the oscillographs always exceeded the frequencies of the filters. For example, on Test 6P-E6, the filters were 220 and 2100 Hz and the galvanometer response frequencies were 1000 and 3000 Hz, respectively.

c. Optical Instrumentation

A large number of different types of cameras were used during this program to record sled and parachute performance characteristics and test operations. These cameras were used for three basic purposes: (1) to provide backup data of sled and parachute performance, Metric Optical Instrumentation; (2) to provide primary data for engineering analysis of parachute performance, Engineering Optical Instrumentation; and (3) to provide Documentary Photography. A listing of the cameras used during this test program is presented in Table 5.

(1) Metric Optical Instrumentation

Ribbon frame type cameras, operating at 90 frames per second, were employed at selected permanent metric optical instrumentation sites alongside the track for this test program. Each camera image related sled and parachute position to precisely surveyed target poles, five to seven of which were within the field of view of each camera site. These cameras were used as a backup system to determine sled and parachute performance characteristics.

(2) Engineering Optical Instrumentation

Maximum use was made of the trackside and sledborne motion picture coverage provided by the Holloman Track to acquire the primary data for engineering analysis of parachute performance.

TABLE 5

CAMERAS USED DURING THE TEST PROGRAM

Camera Type	Track Station Designation	Function Code	Lens Sizes	Frames per Second	Film Type	Used on Sled Tests 6P-
Ribbon Frame	FOX	A	5, 7, 9, and 10 in.	90	B & W	All tests.
16 mm F.F. Fairchild	FX	B	13 and 35 mm	3000	Color	E2, E3, F1, F2, F3, and E6
70 mm F.F. 10B Photosonic	PH	B	135, 180, 250, and 350 mm	360	B&W & C	E2, E3, E6, G1, G2, and G3
70 mm 1/10 F Photosonic	PH	B	3 in.	400	B&W & C	E1, E3, F1, F2, and F3
16 mm 1B Photo-sonic	SX-1	D	17 and 25 mm	1000	B&W & C	All tests.
16 mm 1B Photo-sonic	SX-2	D	17 and 25 mm	500	B&W & C	All tests.
35 mm F.F.Mitchell	TM	C	17 and 20 in.	96	Color	E2, E3, F1, F2, F3, E6, G1, G2, and G3
35 mm 4E Photo-sonic	TM	C	6, 10, and 14 in.	360	Color	G3, H1, H2, H3, E9, E10, G4, and G5
16 mm Locam	A/C,TD, and TM	E&C	6 in. and 200 mm	200&400	Color	All tests after G2.
16 mm FF Nova	FX	B	13 and 25 mm	2000 & 3000	Color	H1
16 mm Hycam	FX	B	13 mm	1000	Color	H1
35 mm 4C Photo-sonic	PH	B	6 in.	2500	Color	All tests after H1.
70 mm 10A Photo-sonic	PH	B	250 mm	60&80	Color	G5, H5, H6, and H7.
70 mm 10R Photo-sonic	PH	B	254 mm	125	Color	H5, H6, and H7

Function Code Key:
A - Metric Optical Instrumentation - Sled and parachute performance (back-up).
B - Track Side - Parachute performance and deployment dynamics.
C - Tracking - Parachute performance and sled operation.
D - On-Board - Parachute oscillation angle and projected area.
E - Documentary.

Abbreviations: B&W -black and white: C-color; A/C-range safety helicopter.

Two on-board cameras, track designations SX-1 and SX-2 and operating at 1000 and 500 frames per second, respectively, were used to obtain test parachute oscillation angle, quadrant angle, and frontal (projected) area as functions of time. Reference dimensions used to reduce the camera coverage data to the desired parachute performance parameters were obtained from photographs taken by these cameras of a ground-fixed reference target board.

Test parachute deployment events and trajectories were determined from fixed trackside motion picture cameras which were located at those track stations where parachute deployment was expected to occur. Reference dimensions used to obtain deployment cone and parachute bag separation distances from the sled as functions of time were determined from a target grid painted on the sled and from known sled dimensions.

A few tracking cameras were also used to provide motion picture coverage of the entire sled run.

(3) Documentary Photography

Pre and post test still photography was employed on each test to provide documentation of the condition of the deployment aids and test parachute during and after installation and after the test run.

Documentary tracking motion picture coverage from on-board the range safety helicopter was obtained on some tests.

d. Timing

Most data collected was correlated by recording time bases and codes which indicated elapsed time. All time bases and codes met Inter-Range-Instrumentation Group (IRIG) standards. One master clock generated all times. Signal distribution for event timing was routed to electronic and photo-optical instrumentation and recording locations.

The photo-optical data (such as from the on-board) cameras) which did not have each camera image marked in coded form was marked with pulses of known frequencies. Events recorded by these cameras were then correlated to the IRIG coded time by use of simultaneous recordings of a light flash from atop the synchronization light stand and an event mark on the oscillograph record.

5. DATA REDUCTION AND PRECISION

The estimated maximum uncertainties of all measured and derived data parameters are listed in Table 6. Discussion of the methods used for data reduction and uncertainty estimations are given below.

a. Time

According to Reference 1, all time bases and codes which meet IRIG standards were recorded with an accuracy of ±50 microseconds. Photo-optical data which was marked with pulses of known frequency (usually 1000 Hz) was estimated to have provided times which were accurate within 0.0005 sec. Times obtained from all photo-optical instrumentation were corrected for the offset of the location of the timing light generator from the event frame, where applicable.

b. Meteorological Data

The estimated maximum uncertainties of the meteorological readings of temperature, pressure, wind speed, wind direction, and relative humidity were taken as ±1 of the last significant figure reported for these readings by the Holloman Air Force Base weather station.

The air density is an indirect measurement which results from a calculation involving the direct measurements of temperature and barometric pressure and standard values for sea level temperature, pressure, and density. That is,

$$\rho = \rho_{SL} \left(\frac{T_{SL}}{P_{SL}}\right) \left(\frac{P}{T}\right) \qquad (1)$$

where:

ρ_{SL} = Standard air density at sea level, 0.002378 slug/cu ft

T_{SL} = Standard air temperature at sea level, 518.69°R

TABLE 6

PRECISION OF THE DATA

Data Parameter, Units	Typical Value	Estimated Maximum Uncertainty (+ and -)
TIME		
IRIG bases and codes, sec	36.54186	0.00005
From pulses of known frequency, sec	0.1779	0.0005
METEOROLOGICAL DATA		
Temperature, °F	67	1
Barometric pressure, in. Hg	25.635	0.001
Wind speed, knots	10	1
Wind direction, deg	210	1
Relative humidity, percent	35	1
Air density, slug/cu ft	0.002037	0.000004
SLED PERFORMANCE DATA		
Primary Velocity Measuring System		
Distance, ft	7536.75	0.20
Velocity, ft/sec	500.0	3.2
Velocity, ft/sec	1000.0	7.0
Velocity, ft/sec	1500.0	12.3
Velocity, ft/sec	2000.0	19.6
Velocity, ft/sec	2500.0	29.7
Acceleration, ft/sec^2	48.8	110-280
Backup Velocity Measuring System		
Distance, ft	7461.0	298
Velocity, ft/sec (percent)	2540.36	(2.44)
Acceleration, g's	4.8	3.5 - 8.7
Metric Optical Instrumentation System		
Distance, ft	3536.51	88
Velocity, ft/sec	500.0	4.7
Velocity, ft/sec	1000.0	11.2
Velocity, ft/sec	1500.0	21.6
Velocity, ft/sec	2000.0	38.1
Velocity, ft/sec	2500.0	62.8
Acceleration, g's	-4.6	6.4-14.7
RELATIVE WIND DATA		
Primary Velocity Measuring System		
True airspeed, ft/sec	500.0	3.4
True airspeed, ft/sec	1000.0	7.1
True airspeed, ft/sec	1500.0	12.3
True airspeed, ft/sec	2000.0	19.6
True airspeed, ft/sec	2500.0	29.7
Mach Number	0.500	0.003
Mach Number	1.000	0.007
Mach Number	1.500	0.012
Mach Number	2.000	0.024

TABLE 6 (Concluded)

PRECISION OF THE DATA

Data Parameter, Units	Typical Value	Estimated Maximum Uncertainty (+ and -)
RELATIVE WIND DATA (Concluded)		
Dynamic Pressure, psf	500.0	10.0
Dynamic Pressure, psf	1000.0	24.0
Dynamic Pressure, psf	3000.0	82.5
Dynamic Pressure, psf	5000.0	190.0
PARACHUTE PERFORMANCE DATA		
Event times, sec	0.456	0.002
Cone and bag separation distance, ft	20.2	0.5
Drag forces, lb	33,227	2500
Drag coefficient		
At a dynamic pressure of 1000 psf	0.163	0.127
At a dynamic pressure of 3000 psf	0.312	0.042
At a dynamic pressure of 5000 psf	0.350	0.025
Projected area, sq ft	8.34	0.35
Oscillation angles		
Stability angle, deg	1.3	0.48
Quadrant angle, deg	26	6.0

P_{SL} = Standard air pressure at sea level, 29.92 in.Hg

ρ = Air density at the Track, slug/cu ft

P = Air pressure at the Track, in. Hg

T = Air temperature at the Track, °R

The maximum uncertainty in air density at the Track was estimated using the method given by Beers (Reference 7) for the propagation of error for a function of any number of independently measured quantities. A maximum uncertainty in air density of ±0.000004 slug/cu ft was obtained using this method.

c. Sled Performance Data

Sled performance data of distance (from the starting point), velocity (speed along the track), and acceleration as functions of time were obtained using primary and backup velocity measuring systems and the metric optical instrumentation system.

(1) Primary Velocity Measuring System

Data reduction under this system began with values for the "raw" times when the sled passed the interrupters. Although the distance between adjacent interrupters was known with a standard error of 0.0005 ft, it was first assumed that interrupters were spaced an even number of feet (for example, 13 ft) apart and that no interrupter failed to produce a pulse. Raw velocity and raw acceleration values were calculated from the differences in the time values and the assumed interrupter distance. This raw data was then "smoothed" by first designating distances from the sled

---

(7) Beers, Yardley: Introduction to the Theory of Error, Addison-Wesley Publishing Company, Inc., Reading, Massachusetts, 1957.

starting point to each interrupter, rounded to the nearest 1/4 ft. The raw times were then "edited", which involved a process for eliminating irregularities that were due to either gaps in the regular sequence of interrupter pulses or to the presence of pulses which were additional to the regular sequence of interrupter pulses. The raw times were further corrected to correlate the computational zero pulse with the time of sled first motion and to account for energy transmission times. These corrected times were then smoothed. Smoothing techniques used during this program included a seven-point moving arc process and a minimum-maximum regression (similar to least squares) method. Smoothed velocity and acceleration values and values for the standard deviation of velocity error were computed from the corrected and smoothed times using these same smoothing techniques.

The largest relative standard deviation in velocity recorded for this program was 0.243 percent for a velocity of 1542 ft/sec. Assuming a normal distribution of the deviations about the mean value, and in accordance with Croxton (Reference 8), it was estimated that approximately 99.95 percent of all variations in velocity at that velocity will fall between ±3.5 times the standard deviation. That is, the maximum relative variation in sled velocity at 1542 ft/sec was estimated to be ±0.85 percent.

Estimation for the maximum variations in sled distance and in velocities other than 1542 ft/sec were made using the method suggested by Beers (Reference 7), the value for the maximum relative variation in velocity at 1542 ft/sec, and the known relationship among the quantities of time,

---

(8) Croxton, Frederick, E., Elementary Statistics with Applications in Medicine and the Biological Sciences. Dover Publications, Inc., New York, 1959.

distance, and velocity. The maximum relative variation in distance was estimated in this way as a constant value of ±0.61 percent. Based on the 13 ft interrupter intervals and adding the initial ±1/8 ft bias for interrupter distance designations from the starting point, a maximum variation of ±0.20 ft for distance was estimated. The maximum relative variations in velocity, R_v , (in percent) were estimated using the following equation.

$$R_v = 9.25 \times 10^{-8} \ V^2 + 0.61 \qquad (2)$$

Maximum variations in acceleration were estimated from the tabulated differences between raw and smoothed acceleration values and between successive smoothed acceleration values. Variations of up to ±280 ft/sec^2 were estimated for those acceleration values that occur during those portions of the run where the level of acceleration was changing rapidly and up to ±110 ft/sec^2 were estimated for those portions of the run which were under essentially constant acceleration.

(2) Backup Velocity Measuring System

Data reduction under this system started with the values for the raw times when the sled passed the sensors which were positioned 208 ft apart. Distances were designated from the sled starting point to each interrupter, rounded to the nearest 1 ft. The raw times were corrected, and were checked for missing pulses; however, no smoothing was done.

Accuracies for the velocity values were estimated from propagations of the primary velocity measuring system errors over 16 interrupter intervals of 13 ft each (to account for the 208 ft interval between sensors). That is, the maximum relative variation in sled velcoity was estimated to be ±2.44 percent. Because of these large

interrupter intervals, the errors in time were negligible compared to the errors in distances. Therefore, the relative variation in sled velocity was estimated as the constant value of ±2.44 percent for all velocity values.

Accuracies of the sled distance and acceleration values were estimated based upon comparison of the tabulated values obtained from the backup and primary velocity measuring systems, for those test runs where the data from both systems were available.

The standard deviation of distance differences was calculated and the maximum variation was taken as 3.5 times the standard deviation. The maximum uncertainty in sled distance, estimated in this manner, was determined to be ±298 ft. While the backup system generally missed the peak acceleration values which were picked up by the primary system, the backup acceleration accuracies were estimated to be on the same order as the primary acceleration accuracies. That is, the maximum relative variations in acceleration were estimated to be from ±3.5 g's for those portions of the run which were under essentially constant acceleration, to ±8.7 g's for those portions of the run where acceleration levels were changing rapidly.

(3) Metric Optical Instrumentation System

For this system, sled performance data was obtained from the reduction of the fixed, ribbon frame camera film. IRIG time and sled position data were referenced to the target grid painted on the sled. Sled position data were computed using a single station (camera) technique utilizing the known position and direction of the track as a constraint and the reference dimensions associated with the trackside target poles. Each value of sled distance, velocity, and acceleration was obtained by evaluating, at the midpoint, the first and second derivatives of a second degree polynomial fitted by least squares procedure to successive values.

Accuracies of the values of the sled performance data were estimated based upon comparisons of the tabulated values obtained from the metric optical instrumentation and primary velocity measuring systems, for those test runs where the data from both systems was reduced. Maximum differences, in all performance data, occurred for those portions of the test run where the sled was just entering or just leaving the field of view of one of the trackside cameras. The standard deviations of differences were calculated, the maximum variations were estimated as 3.5 times the standard deviations, and the errors were combined using the method outlined by Beers (Reference 7). The estimated maximum uncertainties in sled distance, velocity, and acceleration, determined in the above manner, are given in Table 6 and are applicable to the same data ranges as discussed for the primary velocity measuring system.

d. Relative Wind Data

The smoothed velocity data, obtained from the three velocity measuring systems, was combined with the meteorological data to derive indirect measurments of true airspeed, Mach number, and dynamic pressure. The maximum uncertainties in these parameters were estimated using the method given by Beers (Reference 7) for the propagation of errors for functions of any number of independently measured quantities. The values for the estimated uncertainties are given in Table 6 and relationships among the parameters and the direct measurements are given below.

(1) True Airspeed

True airspeed was computed as the absolute value of the vector difference of the velocities of the wind and the sled. That is,

$$V_{TAS} = V_S - V_W \cos \alpha \qquad (3)$$

where:

V_{TAS} = True airspeed, ft/sec

V_S = Velocity (speed) of the sled, ft/sec

V_W = Velocity (speed) of the wind, ft/sec

α = Angle between the headings of the sled and the wind, rad.

For all three velocity measuring systems, the errors in wind velocities were negligible compared to the errors in sled velocities, for sled velocities above 500 ft/sec.

(2) Mach Number

Mach number was computed using the equation:

$$M = V_{TAS} / (49.0192\ T^{1/2}) \qquad (4)$$

where:

M = Mach number

V_{TAS} = True airspeed, ft/sec

T = Air temperature at the Track, °R.

The errors in temperature provided only small contributions to the Mach number variations calculated for the primary velocity measuring system, and were negligible compared to the velocity errors for the other two velocity measuring systems.

(3) Dynamic Pressure

Dynamic pressure was computed using the equation:

$$Q = \frac{1}{2} \rho V_{TAS}^2 \qquad (5)$$

where:

Q = Dynamic pressure, psf
ρ = Air density at the Track, slug/cu ft
V_{TAS} = True airspeed, ft/sec

The errors in density proved to be negligible compared to the velocity errors for all three velocity measuring systems.

e. Parachute Performance Data

Parachute performance data of event times, cone and bag separation distances, and parachute drag forces, coefficient, projected area, and oscillation angles were obtained from the on-board and track-side motion picture coverage and from the tensiometer records.

(1) Event Times

Times for significant events were extracted from the motion picture coverage and the tensiometer record and were tabulated for each test run. The timing for the various instrumentation records was synchronized by identifying the initiation of deployment squib current and the flash of the bulb atop the synchronization light stand. These occurrences, and the fiducial on the oscillograph record, were assumed to be coincident and were set to "time equal to zero." All other event times were decoded and timed relative to this initiation of the deployment sequence.

The maximum variation in event times was estimated from the largest error associated with selecting a particular film frame for an event. This method gave an estimated maximum uncertainty in event times of ±0.002 sec.

(2) Cone and Bag Separation Distances

Deployment cone and parachute bag separation distances (from the sled attachment point to the leading edge of the cone or bag) were determined from the motion picture film provided by the trackside cameras. For each film, the sled was traced once, and the positions of the leading edges of the cone and bag were marked and measured from following frames with sufficient frequency to describe time-displacement curves. The times were decoded from the film and the distances were calculated by taking the ratio of the separation distance image, and the sled overall length image, and multiplying by the measured length of the sled.

The maximum uncertainties in separation distances, determined in this manner, were estimated to be ±0.5 ft.

(3) Drag Forces

Parachute drag force-time histories, recorded on direct print oscillograph records, were reduced by digitizing the trace displacements from the zero load levels and applying the conversion factors determined from the pre-test calibrations. The coincident loads for each test run were then averaged. The graphic presentations of the force-time histories, given in this report, were traced from one oscillogram trace for each test, however, the ordinate scales were established to reflect the average of both traces.

A "snatch" force was tabulated for each test, using as its value, the peak of a force spike that occurred at, or near, the event time of parachute suspension "line stretch." A "maximum force" was also tabulated; using as its value, the peak of a force spike that occurred at, or near, the event time of parachute "canopy first full open."

The accuracy of the drag forces was estimated based upon the average differences between the two drag traces and the accuracy with which the drag trace values could be read and digitized. This gave an estimated maximum uncertainty in drag forces, r_D, of ±2,500 lb. Errors due to the differences between the lines of action of the parachute forces and the directions of the relative winds were insignificant compared to the other errors and were neglected.

(4) Drag Coefficient

Parachute drag coefficient is a derived quantity that was computed using the equation:

$$C_{D_o} = D/ (Q\ S_o) \qquad (6)$$

where C_{D_o} = Parachute drag coefficient

D = Parachute drag force, lb

Q = Dynamic pressure, psf

S_o = Design nominal area of the parachute canopy, 19.635 ft^2.

The maximum variation in drag coefficient, $r_{C_{D_o}}$, was estimated based upon the propagation of errors in drag force and dynamic pressure. The errors in dynamic pressure did not influence drag coefficient errors for dynamic pressures below 3000 psf and only increased drag coefficient errors by less than 2 percent for dynamic pressures above 3000 psf. Therefore, the errors in dynamic pressure were neglected and the maximum uncertainties in drag coefficient were estimated from the following equation.

$$r_{C_{D_o}} = r_D/ (Q\ S_o) = 127/Q. \qquad (7)$$

(5) Projected Area

The parachute canopy projected area-time histories, which are presented in this report, were reduced from the film from one of the on-board cameras for each test. Tracings of the maximum projected area image were periodically taken, and the area measured with a planimeter. These planimeter areas were converted to actual areas by using known target board dimensions and correcting them for the difference in the distances from the camera to the target board and from the camera to the projected diameters as determined from the trackside camera coverage.

The accuracy of the projected areas was determined by combining estimations for the errors associated with the planimeter, the tracings, and the derivation of the conversion factors. This gave an estimated maximum uncertainty in projected area of ±0.35 sq ft.

(6) Oscillation Angles

Parachute stability angle, or oscillation angle, was taken as the angle between a ray constructed from the focal point of the lens of one of the on-board cameras to the center of the parachute vent and the optical axis of the camera. Parachute quadrant angle was taken as the counterclockwise angular displacement of the image of the center of the parachute vent from the positive axis of the on-board camera film plane (looking downstream, zero degrees displacement axis parallel to the earth and to the right). Conversion factors used in the calculations of both these angles were obtained from film images of the target board and known dimensions.

The maximum uncertainties in parachute stability angle and parachute quadrant angle were estimated to be ±0.48 deg and ±6.0 deg, respectively.

6. RUN SUMMARY

Twenty track sled test runs were made in support of this program. Table 7 presents a chronological summary of the test runs in terms of selected parameters of the test matrix.

Difficulties in obtaining satisfactory parachute deployments were experienced in the first three tests, and only one test, 6P-E3, provided usable data. The program was interrupted to establish a reliable deployment technique. Three test runs were made using the Tomahawk sled to investigate deployment system improvements. These were the 6P-F series of tests. The Tomahawk sled was used because it could accept the 2.2 KS 11,000 type rocket motors which were available at no cost to the program at that time. The parachutes which were used on the early 6P-E series of tests were used on the 6P-F series of runs; the riser line attachment loops were repaired after each test, which shortened the riser length by about 1 ft each time they were repaired.

After an acceptable parachute deployment technique was established, the test program continued to completion with only one test failure. On test 6P-H5, the parachute was simultaneously deployed and released.

The results from 14 of the 20 test runs were able to be used for comparative evaluations of nylon and Kevlar parachutes at high dynamic pressures.

TABLE 7

RUN SUMMARY

Test Pun	Test Pun Designation	Date	Sled	Parachute Designation	Parachute Material	Nominal Deployment Mach No.	Deployment Dynamic Pressure, PSF
1	6P-E2	7/14/67	Arrowhead	FDFPA-2	Nylon	*	*
2	6P-E3	9/15/67	Arrowhead	FDFPA-1	Nylon	1.5	2900
3	6P-E4	10/17/67	Arrowhead	FDFPA-4-1	Nylon	*	*
4	6P-F-1	2/2/68	Tomahawk	FDFPA-4-1	Nylon	1.3	2100
5	6P-F2	2/14/68	Tomahawk	FDFPA-2	Nylon	1.3	2100
6	6P-F3	4/11/69	Tomahawk	FDFPA-2	Nylon	1.3	2100
7	6P-E6	9/18/69	Arrowhead	FDFPA-2	Nylon	1.5	2900
8	6P-G1	7/17/70	Arrowhead	FDFPA-3-2	Nylon	1.8	4000
9	6P-G2	10/9/70	Arrowhead	FDFPA-4-2	Nylon	1.8	4000
10	6P-G3	1/5/73	Arrowhead	FEPP-1-1	Nylon	1.8	4000
11	6P-H1	10/10/73	Arrowhead	FEPR-1-2	Nylon	2.2	6500
12	6P-H2	5/24/74	Arrowhead	FEPP-1-3-1	Nylon	2.2	6500
13	6P-H3	5/16/75	Arrowhead	FERP-1-3-2	Nylon	2.2	6500
14	6P-E9	6/13/75	Arrowhead	FERA-1-K	Kevlar	1.5	2900
15	6P-E10	5/27/75	Arrowhead	FERA-2-K	Kevlar	1.5	2900
16	6P-G4	3/26/76	Arrowhead	FERA-3-K	Kevlar	1.8	4000
17	6P-G5	4/9/76	Arrowhead	FERP-1-1-K1	Kevlar	1.8	4000
18	6P-H5	7/7/76	Arrowhead	FERP-1-2-K	Kevlar	*	*
19	6P-H6	7/30/76	Arrowhead	FERP-1-3-K	Kevlar	2.2	6500
20	6P-H7	10/15/76	Arrowhead	FERP-1-4-K	Kelvar	2.2	6500

* Deployment Malfunction (no test data).

- Shortened Riser Lines.

SECTION III
RESULTS AND DISCUSSION

1. SLED TEST RUN RESULTS

a. Deployment Problems on Early Tests

Parachute deployment problems occurred on the first three sled test runs conducted under this program. On the first test, 6P-E2, parachute deployment was initiated where programmed but cone deployment did not occur until 13 sec later. It was suspected that a delayed action blasting cap was inadvertently used in the deployment cone gun. On the second test, 6P-E3, cone deployment occurred where programmed; however, the cone collided with the parachute riser line tie-down trough and with the sled rocket motors. The parachute bag appeared to hesitate on coming out of its container indicating that the force transmitted by the deployment cone may have been marginal. The parachute riser lines exited the bag before they reached line stretch. On the third test, 6P-E4, the deployment cone blasting cap fired where programmed but the shear pin in the mortar body of the deployment cone gun failed to shear. Therefore, no deployment system components were deployed.

b. Deployment Method Selection Runs; $M_\infty = 1.3$

Three sled test runs were conducted using the Tomahawk sled to establish a reliable method for accomplishing parachute deployment; tests 6P-F1, 6P-F2, and 6P-F3. All parachute storage, attachment, deployment, release,and instrumentation components, except the tensiometer, were removed from the Arrowhead sled and mounted on the Tomahawk sled for these tests. Therefore, no parachute drag force data was obtained. Typical sled performance and relative wind curves for these tests are presented in Figure 11.

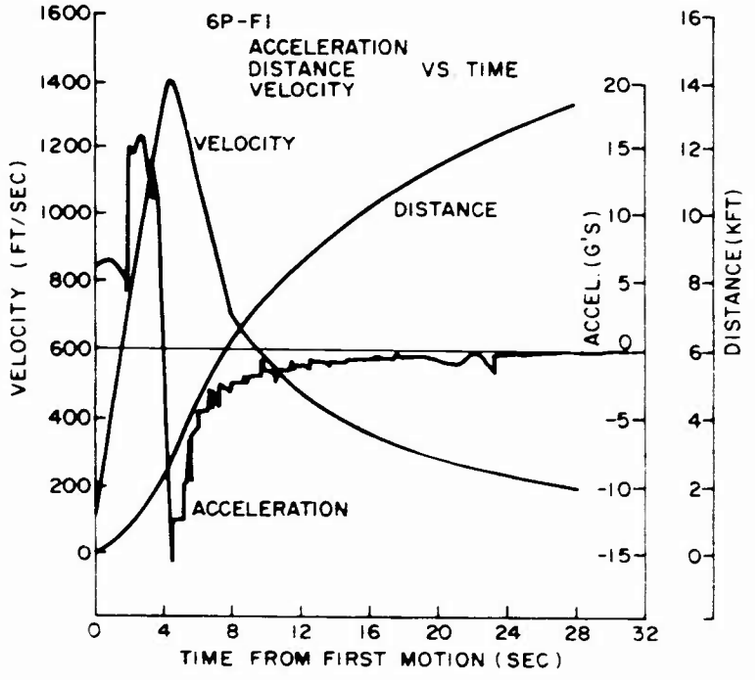

a. SLED PERFORMANCE DATA

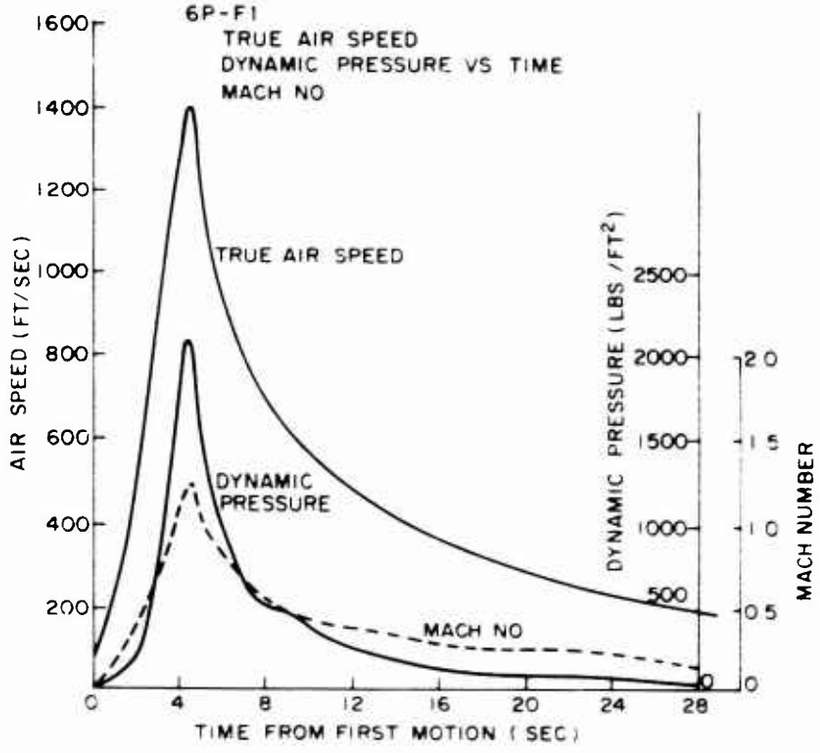

b. RELATIVE WIND DATA

Figure 11. Typical Sled Performance and Relative Wind Curves for the Mach 1.3 Test Runs.

(1) Test 6P-F1

The first deployment system checkout test, 6P-F1, incorporated those deployment system changes which were proposed to correct the problems experienced on the first three sled tests. Pressure relief ports were placed in the side of the parachute container to facilitate the ease with which the parachute could be extracted. A cover was placed over the parachute attachment/deployment/release mechanism and the deployment cone to protect them from wind blast. Two blasting caps were used in the deployment cone drogue gun and the mortar chamber was redesigned to improve cone deployment. An 18 inch diameter Hyperflo pilot chute was incorporated into the deployment system to provide additional extraction force to the test parachute.

All deployment components functioned satisfactorily except for the deployment control break ties which were holding the test parachute lines in the bag. As Figure 12 shows, all the lines and the canopy exited the bag after the bag had separated from the sled a distance of only about 5 ft. This means that the ties were of insufficient number and/or strength.

Figure 13 presents the parachute performance curves for this test. Values for parachute canopy projected area during the inflation phase could not be presented because inflation began before the canopy was in the field of view of the on-board cameras. Also, it was not possible to construct a precise variable area conversion factor for this portion of the run due to lack of accurate time-distance data from the track-side cameras. For this reason, projected area data prior to 0.376 sec was considered unreliable.

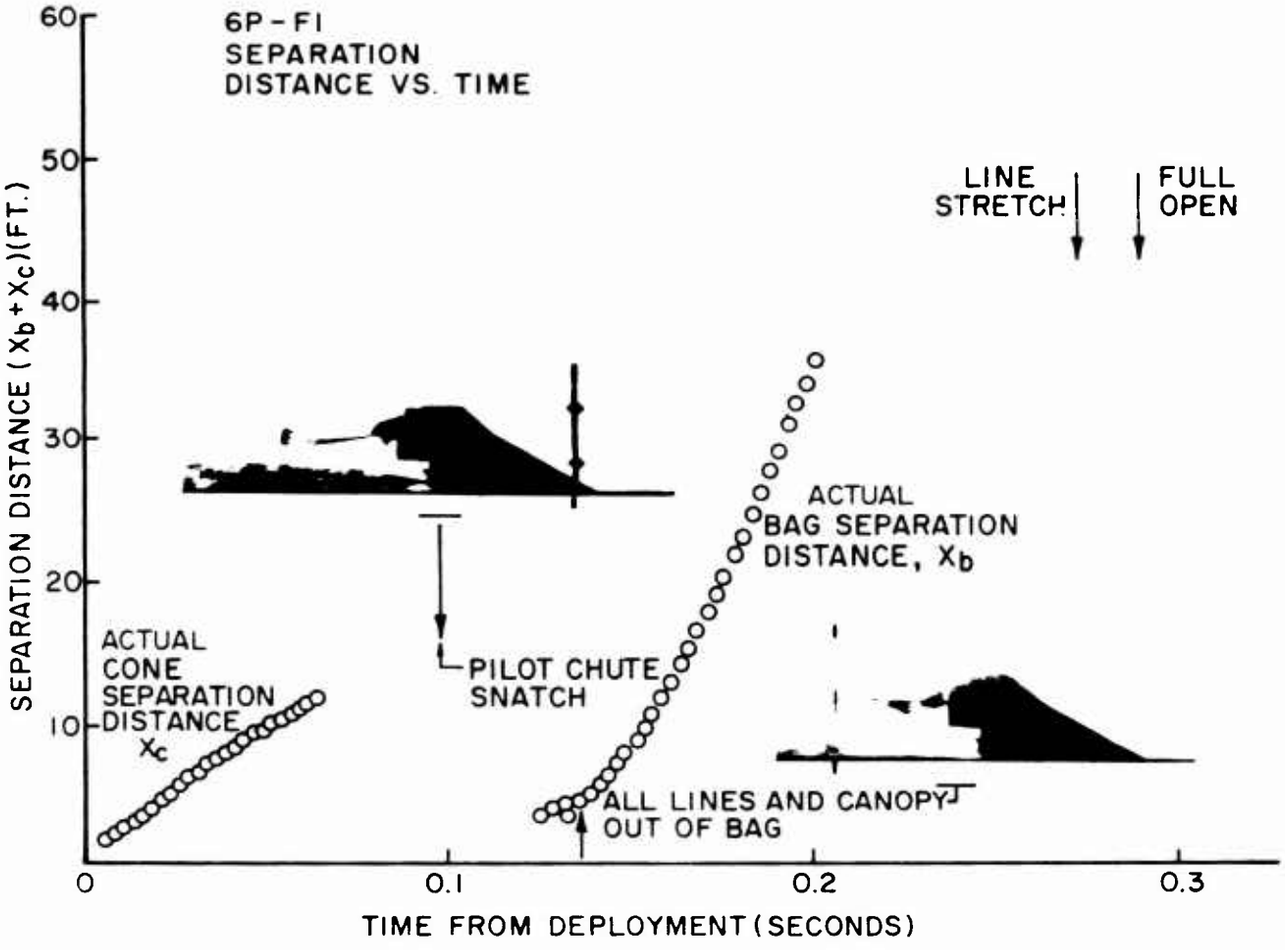

Figure 12. Trajectories of Deployment System Components - Test 6P-F1.

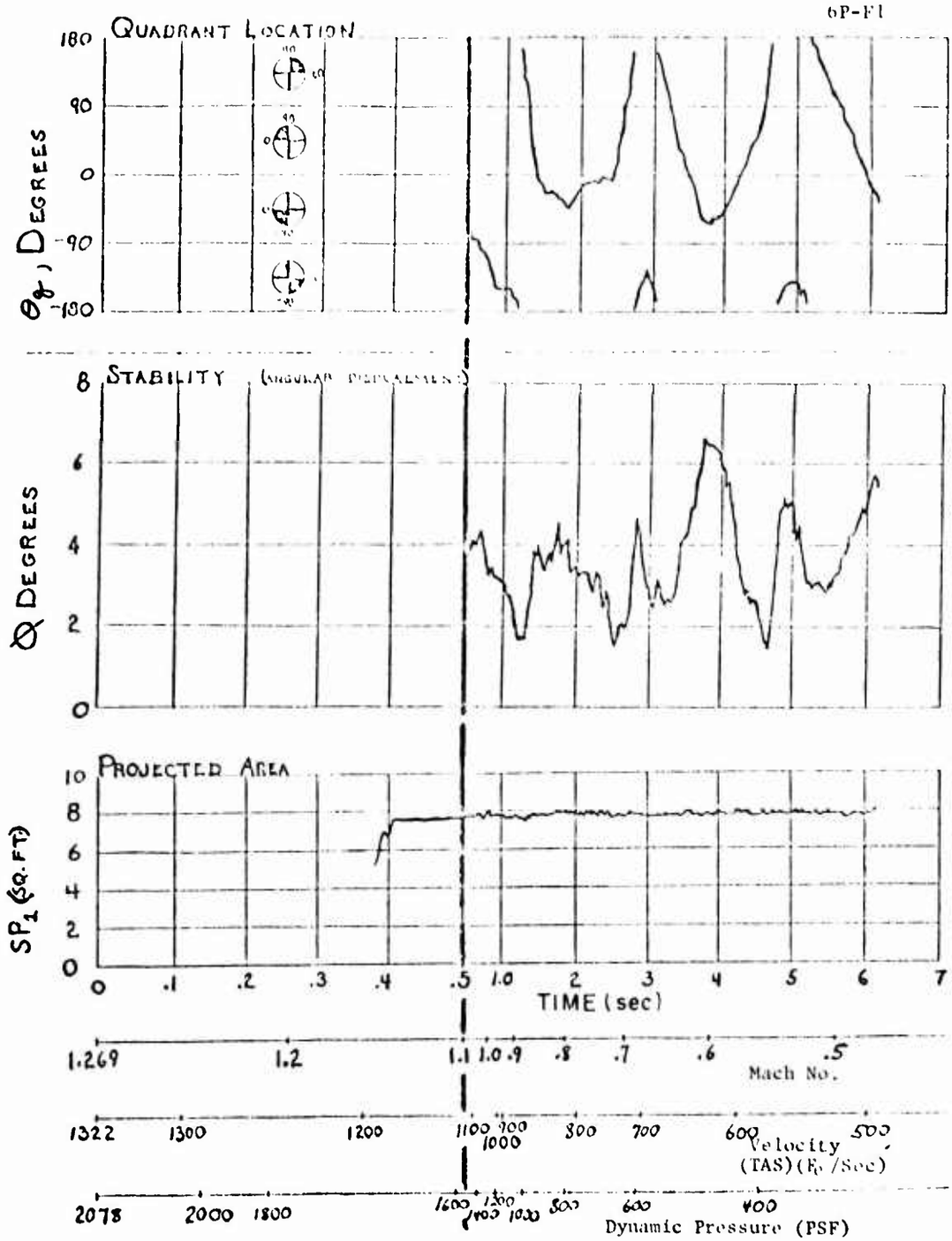

Figure 13. Parachute Performance Curves - Test 6P-F1.

The parachute riser lines were not completely severed and the parachute was not released. This caused the parachute to be dragged along the track late in the run, severely damaging the canopy. The on-board camera coverage showed no evidence of parachute damage prior to its contact with the track.

(2) Test 6P-F2

The second deployment system checkout test, 6P-F2, incorporated an increase in the force of the charge used to sever the parachute riser lines and an increase in the number of parachute deployment control break ties.

All deployment and release systems components functioned satisfactorily except for the break ties. As Figure 14 shows, they were still of insufficient number and/or strength to keep the parachute in the bag until line stretch.

Figure 15 presents the parachute performance curve for this test. No stability data was reduced because the on-board camera film lacked fiducials. The parachute was undamaged.

(3) Test 6P-F3

The third and final deployment system checkout test, 6P-F3, incorporated all the deployment system design features used on all subsequent tests as described in Appendix C. The final change involved the use of the deployment control break ties designed utilizing the calculation method described in Appendix C.

All deployment system components functioned satisfactorily, including the deployment control break ties, as shown by the parachute bag trajectory in Figure 16. Also included in the Figure are the predicted trajectories of the bag as output from the break tie computer program. The actual bag trajectory is closer to the trajectory predicted

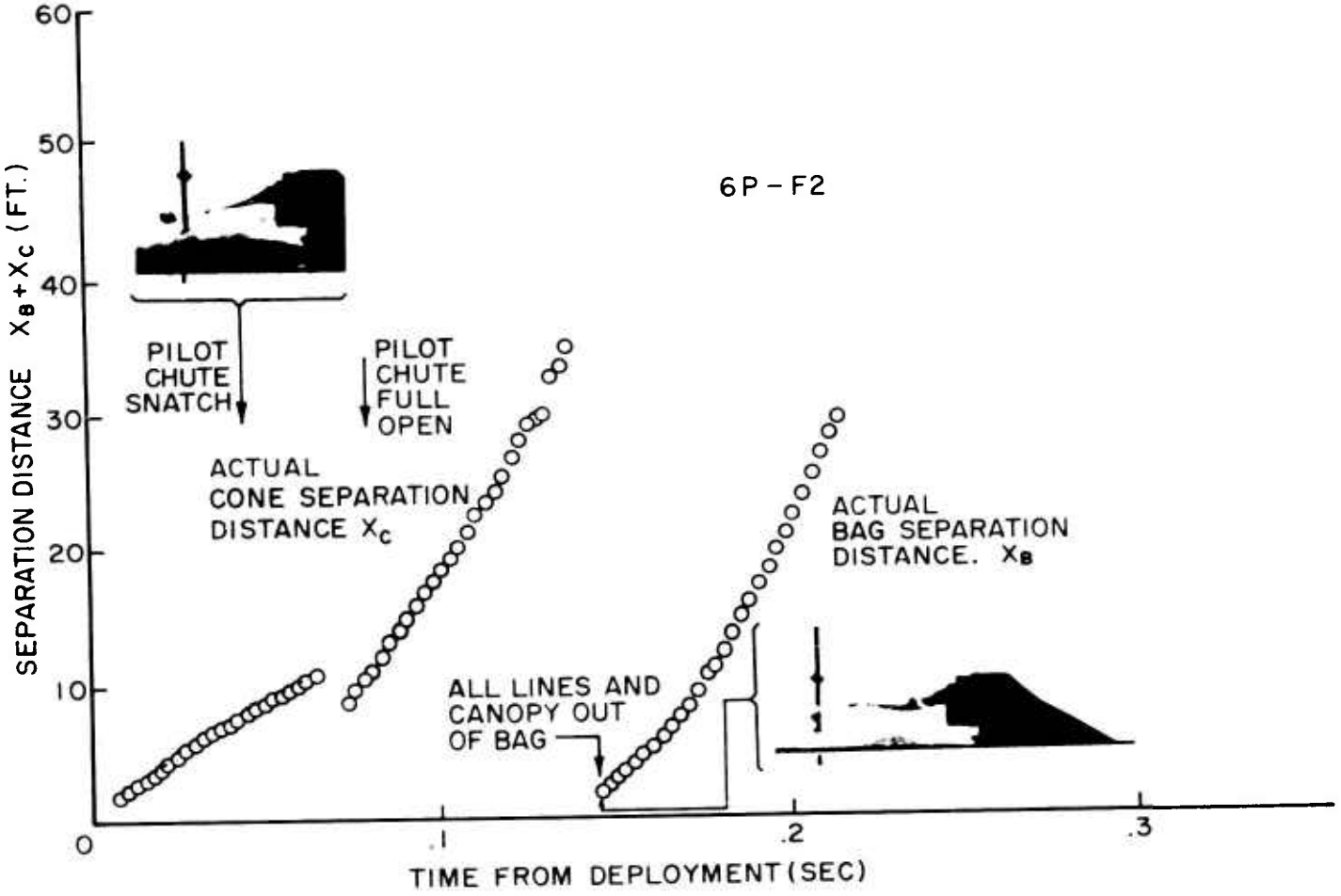

Figure 14. Trajectories of Deployment System Components - Test 6P-F2.

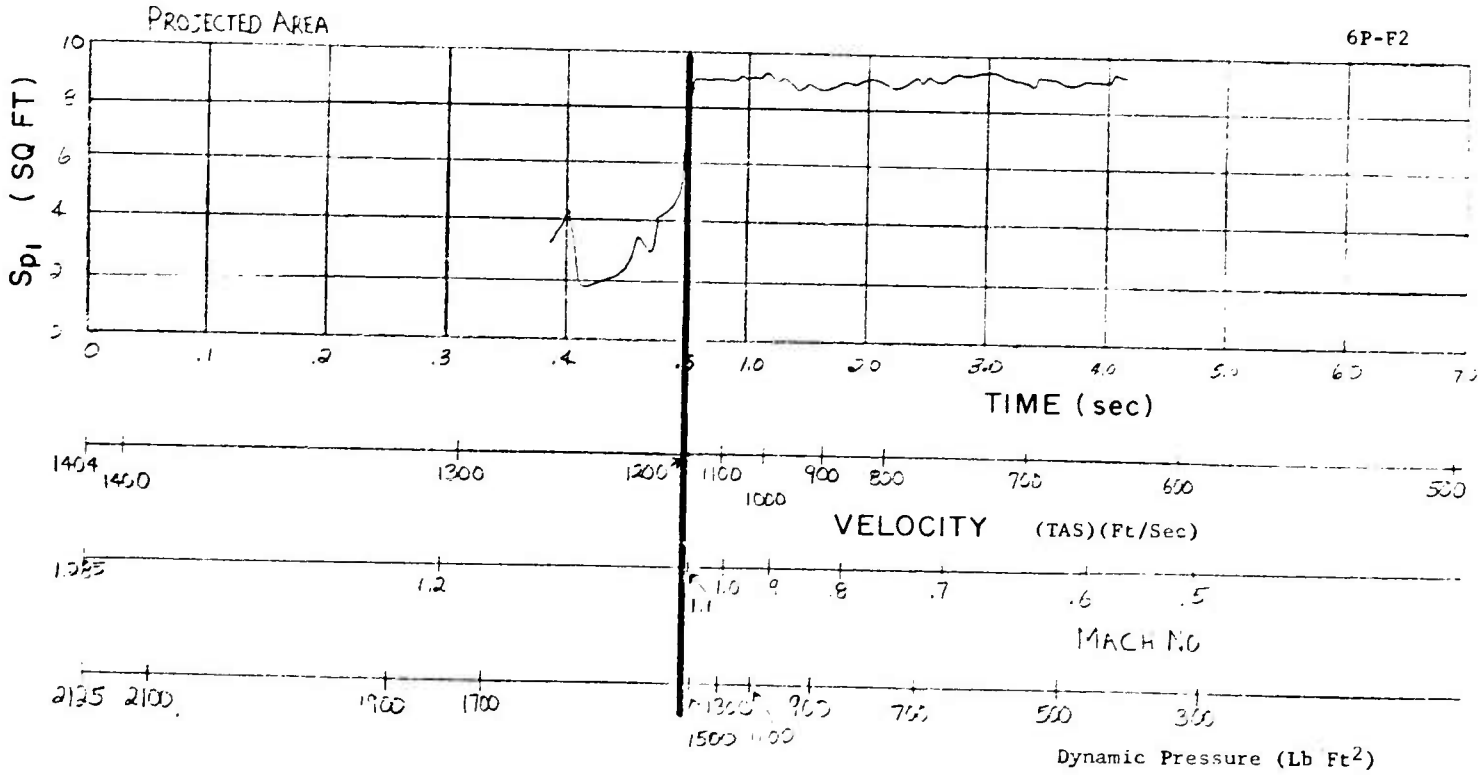

Figure 15. Parachute Performance Curve - Test 6P-F2.

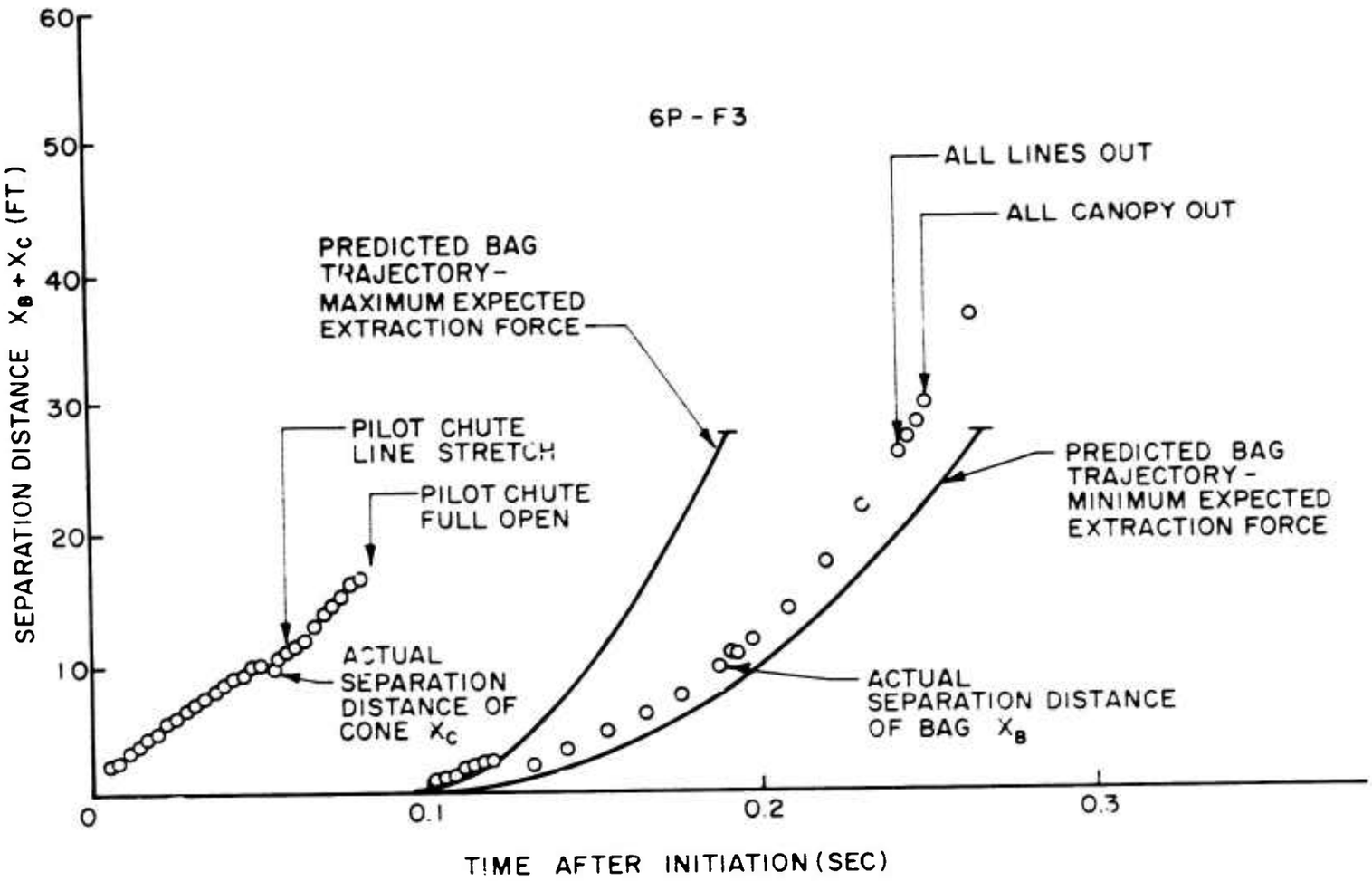

Figure 16. Trajectories of Deployment System Components - Test 6P-F3.

using minimum expected extraction force. This means that there are large dynamic pressure defects in the wake of the sled and/or the lower drag coefficient estimates used in the computer program are more realistic than the higher ones.

Figure 17 presents the parachute performance curves for this test. The parachute appeared fully inflated at 0.399 sec, but this occurred on a rebound after line stretch and the parachute did not attain the average steady state area until 0.740 sec. The parachute was not released from the sled because the electrical arming device on the screenbox which fires the squib and linear shaped charge to sever the riser lines did not operate. The parachute was recovered undamaged, however.

c. Runs at Mach 1.5; Q = 2900 psf

Four sled test runs were made which provided data for the comparative evaluation of nylon and Kevlar hemisflo parachutes at Mach 1.5 and at a dynamic pressure of approximately 2900 psf; tests 6P-E3 and 6P-E6, for nylon, and tests 6P-E9 and 6P-E10 for Kevlar. Typical sled performance and relative wind curves for these tests are presented in Figure 18.

(1) Test 6P-E3; Nylon Parachute

This was one of the early tests which experienced deployment problems as discussed above. However, parachute inflation from line stretch to full-open appeared normal.

Cone and bag separation distance trajectories could not be obtained because sufficient timing and coverage were not provided by the trackside cameras.

Figure 19 presents the parachute performance curves for this test. As the test parachute achieved a full-open condition and generated approximately 31,000 lb of force,

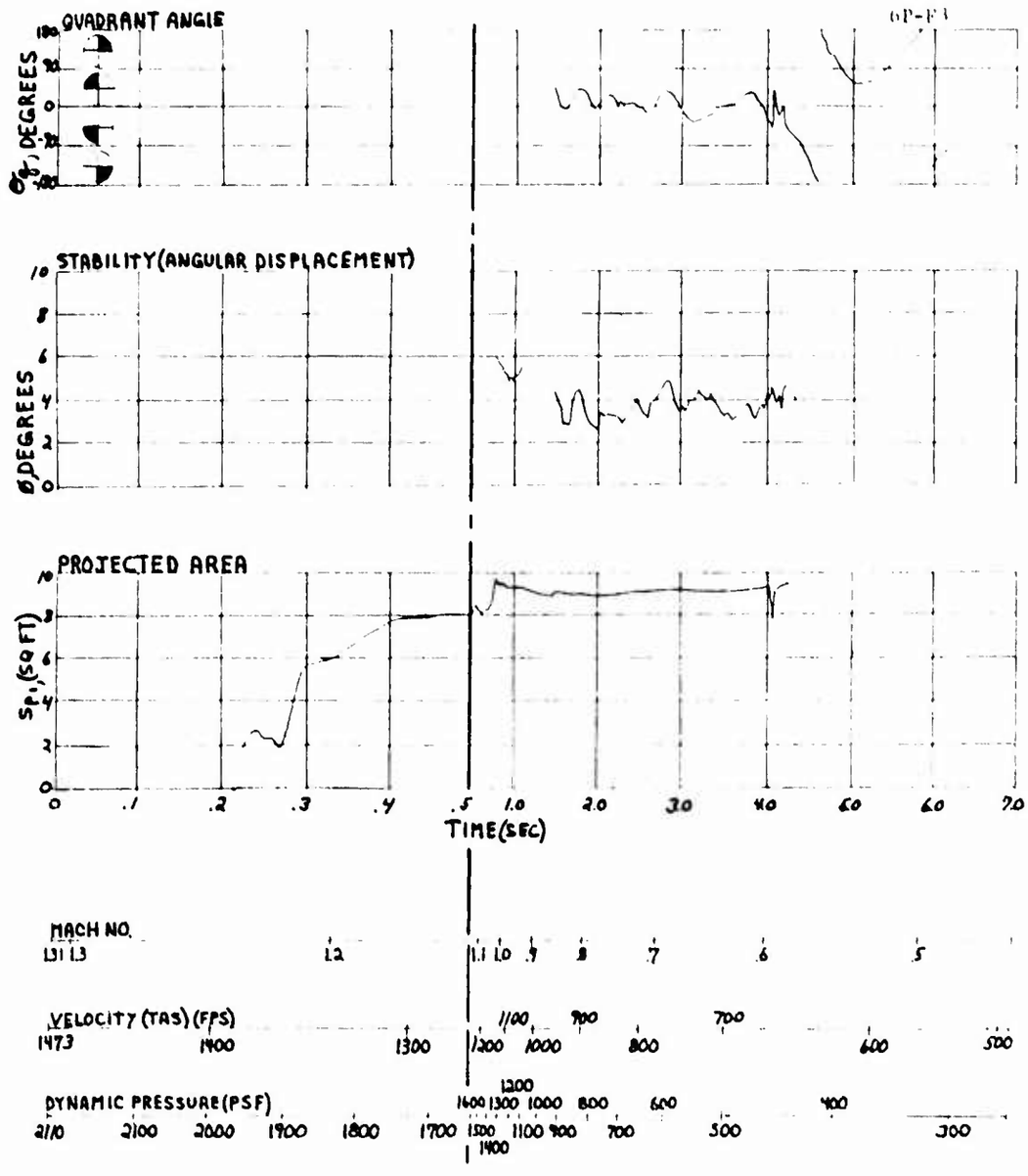

Figure 17. Parachute Performance Curves-Test 6P-F3.

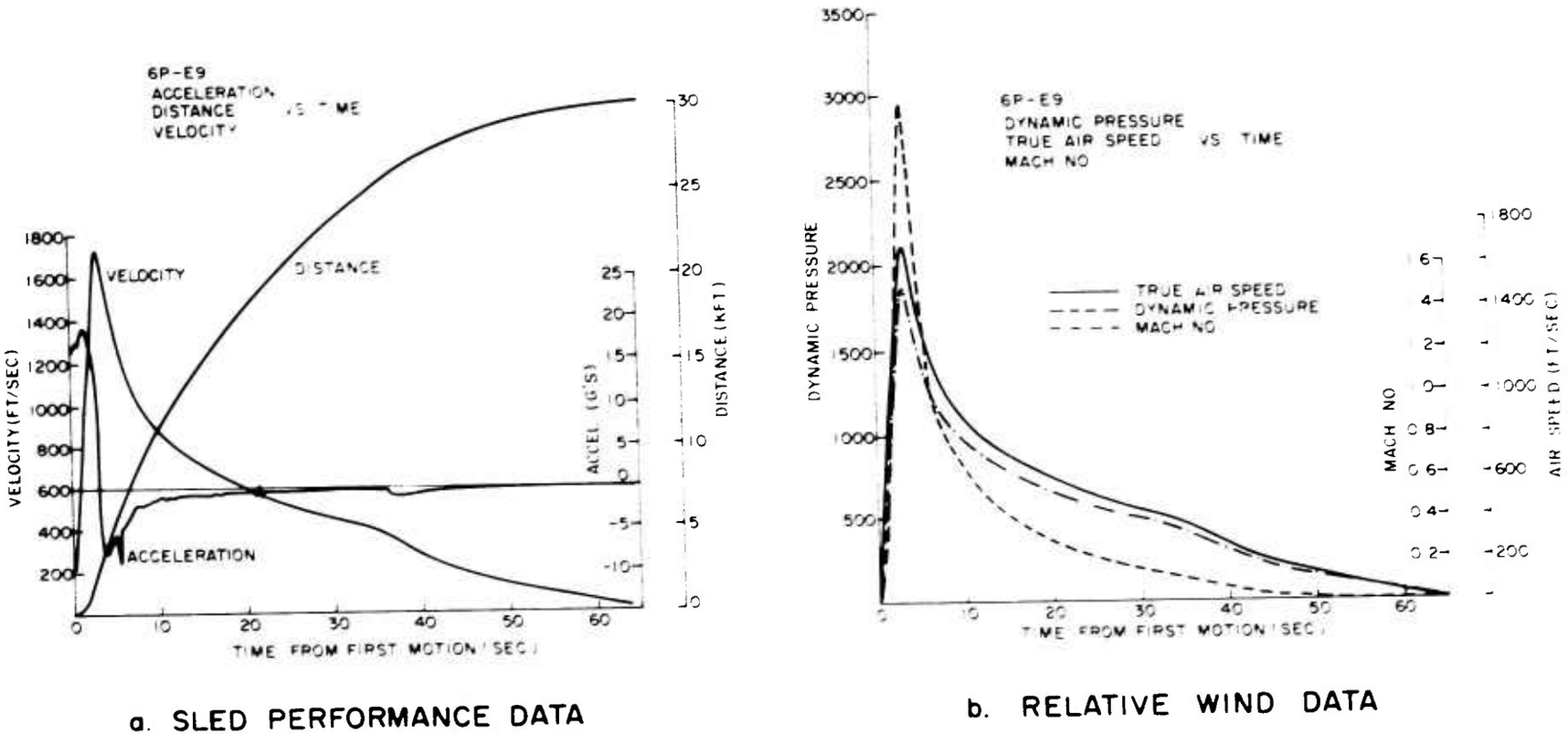

a. SLED PERFORMANCE DATA

b. RELATIVE WIND DATA

Figure 18. Typical Sled Performance and Relative Wind Curves for the Mach 1.5 Test Runs.

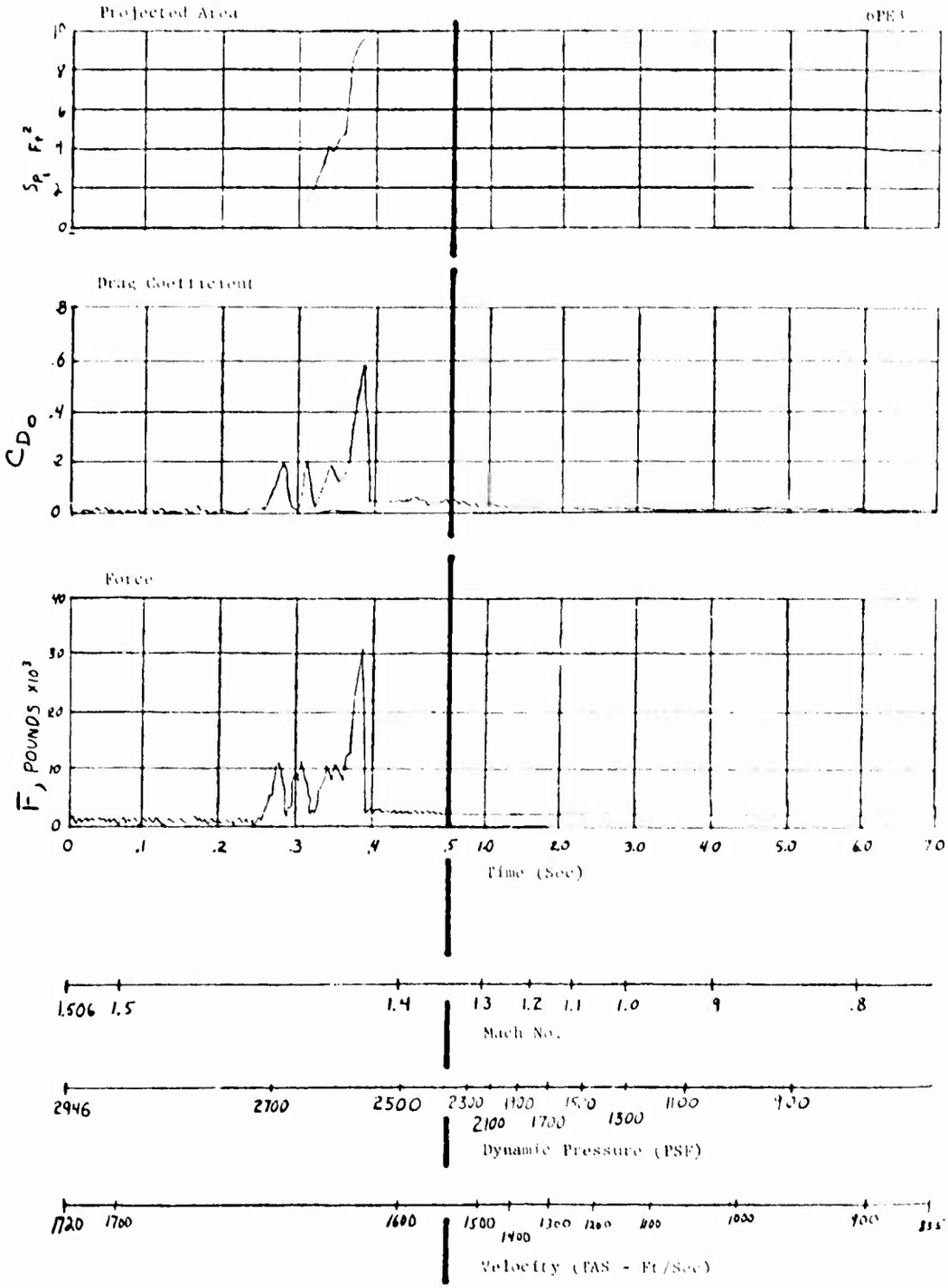

Figure 19. Parachute Performance Curves -Test 6P-E3.

almost simultaneously, two gores split from skirt to vent (including the skirt band but not the vent band) and eleven of the twelve suspension lines broke between the confluence keeper and the canopy skirt. Figure 20 shows the condition of the parachute after the test.

(2) Test 6P-E6; Nylon Parachute

Figure 21 and 22 present the trajectories for the deployment system components and the parachute performance curves, respectively, for this test. All systems performed satisfactorily and the parachute was recovered undamaged; see the photograph in Figure 23.

(3) Test 6P-E9; Kevlar Parachute

As Figure 24 helps to show, all deployment system components functioned satisfactorily. The parachute achieved line stretch at approximately 0.25 sec after deployment initiation and began to inflate shortly thereafter.

Figure 25 presents the parachute performance curves for this test. As the parachute began to inflate, the stitching failed between the vertical ribbons and the skirt band. As parachute inflation continued, the vertical ribbon stitching failure progressed up the canopy gore toward the vent. After the vertical ribbons separated from about five rows of horizontal ribbons, parachute inflation leveled off. As the stitching failure progressed further, the parachute collapsed. Figure 26 shows the condition of the parachute after the test.

(4) Test 6P-E10; Kevlar Parachute

All deployment system components functioned satisfactorily. Figure 27 presents their trajectories.

Figure 20. Post Test Photograph of the Test Parachute - Test 6P-E3.

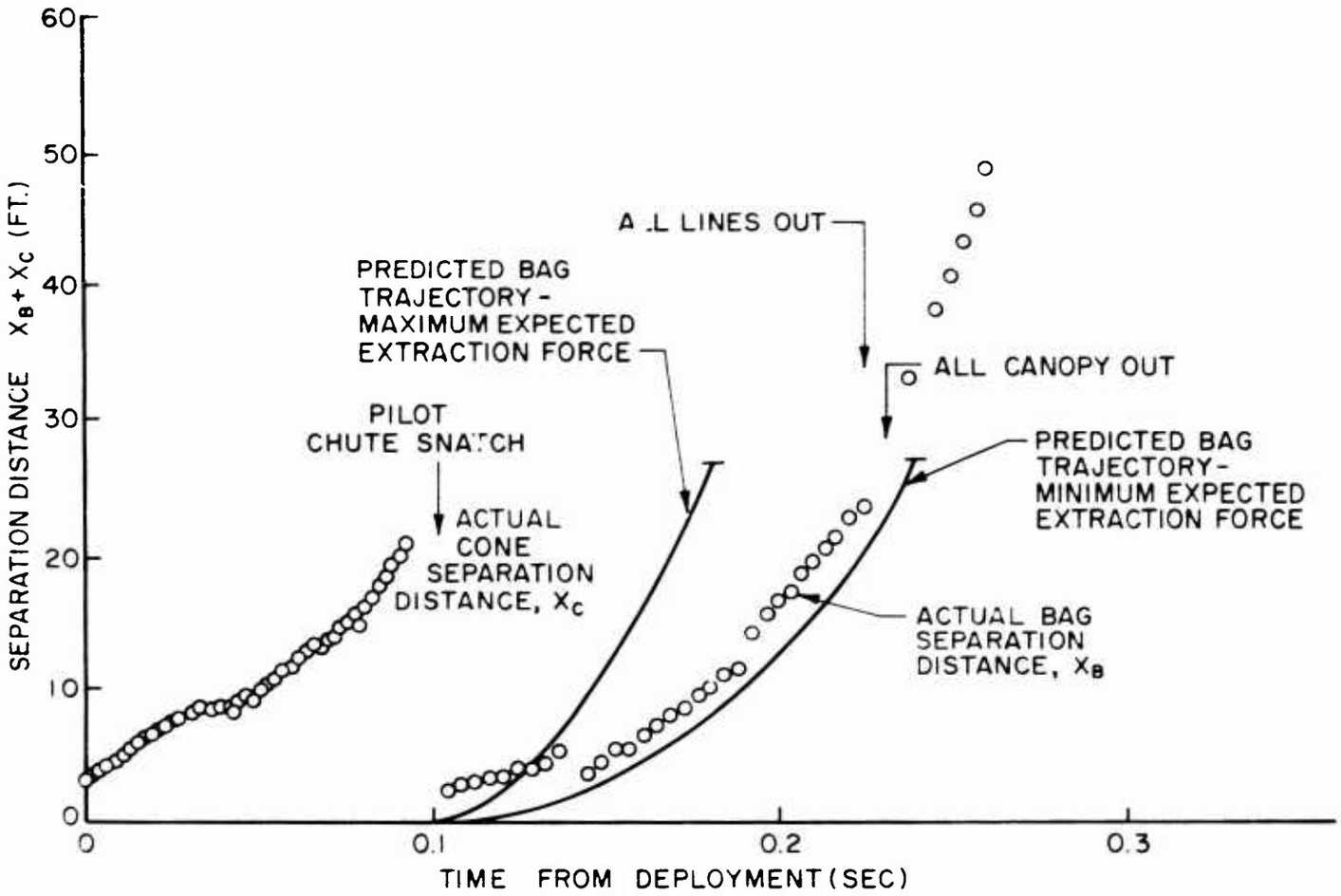

Figure 21. Trajectories of Deployment System Components - Test 6P-E6.

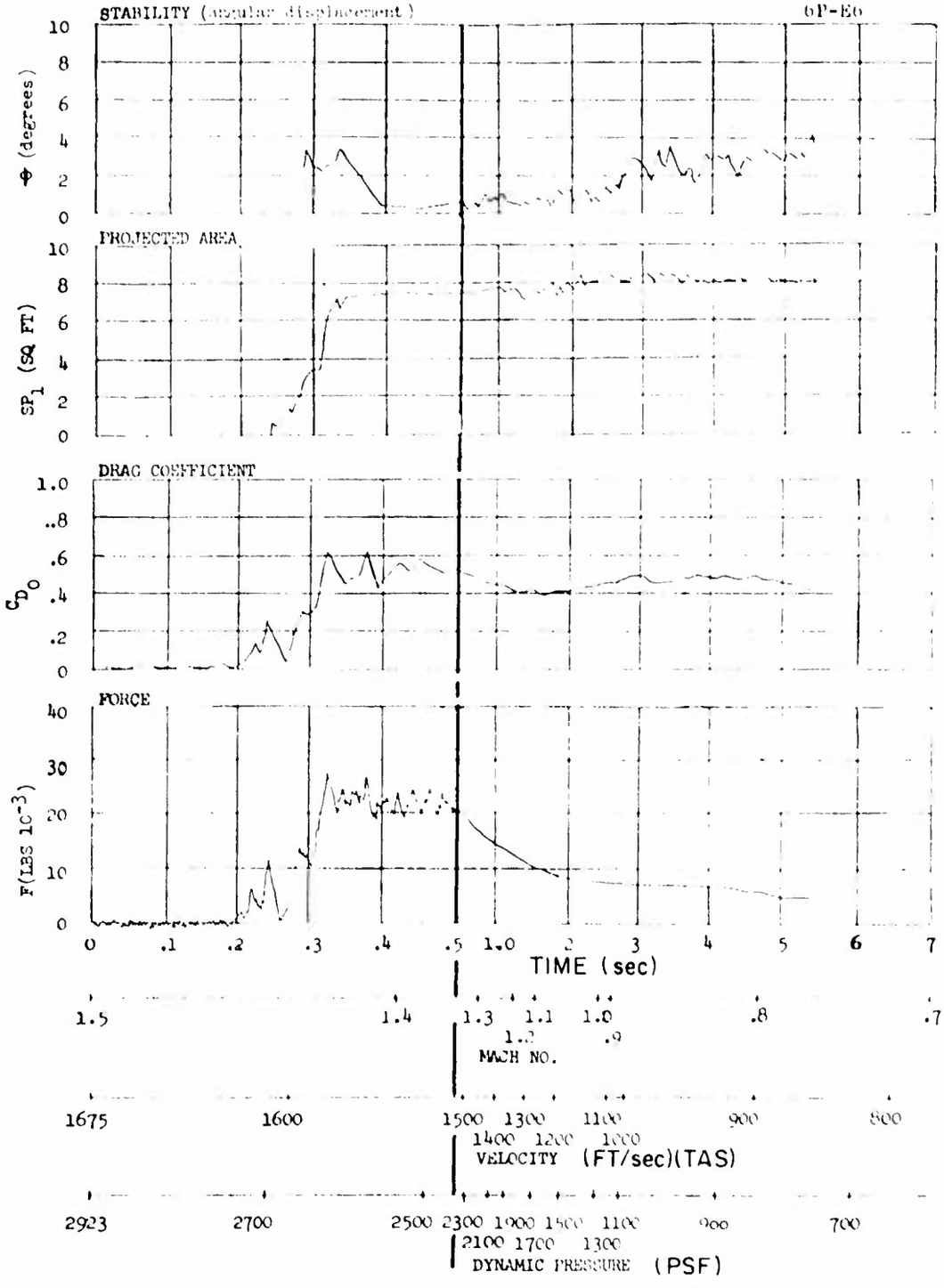

Figure 22. Parachute Performance Curves - Test 6P-E6.

Figure 23. Post Test Photograph of the Test Parachute - Test 6P-E6.

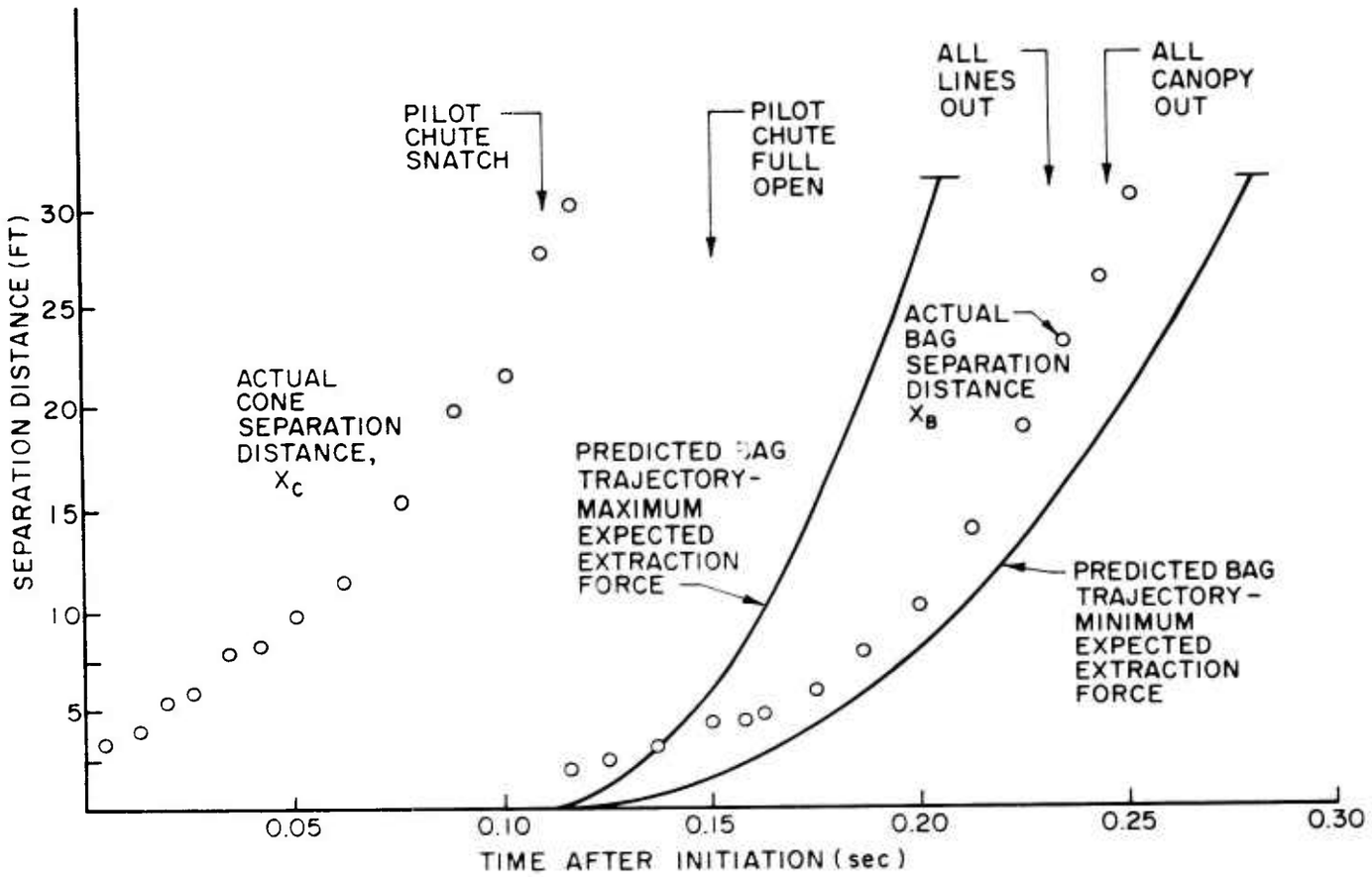

Figure 24. Trajectories of Deployment System Components - Test 6P-E9.

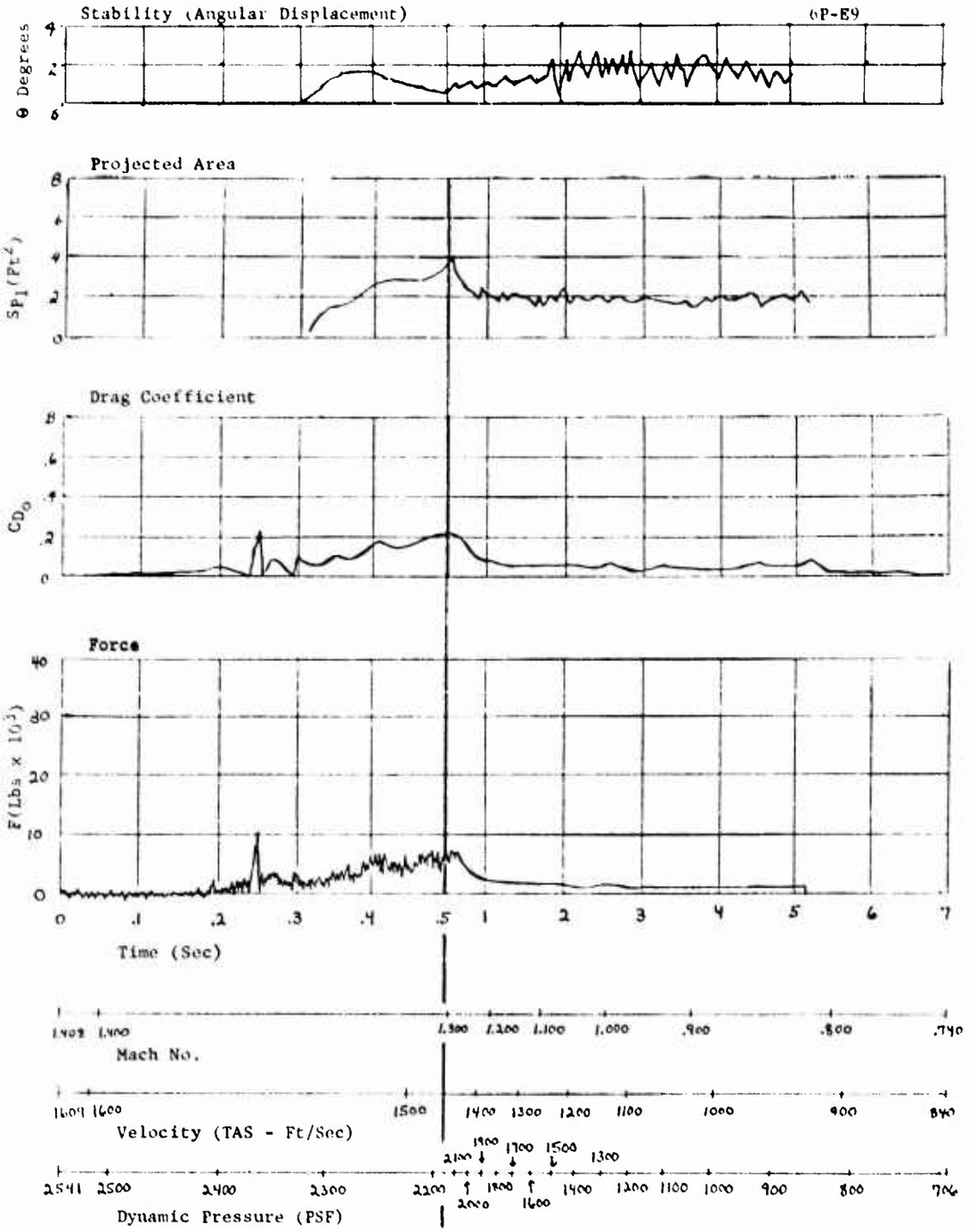

Figure 25. Parachute Performance Curves - Test 6P-E9.

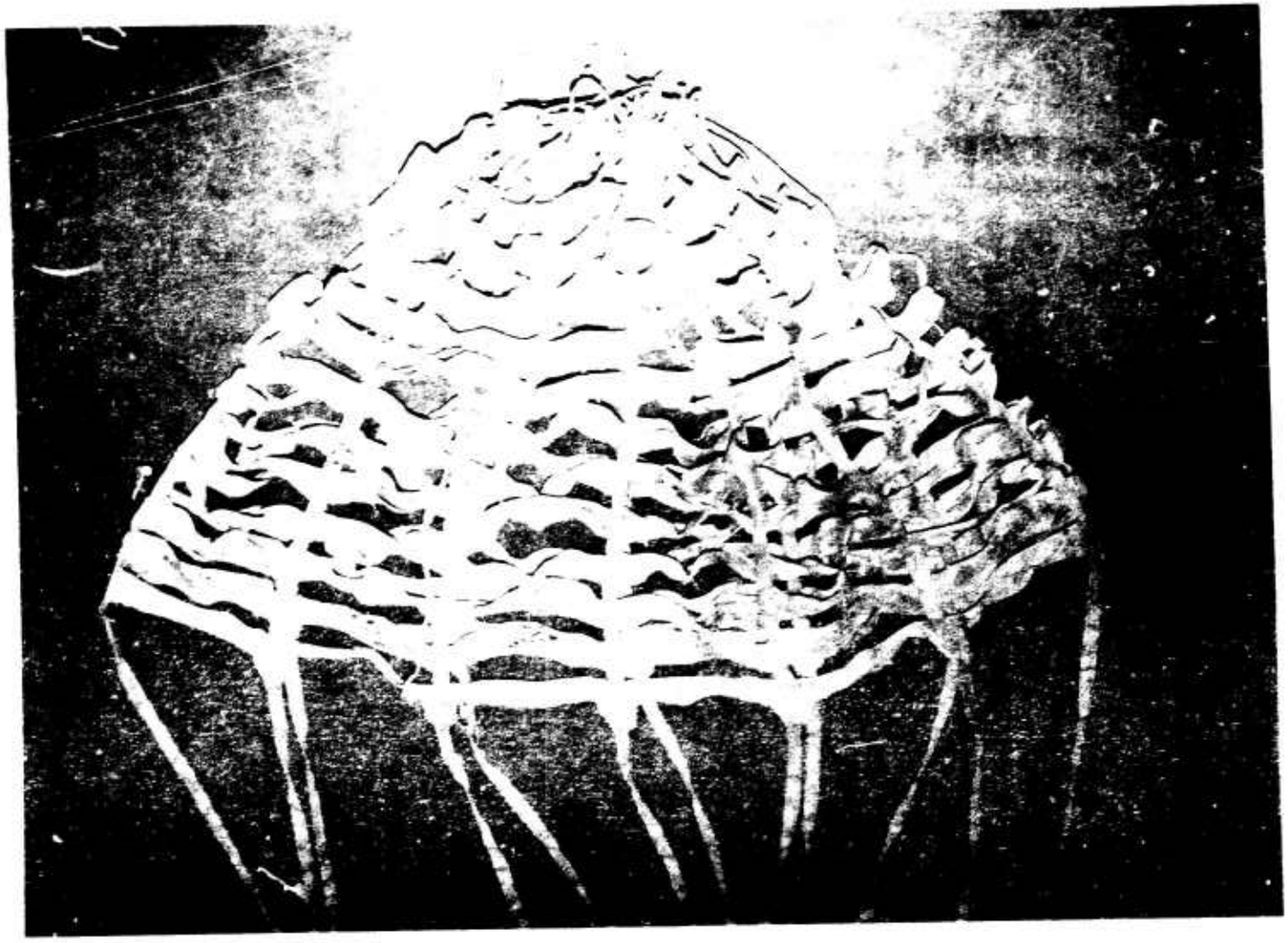

Figure 26. Post Test Photograph of the Test Parachute - Test 6P-E9.

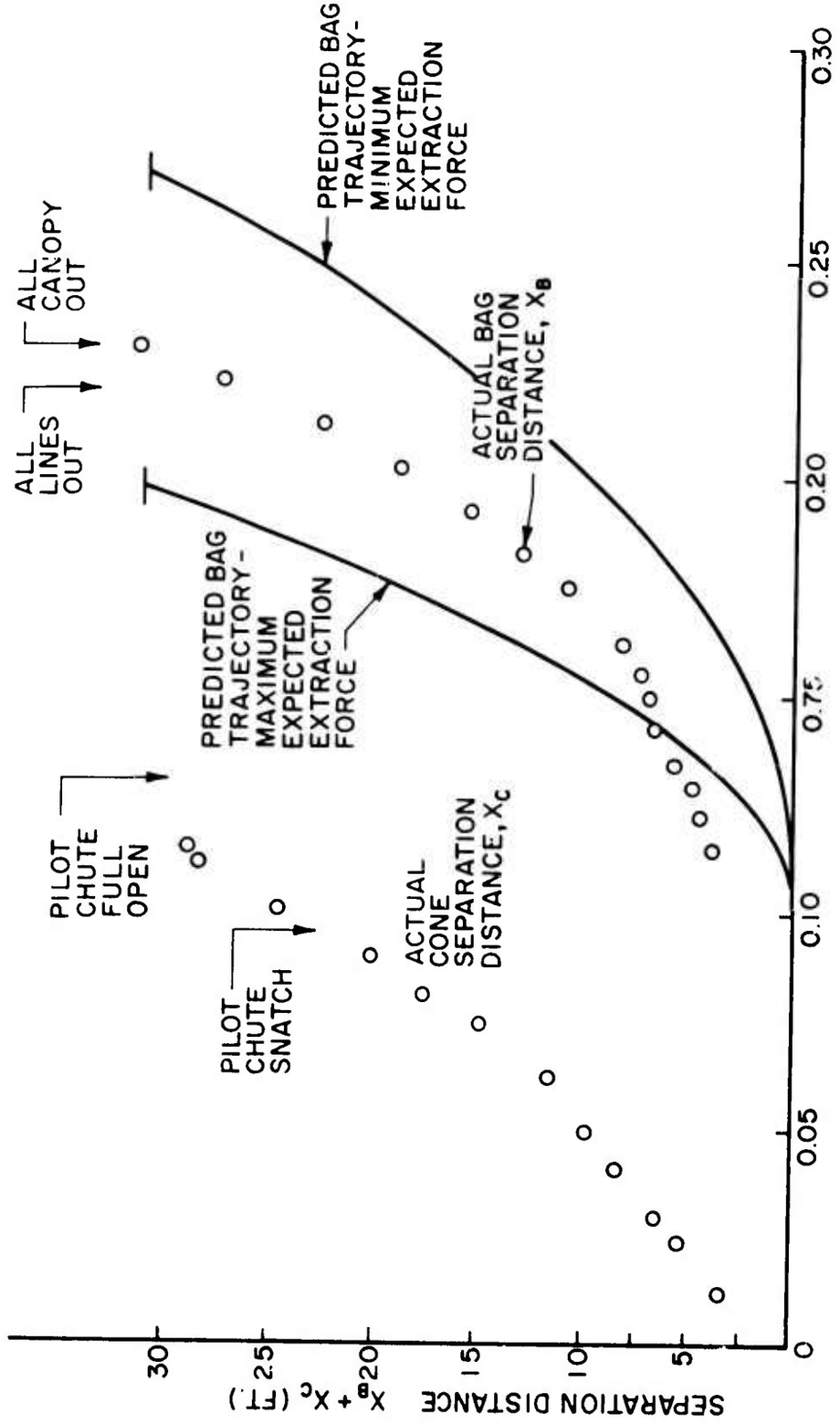

Figure 27. Trajectories of Deployment System Components - Test 6P-E10.

The parachute performance curves for this test are presented in Figure 28. Parachute inflation was normal and the parachute reached full-open at approximately 0.4 sec after deployment initiation. The parachute remained fully inflated with no visible damage for about 0.1 sec, then the stitching started to fail between the vertical ribbons and the skirt band. Progressive stitching failure occurred in the same manner as on test 6P-E9 and the parachute eventually collapsed. Figure 29 shows the condition of the parachute after the test.

d. Runs at Mach 1.8; Q = 4000 psf

Five sled runs were made which provided data for the comparative evaluation of nylon and Kevlar hemisflo parachutes at Mach 1.8 and at a dynamic pressure of approximately 4000 psf; tests 6P-G1, 6P-G2, and 6P-G3 for nylon, and tests 6P-G4 and 6P-G5 for Kevlar. Typical sled performance and relative wind curves for these tests are presented in Figure 30.

(1) Test 6P-G1; Nylon Parachute

All deployment system components functioned satisfactorily, Figure 31 presents their trajectories.

Figure 32 presents the parachute performance curves for this test. Parachute inflation was normal and a peak force of 38,650 lb was produced near the time that the canopy first achieved a full-open condition. The canopy remained fully inflated and produced drag forces in excess of 30,000 lb for about 0.1 sec. Then, the skirt band broke in two places, ten of the twelve suspension lines broke near the skirt, and one gore split from the skirt to the vent band. Figure 33 shows the failure sequence and Figure 34 shows the condition of the parachute after the test.

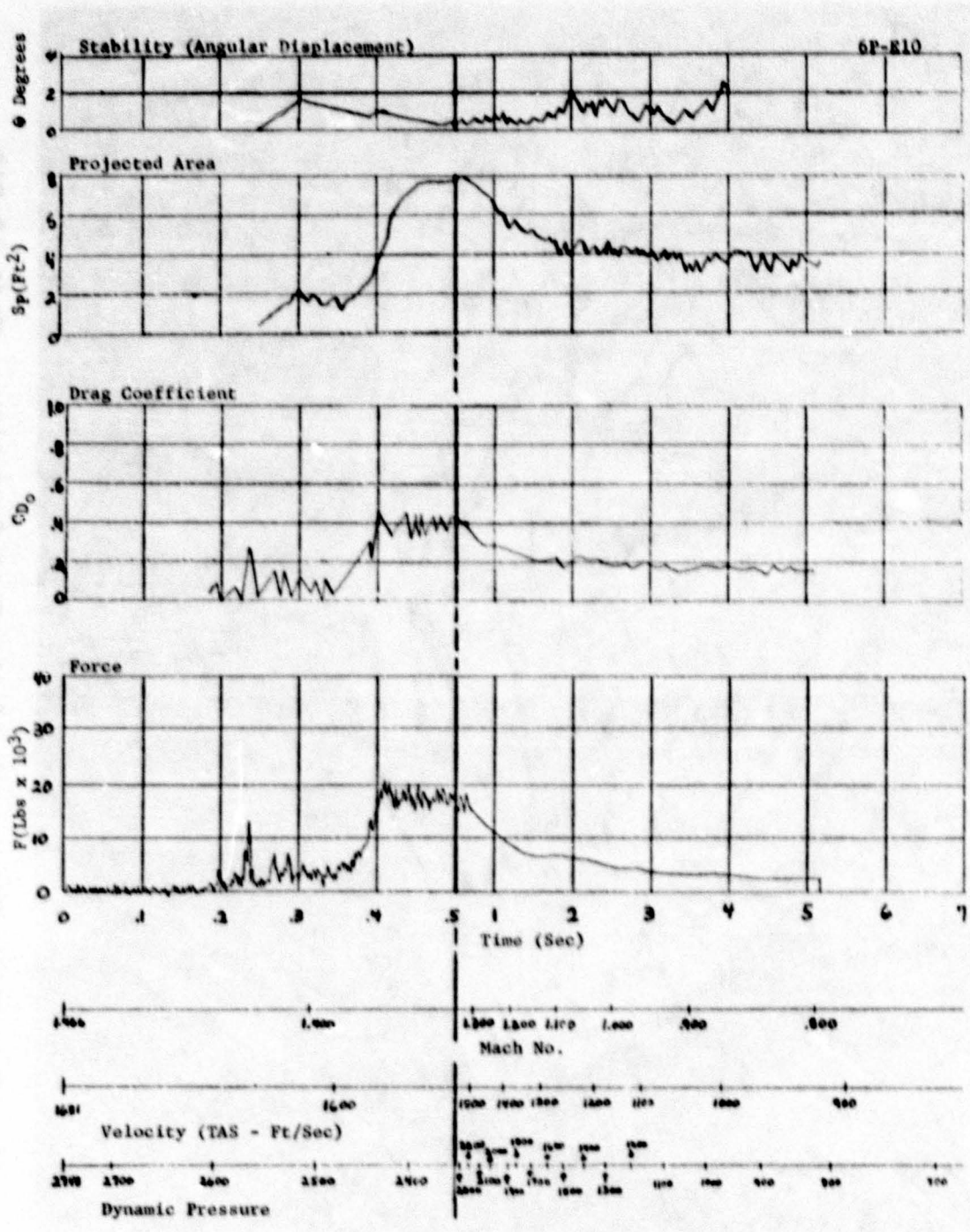

Figure 28. Parachute Performance Curves - Test 6P-E10.

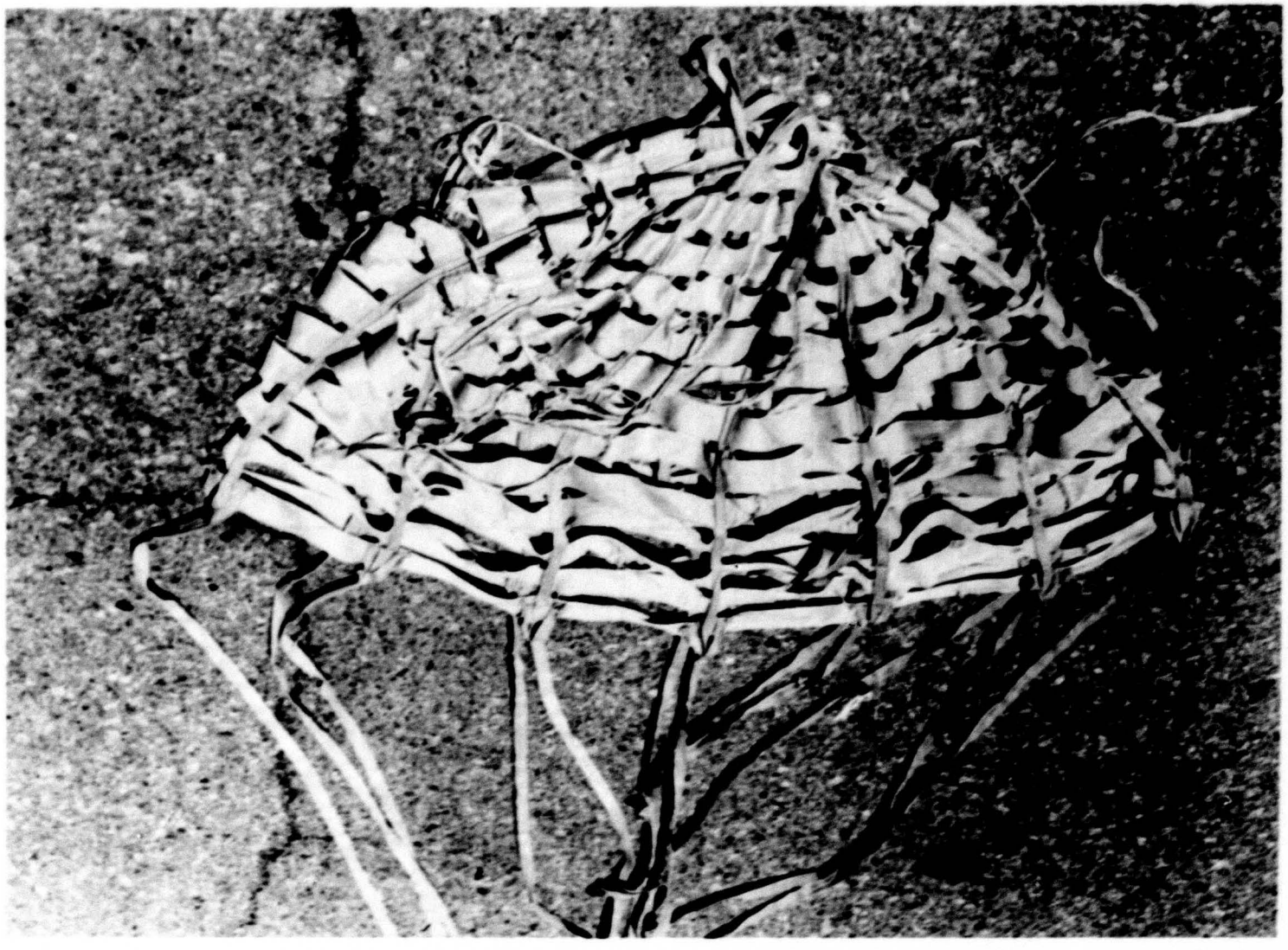

Figure 29. Post Test Photograph of the Test Parachute - Test 6P-E10.

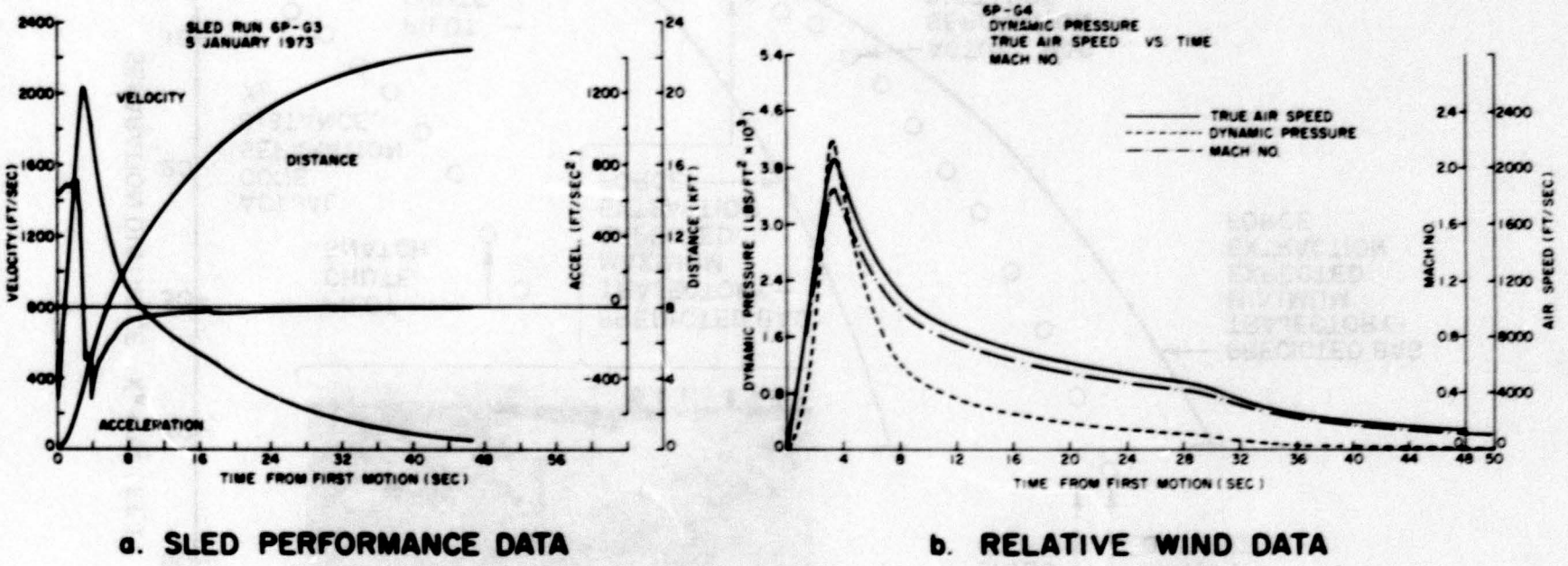

a. SLED PERFORMANCE DATA

b. RELATIVE WIND DATA

Figure 30. Typical Sled Performance and Relative Wind Curves for the Mach 1.8 Test Runs.

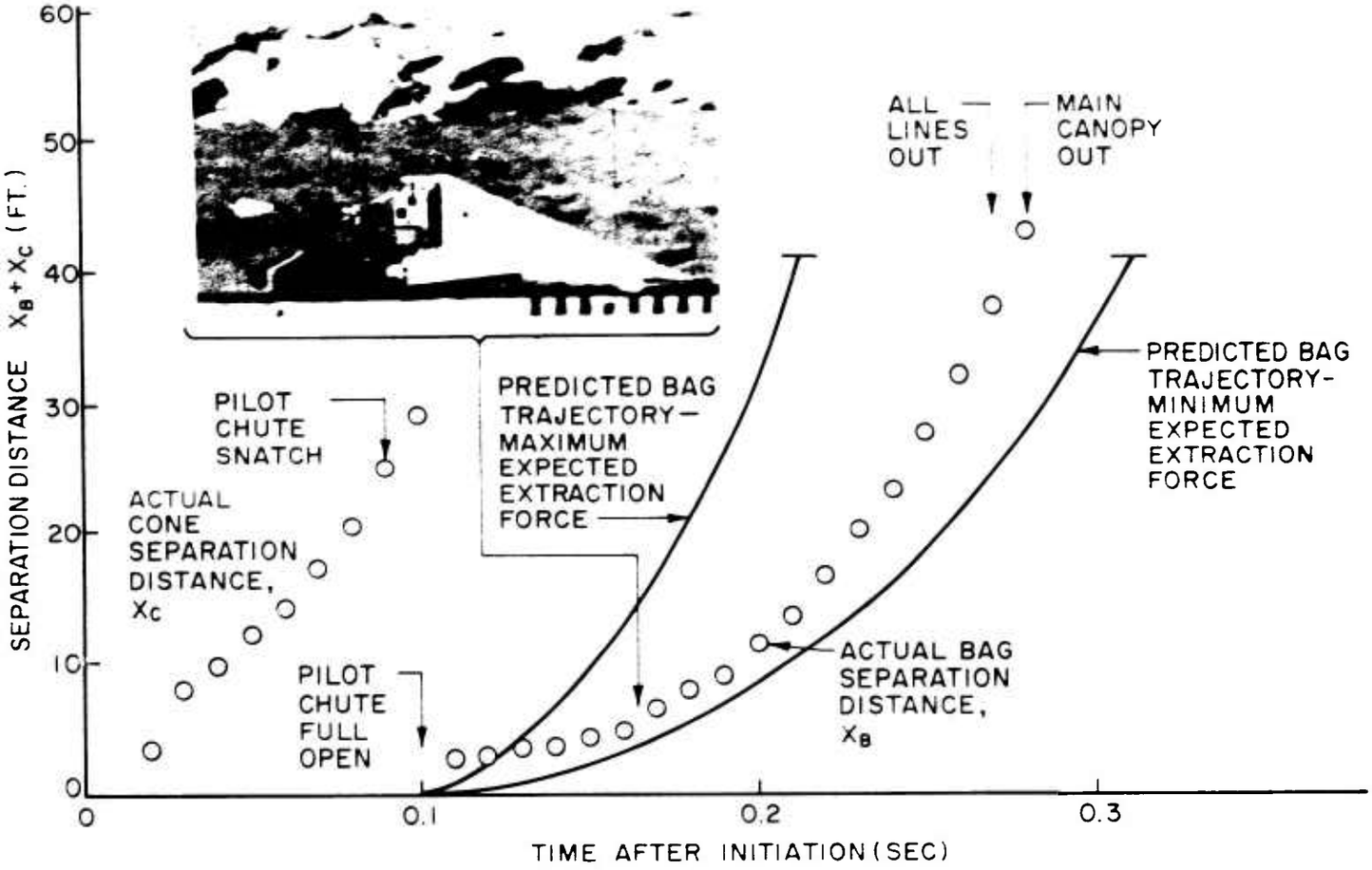

Figure 31. Trajectories of Deployment System Components - Test 6P-G1.

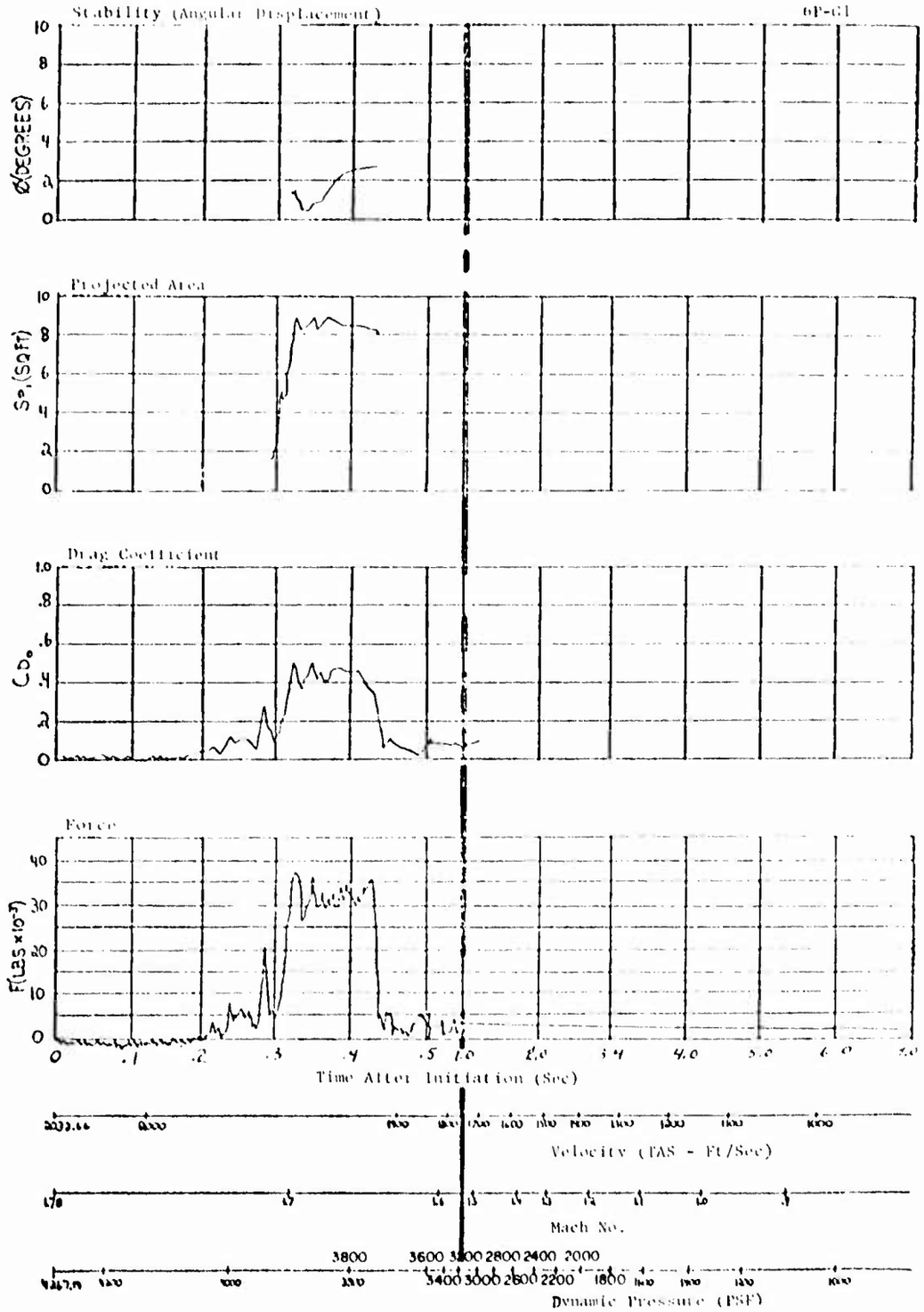

Figure 32. Parachute Performance Curves - Test 6P-G1.

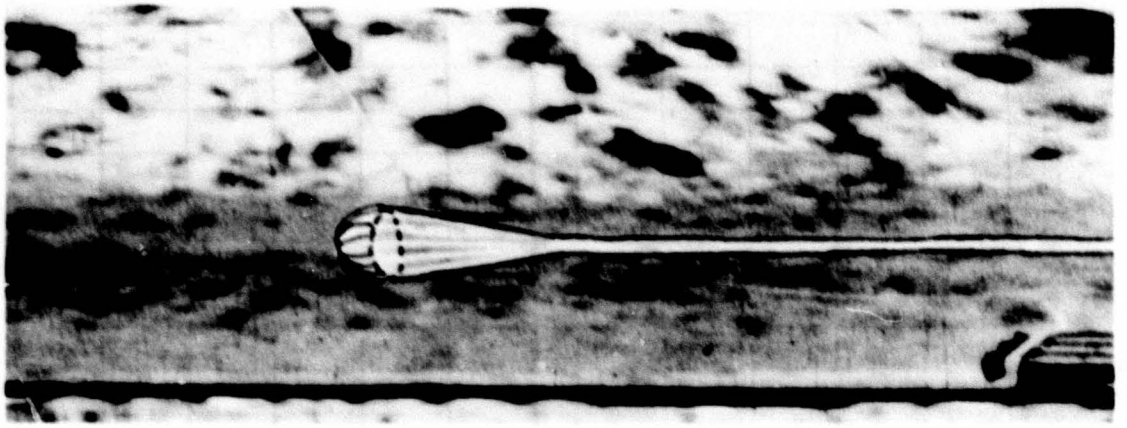

a. TIME FROM DEPLOYMENT = 0.35 sec

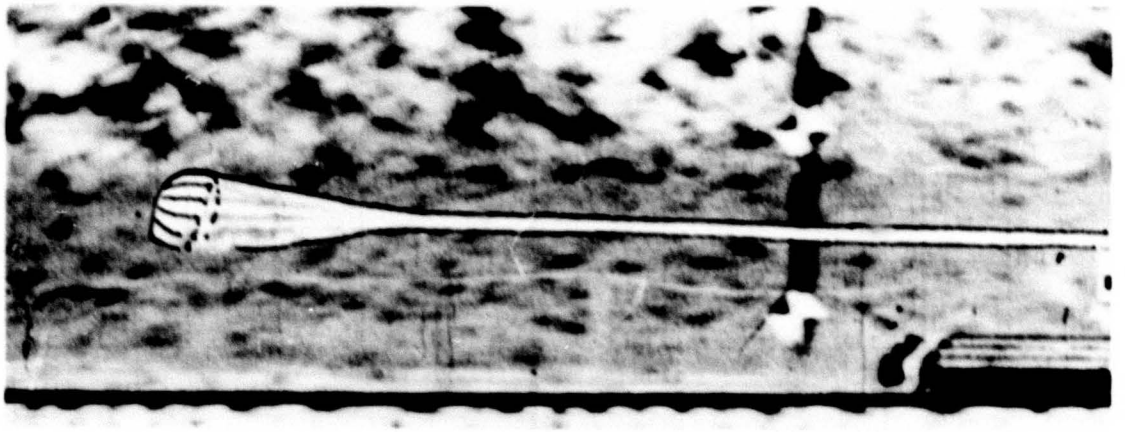

b. TIME FROM DEPLOYMENT = 0.42 sec

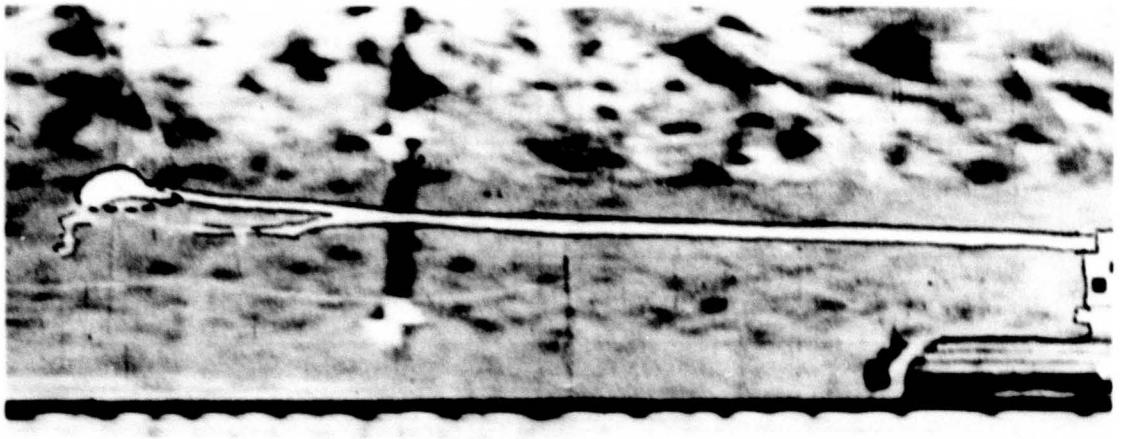

c. TIME FROM DEPLOYMENT = 0.43 sec

Figure 33. Photographs of the Sequence of Parachute Failure - Test 6P-G1. (Photos retouched for clarity.)

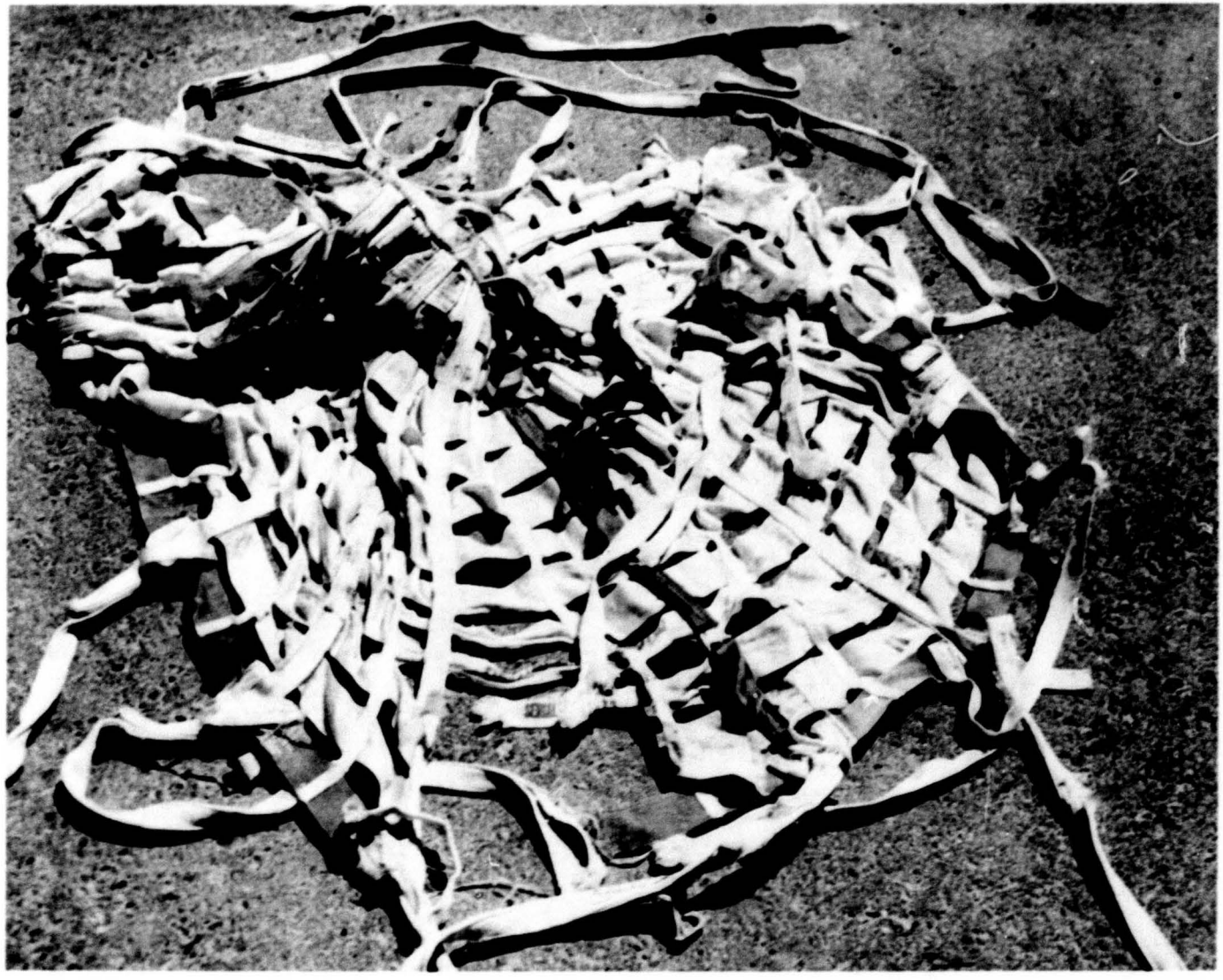

Figure 34. Post Test Photograph of the Test Parachute - Test 6P-G1.

(2) Test 6P-G2; Nylon Parachute

All deployment system components functioned satisfactorily. Deployment cone and bag separation distance trajectories could not be determined because of the inability to discriminate between images of the test items and the background terrain.

Figure 36 presents the parachute performance curves for this test. Parachute performance for this test was similar to that observed for the previous test. Parachute inflation was normal and a peak force of 38,854 lb was produced near the time of canopy first full-open. The canopy remained full-open for about 0.09 sec, at which time the skirt band broke, eight of the twelve suspension lines broke near the skirt, and the canopy collapsed. Figure 36 shows the condition of the parachute after the test.

(3) Test 6P-G3, Nylon Parachute

All deployment system components functioned satisfactorily; Figure 37 presents their trajectories. The deployment cone and bag separation distance had to be scaled from the back-up ribbon frame cameras because the trackside cameras of the primary engineering optical instrumentation system missed the deployment sequence. Deployment event times usually included with the trajectories are not presented in the Figure because they could not be determined with adequate accuracy from the ribbon frame cameras.

Figure 38 presents the parachute performance curves for this test. Parachute inflation to full-open was normal and a peak opening force of 45,869 lb was produced. At approximately the time of the canopy full-open, the confluence keeper broke in four places and the parachute confluence transferred to the first riser line keeper. Figure 39 presents two photographs; one which shows the parachute

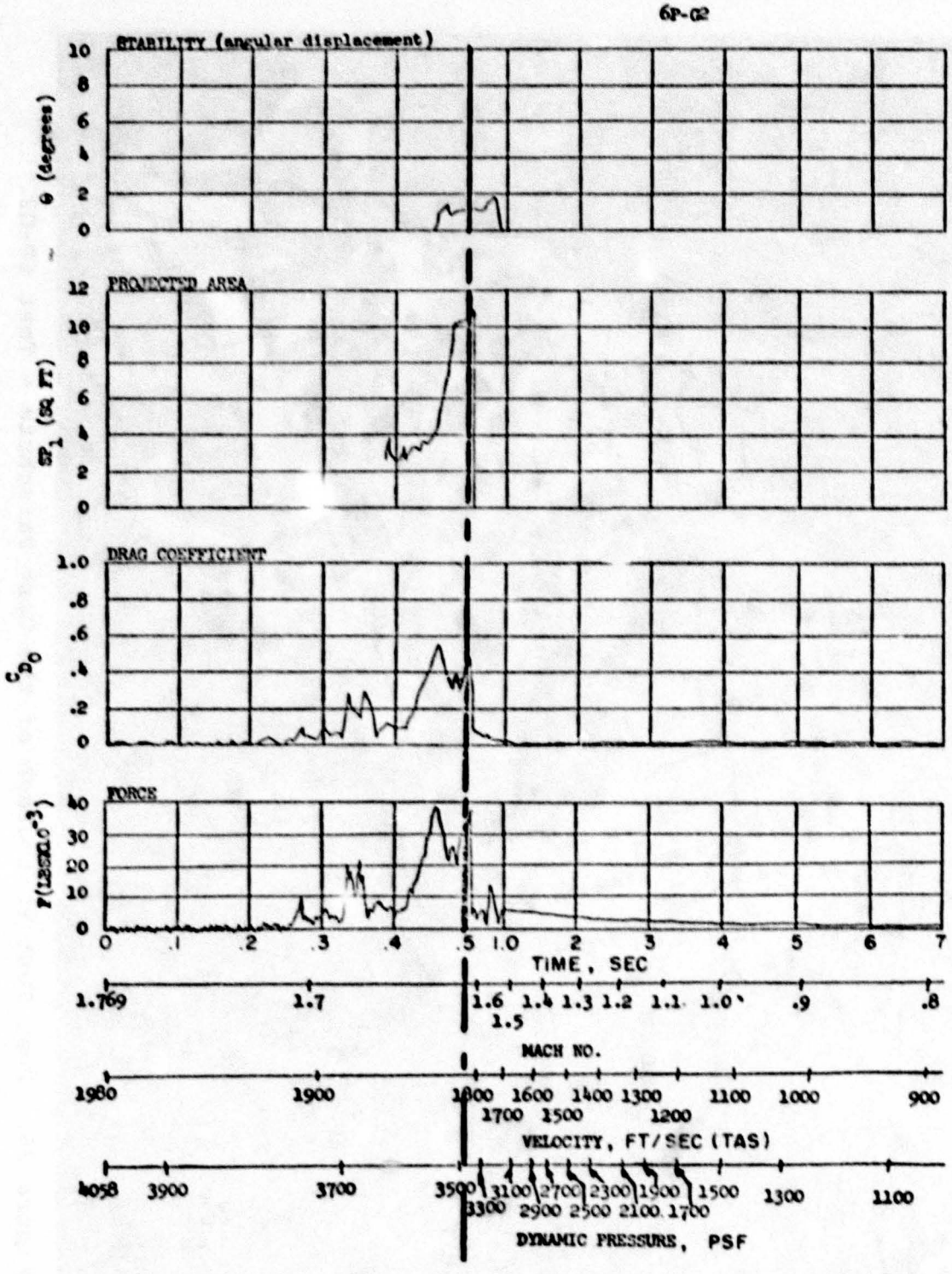

Figure 35. Parachute Performance Curves - Test 6P-G2.

Figure 36. Post Test Photograph of the Test Parachute - Test 6P-G2.

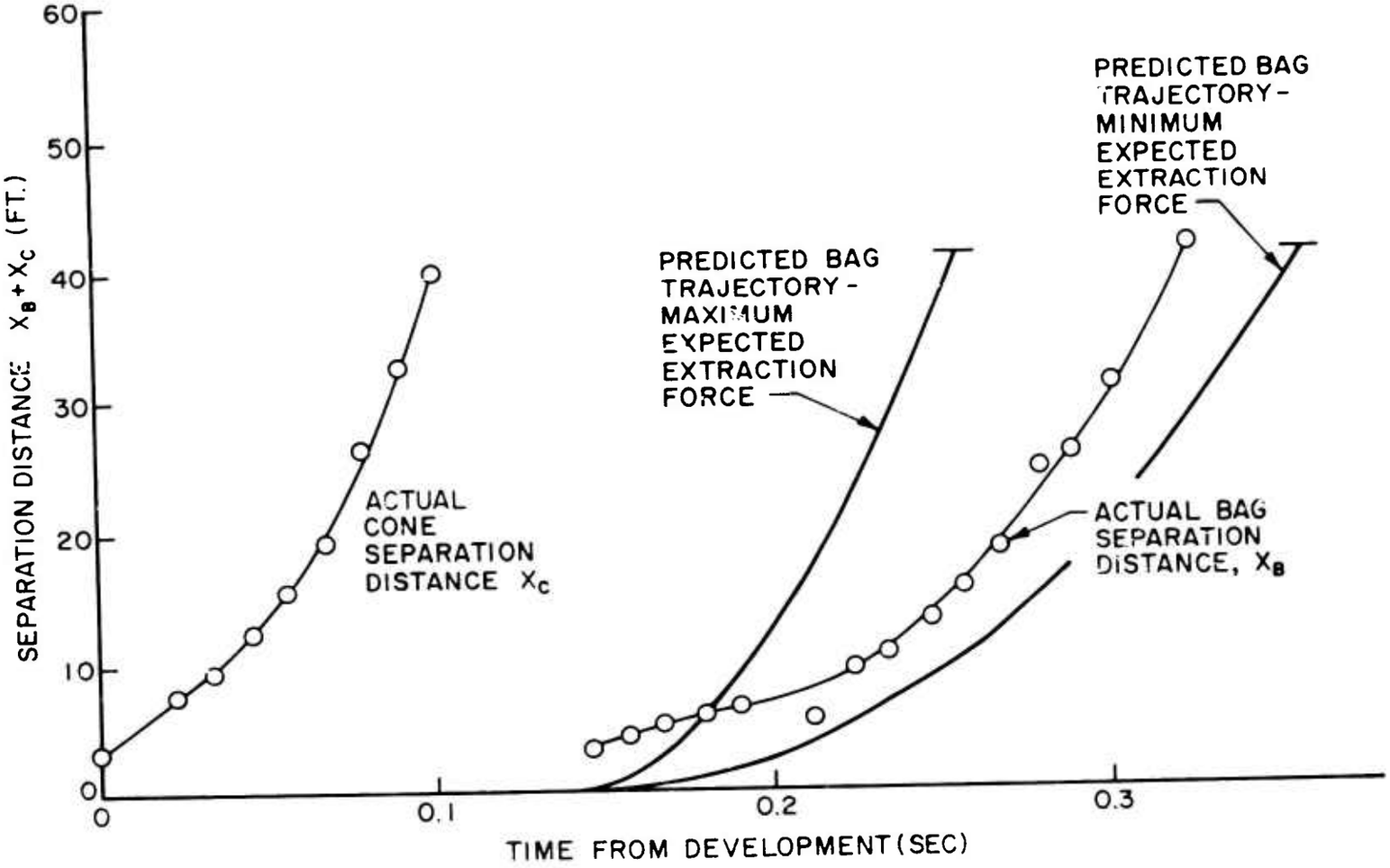

Figure 37. Trajectories of Deployment System Components - Test 6P-G3.

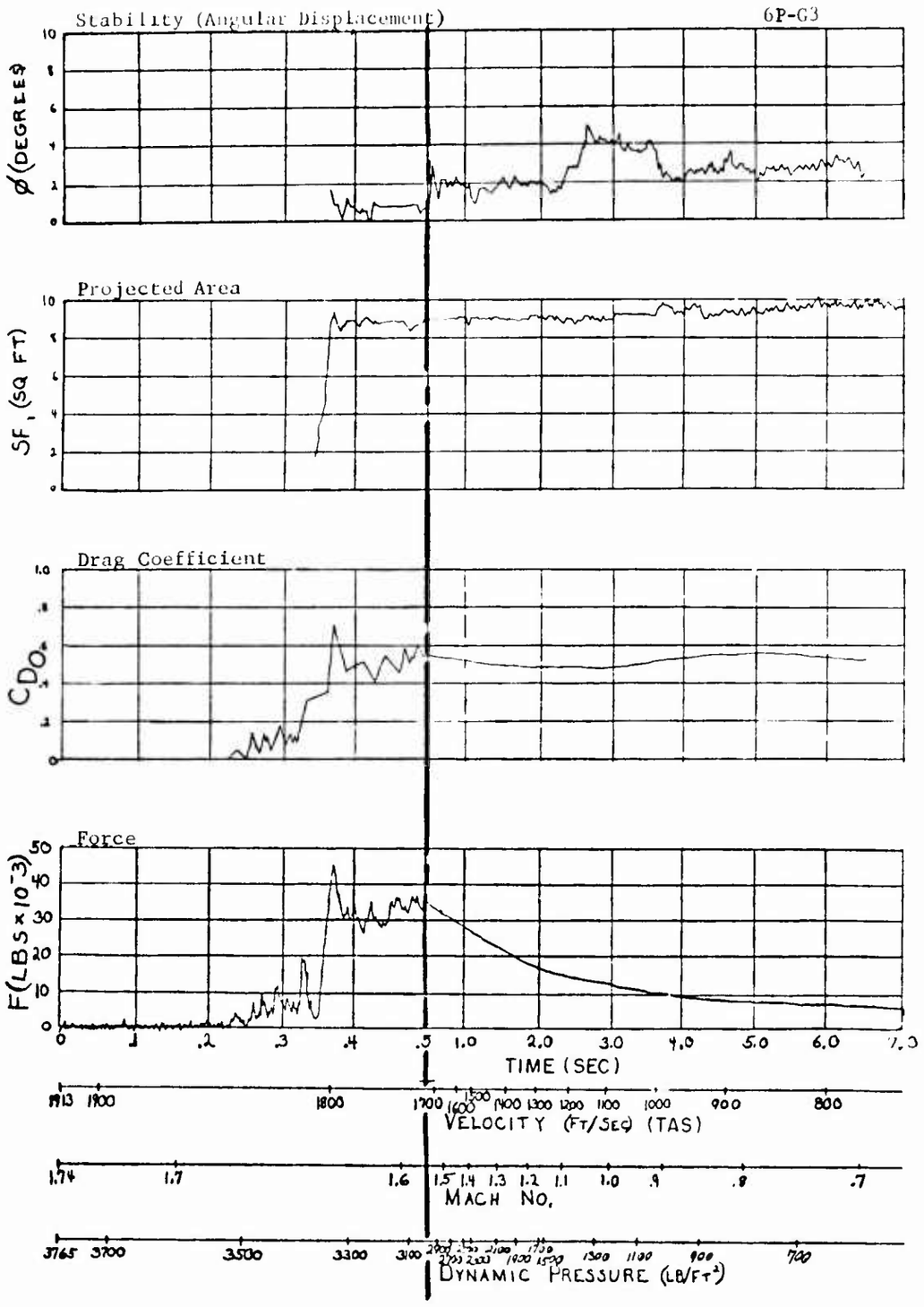

Figure 38. Parachute Performance Curves - Test 6P-G3.

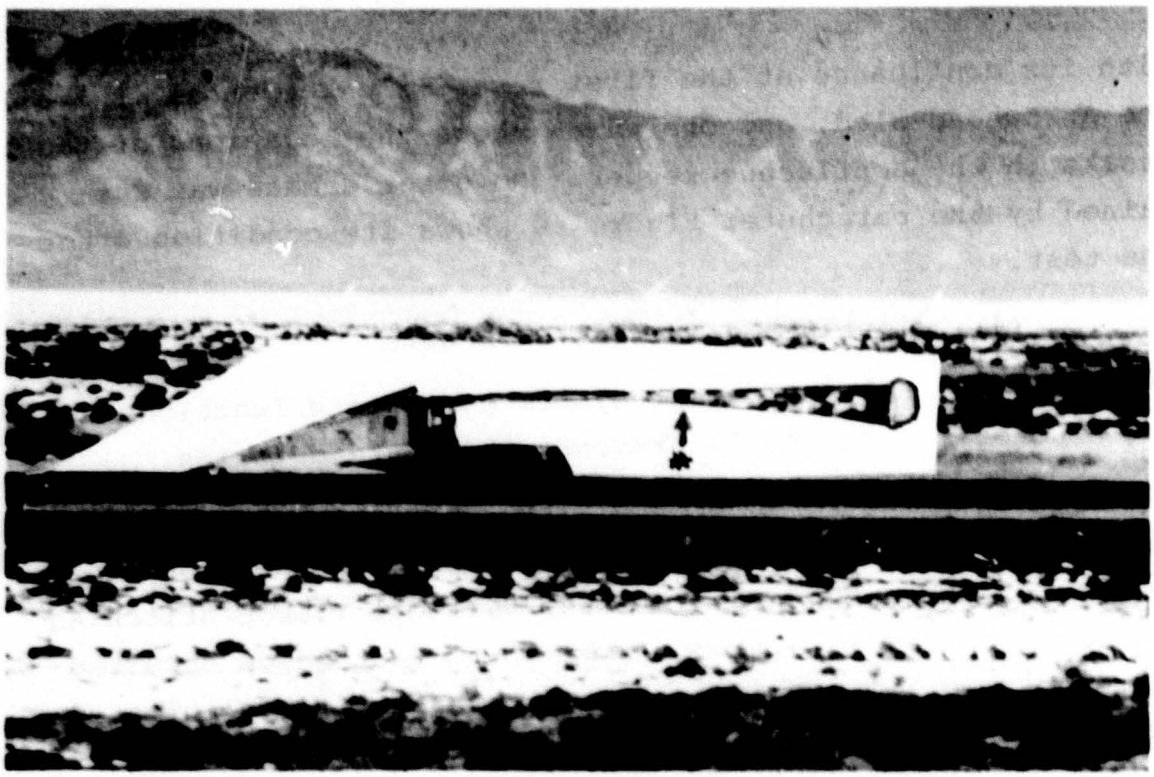

a. *Location of Parachute Confluence During Test

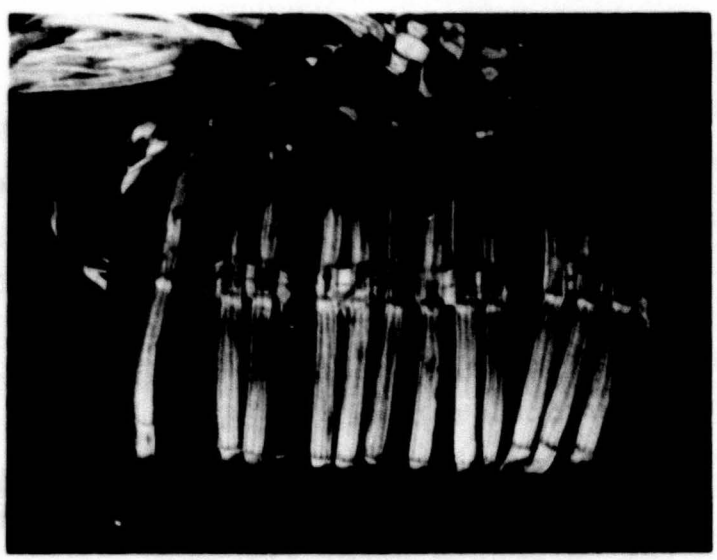

b. Location of Keeper Breaks

Figure 39. Photographs Showing the Damaged Confluence Keeper on Test 6P-G3. (Photo retouched for clarity.)

with its confluence at the first riser line keeper as it trails the Arrowhead sled, and one which shows the locations of the breaks in the confluence keeper. No other damage was sustained by the parachute; Figure 40 shows its condition after the test.

(4) Test 6P-G4; Kevlar Parachute

All deployment system components functioned satisfactorily; Figure 41 presents their trajectories.

Figure 42 presents the parachute performance curves for this test. Parachute inflation was not normal. As the parachute began to inflate, vertical ribbon stitching failure occurred in a manner similar to that which occurred on test 6P-E9. The canopy never did reach a fully inflated shape (Figure 43 shows the maximum stage of inflation) and became severely damaged during the run. Figure 44 shows the condition of the canopy after the test.

(5) Test 6P-G5; Kevlar Parachute

All deployment system components functioned satisfactorily; Figure 45 presents their trajectories.

Figure 46 presents the parachute performance curves for this test. Parachute inflation was normal and the parachute reached full-open at approximately 0.45 sec after deployment initiation. The parachute remained fully inflated, as shown in Figure 47, with no visible damage for about 10 sec. Vertical ribbon stitching failure began to occur just prior to parachute release and progressed from the skirt band to the fifth row of ribbons. Figure 48 shows the condition of the parachute after the test.

e. Runs at Mach 2.2; Q = 6500 psf

Five sled runs were made which provided data for the comparative evaluation of nylon and Kevlar hemisflo parachutes

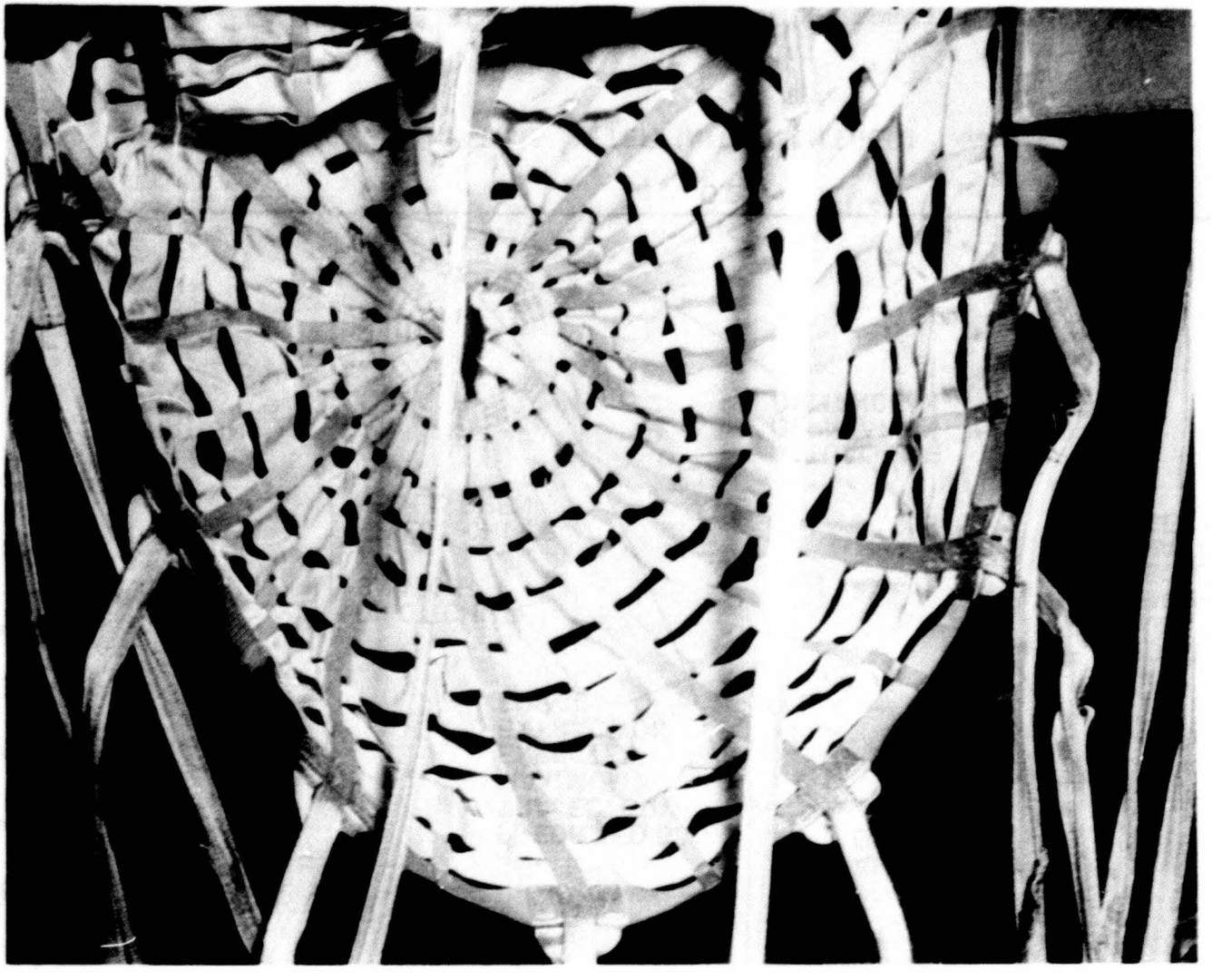

Figure 40. Post Test Photograph of the Test Parachute - Test 6P-G3.

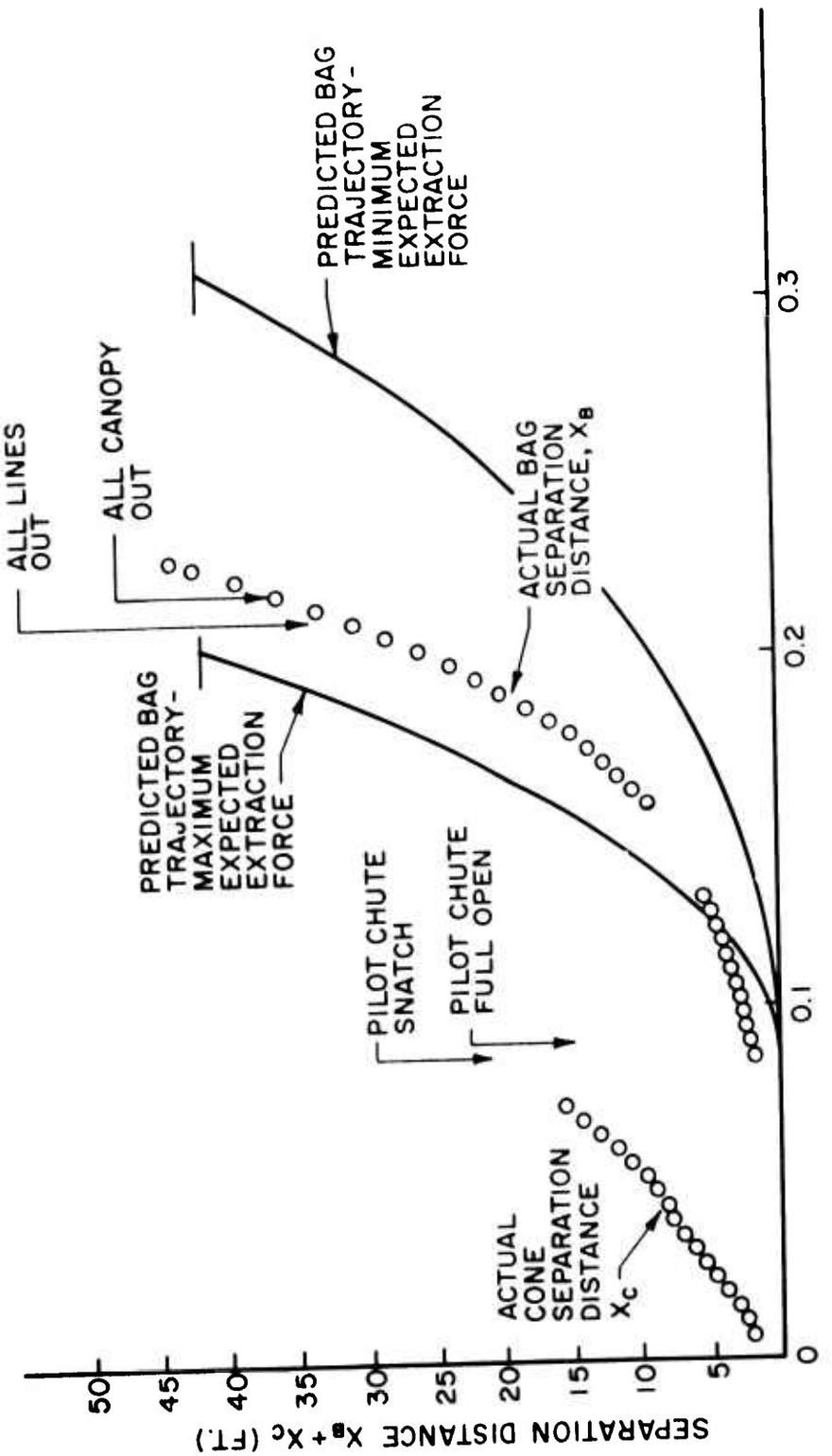

Figure 41. Trajectories of Deployment System Components - Test 6P-G4.

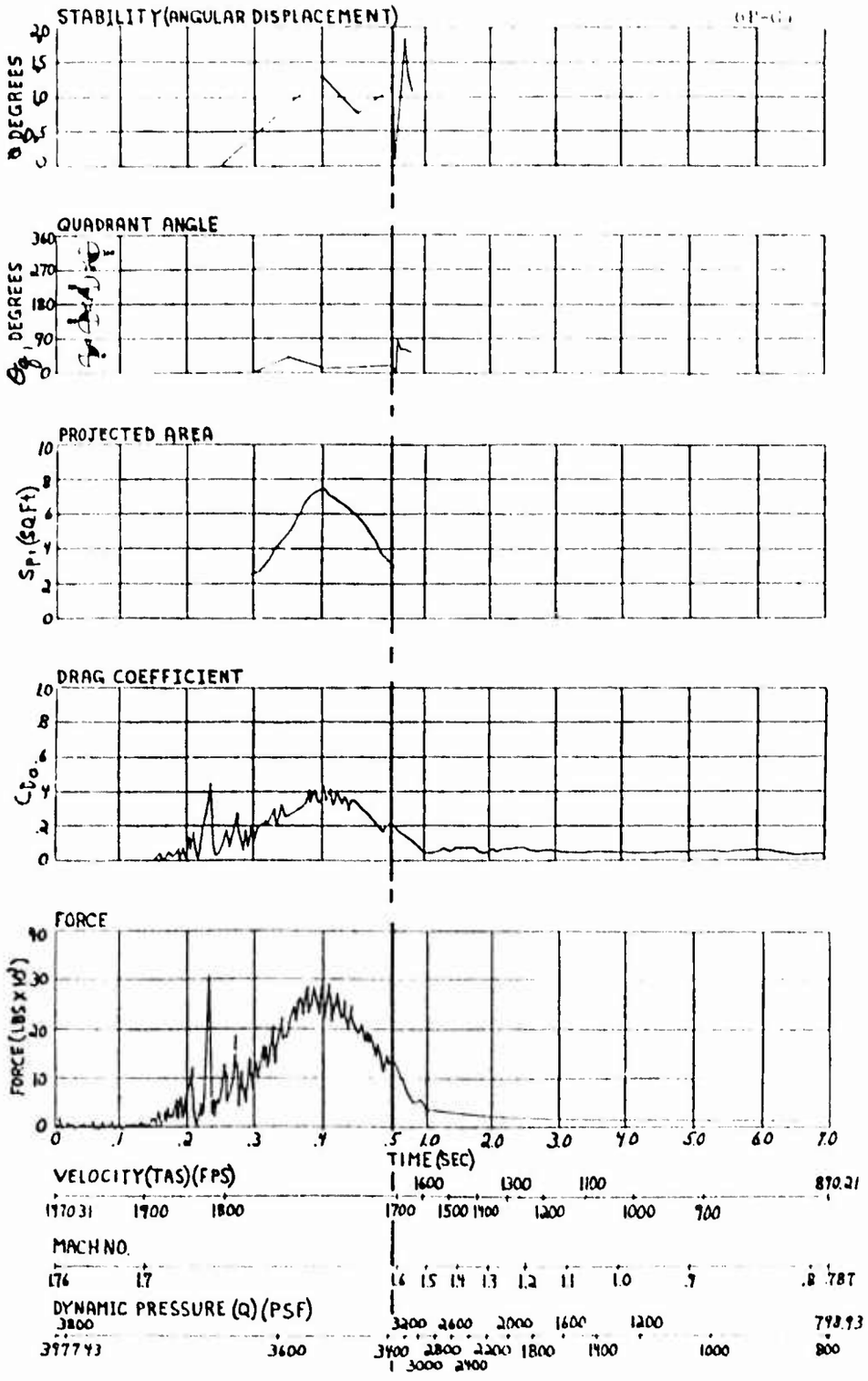

Figure 47. Parachute Performance Curves - Test 6P-64.

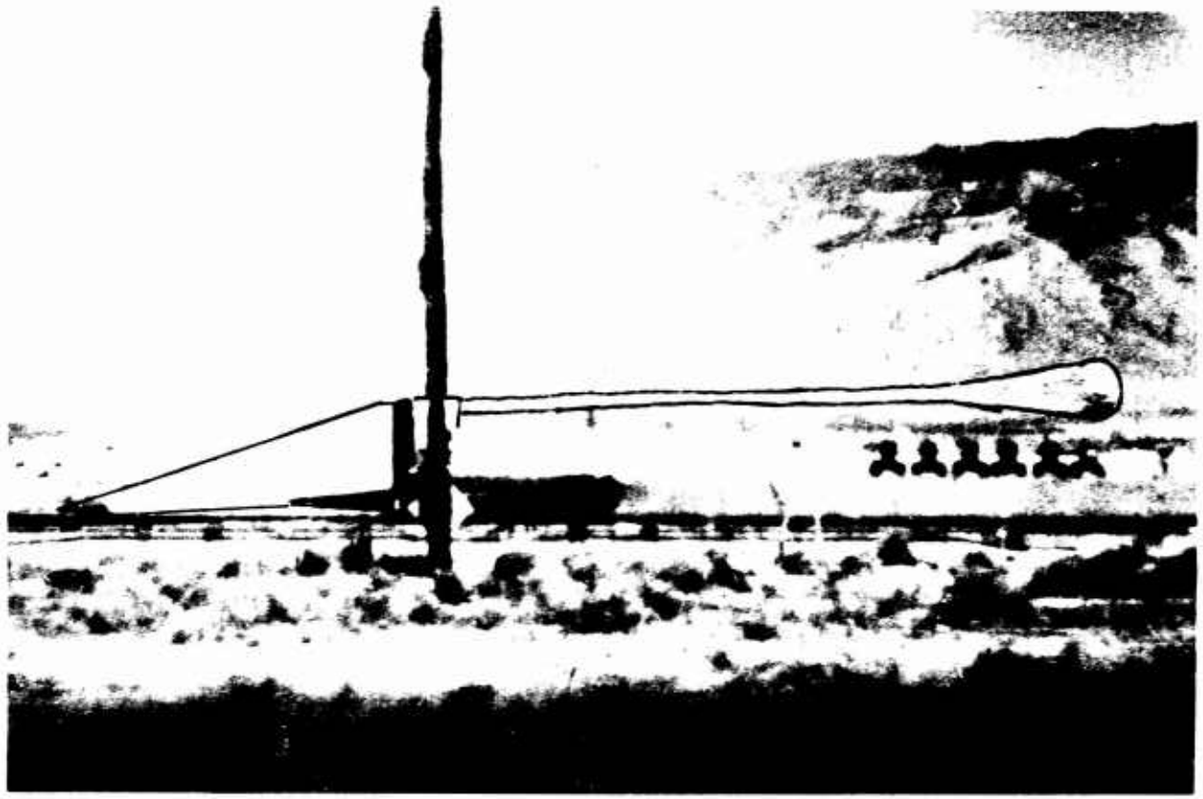

Figure 43. Photograph Showing Partial Inflation of the Test Parachute - Test 6P-G4. (Photo retouched for clarity.)

Figure 44. Post Test Photograph of the Test Parachute - Test 6P-G4.

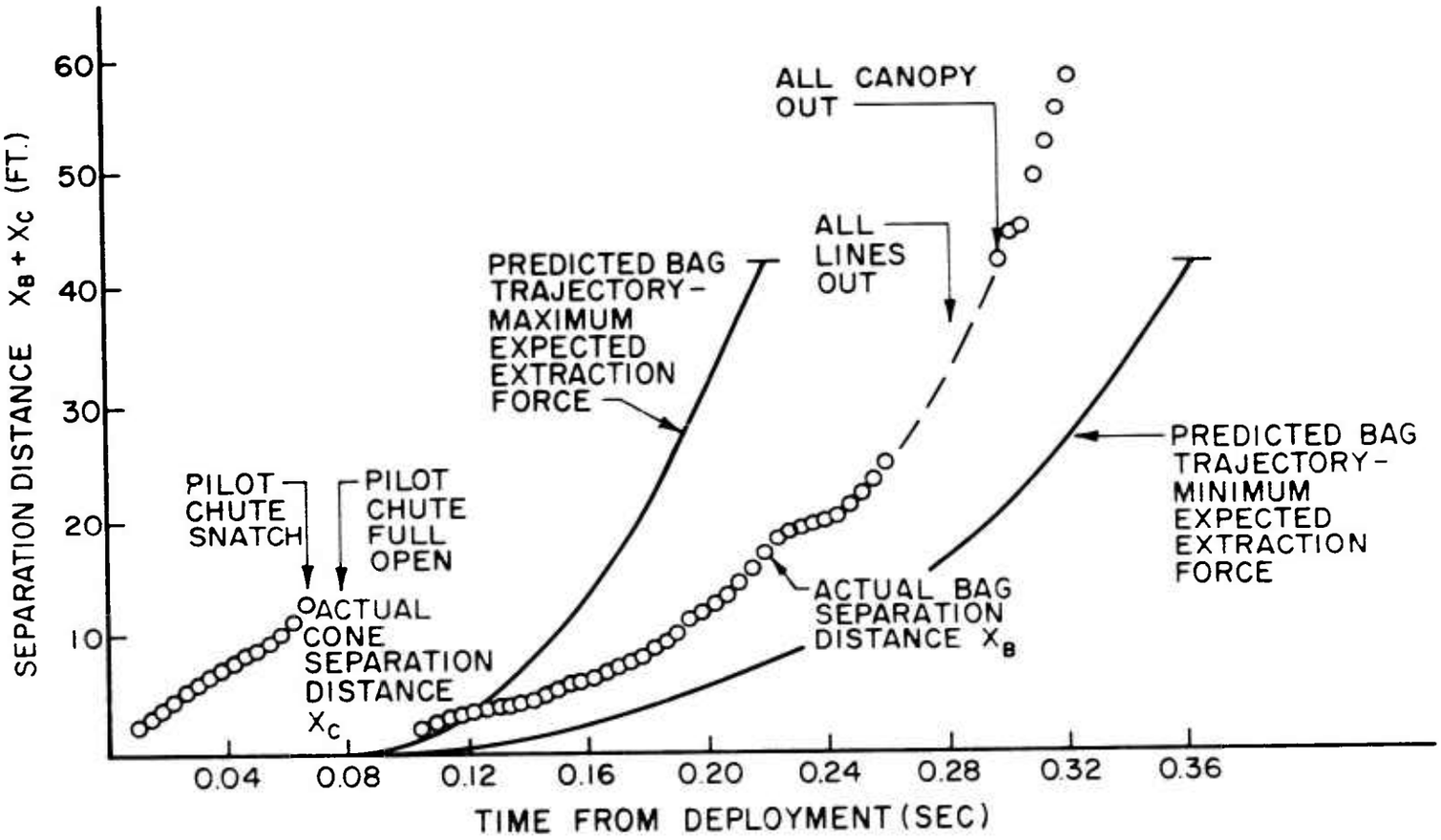

Figure 45. Trajectories of Deployment System Components - Test 6P-G5.

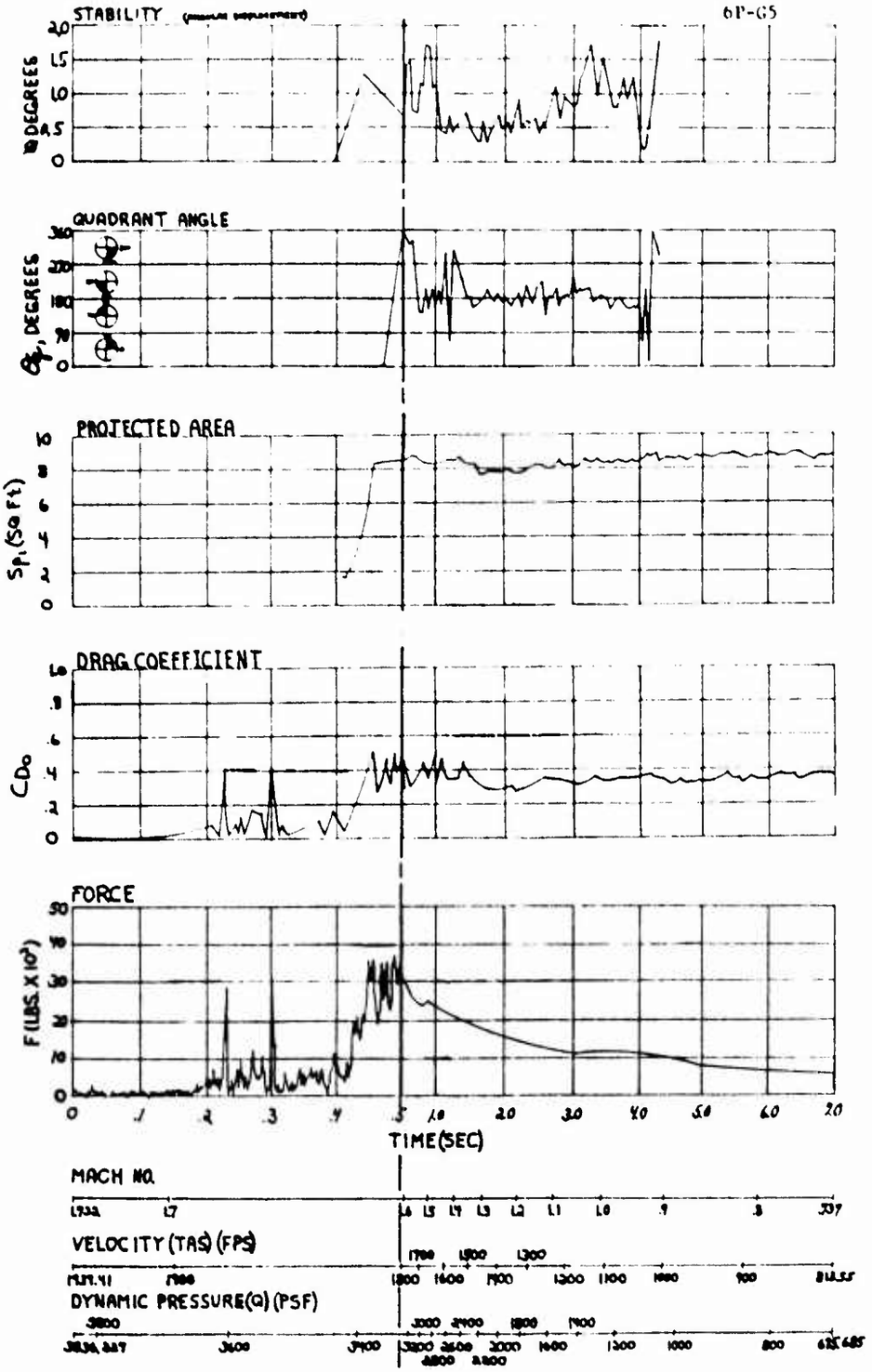

Figure 46. Parachute Performance Curves - Test 6P-G5.

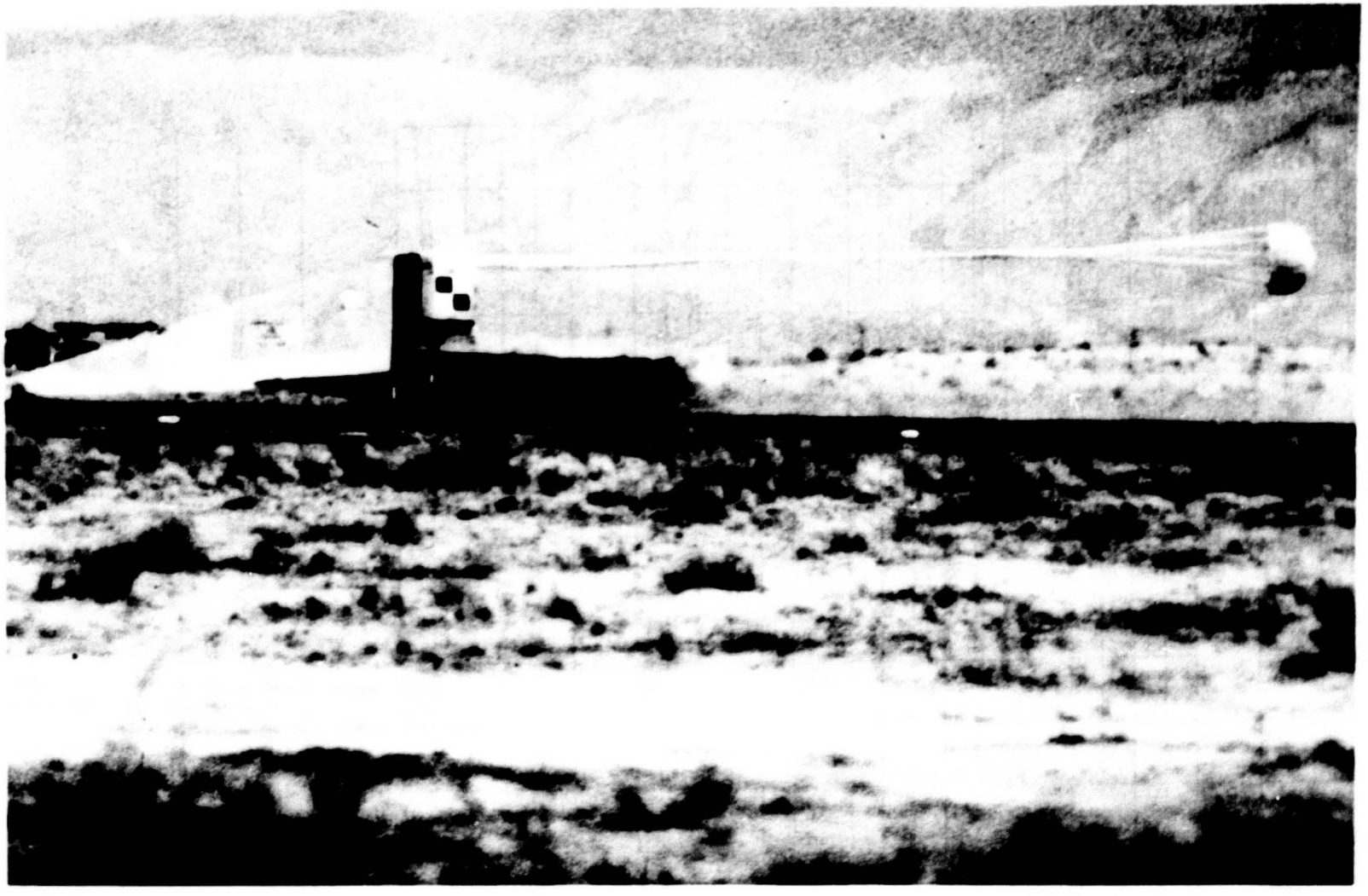

Figure 47. Photograph Showing Full Inflation of the Test Parachute - Test 6P-G5.

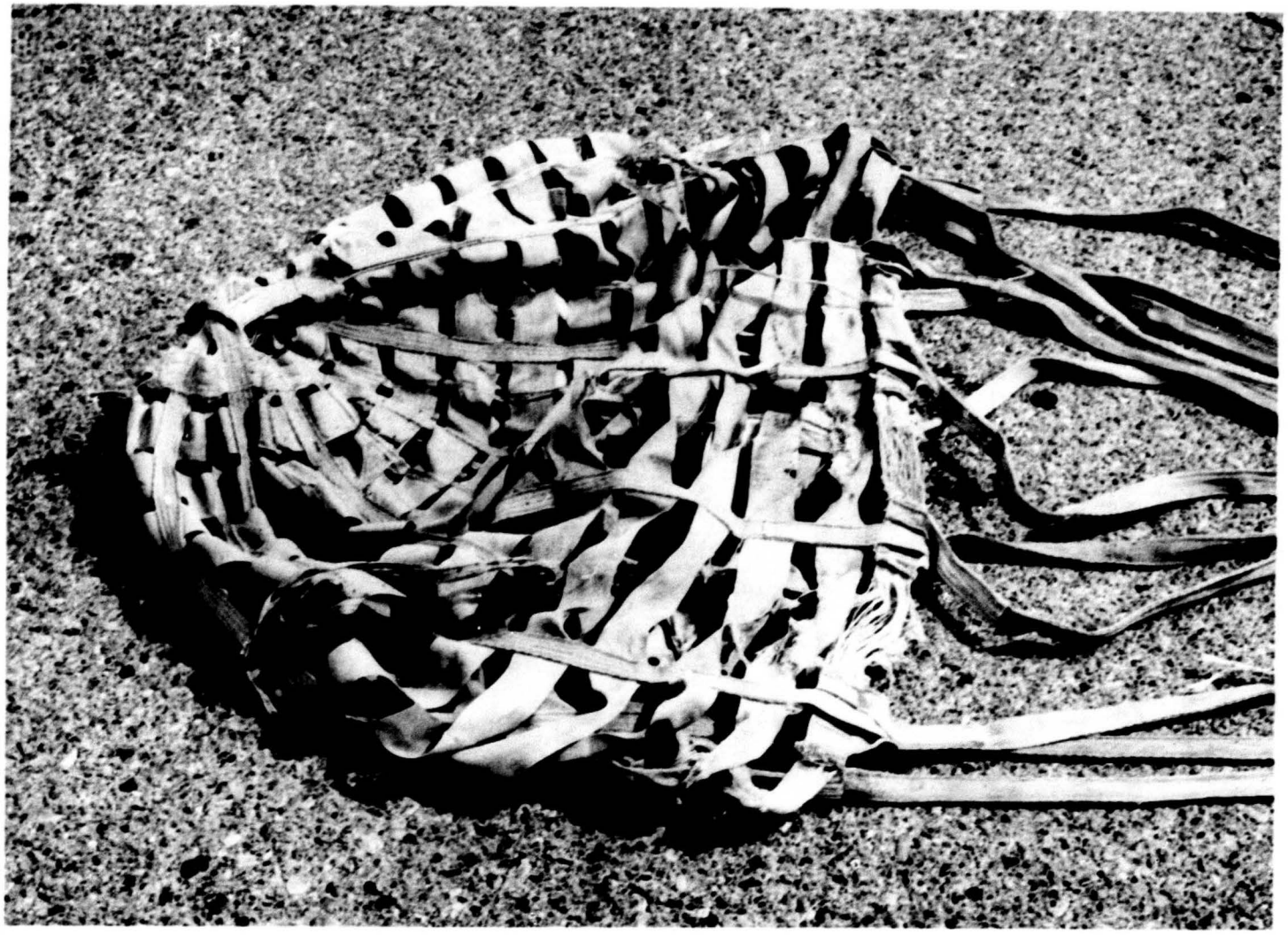

Figure 48. Post Test Photograph of the Test Parachute - Test 6P-G5.

at Mach 2.2 and at a dynamic pressure of approximately 6500 psf; tests 6P-H1, 6P-H2, and 6P-H3 for nylon, and tests 6P-H6 and 6P-H7 for Kevlar. Typical sled performance and relative wind curves for these tests are presented in Figure 49.

(1) Test 6P-H1; Nylon Parachute

All deployment system components functioned satisfactorily. No separation trajectories are presented because only the trajectory for the deployment cone was obtained. The trackside cameras were positioned incorrectly and missed most of the deployment and inflation processes.

Figure 50 presents the parachute performance curves for this test. The parachute reached line stretch at approximately 0.22 sec after deployment initiation where it generated a snatch force of 55,692 lb. The lines became slack as the parachute rebounded from line stretch. The canopy started to inflate during the rebound and reached approximately 80 percent of its full-open area when the lines were stretched for the second time and a force of over 70,000 lb was generated. At the time of the second line stretch, nine of the twelve parachute suspension lines broke between the confluence keeper and the canopy skirt, three vertical ribbons broke, and the stitching between the vent band and six radials broke. Figure 51 shows the condition of the parachute after the test.

(2) Test 6P-H2; Nylon Parachute

All deployment system components functioned satisfactorily; Figure 52 presents their trajectories.

Figure 53 presents the parachute performance curves for this test. The parachute produced a snatch force of 41,867 lb at line stretch and started to inflate approximately 0.02 sec later. Inflation was not normal, however. The canopy inflated to only approximately 30 percent of its full open area

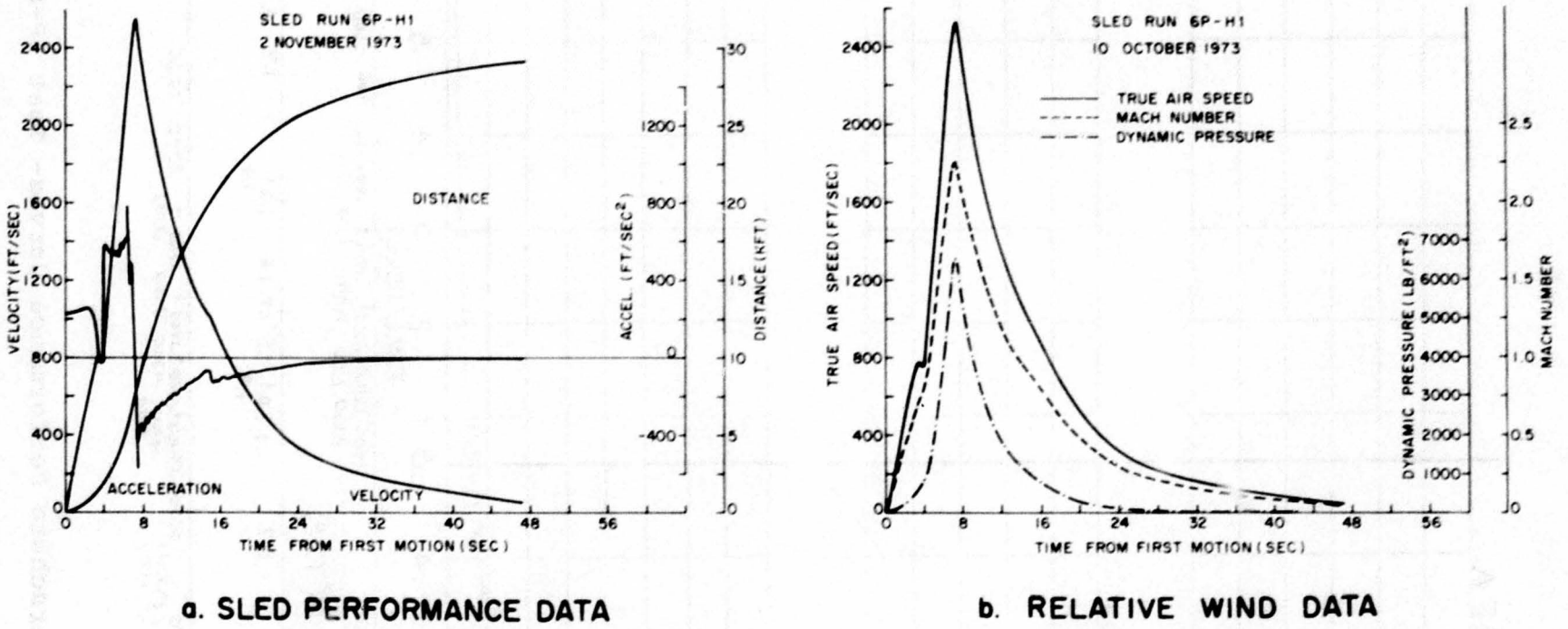

Figure 49. Typical Sled Performance and Relative Wind Curves for the Mach 2.2 Test Runs.

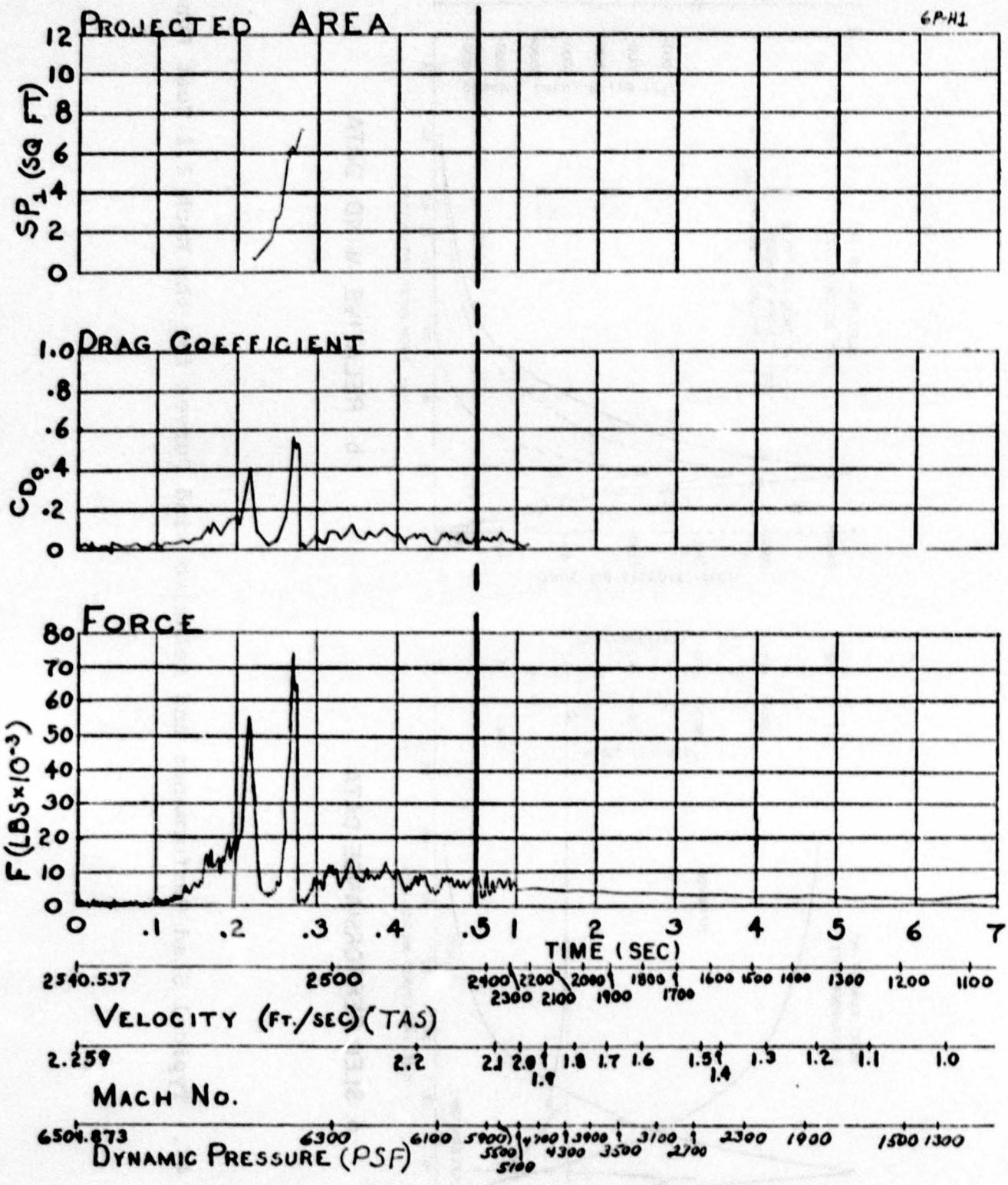

Figure 50. Parachute Performance Curves- Test 6P-H1.

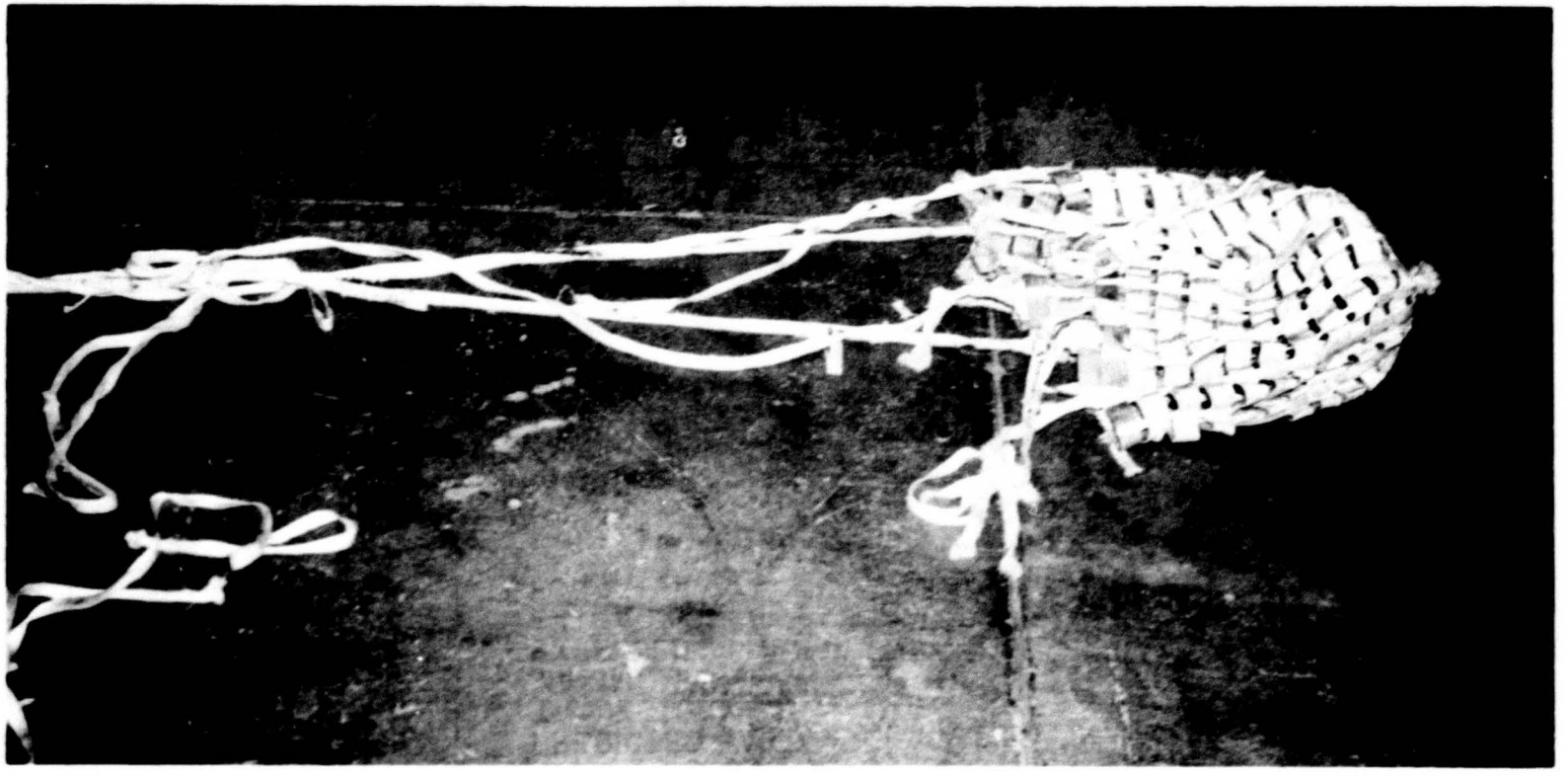

Figure 51. Post Test Photograph of the Test Parachute - Test 6P-H1.

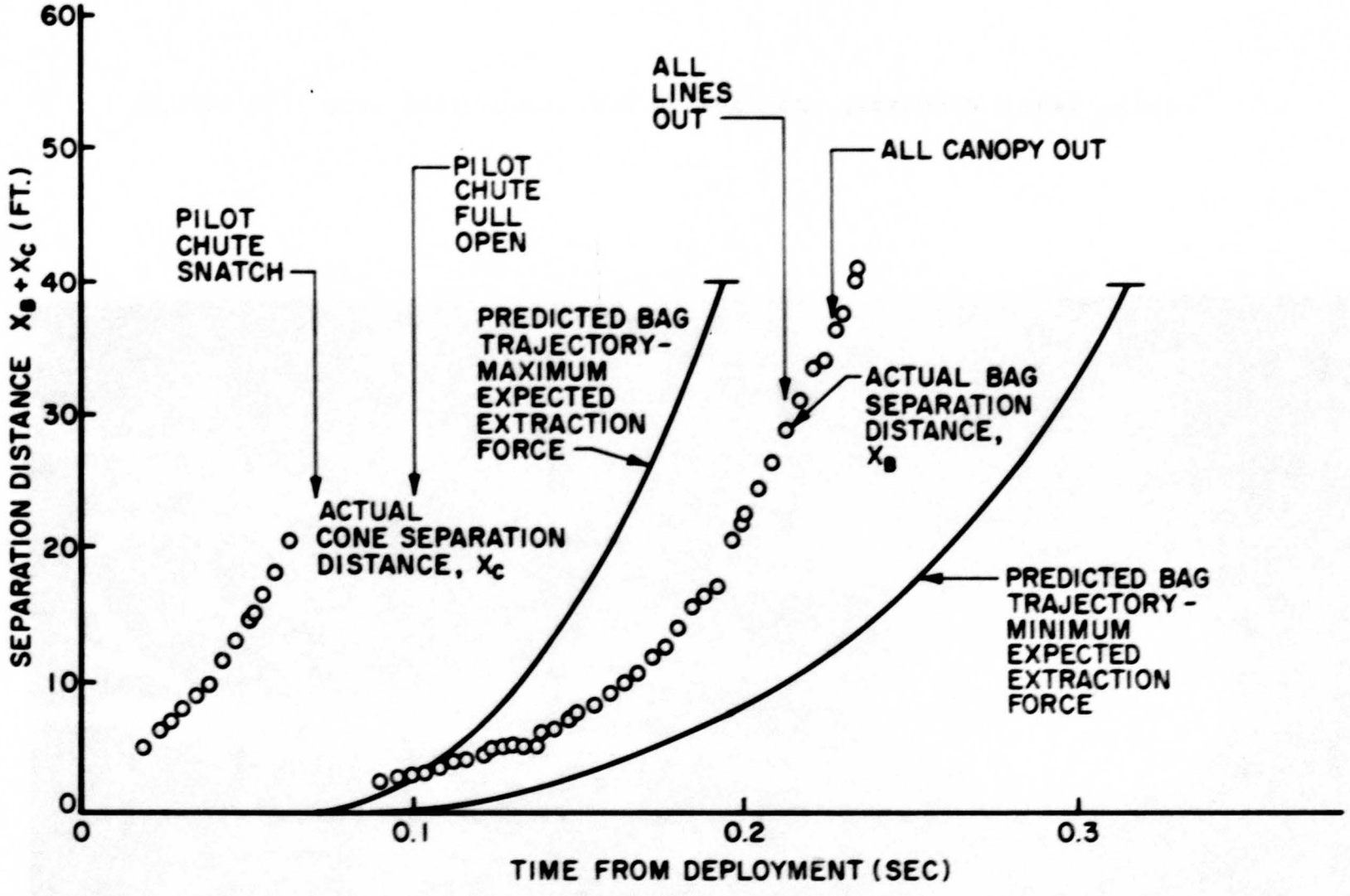

Figure 52. Trajectories of Deployment System Components - Test 6P-H2.

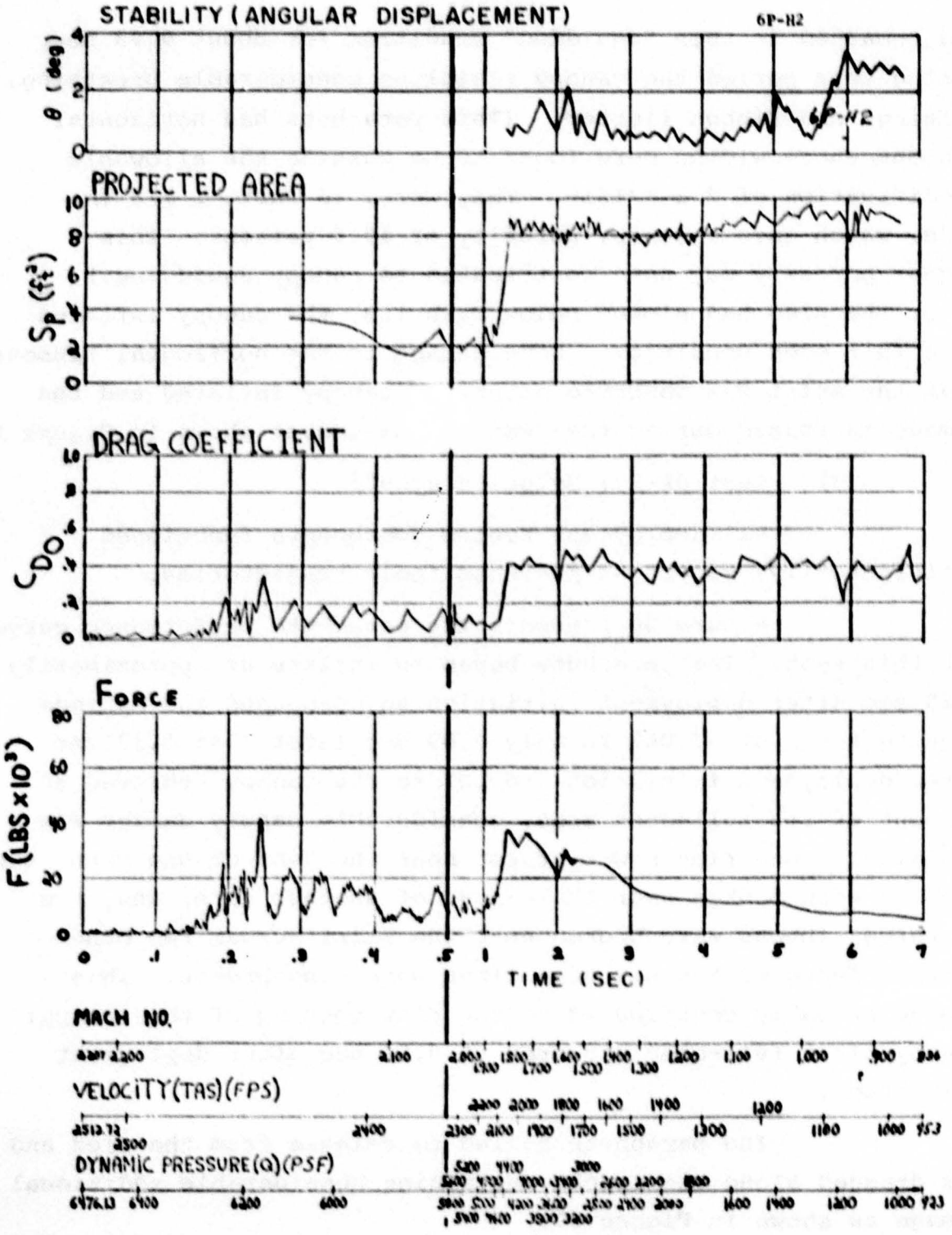

Figure 53. Parachute Performance Curves - Test 6P-H2.

and remained in this "squidded" condition for about 0.93 sec. During this period the canopy exhibited considerable breathing, pulsing, and ribbon flutter. (This parachute had horizontal ribbons whose widths were found to be outside the allowable specification of 2 ± 1/16in. They were, in fact, 1 7/8 in. wide, which gave a canopy porosity of 19.9 percent. This higher porosity may have contributed to canopy squidding.) After the sled had slowed below Mach 1.9, the canopy inflated to a full open condition. Some damage to the horizontal ribbons near the skirt was observed after the canopy inflated and the damage increased during the test to the amount shown in Figure 54.

(3) Test 6P-H3; Nylon Parachute

All deployment system components functioned satisfactorily; Figure 55 presents their trajectories.

Figure 56 presents the parachute performance curves for this test. The parachute began to inflate at approximately 0.25 sec after deployment initiation and produced the maximum opening force of 57,067 lb only 0.03 sec later. At 0.32 sec after deployment initiation and before the canopy achieved 80 percent of its full-open area, considerable canopy damage was sustained. One ribbon was broken near the vent of one gore; two ribbons were broken near the center of another gore; and, two or three ribbons were broken near the skirt across two other gores. Three of the six vent lines were also broken. This damage probably contributed to the slow opening of the canopy; canopy first full-open occurred at 0.54 sec after deployment initiation.

The parachute failed to release from the sled and was dragged along the track, sustaining considerable additional damage as shown in Figure 57.

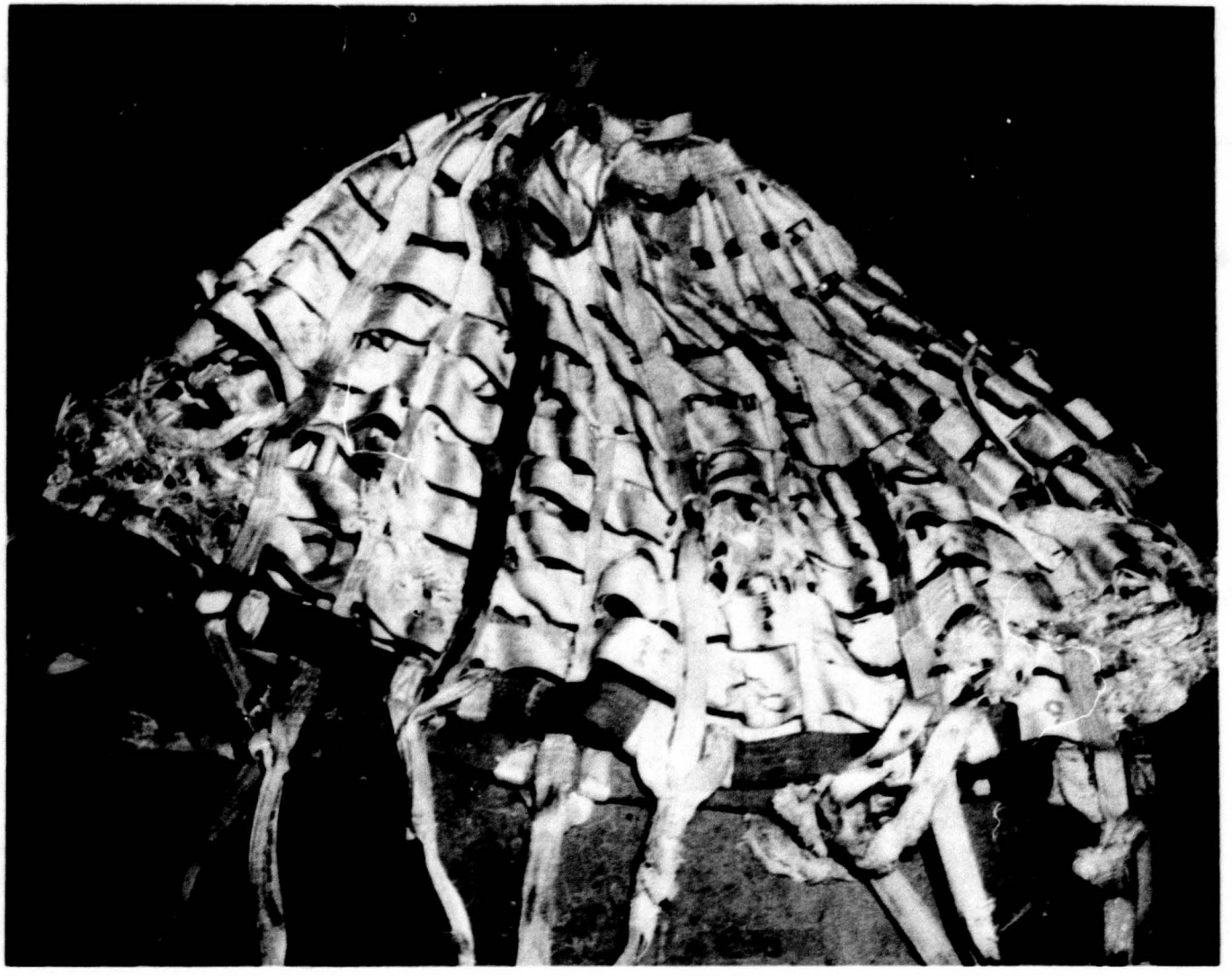

Figure 54. Post Test Photograph of the Test Parachute - Test 6P-H2.

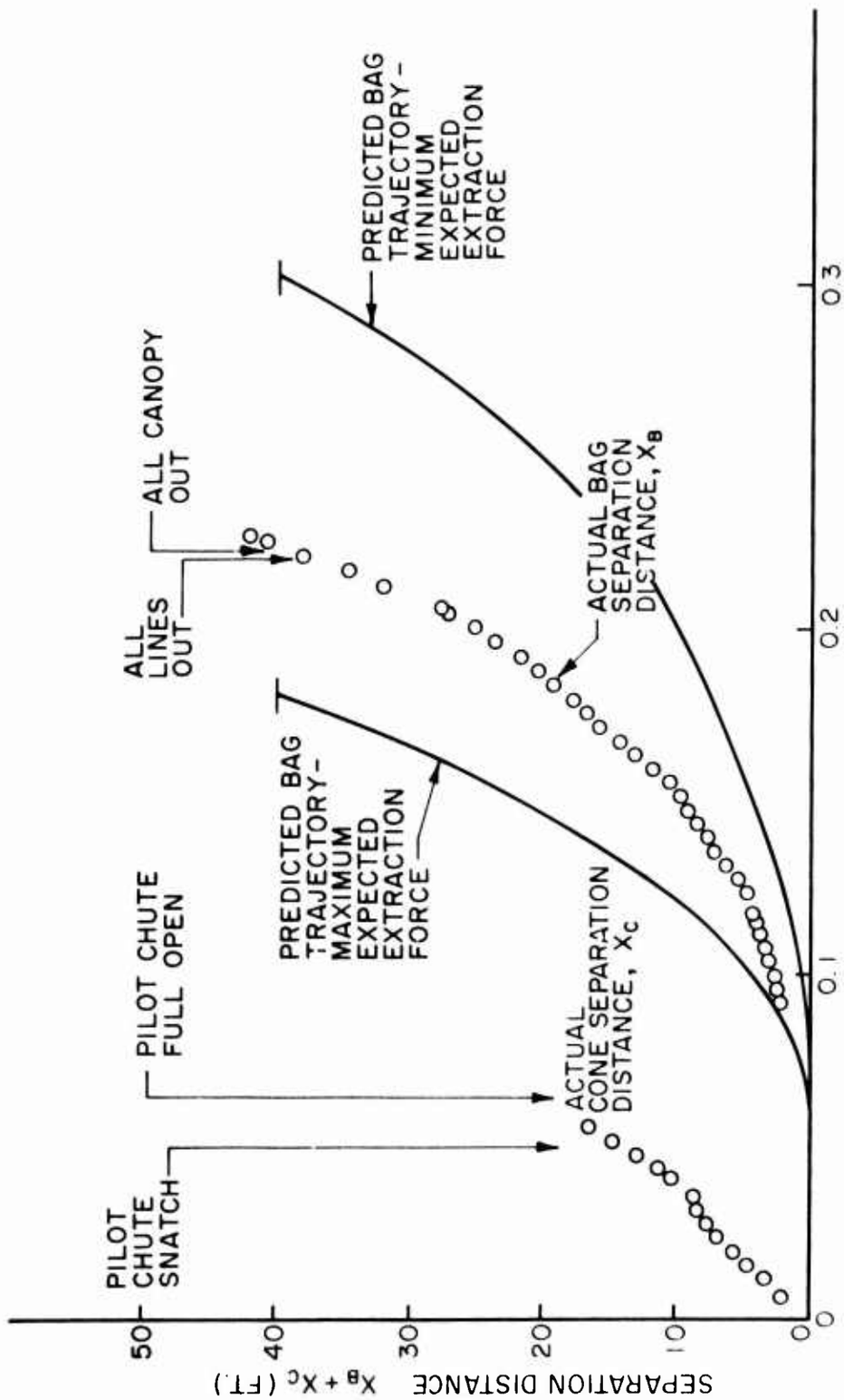

Figure 55. Trajectories of Deployment System Components - Test 6P-H3.

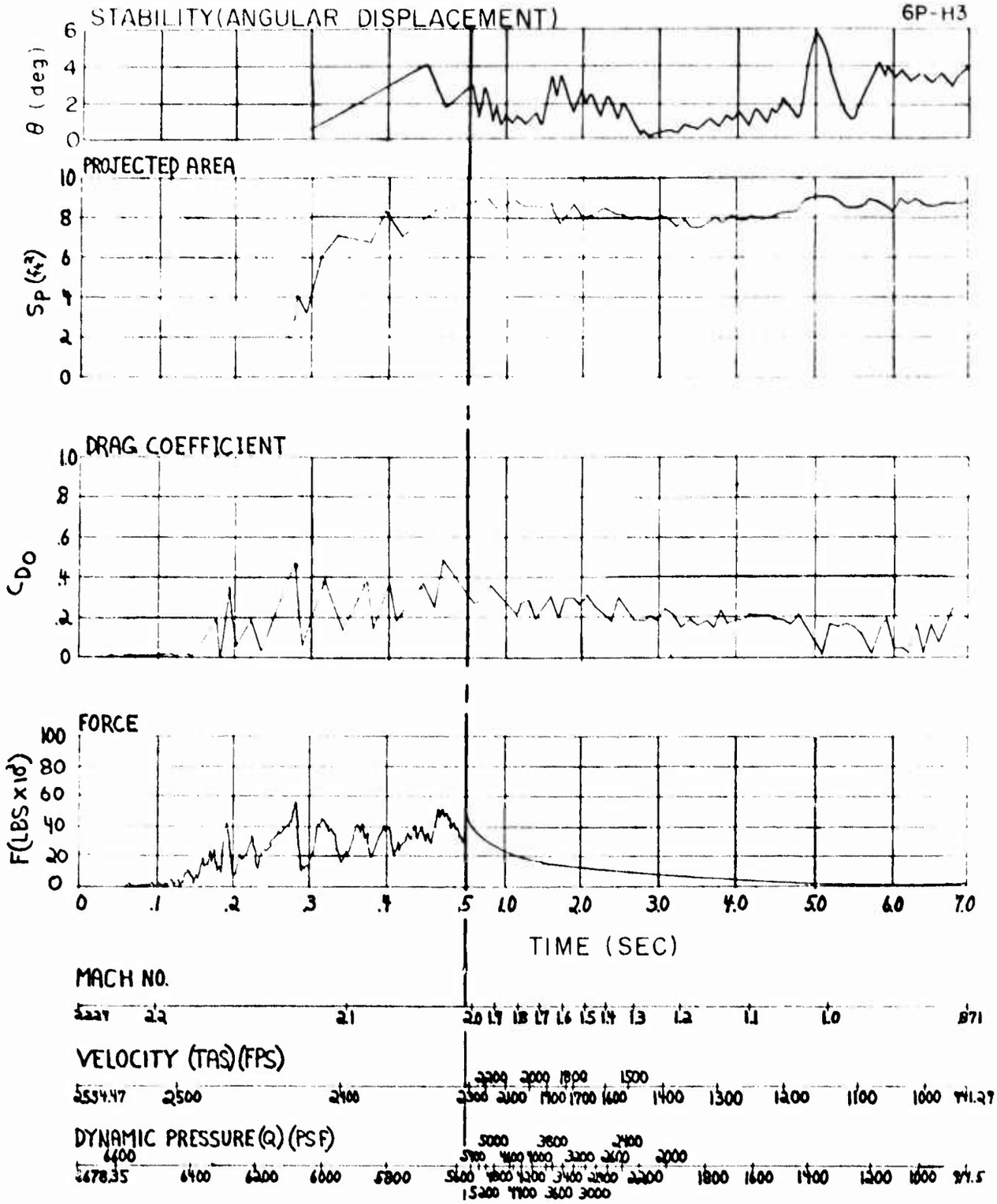

Figure 56. Parachute Performance Curves - Test 6P-H3.

Figure 57. Post Test Photograph of the Test Parachute - Test 6P-H3.

(4) Test 6P-H6; Kevlar Parachute

Parachute deployment was not normal. The cone riser broke at the pin link of the deployment cone immediately after the riser became stretched. Pilot chute deployment and inflation were normal, however. As the test parachute was separating from the sled, the bag turned sideways and exposed a group of lines to the airstream. This group of lines exited the bag prematurely and initiated deployment of the remaining lines and canopy before the bag could fully separate from the sled. Figure 58 shows that all the lines and canopy were out of the bag before the bag had completed 50 percent of its required separation distance from the sled.

Figure 59 presents the parachute performance curves for this test. The parachute reached line stretch with the canopy inflated to approximately 20 percent of its full-open area. A snatch force of 53,674 lb was produced and the canopy was severely damaged. The on-board camera coverage showed that, immediately after line stretch, a number of horizontal ribbons were broken and most of the vertical ribbons were pulled away from the horizontal ribbons. The canopy remained only partially inflated throughout the test run, sustaining considerable additional damage as shown in Figure 60.

(5) Test 6P-H7; Kevlar Parachute

All deployment system components functioned satisfactorily; Figure 61 presents their trajectories.

Parachute operation after line stretch was not normal, however. Immediately upon line stretch, the canopy generated 62,000 lb of snatch force and the confluence keeper broke in two places separating the suspension lines into two groups. Immediately after line stretch, the canopy rebounded toward the sled and the lines went slack. Four more line stretch and rebound cycles followed before the canopy started to inflate.

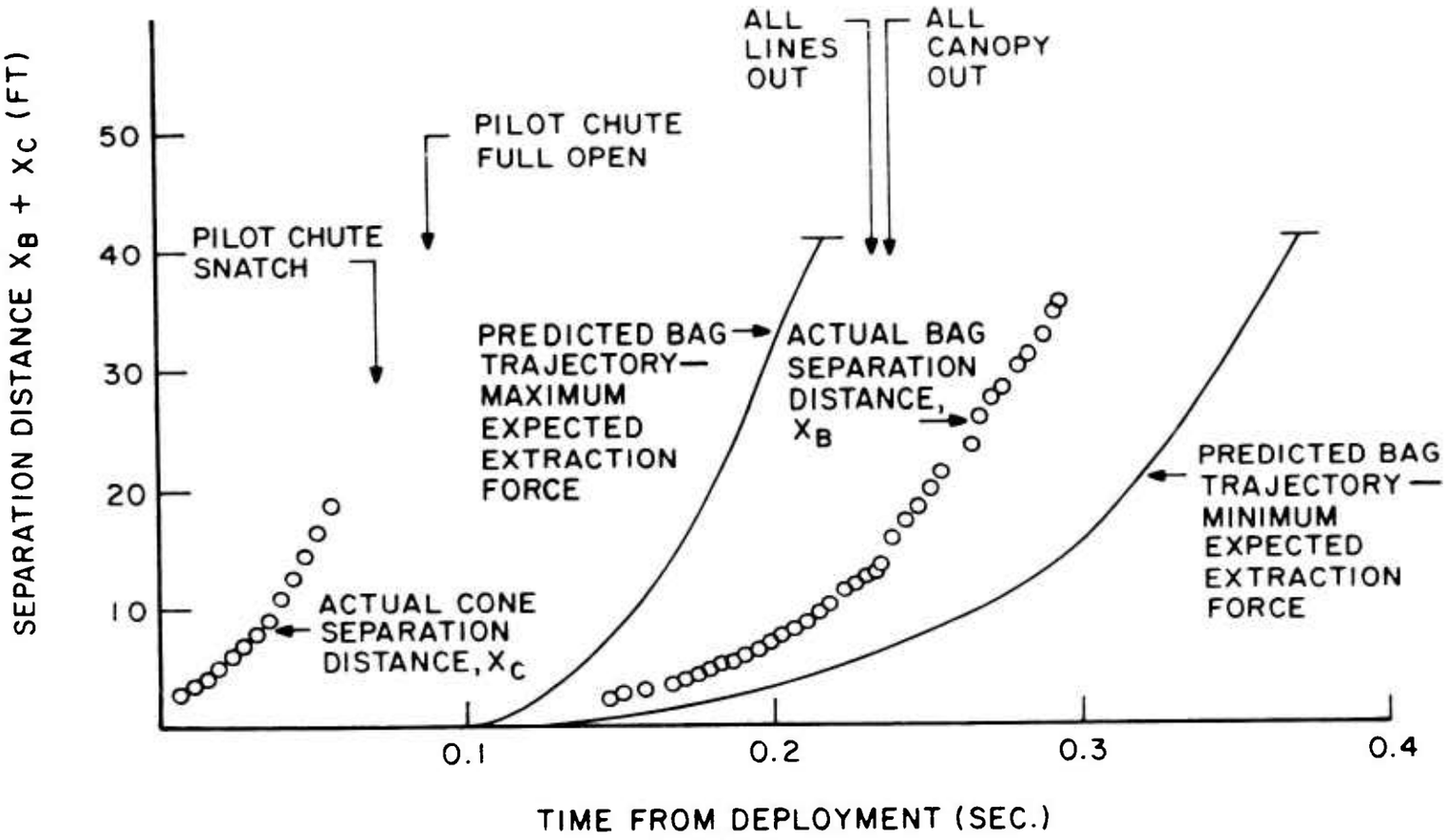

Figure 58. Trajectories of Deployment System Components - Test 6P-H6.

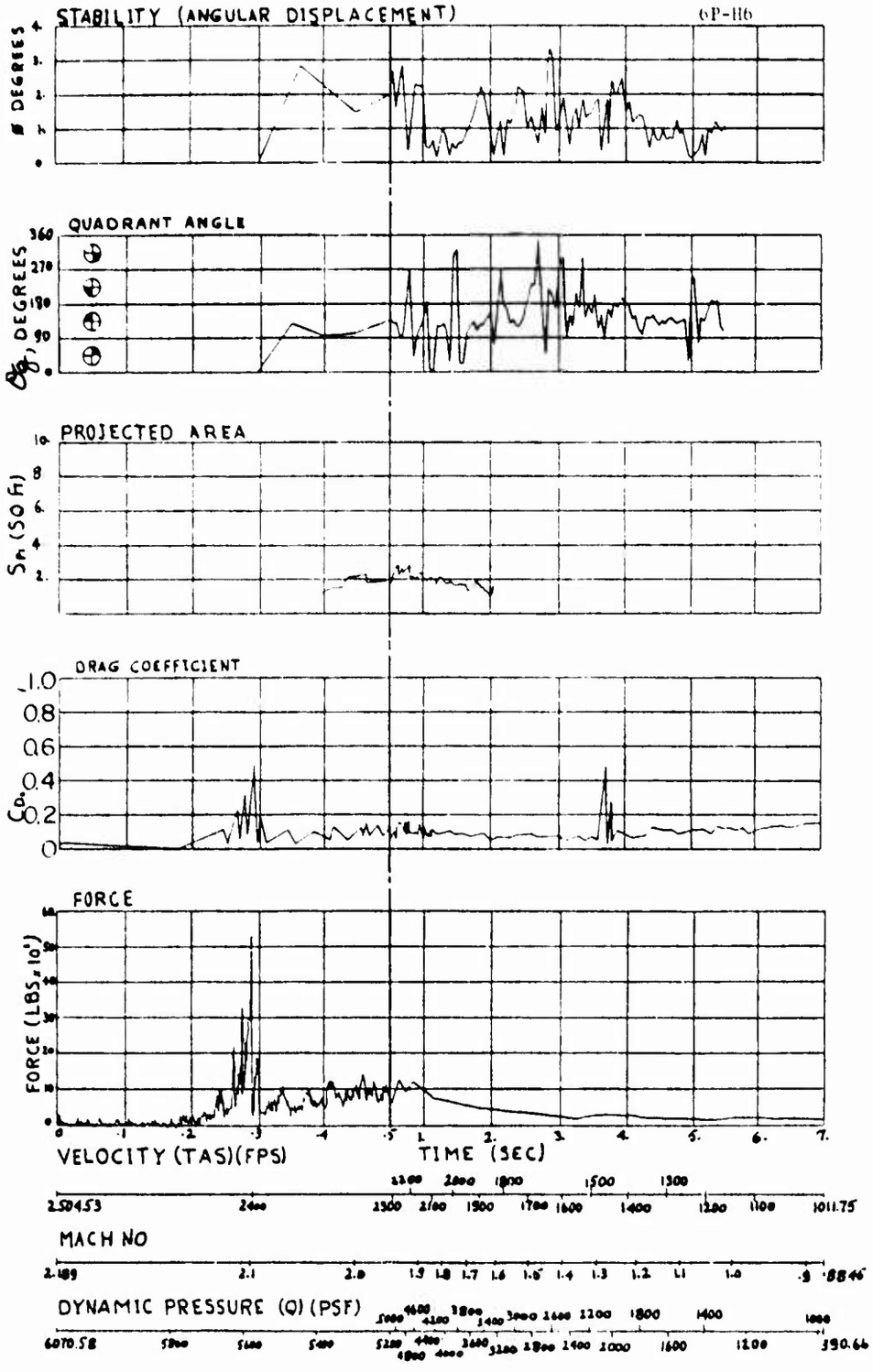

Figure 59. Parachute Performance Curves - Test 6P-H6.

Figure 60. Post Test Photograph of the Test Parachute - Test 6P-H6.

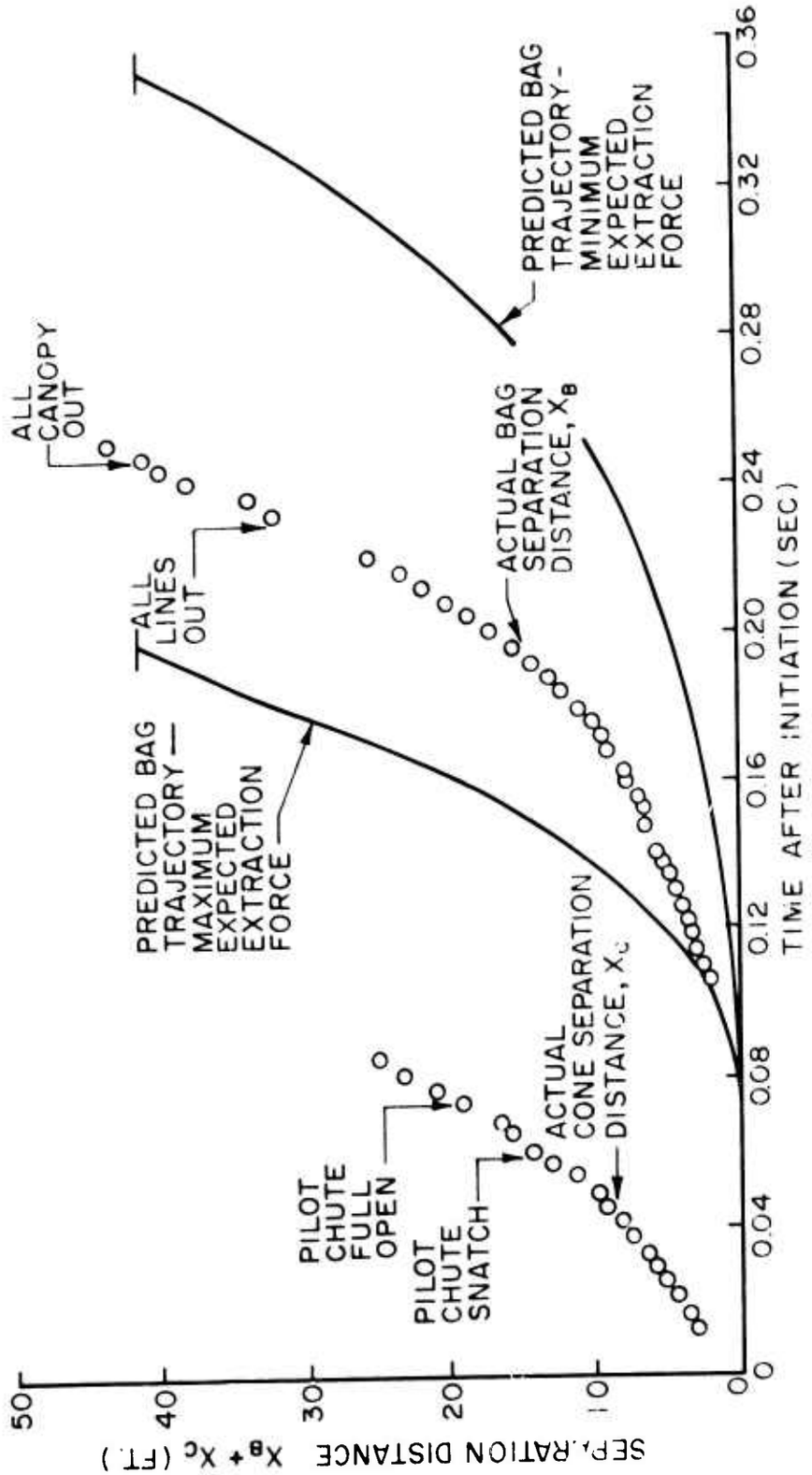

Figure 61. Trajectories of Deployment System Components - Test 6P-H7.

Figure 62 presents the parachute performance curves for this test. Once the parachute became fully inflated, major damage to the vertical ribbons near the canopy skirt could be observed. The canopy remained fully inflated for about 0.25 sec before it collapsed. During this period, the vertical ribbons pulled away from the first four or five rows of horizontal ribbons. This apparently increased canopy porosity an amount sufficient to cause its collapse at a speed of about Mach 1.3. After the sled slowed to about Mach 0.9, the canopy reinflated to full-open. The canopy remained inflated until just before it was released. Canopy damage continued during this period, to the amount shown in Figure 63, and the canopy eventually collapsed.

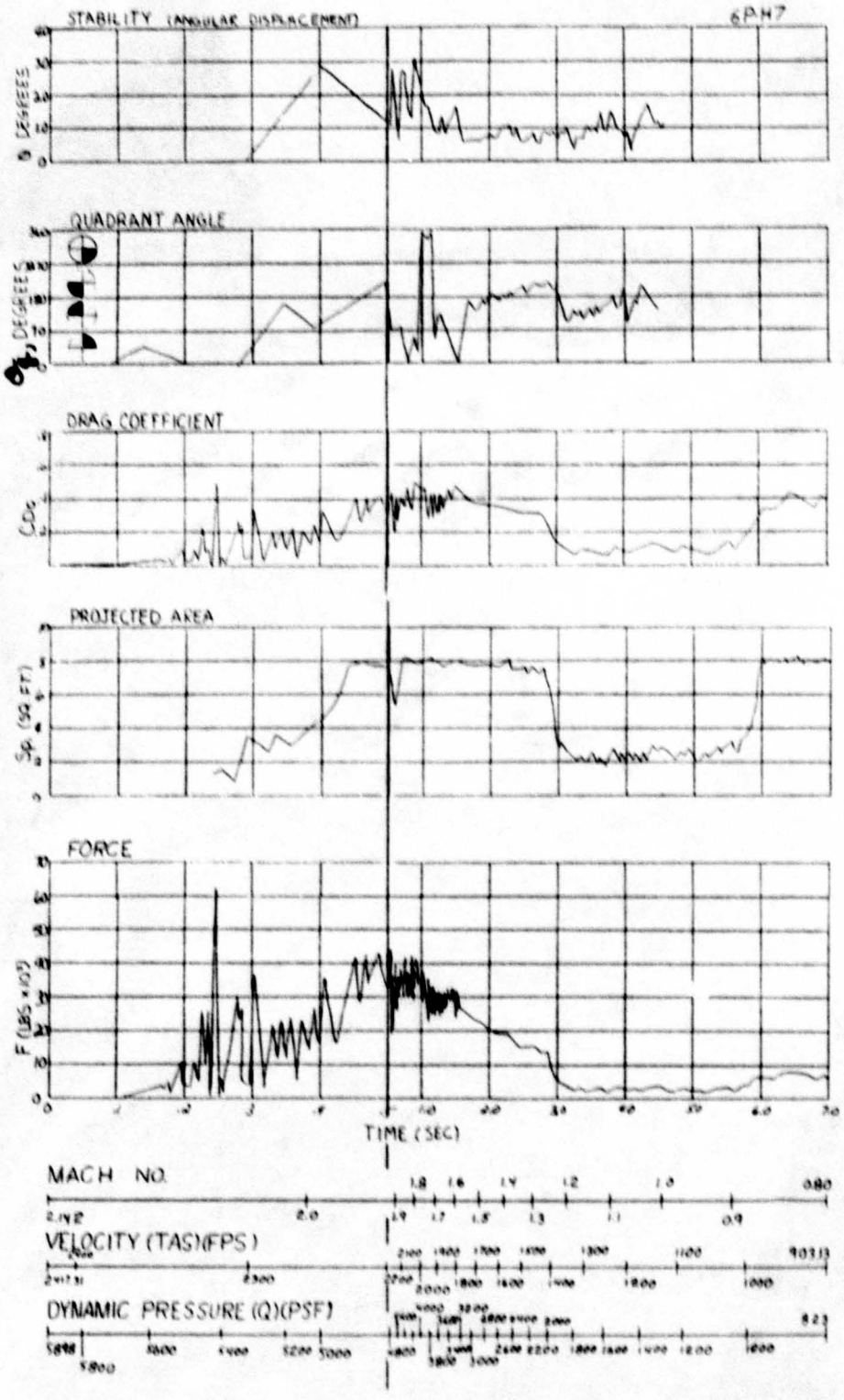

Figure 62. Parachute Performance Curves - Test 6P-H7.

Figure 63. Post Test Photograph of the Test Parachute - Test 6P-H7.

2. PERFORMANCE OF THE DEPLOYMENT SYSTEM COMPONENTS

All sled test runs after 6P-F2 (runs 6 through 20) incorporated the deployment system components described in Appendix C. These components functioned satisfactorily on all but two of the tests. On test 6P-H5, the parachute attachment/deployment/release mechanism malfunctioned and released the parachute immediately upon deployment initiation. On test 6P-H6, the deployment control break ties did not hold the parachute in the bag for the full separation distance of the bag from the sled.

For all tests that provided data and where the deployment system components functioned satisfactorily, the actual separation distance-time histories of the bag fell within the band of trajectories predicted by the calculation technique used to select the strengths of the deployment control break ties. This means that, although little was known about the aerodynamic performance characteristics of the deployment components in the wake of the Arrowhead sled, estimation of minimum and maximum expected performance levels can be used to obtain reasonable results.

Therefore, the deployment control break tie design calculation technique described in Appendix C has been shown to be a satisfactory method which can be used to determine the number, locations, and strengths of parachute break ties that will control the deployment of nylon and Kevlar hemisflo ribbon parachutes at supersonic speeds and high dynamic pressures.

3. PERFORMANCE OF THE TEST PARACHUTES

Values for the important performance parameters of the nylon and Kevlar 5 ft diameter hemisflo parachutes are summarized in Table 8. At each of the three nominal deployment Mach numbers, Mach 1.5, 1.8, and 2.2, sufficient data was obtained to allow for comparative evaluations of the deployment forces, canopy inflation characteristics, steady state performance, and material structural integrity of the nylon and Kevlar parachutes.

a. Deployment Forces

During the period from parachute deployment initiation until the parachute canopy started to inflate, a number of force spikes were recorded on the oscillograph record for each test. The largest force spike usually occurred just before the canopy started to inflate when the lines and canopy were all stretched out and were "snatched" up to the velocity of the sled; that is, at line stretch. This force was called the snatch force. However, on three of the tests the largest force spike occurred prior to line stretch. Values for the maximum force spikes which occurred during deployment were plotted as functions of the freestream dynamic pressure at deployment initiation and are presented in Figure 64. The maximum deployment force increased almost linearly with dynamic pressure for both the nylon and Kevlar parachutes. The Kevlar parachutes exhibited considerably higher deployment forces than the nylon parachutes for dynamic pressures above 3,000 psf.

b. Canopy Inflation Characteristics

(1) Filling Time

The filling time, t_f was taken as the difference between the time of line stretch, t_{LS}, and the time of canopy first full-open, t_{FO}. That is,

TABLE 8

5 ft D_o HEMISFLO RIBBON PARACHUTE PERFORMANCE CHARACTERISTICS

Performance Parameters \ Sled Test	6P-E3	6P-E6	6P-E9	6P-E10	6P-G1	6P-G2	6P-G3	6P-G4	6P-G5	6P-H1	6P-H2	6P-H3	6P-H6	6P-H7
DEPLOYMENT INITIATION														
Time (sec)	0.000	0.000	0.000	0.000	0.000	0.000	0.000	0.000	0.000	0.000	0.000	0.000	0.000	0.000
Mach Number	1.51	1.5	1.41	1.47	1.78	1.77	1.74	1.76	1.73	2.26	2.21	2.23	2.19	2.14
Dynamic Pressure (psf)	2946	2923	2541	2748	4267	4058	3765	3977	3836	6505	6476	6678	6071	5898
MAXIMUM DEPLOYMENT FORCE														
Time (sec)	0.275	0.249	0.251	0.235	0.285	0.340	0.330	0.236	0.30	0.215	0.246	0.194	0.290	0.247
Force (lb)	11,712	12,954	11,021	12,953	22,667	21,318	20,000	30,914	31,500	55,692	41,867	44,267	53,674	62,000
LINE STRETCH														
Time, t_{LS} (sec)	0.301	0.249	0.251	0.235	0.285	0.340	0.330	0.236	0.395	0.215	0.246	0.233	0.290	0.247
Mach Number, M_{LS}	1.44	1.44	1.36	1.42	1.71	1.67	1.64	1.67	1.63	2.24	2.16	2.16	2.10	2.05
Dynamic Pressure, Q_{LS} (psf)	2675	2700	2380	2580	3950	3650	3400	3650	3440	6380	6170	6200	5587	5410
Snatch Force, F_{LS} (lb)	10,513	12,954	11,021	12,953	22,667	21,318	20,000	30,914	11,080	55,692	41,867	32,000	53,674	62,000
CANOPY INFLATION														
Time (sec)	0.380	0.322	---	0.406	0.325	0.463	0.372	---	0.456	0.270	1.301	0.280	---	0.566
Mach Number	1.42	1.42	---	1.36	1.69	1.62	1.63	---	1.61	2.23	1.82	2.12	---	1.90
Dynamic Pressure (psf)	2610	2650	---	2430	3900	3540	3400	---	3370	6340	4400	6086	---	4800
Opening Force, F_o, (lb)	30,719	28,897	---	20,645	38,640	38,854	45,869	---	33,227	73,650	35,200	57,067	---	44,580
Opening Shock Factor, X	---	1.09	---	1.04	1.11	---	1.32	---	1.29	---	---	---	---	1.12
FIRST FULL-OPEN														
Time, t_{FO} (sec)	0.380	0.322	---	0.457	0.334	0.442	0.368	---	0.456	---	1.357	0.541	---	0.438
Mach Number	1.42	1.42	---	1.36	1.69	1.63	1.63	---	1.61	---	1.82	2.02	---	1.97
Dynamic Pressure, Q_{FO} (psf)	2610	2650	---	2430	3900	3550	3350	---	3370	---	4400	5450	---	4900
Filling Time, $t_f = t_{FO} - t_{LS}$ (sec)	0.079	0.073	---	0.222	0.049	0.101	0.038	---	0.061	---	---	---	---	0.191
STEADY STATE (Average for first Second)														
Drag Coefficient, C_{D_o}	---	0.50	---	0.39	0.45	---	0.52	---	0.38	---	0.40	---	---	0.38
Stability Angle, θ (deg)	---	0.8	---	0.6	2.0	---	2.0	---	0.8	---	1.5	---	---	1.0
Projected Area, (sq ft)	---	7.6	---	7.6	8.6	---	9.0	---	8.4	---	8.5	---	---	7.8
PARACHUTE COMPONENTS														
Material Type	Nylon	Nylon	Kevlar	Kevlar	Nylon	Nylon	Nylon	Kevlar	Kevlar	Nylon	Nylon	Nylon	Kevlar	Kevlar
Time of Failure (sec)	0.380	---	0.251	0.75	0.43	0.550	---	0.26	---	0.270	---	0.32	0.290	0.438
Suspension Line Strength (lb)	6000	6000	6000	6000	8000	12,000	12,000	8000	12,000	15,000	18,000	18,000	18,000	24,000
Suspension Line Damage	Major	None	None	None	Major	Major	None	None	None	Major	None	None	None	None
Horizontal Ribbon Strength (lb)	2000	3000	2000	3000	3000	4000	4000	3000	4000	5000	6000	6000	6000	8000
Horizontal Ribbon Damage	Major	None	Minor	Minor	Major	Major	None	Major	None	None	Minor	Major	Major	None
Vertical Ribbon Strength (lb)	1250	1250	1500	1500	1250	1250	1250	1500	1500	2500	2500	2500	3000	3000
Vertical Ribbon Damage	None	None	Major	Major	None	None	None	Major	None	Major	None	None	Major	Major
Skirt Band Strength (lb)	4500	6500	4500	6500	6500	8700	8700	6500	8700	11,000	13,000	13,000	13,000	17,400
Skirt Band Damage	Major	None	None	None	Major	Major	None	None	None	None	None	None	None	None

$$t_f = t_{FO} - t_{LS} \qquad (8)$$

where canopy first full-open was defined as that event where the value of the canopy projected area during inflation first equaled the steady state projected area.

Filling times are tabulated in Table 8 only for those tests where canopy inflation was considered normal. All filling times were relatively short, less than 0.23 seconds, and did not appear to be influenced by deployment conditions or parachute material type.

(2) Opening Force

The opening force, F_o, was defined as that peak force which occurred during canopy inflation or just after canopy first full-open. Values for the opening force are plotted as functions of dynamic pressure in Figure 65. For given line stretch dynamic pressures, the opening forces for the Kevlar parachutes were lower than the opening forces for the nylon parachutes.

Also plotted on Figure 65 are the straight lines obtained using the equation on page 164 of the "Parachute Handbook" (Reference 6) which is recommended for calculating opening forces. This equation was written as:

$$F_o = C_{D_o} S_o Q_{LS} X \qquad (9)$$

where: (1) C_{D_o} was the average value of the steady state drag coefficients, 0.468 for the nylon parachute and 0.383 for the Kevlar parachutes; (2) S_o was the nominal canopy area, 19.635 sq ft for both parachute types; (3) Q_{LS} was the independent parameter of dynamic pressure at line stretch; and (4) X was the average value of the opening shock factors, 1.17 for the nylon parachute and 1.15 for the Kevlar parachutes. Because the data groups closely around the straight

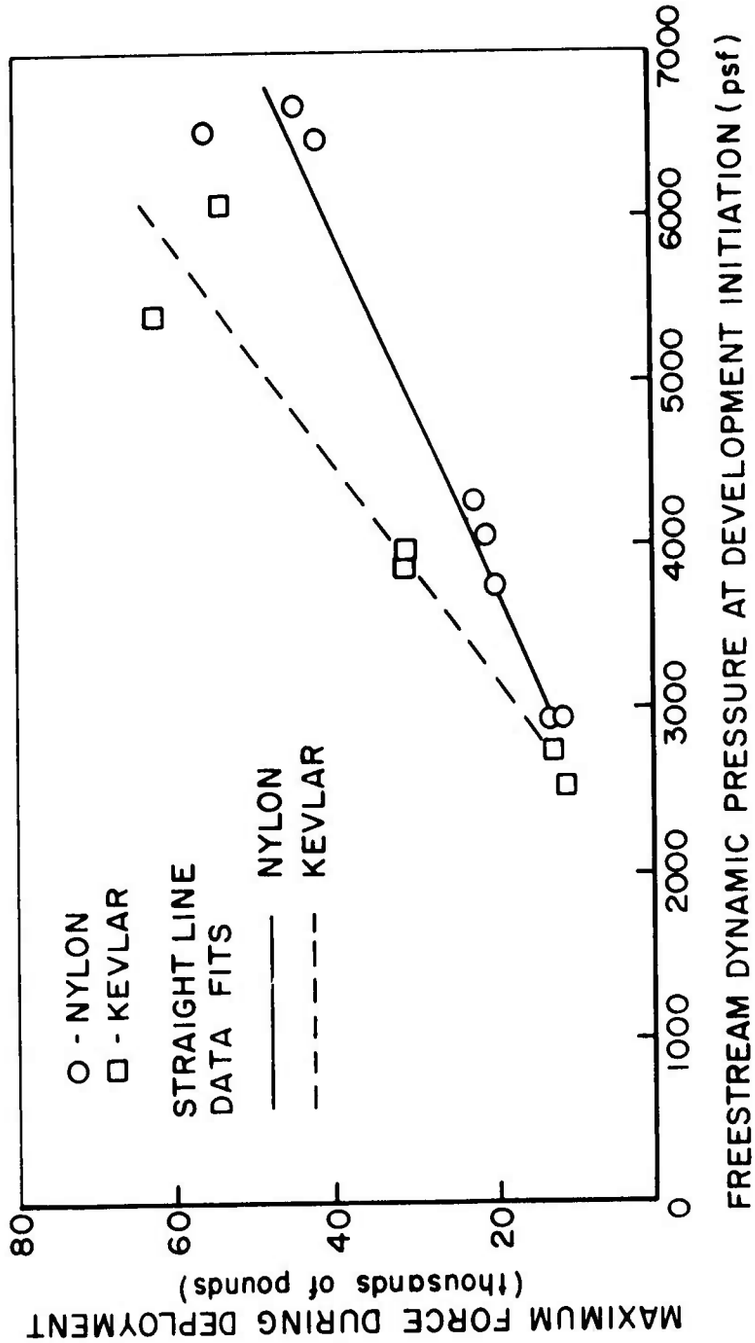

Figure 64. Variation of Deployment Force with Dynamic Pressure for Nylon and Kevlar Parachutes.

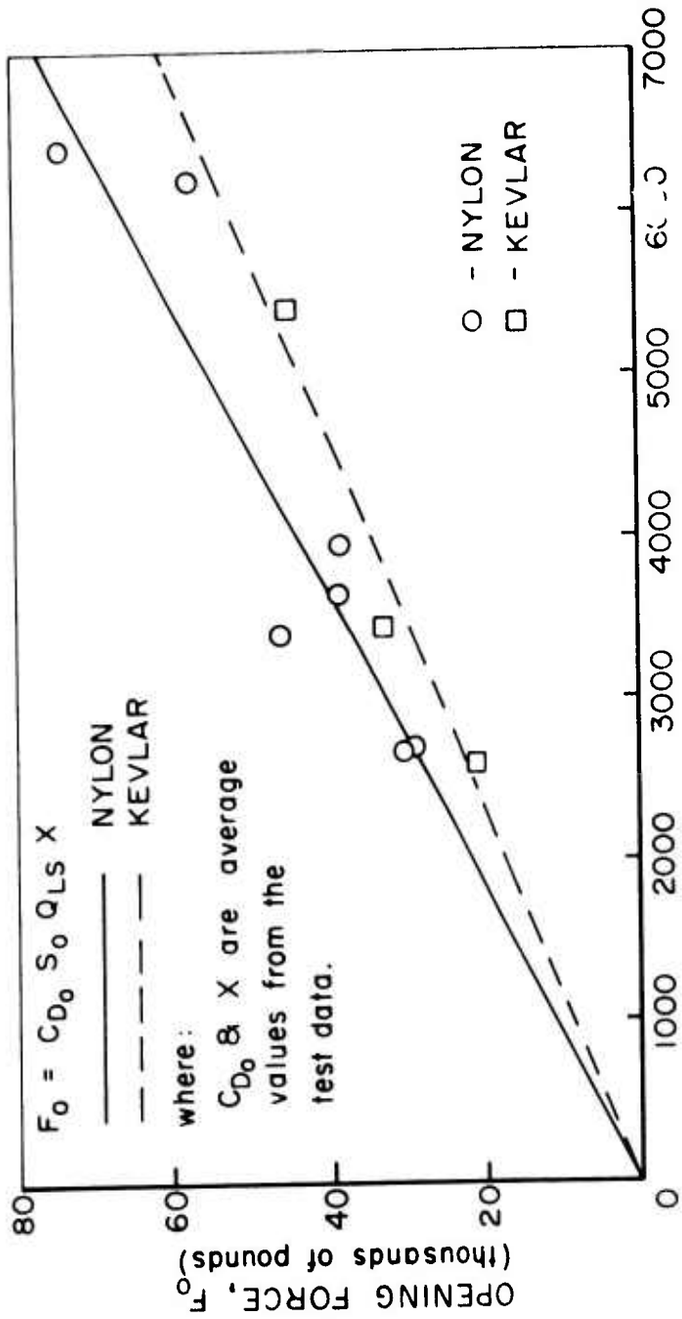

Figure 65. Variation of Opening Force with Dynamic Pressure for Nylon and Kevlar Parachutes.

lines, it is apparent that Equation 9 can be used to yield reasonable approximations of the peak forces generated during canopy inflation of nylon and Kevlar hemisflo ribbon parachutes at supersonic speeds and high dynamic pressures.

(3) Opening Shock Factor

An opening shock factor, X, was defined as the ratio of the opening force, F_o, and the product of the average steady state drag coefficient, C_{D_o}, the nominal canopy area, S_o, and the dynamic pressure at line stretch, Q_{LS}. That is:

$$X = F_o/(C_{D_o} S_o Q_{LS}). \quad (10)$$

A value for opening shock factor was calculated only for those tests which had normal canopy inflation and from which a steady state drag coefficient was obtained.

The average opening shock factors for the nylon and Kevlar hemisflo ribbon parachutes were approximately the same, 1.17 for nylon and 1.15 for Kevlar.

c. Steady State Performance

(1) Drag Coefficient

The steady state drag coefficient, C_{D_o}, was defined as the ratio of the instantaneous parachute drag force, D, and the product of the instantaneous dynamic pressure, Q, and the nominal canopy area, S_o. That is:

$$C_{D_o} = D/(Q S_o) \quad (11)$$

An average value for the steady state drag coefficient over approximately 1 sec of parachute operation is tabulated

in Table 8 for each test that had normal steady state parachute operation. These were the values used in the opening shock factor equation. Averages of these values were used in the opening force equation. The overall average steady state drag coefficient for the nylon parachutes of 0.468 was 22 percent higher than the average value of 0.383 for the Kevlar parachutes.

Steady state drag coefficients were also plotted as functions of Mach number and dynamic pressure and are presented in Figures 66 and 67 The drag coefficients for the nylon parachutes were higher than for the Kevlar parachutes for all Mach numbers and dynamic pressures.

Various suspected causes for these differences in drag coefficients were analyzed, including differences in canopy projected area, increased canopy porosity due to vertical ribbon damage on some of the Kevlar parachutes, and parachute stability. No explanation was found for the fact that the nylon hemisflo ribbon parachutes exhibited higher steady state drag coefficients than their Kevlar counterparts.

(2) Stability Angle

After the parachute became full-open, the oscillation angles for all parachute types were very small, usually less than 2 deg. Therefore, the oscillatory stability for both nylon and Kevlar hemisflo ribbon parachutes operating at supersonic speeds and high dynamic pressures can be considered excellent.

(3) Projected Area

The average full-open projected area (for approximately 1 sec after first full-open) of the undamaged nylon parachutes ranged from 7.6 to 9.0 sq ft, with an overall average value of 8.4 sq ft. The projected area of the Kevlar

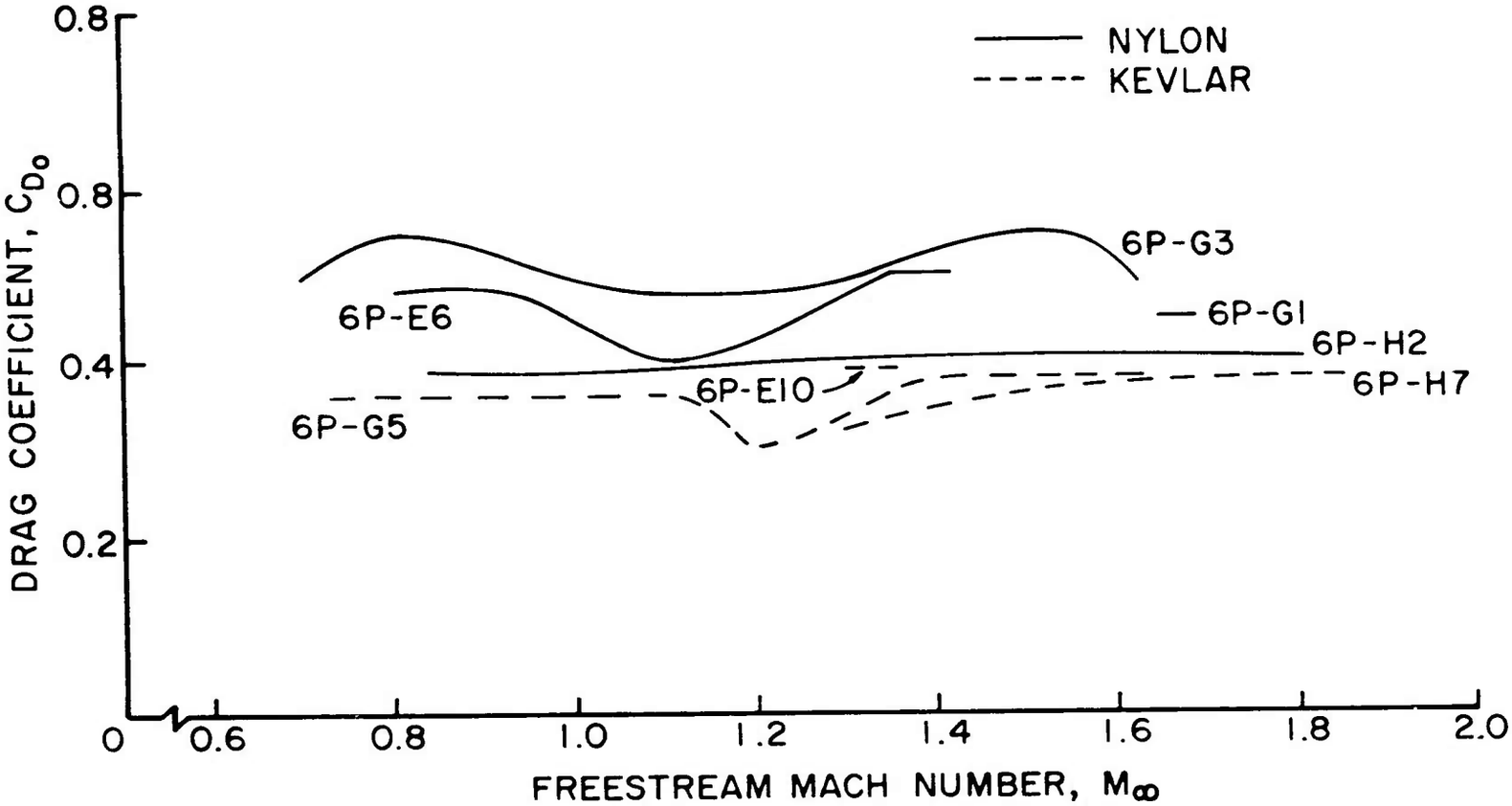

Figure 66. Variation of Drag Coefficient with Mach Number for Nylon and Kevlar Parachutes.

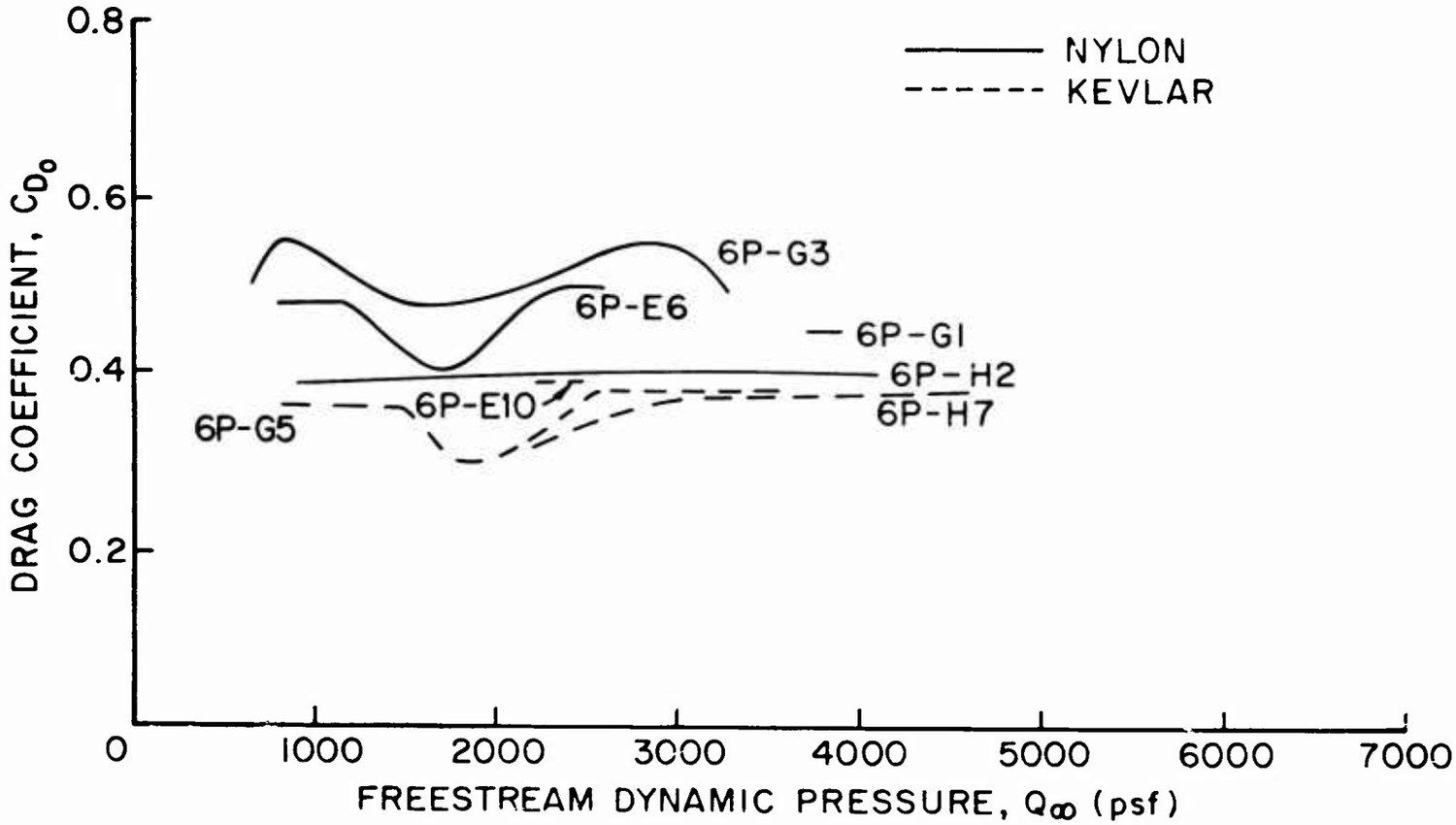

Figure 67. Variation of Drag Coefficient with Dynamic Pressure for Nylon and Kevlar Parachutes.

parachutes ranged from 7.6 to 8.4 sq ft, with an overall average value of 7.9 sq ft. The average projected area of the nylon parachutes, then, was 6 percent higher than the average projected area of the Kevlar parachutes.

The average projected areas yield average inflated diameters of 3.3 and 3.2 ft, respectively, for the nylon and Kevlar parachutes.

d. Material Structural Integrity

Since one of the basic objectives of the test program was to determine design criteria for the strength of the material components of the nylon and Kevlar parachutes, the test conditions and material strengths were chosen such that ultimate loads might be determined for the suspension lines, horizontal ribbons, and the skirt band. Assessment of the damage incurred during specific portions of the test run has yielded some measure of the structural integrity of certain material components of nylon and Kevlar hemisflo ribbon parachutes operating at supersonic speeds and high dynamic pressures.

(1) Suspension Lines

The nominal rated breaking strengths of the suspension lines, SLS, are plotted as functions of the peak opening force, or snatch force where appropriate, in Figure 68. Also plotted in the Figure is the straight line described by the equation which is recommended on page 378 of the "Parachute Handbook" (Reference 6) for selecting the strength of the suspension lines for deceleration (drogue) parachutes of aerospace vehicle recovery systems.

For the nylon parachutes, all but one of the parachutes which had suspension line strengths below the design line exhibited major structural damage to the lines. And, all but one of the nylon parachutes which had suspension

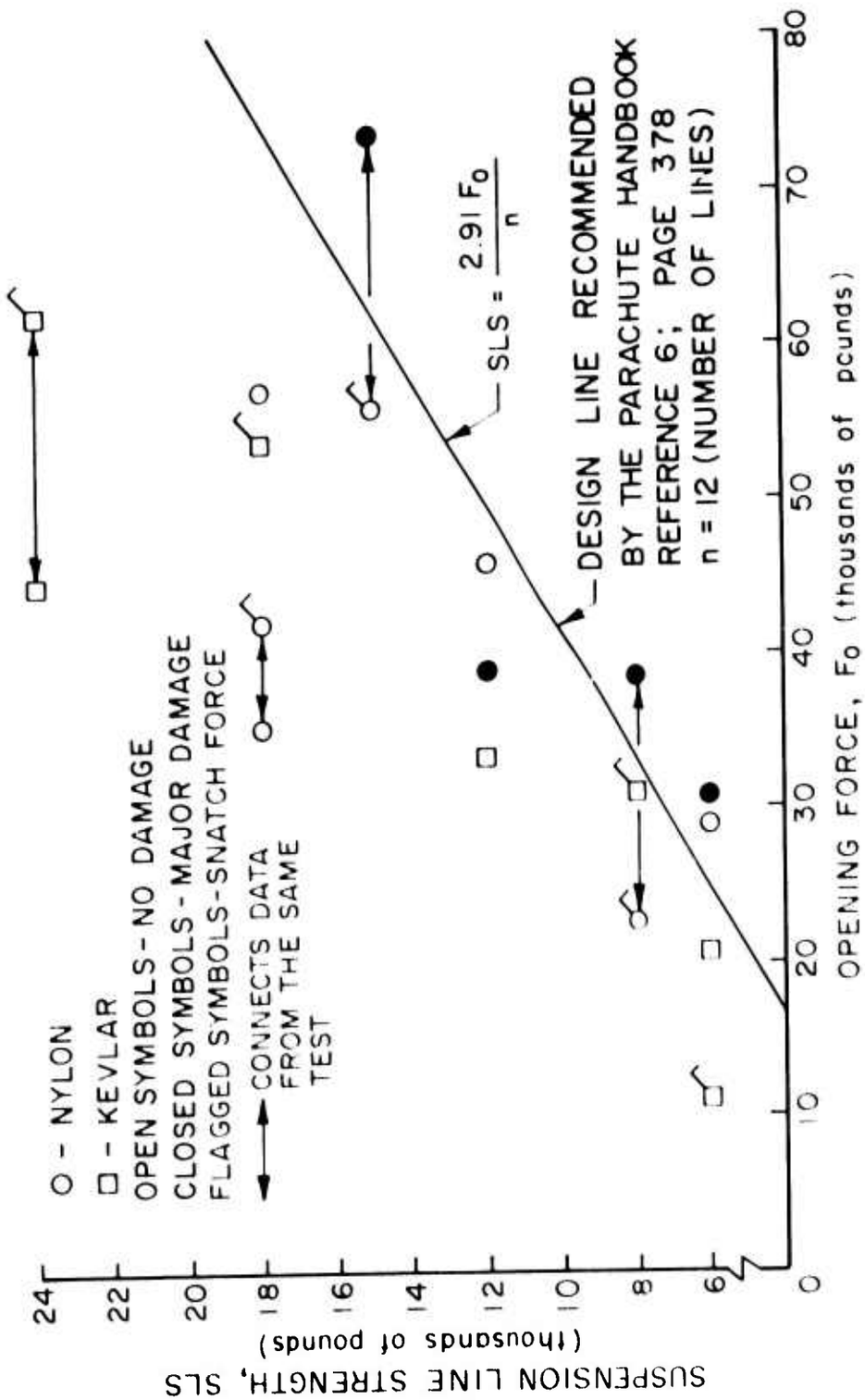

Figure 62. Suspension Line Damage as a Function of Line Strength and Opening Force.

line strengths above the design line exhibited no structural damage to the suspension lines. This means that the line described by the Handbook Equation is a better approximation of the ultimate suspension line load rather than a design line to be used for selecting adequate suspension line strengths for nylon hemisflo parachutes which operate at supersonic speeds and high dynamic pressures.

No Kevlar suspension lines failed during this test program and no Kevlar parachute produced opening or snatch forces sufficiently large enough to yield suspension line strengths below the design line. Therefore, no design criteria could be established for the suspension lines of the Kevlar parachutes.

(2) Horizontal Ribbons

The nominal rated breaking strengths of the horizontal ribbons, HRS, are plotted as functions of the peak opening force in Figure 69. Also plotted in the Figure is a line through the data which is described by the equation

$$HRS = 0.12\ F_o \qquad (12)$$

Because none of the nylon or Kevlar parachutes which had ribbon strengths above the line exhibited any structural damage to the horizontal ribbons, while some of those below the line did show major ribbon damage, Equation 12 can be used as a first approximation of the ultimate load in the horizontal ribbons of nylon and Kevlar hemisflo parachutes operating at supersonic speeds and high dynamic pressures.

(3) Vertical Ribbons

While the vertical ribbons are not generally considered a major structural load-carrying component of

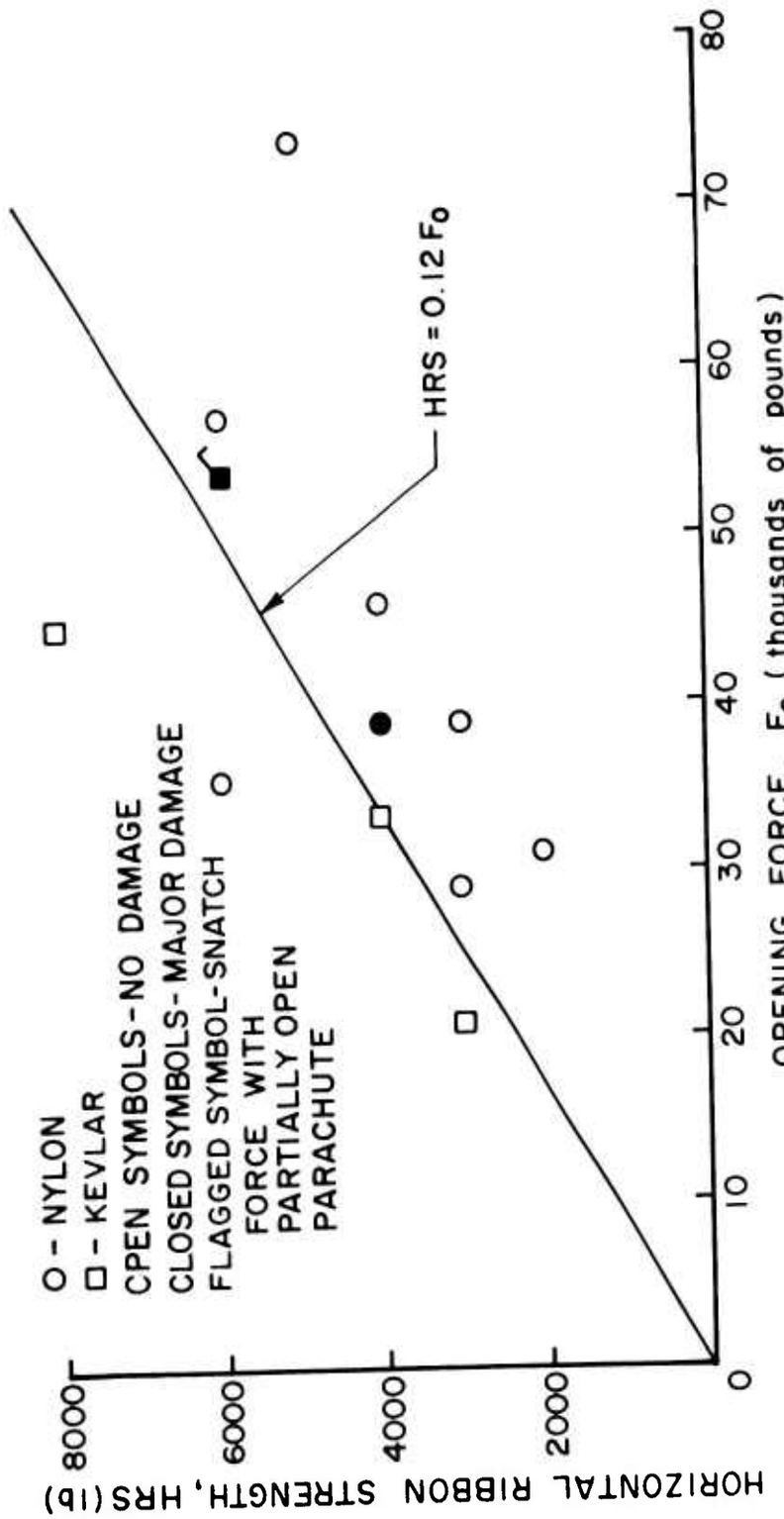

Figure 69. Horizontal Ribbon Damage as a Function of Ribbon Strength and Opening Force.

ribbon parachutes, the amount of damage sustained by these ribbons during this test program may justify a reapraisal of that philosophy; especially for Kevlar ribbon hemisflo parachutes operating at supersonic speeds and high dynamic pressures. Five out of the six Kevlar parachutes tested during this program sustained major damage to the vertical ribbons; on three of the tests they were the only components to sustain major damage.

(4) Other Components

Structural damage to other parachute material components such as skirt and vent bands, radial webbings, and vent lines did not occur over a wide enough range of test and performance parameters to permit the establishment of any structural design criteria for them.

SECTION IV
CONCLUSIONS

A total of 20 sled test runs were made during this test program; 3 tests provided no parachute performance data because of deployment system malfunctions, 3 tests were made at Mach 1.2 to establish a high speed, high dynamic pressure deployment technique, and 14 tests provided sufficient data at each of three nominal deployment Mach numbers, Mach 1.5, 1.8, and 2.2, to allow for the comparative evaluations of the performance characteristics of 5 ft diameter nylon and Kevlar hemisflo parachutes operating at dynamic pressures up to 6000 psf.

(1) The maximum deployment forces increased almost linearly with deployment dynamic pressures for both the nylon and Kevlar parachutes. The Kevlar parachutes exhibited approximately 50 percent higher deployment forces than the nylon parachutes for dynamic pressures from 4000 to 6500 psf; at 3000 psf, the deployment forces for the nylon and Kevlar parachutes were approximately equal.

(2) The filling times for both parachutes were relatively short, less than 0.23 sec, and did not appear to be influenced by deployment conditions or parachute material type.

(3) For line stretch dynamic pressures from 2600 to 6400 psf, the opening forces for the Kevlar parachutes were approximately 22 percent lower than for the nylon parachutes.

(4) The average opening shock factors for the nylon and Kevlar hemisflo ribbon parachutes were approximately the same, 1.17 for nylon and 1.15 for Kevlar.

(5) The overall average steady-state drag coefficient for the Kevlar parachutes of 0.383 was 18 percent lower than the average value of 0.468 for the nylon parachutes.

(6) The steady-state oscillatory stability for both nylon and Kevlar hemisflo parachutes was considered excellent; stability angles were 2.0 degrees or less.

(7) The average, full-open projected area of the nylon parachutes of 8.4 sq ft was 6 percent higher than the average projected area of the Kevlar parachutes of 7.9 sq ft.

Assessment of the damage incurred during specific portions of the test runs has yielded some measure of the structural integrity of certain material components of nylon and Kevlar parachutes operating at supersonic speeds and high dynamic pressures.

(1) The "Parachute Handbook" Equation of SLS = 2.91 F_o/n (Reference 6), which has been used in the past to select suspension line strengths, SLS, for droque type parachutes in terms of parachute opening force, F_o, and the number of suspension lines, n, has been shown to give a good approximation of the ultimate load in the suspension lines of nylon hemisflo parachutes operating at line stretch dynamic pressures from 2400 to 6400 psf.

(2) The ultimate load in the horizontal ribbons, HRS, of nylon and Kevlar hemisflo parachutes operating at line stretch dynamic pressures from 2400 to 6400 psf can be approximated by the Equation HRS = 0.12 F_o.

(3) The considerable amount of damage sustained by the vertical ribbons, especially on the Kevlar parachutes, during this test program indicates that the generally accepted practice of assuming that the vertical ribbons are not a major load-carrying component may have to be revised.

For approximately equal strength hemisflo parachutes, the weights of the Kevlar canopies were between 38 and 55 percent of the weights of the nylon canopies. Thus, the results from this test program have shown the realization

of the potential weight savings of Kevlar substitution for nylon in hemisflo ribbon parachutes.

There were no significant difficulties associated with the fabrication of the parachutes made from the new high-strength, low-modulus Kevlar materials.

The deployment control break tie design calculation technique presented in this report has been shown to be a satisfactory method which can be used to determine the number, locations, and strengths of parachute break ties that will control the deployment of nylon and Kevlar hemisflo ribbon parachutes at supersonic speeds and high dynamic pressures. This calculation technique also provides satisfactory predictions of separation distance- time histories of the parachute bag during deployments from the Arrowhead and Tomahawk sleds.

The Supersonic-X-3 parachute performed well as a pilot chute on all tests during this program; for deployment Mach numbers from 1.2 to 2.2 and deployment dynamic pressures from 2110 to 6678 psf.

APPENDIX A
DESCRIPTION OF THE ARROWHEAD SLED

1. PRELIMINARY DESIGN

a. Design Requirements for a Mach 3 Sled

In June 1960, what is now the Recovery and Crew Station Branch of the Air Force Flight Dynamics Laboratory awarded a contract to the Cook Research Laboratories (CRL), a division of the Cook Electric Company, Chicago, Illinois, to develop, design, construct, and test a parachute ground-borne rocket propelled test vehicle capable of deploying deceleration devices at a sea level speed of Mach 3.

Specifically: the test vehicle was to be suitable for operation on the (then) 20,000 ft track at Edwards Air Force Base, California; a pusher type sled vehicle was to be considered; the maximum sled weight, not including the solid-fuel rocket motors, was not to exceed 5,000 lb; a minimum speed of 3,300 ft/sec was to be obtained at the time of parachute deployment; the minimum distance between fore and aft slipper pairs was to be 18 ft; the minimum height of attachment point for the aerodynamic deceleration device was to be 7 ft above the top of the rails; the subsonic drag area of the sled was to be less than 12 sq ft; the structure of the test vehicle was to be designed to accommodate a maximum horizontal drag load of 200,000 lb, and a lateral load up to 30,000 lb, to be applied at the parachute attachment point; a rectangular container with a clear storage volume of 2.5 cu ft for storing the parachute was to be provided; and, the vehicle was to be capable of withstanding all forces and accelerations imposed upon it during operation.

b. Basic Configuration

The sled configuration selected by CRL to meet the above requirements had as its primary member a swept vertical fin whose plan form described a half-delta section. This fin member positioned the parachute attachment point seven feet above the track rail and transferred loads developed by the parachute to fore and intermediate cross members. These structural cross members distributed the loads through the slippers equally to each of the track rails. Power to drive the sled was to be provided by five rocket motors positioned in-line in a horizontal plane and mounted to the aft face of the intermediate cross member at the base of the vertical fin. Fairings were provided ahead of each of the sled cross members to minimize drag and flow field interferences. A third cross member supported the nozzle end of the rocket motors. Spacers were provided at the head end of the rocket motors to permit installation of the motor ignitors.

The CRL sled design called for the use of the slippers, the water brake, and the pusher sled which were available at the Edwards Track and would be adaptable for use with either Genie or Nike rocket motors.

Several innovations, unique for parachute sleds, were incorporated in the CRL design to minimize weight and insure structural integrity. A large portion of the water brake was to be buried within the sled structure. Honeycomb panels were to be used in place of sheet metal skin over most of the external surface. And, the leading edge fairing of the swept vertical fin would also serve as part of the main parachute load tension member.

The sled control system and instrumentation electronics were to be packaged in a compartment in the horizontal structure forward of the intermediate cross member. The movie

cameras were to be mounted in a compartment below the parachute storage compartment on the aft face of the vertical fin.

A sketch of the Mach 3 sled configuration selected by the Cook Research Laboratories is shown in Figure A-1.

c. Wind Tunnel Tests

Wind tunnel tests were performed at the CRL wind tunnel to compare characteristics of two basic sled shapes and to confirm performance predictions. The test program investigated the variation of drag area, normal force, and wake interference effects for the candidate configurations. The Mach number range covered was from 1.84 to 2.00. Figure A-2 shows a photograph of the wind tunnel models tested.

The wind tunnel test results indicated that the in-line configuration results in higher performance than the up-swept configuration and that the up-loads for both configurations were within maximum allowable track limits. Analysis of schlieren photographs indicated that both configurations exhibit similar flow field characteristics. The results from analyses of the schlieren photographs and wake survey pressure measurements are presented in Figure A-3.

The above information on the preliminary design of the Arrowhead sled was obtained from Reference 9.

---

(9) Broderick, Milan A.: Study, Design and Fabrication of a Supersonic Parachute Sled Test Vehicle, Contract No. AF 33(616)-7407), Cook Research Laboratories Design Analysis Report P-2019, November 1960, and Progress Reports P-2019, 1 through 5, August 1960 through April 1961.

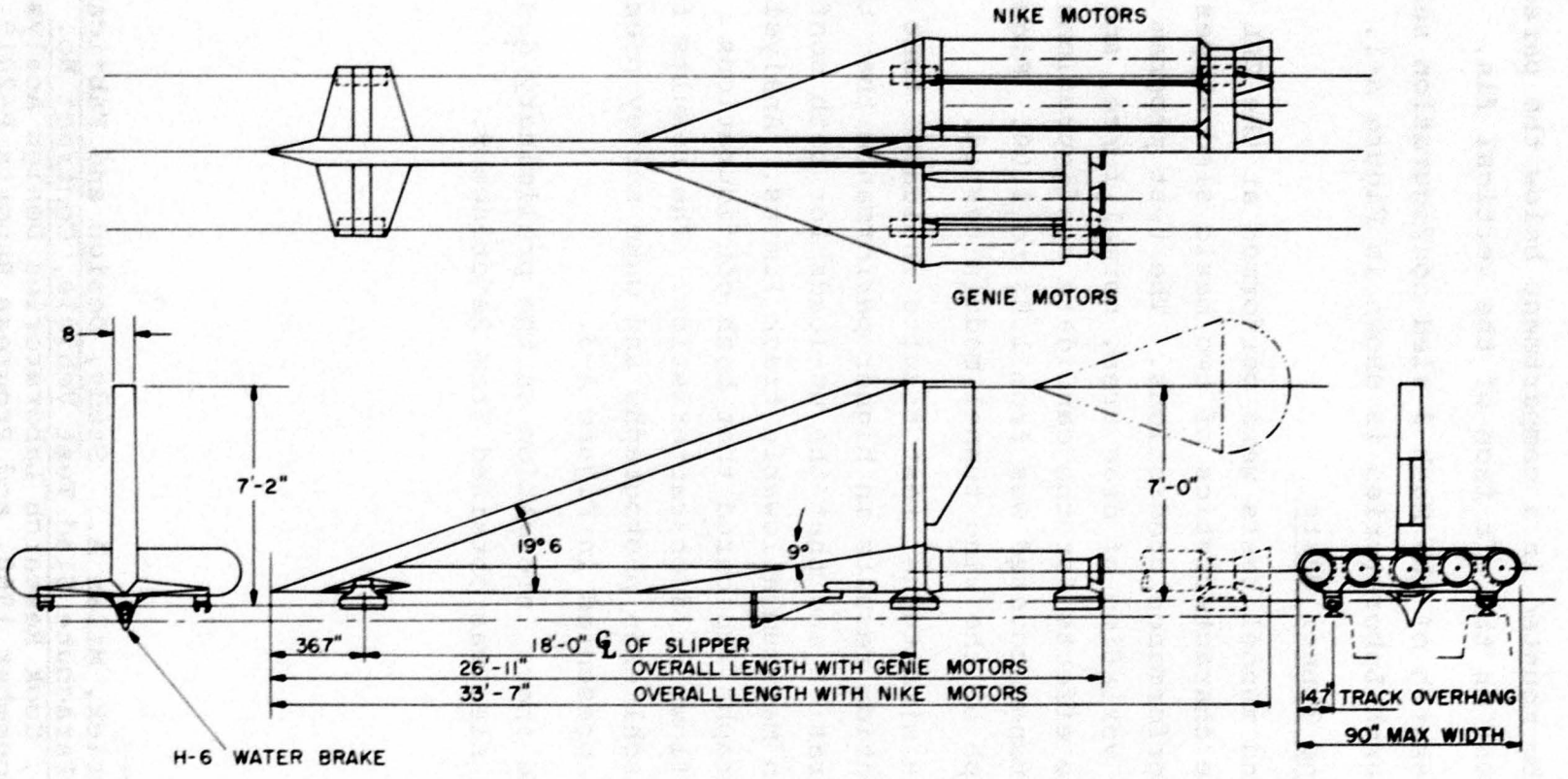

Figure A-1. Sketch of the Preliminary Mach 3 Sled Configuration.

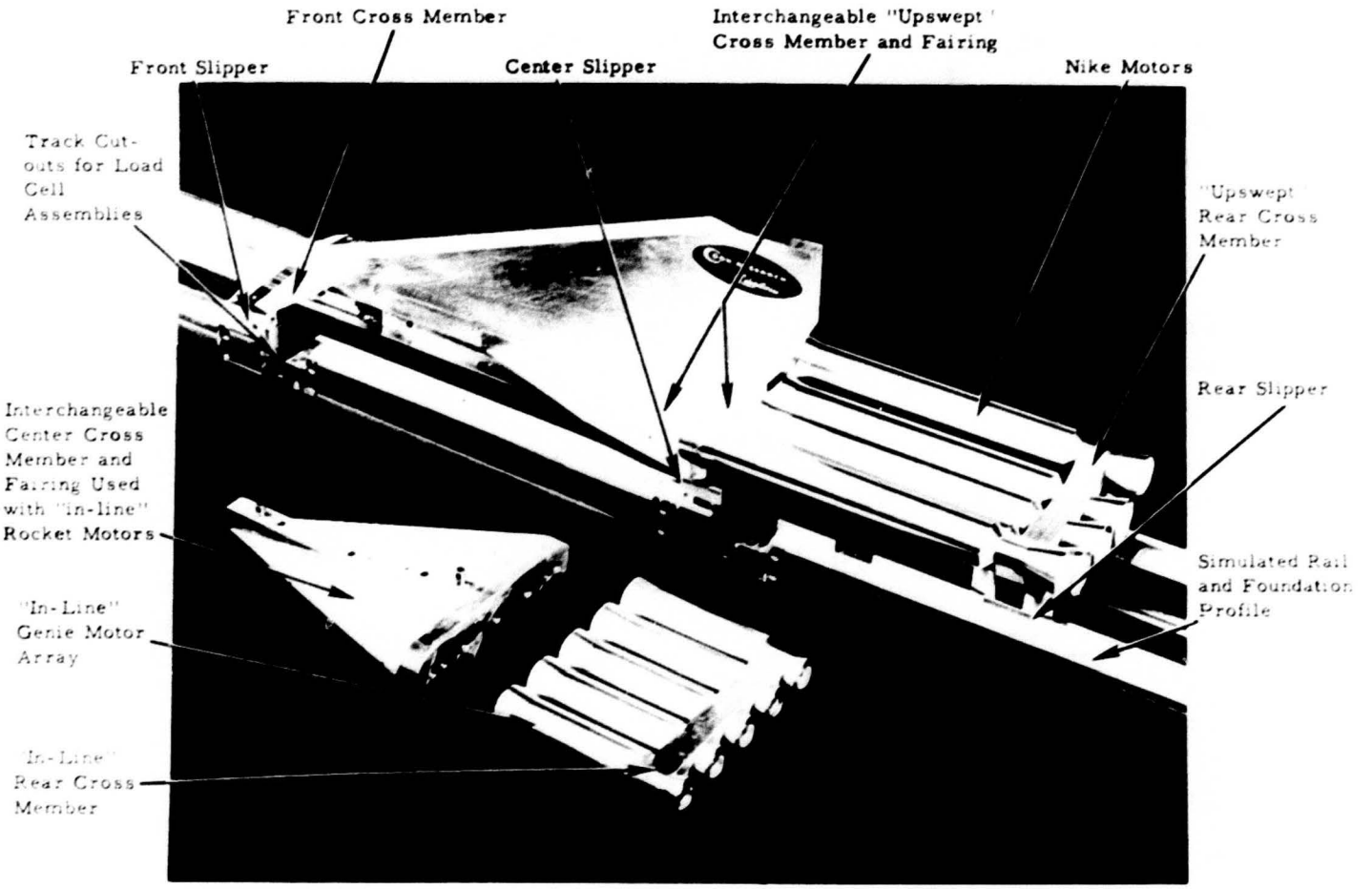

Figure A-2. Wind Tunnel Models of the Preliminary Mach 3 Sled Configuration.

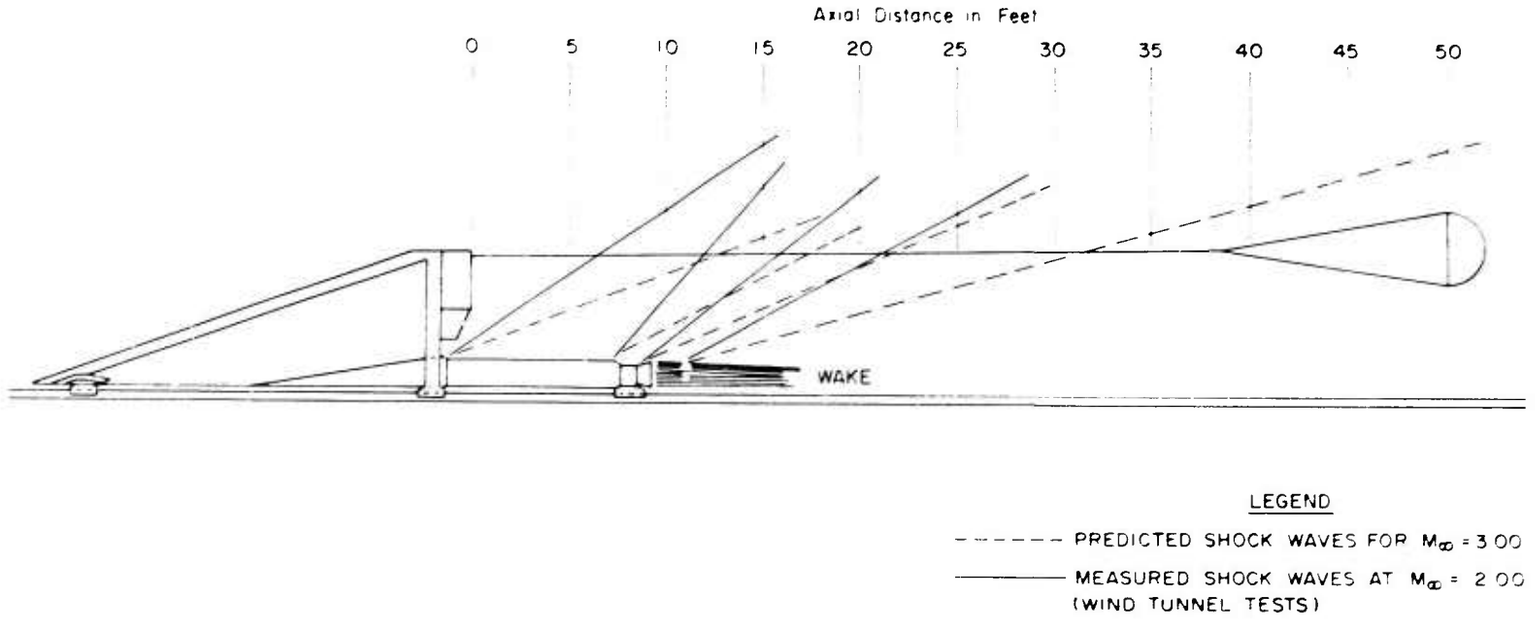

Figure A-3. Measured and Predicted Shock Wave Patterns for the Preliminary Mach 3 Sled.

2. INTERMEDIATE DESIGN

a. Design Requirements for the Arrowhead Sled

In 1961, Air Force track testing was transferred from the Edwards Track to the (then) 35,000 ft Holloman Track and the Mach 3 sled contract with Cook Research Laboratories was terminated. The Holloman Track then undertook the in-house redesign and fabrication of the Mach 3 sled for operation on the wider track gage at the Holloman Track. In an effort to reduce the design sophistication and the projected high operating costs, the operational and physical design requirements for the supersonic aerodynamic decelerator sled test vehicle were modified by the Air Force Flight Dynamics Laboratory.

Specifically, the new sled was to provide a decelerator deployment speed regime from 1500 to 2750 ft/sec. This reduction in maximum sled velocity also resulted in lowering the maximum longitudinal and lateral forces applied to the sled to 150,000 and 15,000 lb,respectively. As required for the Mach 3 sled, the redesigned sled was to incorporate a 2.5 cu ft storage compartment for the test item, a test item deployment system, test item disconnect, and the necessary on-board instrumentation to sense, telemeter, and photograph the test item performance data. An aerodynamically clean and faired sled superstructure was desired to minimize sled wake effects on decelerator performance.

b. Candidate Configurations

The Holloman Track considered two basic sled configurations. Both incorporated the basic characteristics of the Cook Research Laboratores Mach 3 sled design and consisted of two stages; the foresled and booster package and the pusher sled.

The foresled was composed of a vertical fin, forward wedge, and aft wedge. The vertical fin was made up of a leading edge structure, a diagonal tension member, a vertical column, a longitudinal column, vertical bulkheads, a nose cone fairing and skin panels. The forward wedge consisted of a forward slipper beam and fairing and necessary lugs and provisions for attaching the wedge to the vertical fin. The aft wedge consisted of an aft slipper beam, aft fairing, instrumentation compartments, and necessary access doors and fairing attachment provisions. The foresled design also incorporated the test item container, camera container, and release mechanism in the manners designed by CRL, except for slight modifications. The booster package consisted of a nozzle support beam, motor adapters, thrust beam, probe brake, and latch mechanism.

The pusher sled consisted of a nozzle support beam, motor adapters, forward beam, pusher adapters, and probe brake.

The major differences between the two basic sled configurations were in the slope and shape of the bottom surface. The bottom surface was flat and parallel to the rails on one sled design, whereas on the other, the cross section at the aft slipper wedge had a bottom surface shape of an inverted "V" and the sled bottom was at a slight angle to the rails.

c. Wind Tunnel Tests

Wind tunnel tests were performed at the Arnold Engineering Development Center, von Karman Gas Dynamics Facility to determine the static aerodynamic force characteristics and the bottom surface pressure distributions for the two configurations in the Mach number range from 1.42 to 3.00.

Descriptions of the test set-up, instrumentation, procedure, models, hardware, and selected results from these tests can be found in References 10, 11, and 12.

In the first wind tunnel test series (Reference 10) several modifications of the two basic sled designs were tested with the models mounted in the presence of a ground plane and at zero angle of attack with rails designed to simulate the Holloman track and trough. On the V-bottom sled, the leading edge of the aft slipper wedge was sharp, and both sharp and blunt leading edges were tested on the flat-bottom sled. On both basic sled models the vertical fin leading edge could be either sharp or blunt. Two booster configurations were tested with each sled model: a cluster of five Genie motors and a cluster of five Nike motors. In addition, two V-bottom configurations were tested with and without model parachutes deployed at various distances aft of the sled. During the force phase, 17 sled configurations were tested and 10 configurations were tested during the pressure phase, at Mach numbers of 1.47, 1.75, 2, 2.5, and 3. Regular and schlieren photographs from three tests of the V-bottom sled model with Genie boosters and a trailing model parachute are presented in Figure A-4.

---

(10) Jenke, L.M.: Supersonic Wind Tunnel Tests of the IDS-6328 Parachute Test Sled, Arnold Engineering Development Center Report AEDC-TDR-64-38, (AD 431 849), March 1964.

(11) Jenke, L.M. and Lucus, E.J.: Supersonic Wind Tunnel Tests of a Parachute Test Sled, Arnold Engineering Development Center Report AEDC-TDR-64-203, (AD 448 066), October 1964.

(12) Lucus, E.J. and Jenke, L.M.: Supersonic Wind Tunnel Tests of an Outrigger Rocket Sled and Two Dual Rail Sleds, Arnold Engineering Development Center Report AEDC TR-65-168, (AD 468 970), August 1965.

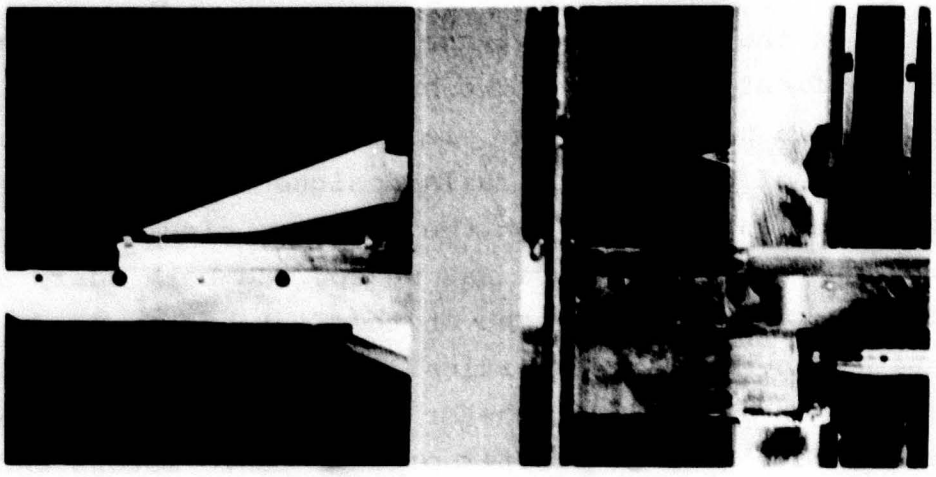

a. Regular Photograph; V-Bottom Model with Genie Boosters and Hyperflo Parachute.

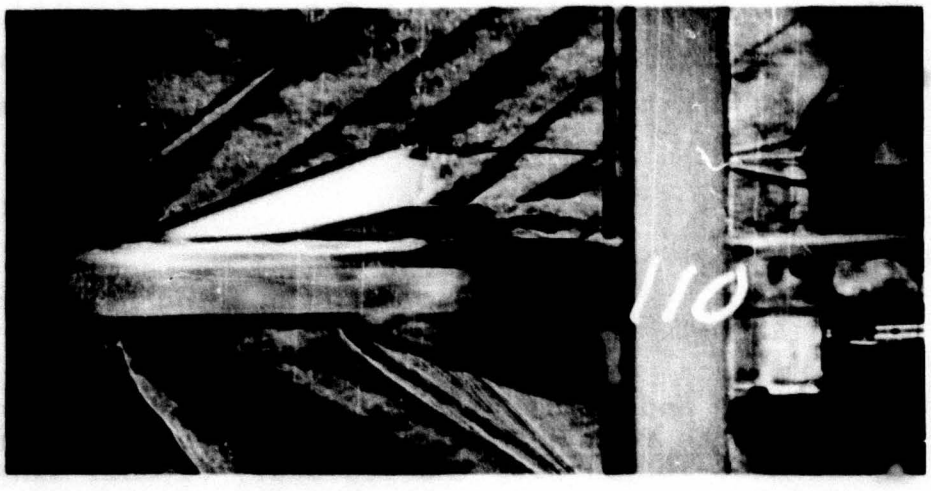

b. Schlieren Photograph; V-Bottom Model with Genie Boosters and Hyperflo Parachute.

Figure A-4. Regular and Schlieren Photographs of the Intermediate Design Arrowhead Sled Wind Tunnel Model During a Mach 1.5 Test (From Reference 10).

In the second wind tunnel test series (Reference 11) two sled configurations were investigated which were identical except for the rear slipper wedge design. For both configurations, the lateral cross section of the aft wedge had a bottom surface of an inverted "V". The differences in the two were in the leading edge droop angle and the planform area. Both configurations used a booster model of five Nike rocket motors. Force data was obtained at Mach numbers 1.42, 1.72, 2, 2.49, and 2.97.

The most promising sled configuration from these two test series was selected for the third series of tests (Reference 12). The details of the selected model are presented in Figure A-5. The results from the second series tests of this model indicated that significant changes in the aerodynamic forces occurred between Mach 1.5 and 2.0. The third series of tests was made to determine the sled forces at intermediate Mach numbers within this range. Data was obtained at Mach numbers 1.5, 1.62, 1.75, 1.87, 2.0, 2.5, and 3.0. A schlieren photograph from these tests is presented in Figure A-6.

3. FINAL DESIGN

A three-veiw sketch of the Arrowhead sled configuration which was selected by the Holloman Track for detail design and fabrication is presented in Figure A-7. The swept vertical fin slopes upward along the bottom from front to rear, the shape of the intermediate and aft wedges is an inverted "V", and all leading edges are sharp. The captive booster package will accommodate up to five Nike rocket motors and incorporates the probe brake. The test parachute attachment point is located 7 ft above the rails as required. The parachute attachment, attachment cover, and box, and camera box assemblies all attach to the vertical column of the swept fin and are

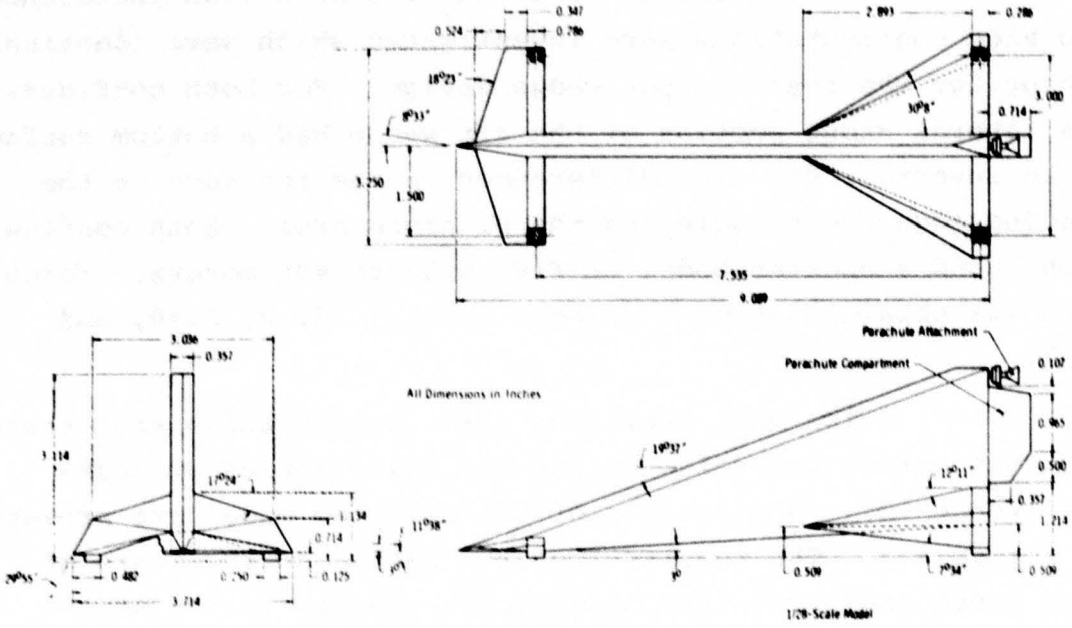

a. Details of the Foresled.

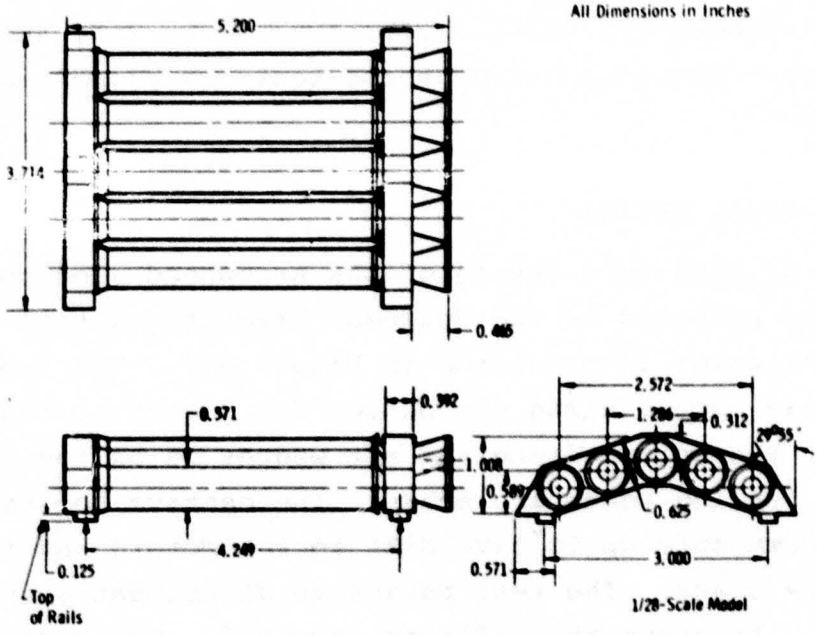

b. Details of the Booster Package.

Figure A-5. Final Design Arrowhead Sled Wind Tunnel Model (From Reference 12).

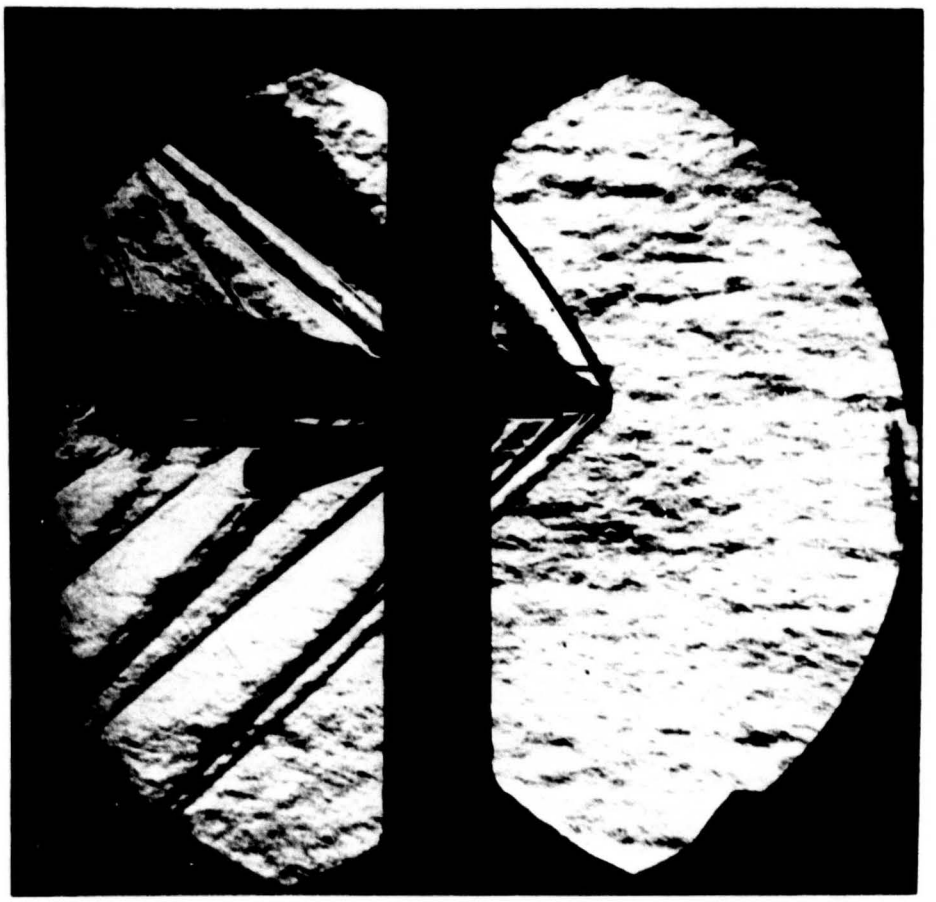

Figure A-6. Schlieren Photograph of the Final Design Arrowhead Sled Wind Tunnel Model; V-Bottom Model with Nike Boosters at Mach 1.5 (From Reference 12).

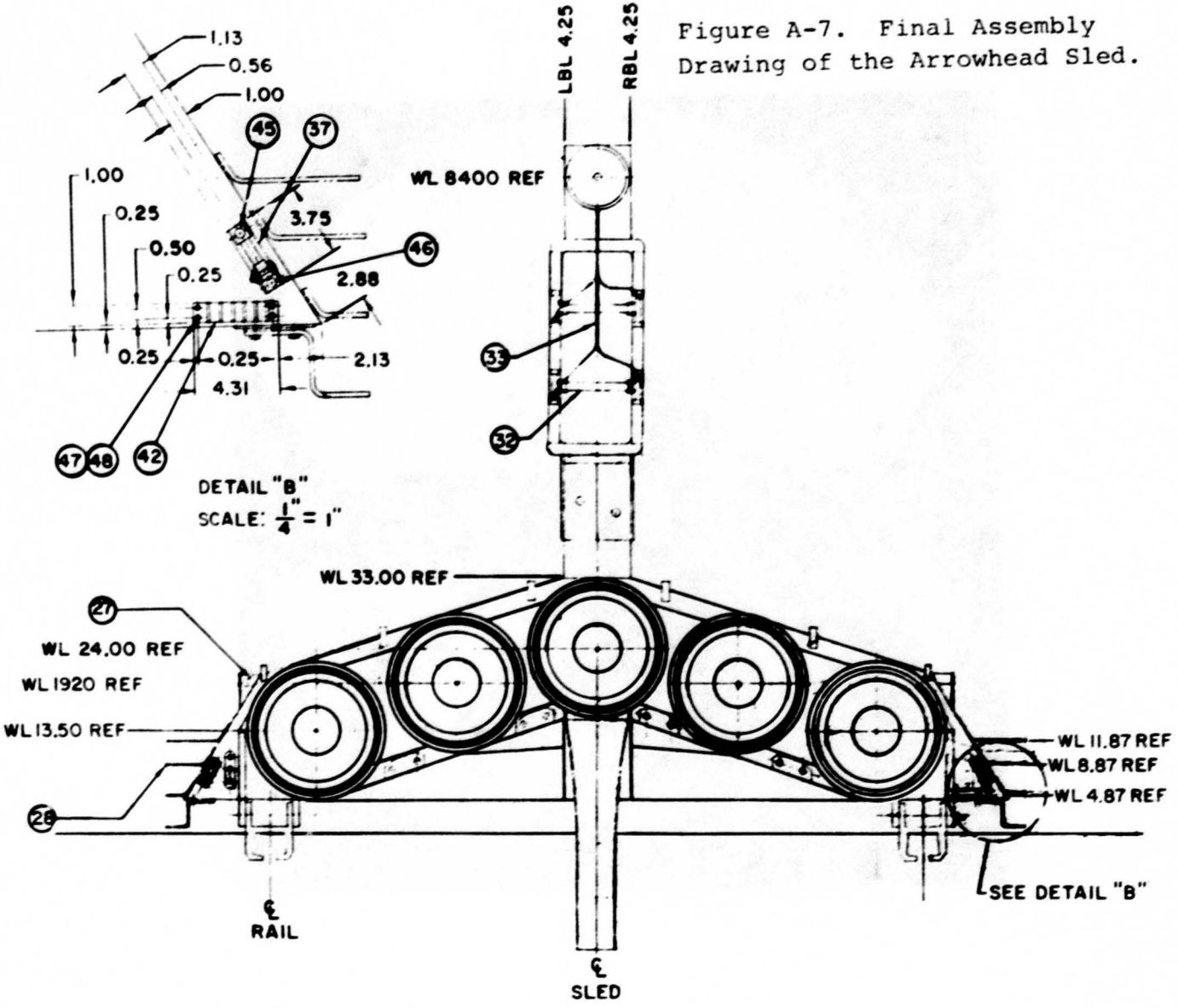

Figure A-7. Final Assembly Drawing of the Arrowhead Sled.

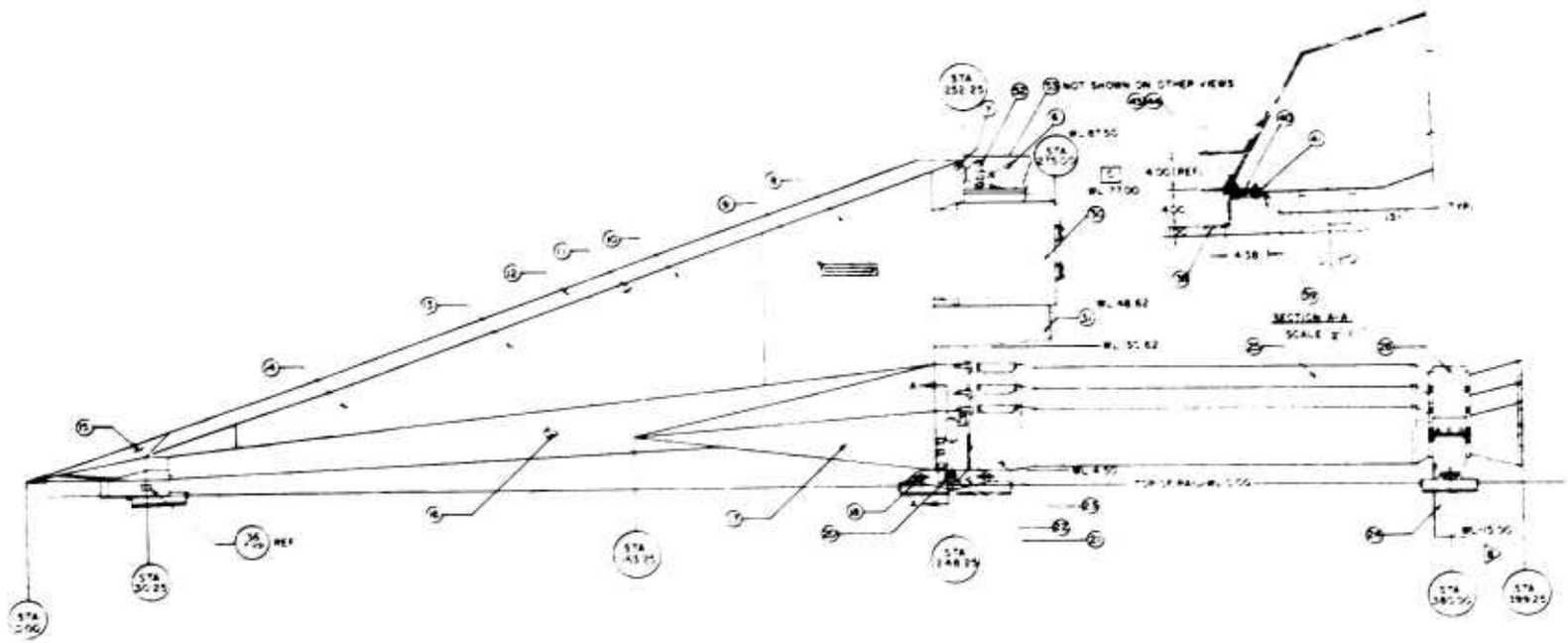

Figure A-7 (Continued). Final Assembly Drawing of the Arrowhead Sled.

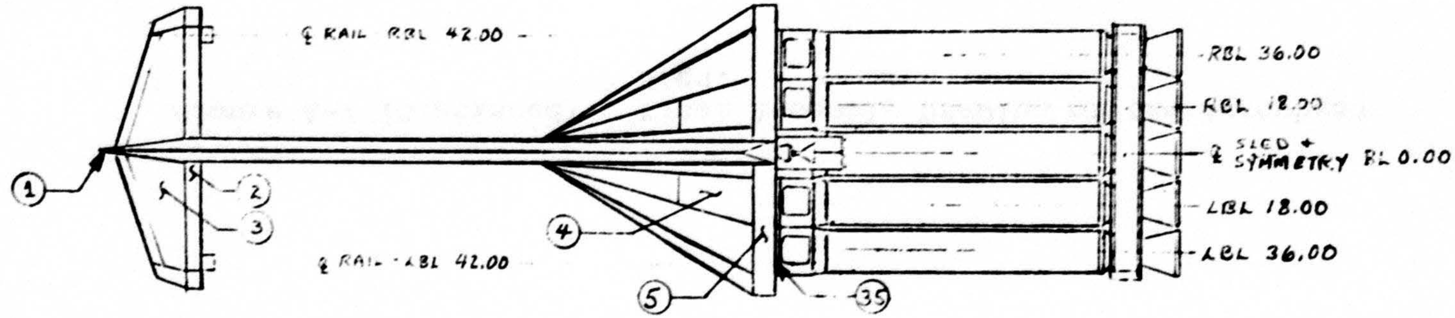

Rev	Item	Qty		Part No.	Description
A	53	1		7422259-10	PARACHUTE ATCH COVER ASSY
A	52	1		7422253-10	PARACHUTE ATCH ASSY
D	51	1		70C46372-10	ASSY-NOSE COVER
D	50	2		70B46474-1	COVER-FRONT FAIRING
B	49	2		70B46474-3	COVER-FRONT FAIRING
	48	AS REQ		MS20995C[illegible]	WIRE LOCK
	47	4		MS35265-47	SCREW 8-32UNF-3A
	46	2		AN509-416-14	SCREW $\frac{1}{4}$-28UNF-3A
	45	2		AN4-14A	BOLT $\frac{1}{4}$-28UNF-3A
	44	4		MS21042-4	NUT $\frac{1}{4}$-28UNF-3B
	43	4		AN4-15A	BOLT $\frac{1}{4}$-28UNF-3A
	42	1		CONTACT STRIP	TO BE SUPPLIED BY INSTR. DEPT.
	41	4		70B46811-3	INSULATION PLATE
	40	2		70B46811-1	INSULATION PLATE
	39	2		70B46810-1	INSULATION PLATE -OLDER
	38	2		70C46[illegible]	KNIFE BLADE
	37	1		70C468[illegible]	ASSY, CUTTER MOUNT
	36	2		64-054-C314	SLIPPER PIN BRACE
A	35	1		64-054-J226	BOOSTER PACKAGE FWD. BEAM
C	34				
C	33	2		XRRB18854	ASSY, [illegible] CABLE
	32	2	X	64-054-C295	STRAP-PARACHUTE RETAINING
	31	1	X	64-054-E271	ASSY-CAMERA BOX
	30	1	X	64-054-E2[illegible]	ASSY-PARACHUTE BOX
	29	4			
	28	4		64 054-B199	KNIFE BLADES
	27	1		64 054-D223	ASSY-LATCH
	26	1		64-054-J12	ASSY-NOZZLE SUPPORT BEAM
	25	5	X	64-054-B100	MODEL NIKE MOTOR
	24	1		64-054-C249	PROBE BRAKE
	23	1		64-054-F35	ASSY-MOTOR ADAPTER
	22	2		64-054-F60	ASSY-BOGIE BEAM
	21	2		64-054-C166	BOGIE PIN
	20	2		64-054-B69	BEARING-BOGIE PIN
C	19				
	18	8		64-054-B29	BEARING-SLIPPER PIN
	17	2		64-054-E143	ASSY-AFT FAIRING
	16	1		64-054-E130	ASSY-LONGITUDINAL COLUMN
	15	1		64-054-E59	ASSY-NOSE CONE
	14	2		64-054-E49-1.5	ASSY-HONEYCOMB PANEL, VERTICAL, FIN
	13	2		64-054-E43-2.6	ASSY-HONEYCOMB PANEL, VERTICAL FIN
	12	1		64-054-J103	ASSY-LEADING EDGE
	11	1		64-054-J91	ASSY-DIAGONAL TENSION-MEMBER
	10	2		64-054 E48-247	ASSY-HONEYCOMB PANEL, VERTICAL FIN
	9	1		64-054-D57	ASSY SLOT ANTENNA
	8	2		64-054-E48 4.6	ASSY-HONEYCOMB PANEL VERTICAL FIN
	7	1		64-054-C106	ASSY-VERTICAL COLUMN
	6	1	X	64-054-D221	ASSY-DRAG CONE
	5	1		64-054-J57	ASSY-AFT SLIPPER BEAM
	4	2		64-054-F158	ASSY-INSTRUMENTATION PALLET
	3	2		64-054-E92	ASSY-FWD BEAM FAIRING
	2	1		64 054-[illegible]	ASSY-FWD SLIPPER BEAM
	1	1		64 054-D92	TIP-NOSE CONE
	ITEM	QTY		PART NO.	DESCRIPTION

BILL OF MATERIAL

Figure A-7 (Concluded). Final Assembly Drawing of the Arrowhead Sled.

readily removable. The storage volume of the parachute box is the required 2.5 cu ft and parachute restraining/release mechamisms are provided on the parachute box.

4. SLED FABRICATION

Fabrication of the Arrowhead sled began early in 1964 and was accomplished almost entirely at the Holloman Track. Some steel and aluminum materials procured under the Mach 3 sled contract with Cook Research Laboratories were used and some machining was done at the Air Force Flight Dynamics Laboratory (AFFDL). The Holloman Track and the AFFDL shared the cost of the instrumentation and the AFFDL supplied the Nike rocket motors. Fabrication was completed in mid 1965, and the Holloman Track designated the Arrowhead sled as IDS 6328.

5. SLED CHECKOUT RUNS

The first checkout run, 6P-A1, was conducted on 2 September 1965 to verify sled performance and establish sled acceleration and structural loadings. Photographs of the Arrowhead sled which were taken just prior to launch are presented in Figure A-8. The captive pusher sled was loaded with three live and two inert Nike rocket motors. Immediately after initiation of rocket ignition; one motor ignited and burned normally, one motor failed to ignite due to a faulty ignitor, and the third motor blew the ignitor out of the case. The resultant release of flame and hot gases from the head end of the booster extensively damaged the sled structure and destroyed the telemetry system except for the transmitter and four amplifiers. The photograph presented in Figure A-9 shows the damage area.

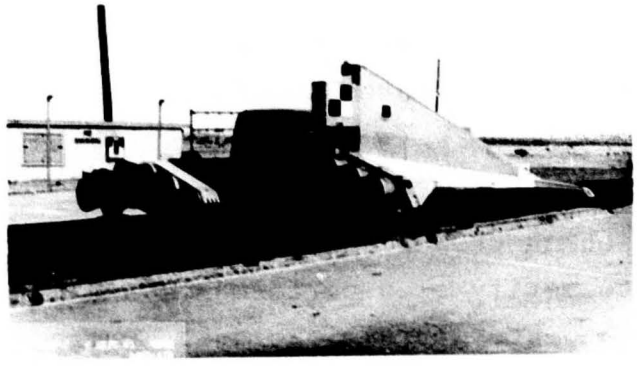

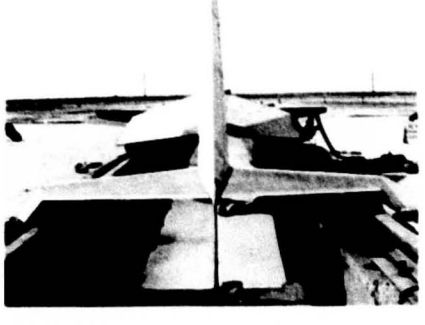

Figure A-8. Photographs of the IDS 6328 Arrowhead Sled Taken Just Prior to Its First Launch.

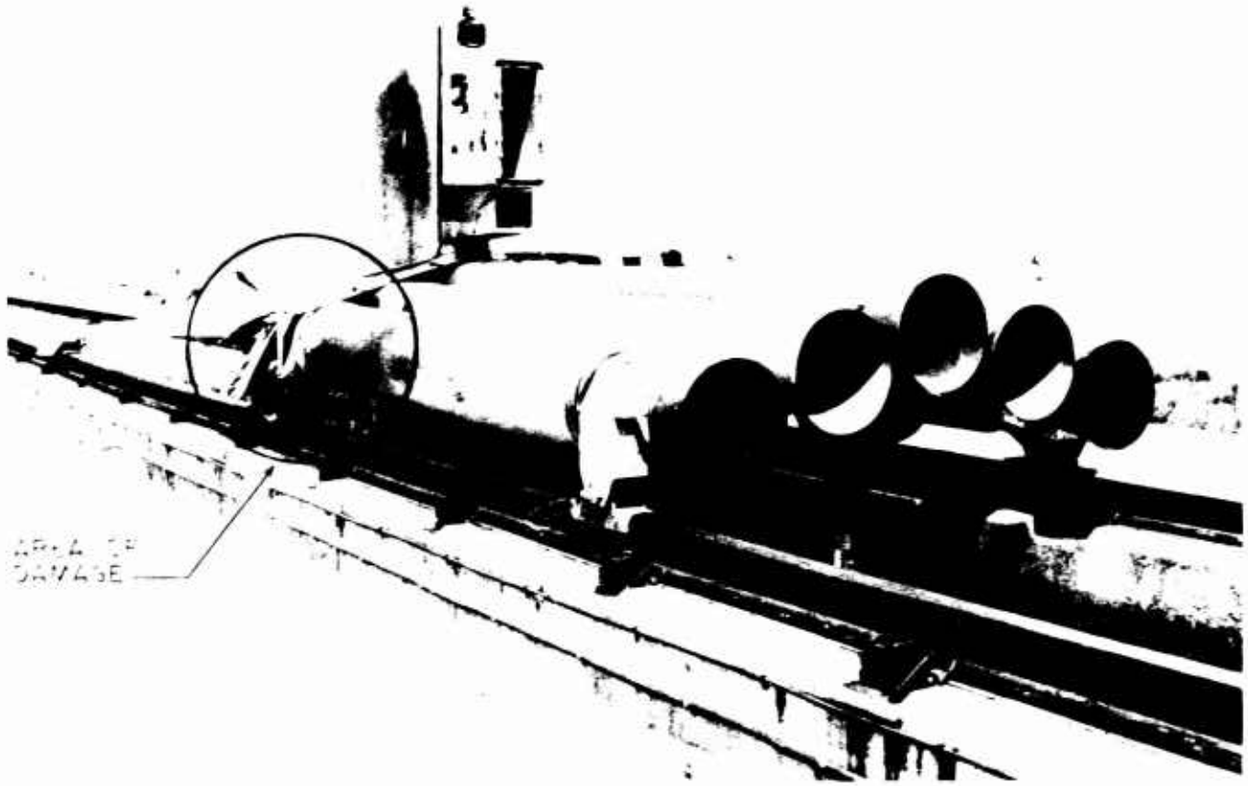

Figure A-9. Photograph of the Arrowhead Sled After its First Launch Showing the Area of Damage.

The Holloman Track repaired the damage, replaced the telemetry system, and conducted the second checkout run, 6P-C1, on 14 April 1966. The booster configuration was the same as for the first checkout run. All motors ignited and burned properly. The Arrowhead sled and captive pusher were accelerated to Mach 0.95.

The third checkout run, 6P-B1A, was conducted on 26 April 1966 and was also a success. Five Nike motors accelerated the sled to Mach 1.89.

The fourth checkout run, 6P-D1, was conducted on 17 June 1966. The Arrowhead sled for this run was the "full-up" configuration. A full complement of 10 Nikes were loaded on the pusher sleds, all test parachute attachment, restraining, deployment, and releasing components were installed and a sample test parachute was packaged in the parachute box. The second stage Nike cluster failed to ignite and a maximum speed of only Mach 1.11 was obtained. Parachute deployment occurred at Mach 0.56.

The fifth and final checkout run, 6P-D2, was conducted on 22 July 1966. This was also a full-up Arrowhead sled configuration. All Nike motors operated as planned and a maximum speed of 2886 ft/sec, or Mach 2.55, was achieved. Minor damage and structural overloads were sustained by the booster packages and parachute deployment occurred prematurely.

Holloman redesigned and rebuilt the lower aft slipper beam of the noncaptive pusher sled, reinforced the aft slipper beam of the captive pusher sled, installed a channel on top of the parachute box to provide additional parachute tie-down locations, and declared the IDS 6328 Arrowhead sled fully operational in early 1967.

APPENDIX B

DESCRIPTION AND DESIGN OF THE 5 FT
NOMINAL DIAMETER HEMISFLO PARACHUTES

1. GENERAL DESCRIPTION

The hemisflo parachute has a canopy which is designed as a hemisphere with a truncated cone extension beginning at the periphery of the hemisphere. The slant height of the truncated cone is equal to one-twentieth of the circumference of a great circle of the hemisphere. The included angle of the cone is equal to the angle between two diametric suspension lines. The suspension lines have a free length (from the canopy skirt to the confluence) equal to the circumference of a great circle of the hemisphere. The hemisphere and truncated cone actually have a lateral cross section of a regular polygon of n sides because the canopy is constructed using n gores, where n also equals the number of suspension lines. The entire canopy is of ribbon construction. Riser lines are used to position the canopy at the proper location downstream of the test vehicle.

2. MAJOR COMPONENTS

a. Canopy

The hemisflo canopy was designed in accordance with the method outlined on pages 517 through 522 of the "Parachute Handbook" (Reference 6) which gives sample calculations and design equations for hemispherical canopies. The input parameters were a nominal diameter of 5 ft (or a nominal total surface area, S_o, of 19.635 sq ft) and 12 gores. The results of the calculations yielded the dimensions and coordinates of a canopy gore and the effective length and confluence angle of the suspension lines.

b. Suspension Lines

An integral two-ply suspension line, riser line, radial, and vent line arrangement was chosen for use with the parachutes. For this type arrangement: the two-ply lines proceed from an attachment point as riser lines, passing through riser keepers, to a confluence keeper; from the confluence keeper to the canopy skirt the lines serve as two-ply suspension lines; at the skirt, the lines divide, with one ply passing outside the canopy and the other inside the canopy, thus forming radial pairs; the lines meet again at the vent becoming two-ply vent lines; they divide again on the diametric side of the canopy, forming another pair of radials, and meet at the skirt; from the skirt, the two-ply suspension lines pass through the confluence keeper, become radial lines, and terminate in a second attachment point.

With this arrangement, the suspension lines are brought together at a circular confluence keeper and do not meet at a confluence. This means that the actual suspension line length must be shorter than the calculated length to maintain the required confluence angle. Since the confluence keeper holds the suspension lines in a circle with a radius of 3.1 in., a suspension line length from canopy skirt to confluence keeper of 100 in. was required to be used. Each parachute had 12, two-ply, 100 in. long suspension lines.

c. Riser Lines

The 12, two-ply riser lines were continuous from the attachment point to the confluence keeper for each parachute. Riser keepers helped maintain the position of the riser lines and were located every 10 ft from the confluence keeper.

The risers were used to position the canopy downstream of the strong shock waves generated by the Arrowhead test sled. These shock waves for two freestream Mach numbers

are shown in Figure A-3 of Appendix A. Risers 20 ft long were used for the parachutes tested up to Mach 1.5 and risers 30 ft long were used for the tests at higher Mach numbers.

d. Confluence and Riser Keepers

Fixed line circular keepers were used for the confluence keeper and the one or two riser keepers used on each test parachute. The design of all keepers was the same except for the strengths of the keeper webbing band and sewing thread. A sketch of the confluence and riser keepers is presented in Figure B-1.

e. Attachment Loops

Each of the 12, two-ply riser lines terminated in a loop which was used to mate with the attachment/deployment/release mechanism on-board the test sleds. A sketch showing the design details of the attachment loops which were used on each parachute is presented in Figure B-2.

3. CANOPY COMPONENTS

a. Horizontal Ribbons

Eleven, 2 in. wide horizontal ribbons were equally spaced between the vent and skirt bands of each canopy. Each ribbon was continuous around the canopy with one lap splice per ribbon made between the radials. The locations of the splices were staggered around the canopy.

On parachutes with horizontal ribbons of two-ply, the ribbons were sewn together with four or six rows or stitching prior to assembly on the canopy.

b. Vertical Ribbon

One, 5/8 in. wide tape served as a vertical ribbon on each canopy gore to help control the spacing of the horizontal ribbons. The vertical ribbon was located in the

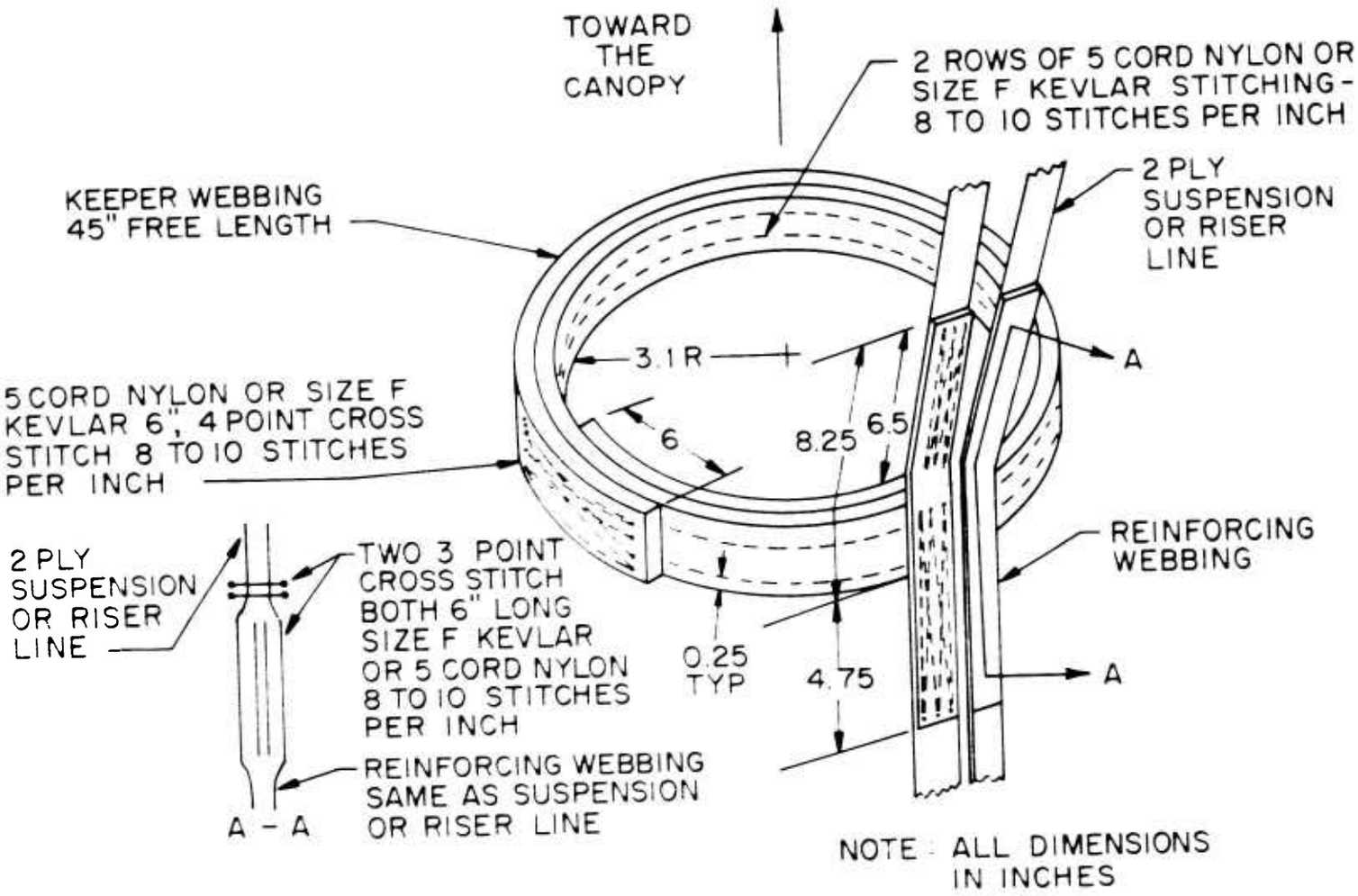

Figure B-1. Confluence and Riser Keeper Design Details.

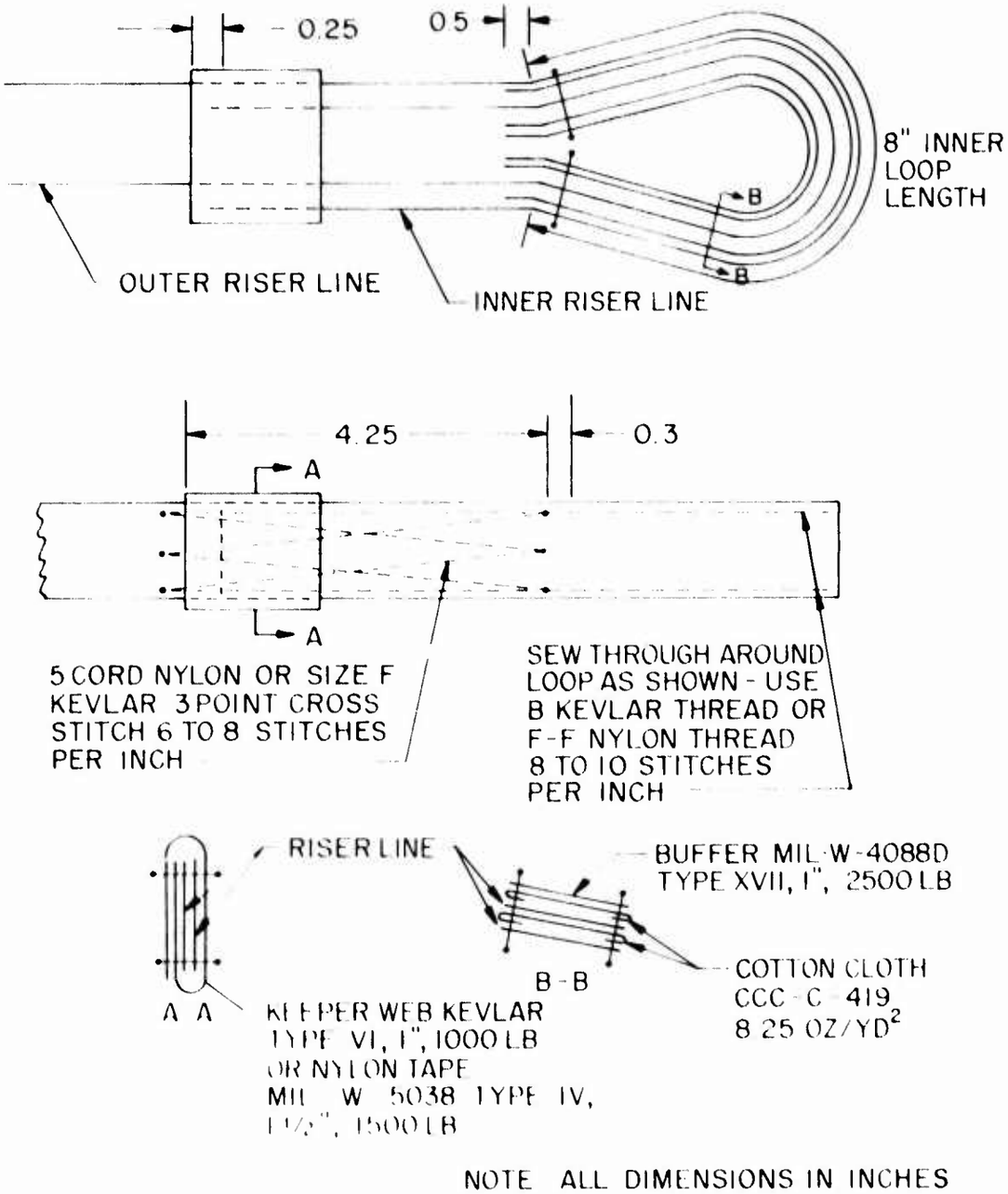

Figure B-2. Design Details of the Riser Line Attachment Loops.

center of the gore and extended from the vent band to the skirt band. Each vertical ribbon was either two or four ply, with half the plies on the inside of the canopy and half on the outside; thus, the horizontal ribbons were sandwiched between the vertical ribbon plies. Three rows of straight stitching, which extended from the canopy skirt to the vent, were used to fasten the vertical ribbons to the horizontal ribbons and to the skirt and vent bands. The length of each vertical ribbon was equal to the finished gore height of 31.9 in.

c. Radials and Radial Tapes

The radials were formed by the separated suspension lines where they passed over the canopy. Four rows of straight stitching, which extended from the canopy skirt to the vent, were used to fasten the radials to the horizontal ribbons and to the skirt and vent bands. Horizontal ribbon and skirt band lengths between the centerlines of adjacent radials were determined from the gore coordinate calculations.

For those test parachutes which had 3/4 in. wide radials, a 1 in. wide radial tape was placed between the radials to provide a canopy porosity equal to that of the canopies with 1 in. wide radials.

d. Skirt Band

A separate 1 3/4 in.wide skirt band was used on each test parachute. The band was continuous around the canopy with one lap splice each inside a radial pair. When two-ply skirt bands were used, one ply was placed inside the radial pair and the other ply was placed on top of a radial on the outside of the canopy. Four rows of straight stitching were used to join the plies and fasten the skirt band to the radials and vertical ribbons.

The skirt band provided a skirt circumference of 112 in., which is equal to the finished gore width at the skirt, 9.3 in., times the number of gores, n = 12.

e. Vent Band

A separate 1 3/4 in. wide, multiple ply vent band, was used on each test parachute. The band was continuous around the canopy, passing inside the radial pairs and outside the canopy for two-ply vent bands and passing inside the radial pairs and both inside and outside the canopy for three-ply vent bands. Four rows of straight stitching were used to join the plies and fasten the vent band to the radials and vertical ribbons.

The length of the vent band was determined based upon the number of plies used, the length of the splice or splices (usually 6 in. each), and the requirement for maintaining a finished dimension of 1.43 in. between the centerlines of adjacent radials at the vent. This dimension is 0.19 in. shorter than the calculated gore width at the vent. This take-up was incorporated to increase the share of canopy stress loads taken by the vent band and decrease the share taken by adjacent ribbons.

f. Vent Lines

The vent lines were formed where the 12, two-ply radials crossed over the vent. This gave six, two-ply vent lines for each parachute. The finished length of each vent line (measured under 40 lb tension) was 5.0 in. This length is 0.8 in. shorter than the calculated gore length across the vent and was also used to carry canopy stress loads away from the ribbons near the vent and into the vent band and vent lines.

4. CANOPY POROSITY

Graphical layouts and calculations such as given on pages 520 through 522 of the Parachute Handbook (Reference 6) were used to determine the horizontal ribbon arrangement which would provide the desired 14 to 18 percent geometric porosity.

Eleven, 2 in. wide horizontal ribbons spaced equally between 1 3/4 in. wide vent and skirt bands gave a canopy geometric porosity of 16.47 percent. The 12 spaces between the ribbons and the bands were all 0.537 in. wide.

One test parachute, FERR-1-3-1, which was used on test 6P-H2, had horizontal ribbons with widths outside the allowable specification of 2 ± 1/16 in. The ribbons measured 1 7/8 in. in width. This means that the parachute had a canopy porosity of 19.9 percent and a ribbon spacing of 0.651 in.

5. PARACHUTE MATERIALS

The major structural components were analyzed to estimate strength requirements and select materials.

a. Strength Requirements

(1) Parachute Opening Force

As pointed out on page 369 of the Parachute Handbook (Reference 6) the overall strength requirements for parachute components are usually established by applying a design factor to the expected maximum parachute opening force, F_o. Pages 163 and 164 of Reference 6 present a method for estimating F_o which is applicable to this test program; that is,

$$F_o = C_{D_o} S_o Q_{LS} X \qquad \text{(B-1)}$$

where

F_o = Opening force, lb

C_{D_o} = Parachute drag coefficient

S_o = Design nominal area of the parachute canopy, 19.635 sq ft

Q_{LS} = Dynamic pressure at parachute line stretch, psf

X = Opening shock factor.

Average performance data from previous sled tests of hemisflo parachutes (Reference 3) were used to estimate values for C_{D_o} and X. From Reference 3,

$$C_{D_o} = 0.42 \qquad \text{(B-2)}$$

$$X = 1.3 \qquad \text{(B-3)}$$

For the three nominal test Mach numbers of interest, M_∞ = 1.5, 1.8, and 2.2, the track dynamic pressures at line stretch, Q_{LS}, were expected to be approximately 2900, 4000, and 6500 psf, respectively.

Input of the known and estimated values into Equation B-1 gave the following expected maximum parachute opening forces for the three test conditions:

M_∞	F_o (lb)
1.5	31,090
1.8	42,883
2.2	69,685

(2) Suspension Lines, Riser Lines, Vent Lines, and Radials

The strength requirements for these components were estimated based upon the method established for suspension lines, since all these components are to be the same material as, and continuations of, the suspension lines. The method used is presented on page 378 of the Parachute Handbook (Reference 6) and can be expressed as

$$SLS = (2.91)\ (F_o)/n \qquad \text{(B-4)}$$

where

SLS = Suspension line strength, lb

2.91 = Design factor for deceleration parachutes of aerospace vehicle recovery systems, given on page 370 of Reference 6

F_o = Maximum opening force, lb

n = Number of suspension lines, 12.

This expression gave the following suspension line strength requirements for the three test conditions:

M_∞	SLS (lb)
1.5	7,540
1.8	10,400
2.2	16,900

Suspension lines with these strengths were expected to survive, undamaged, when subjected to the expected maximum opening forces at the three test Mach numbers. This is illustrated on Figure B-3.

Also shown on Figure B-3 are the suspension line strengths chosen for use on this program. They are plotted at each of the three test Mach numbers. It was expected that a sufficiently large range of strengths would be available for testing such that the ultimate suspension line load could be determined as a function of opening force.

(3) Horizontal Ribbons

The strength requirements for the horizontal ribbons were estimated by averaging the requirements specified in Table 7-5 on page 376 of the Parachute Handbook (Reference 6) and the strengths used on actual hemisflo parachutes tested previously on a high-speed sled (Reference 3). The required horizontal ribbon strength, HRS, for 2 in. ribbons, was estimated in terms of the suspension line strength, SLS, to be

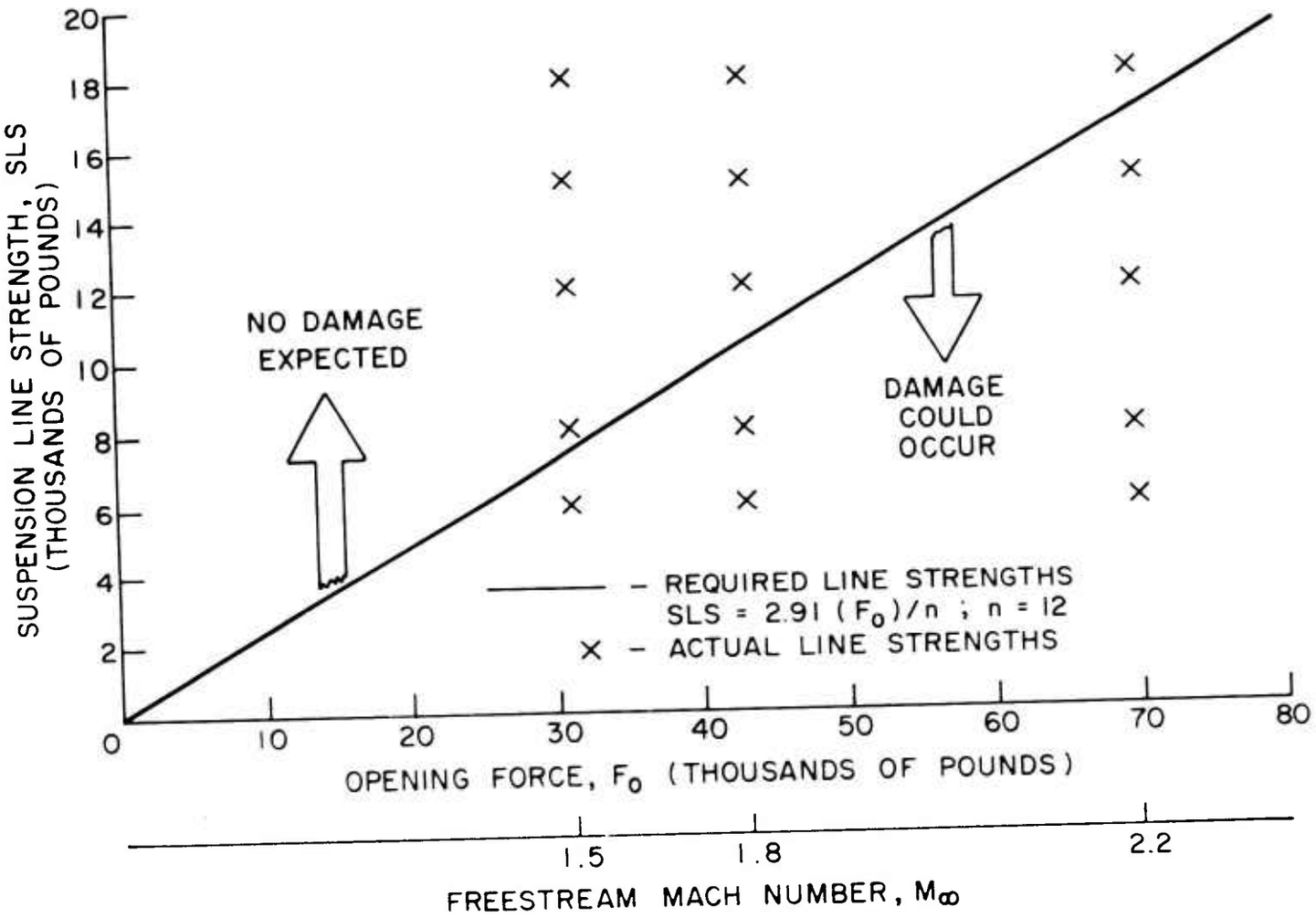

Figure B-3. Suspension Line Strengths as Functions of Opening Force and Freestream Mach Number.

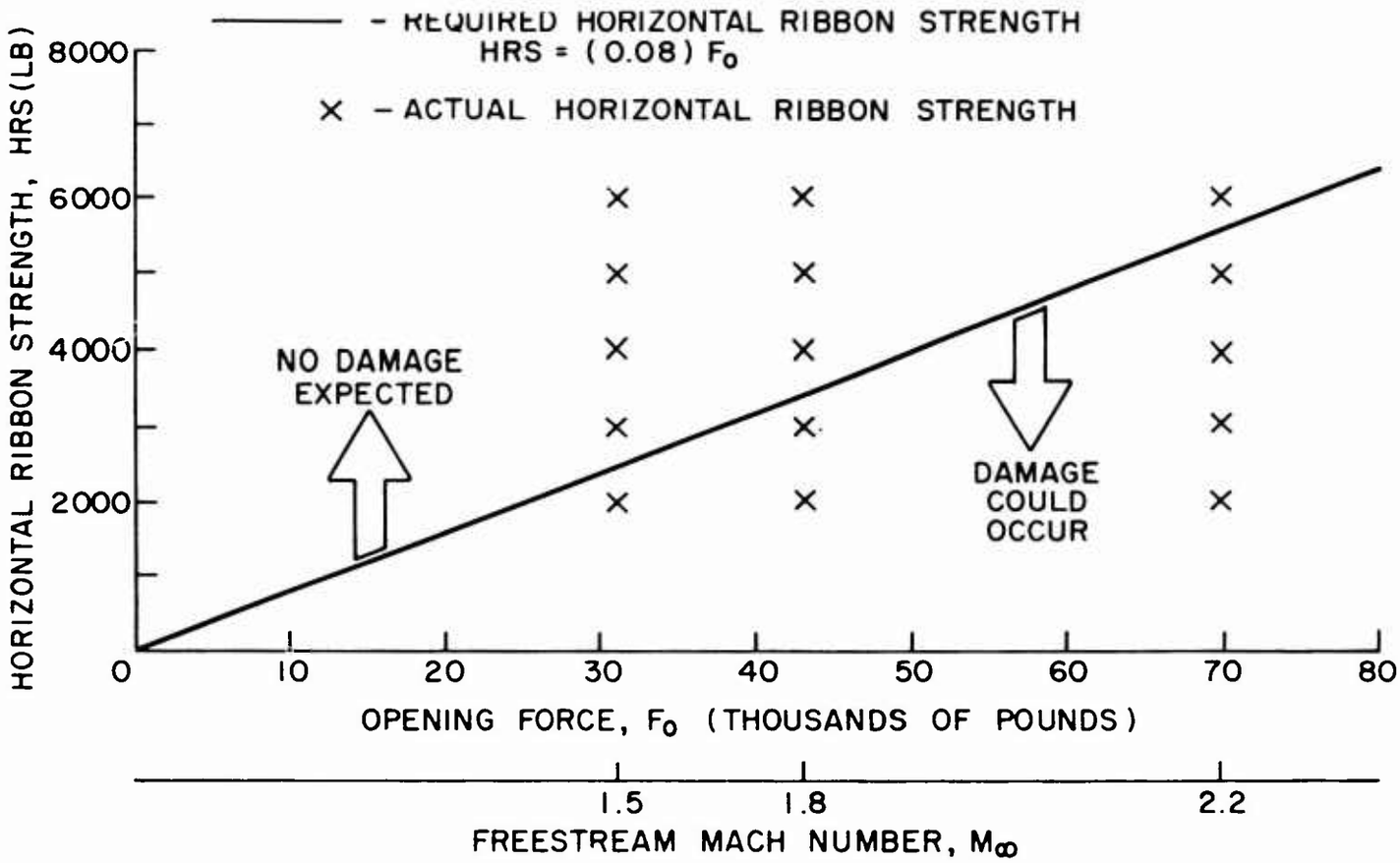

Figure B-4. Horizontal Ribbon Strengths as Functions of Opening Force and Freestream Mach Number.

$$HRS = (1/3)\ SLS \qquad (B-5)$$

or, in terms of the maximum parachute opening force, F_o,

$$HRS = (0.08)\ F_o \qquad (B-6)$$

Horizontal ribbons with strengths determined from Equation B-6 were expected to survive undamaged when subjected to the expected maximum opening forces at the three test Mach numbers. This is illustrated in Figure B-4.

Also shown in Figure B-4 are the horizontal ribbon strengths chosen for use on this program. They are plotted at each of the three test Mach numbers. It was expected that a sufficiently large range of strengths would be available for testing such that the ultimate horizontal ribbon load could be determined as a function of opening force.

(4) Skirt Band

The requirements for the skirt band strength, SBS, of each parachute were determined using the following expression:

$$SBS = (0.72)\ SLS \qquad (B-7)$$

Or, in terms of the maximum parachute opening force, F_o,

$$SBS = (0.175)\ F_o \qquad (B-8)$$

(5) Vent Band

The requirements for the vent band strengths, VBS, of each parachute were determined using the expression

$$VBS = (1.11)\ SLS \qquad (B-9)$$

or, in terms of the maximum parachute opening force, F_o,

$$VBS = (0.27)\ F_o \qquad (B-10)$$

(6) Confluence Keeper

No strength requirements were originally estimated for the confluence keeper bands. The confluence and riser keepers were initially identical, each incorporating a two-ply, 1 3/4 in. wide, 3600 lb webbing as the band material. After a structural failure of the confluence keeper band on test 6P-G3, all subsequent confluence keeper band strengths were made approximately equal to the vent band strengths.

(7) Other Components

Strength requirements for other parachute components such as the riser keeper bands and the vertical ribbons were not established. The strengths of these components were selected somewhat arbitrarily but with consideration of strengths previously used on other parachutes tested at high dynamic pressures.

b. Material Characteristics

General characteristics of the materials selected for the various components of each test parachute used on this program are summarized in Tables 2 and 3 of Section II.

(1) Nylon Materials

Detailed construction descriptions and other characteristics of the nylon materials used in the fabrication of the test parachutes can be found in the applicable Military and Federal specifications which were in effect at the time of parachute manufacture.

(2) Kevlar Materials

The Kevlar parachute materials used in the fabrication of the test parachutes were in various stages of development by the Fabric Research Laboratories (FRL) under

contract to the Air Force Flight Dynamics Laboratory and the Air Force Materials Laboratory (Reference 13). Design details, construction descriptions, weaving requirements, and material characteristics for the final Kevlar materials developed under the FRL program are documented in References 14 and 15. The construction and characteristics of the Kevlar materials used in the fabrication of the test parachutes are summarized in Table B-1.

6. PARACHUTE FABRICATION

a. Manufacturing Technique

All test parachutes were manufactured in accordance with the Military Specification for continuous ribbon, heavy duty type parachute systems (Reference 16). This Specification includes descriptions of the manufacturing techniques associated with stitching, seaming, splicing, measuring, finishing, marking, and inspecting the test parachutes.

---

(13) Babish, C.A.: Development and Evaluation of Kevlar 29 Materials for Air Force Weapon System Parachute Applications, paper presented at the Workshop on Superstrength Fiber Applications, Dayton, Ohio, April 20 and 21, 1977.

(14) Abbott, N.J., et al., Design of Parachute Component Materials from Kevlar 29 and 49, Air Force Materials Laboratory Report, AFML-TR-74-65, Part IV, July 1976.

(15) United States Air Force Draft Tentative Military Specifications for: Webbing, Textile, Kevlar; Tubular Webbing, Textile, Kevlar; Tape, Textile Kevlar; Coreless Cord, Kevlar; and Thread, Kevlar, October 1976.

(16) Military Specification: MIL-P-25716, Parachute System, Heavy Duty, General Specification For.

TABLE B-1

CONSTRUCTION AND CHARACTERISTICS OF THE KEVLAR 29 MATERIALS

Material Type	Prelim. Draft Spec. Type *	Width (in.)	Rated Breaking Strength (lb min.)	Tested Breaking Strength (lb avg)	Thickness (in.)	Weight (oz/yd)	Weave Type	Warp Construction		Filling Construction	
								denier/ply/ twist[1]	Total Ends	denier/ply/ twist[1]	Total Ends
Webbing	II	3/4	3000	3091	0.043	0.407	Plain	1500/2/1/8	31	1000/1/4	12
Webbing	II a	3/4	4000	4101	0.046	0.526	Plain	1500/2/1/8	41	1000/1/4	11
Webbing	IV	1	2500	2796	0.029	0.365	Plain	1000/1/4	71	1000/1/4	22
Webbing	V	1	3500	4293	0.050	0.596	Plain Tubular	1500/1/3	81	1500/1/3	28
Webbing	V	1	6000	6675	0.067	0.924	2x2HB[2]	1500/3/1.6	49	1500/1/3	12
Webbing	VI	1	9000	9202	0.104	1.422	Double Plain	1500/3/1.6	76	1500/1/3	8
Webbing	VII	1	12000	12,063	0.113	1.418	Double Plain	1500/3/1.6	77	1500/1/3	9
Webbing	XIV	1 3/4	3600	4540	0.025	0.528	Plain	1000/2/2.1	55	1000/1/4	16
Webbing	XV	1 3/4	4500	4855	0.029	0.644	Plain	1000/1/4	130	1000/1/4	22
Webbing	XVI	1 3/4	6500	7500	0.038	0.862	Plain	1500/1/3	140	1500/1/3	11
Webbing	XVIII	1 3/4	8700	8815	0.046	1.069	Plain	1500/2/1.8	88	1000/1/4	10
Tape	V	5/8	625	795	0.014	0.092	Plain	400/1/5	47	400/1/5	22
Tape	VI	1	1000	1199	0.014	0.140	Plain	400/1/5	74	400/1/5	21
Ribbon	XII	2	2000	2496	0.014	0.286	Plain	400/1/5	148	400/1/5	21
Ribbon	XIII	2	3000	3194	0.021	0.516	Plain	1500/1/3	64	1000/1/4	22
Ribbon	XIV	2	4000	4965	0.024	0.594	Plain	1000/2/2.1	60	1000/1/4	18

Material Type	Letter Size	Dia. (in.)	Rated Breaking Strength (lb)	Tested Breaking Strength (lb avg.)	Nominal Weight (yd/lb)	Yarn denier/ ply	Single Twist (tpi)	Ply Twist (tpi)
Thread	B	0.013	16	20	10,000	200/2	12S	6Z
Thread	E	0.015	25	31	6,700	200/3	12S	6Z
Thread	FF	0.021	60	59	3,350	400/3	8S	4Z

[1] When a plied yarn is used, this is the value of the ply twist. Singles twist is always zero, or producers twist. Twist is in turns per inch, tpi.

[2] 2 x 2 herringbone twill, center reversal.

*Note that preliminary draft specification type numbers may not correspond to the numbers in the final specifications.

b. Major Seams and Joints

Because the test parachutes were manufactured using the continuous ribbon technique, very few major seam and joint types were required during fabrication. Continuous rows of straight stitching along the radials and vertical ribbons were used to join them to the horizontal ribbons and to the skirt and vent bands. Continuous rows of straight stitching along the multiple ply skirt and vent bands were used to join the plies and fasten the bands to the radials and vertical ribbons.

Details of the ribbon splice and the skirt band splice and the suspension line to skirt reinforcement joint are given in Figures B-5 and B-6. While the construction of the splices were the same for the nylon and Kevlar parachutes, the number of stitches per inch and the thread type were different. The nylon parachutes were stitched in accordance with Reference 16 to provide splices that would withstand ultimate loads of at least 90 percent of the ultimate strengths of the component materials (joint efficiencies of 90 percent or greater). The Kevlar parachutes provided joint efficiencies of: (1) from 69 to 87 percent for the ribbon splices; (2) from 70 to 94 percent for the skirt band splices; and, (3) from 76 to 87 percent for the suspension line to skirt reinforcement joints.

7. PARACHUTE WEIGHTS

All test parachutes were weighed prior to packing. Total parachute weights included the weights of all major parachute components; the canopy, suspension lines, and riser lines. Canopy weights were estimated as an average of two weighings. The first weighing involved placing the canopy portion on the scale and supporting the remainder of the parachute in such a manner that little weight was added to, or subtracted from, the canopy weight by the support of the rest of the parachute. The second weighing involved placing all

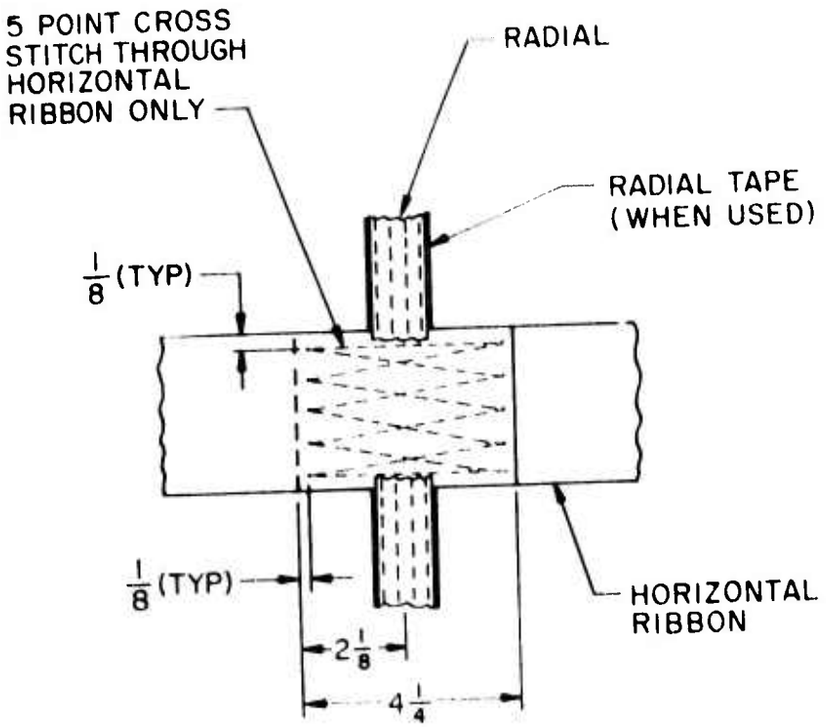

Figure B-5. Design Details for a Typical Horizontal Ribbon Splice.

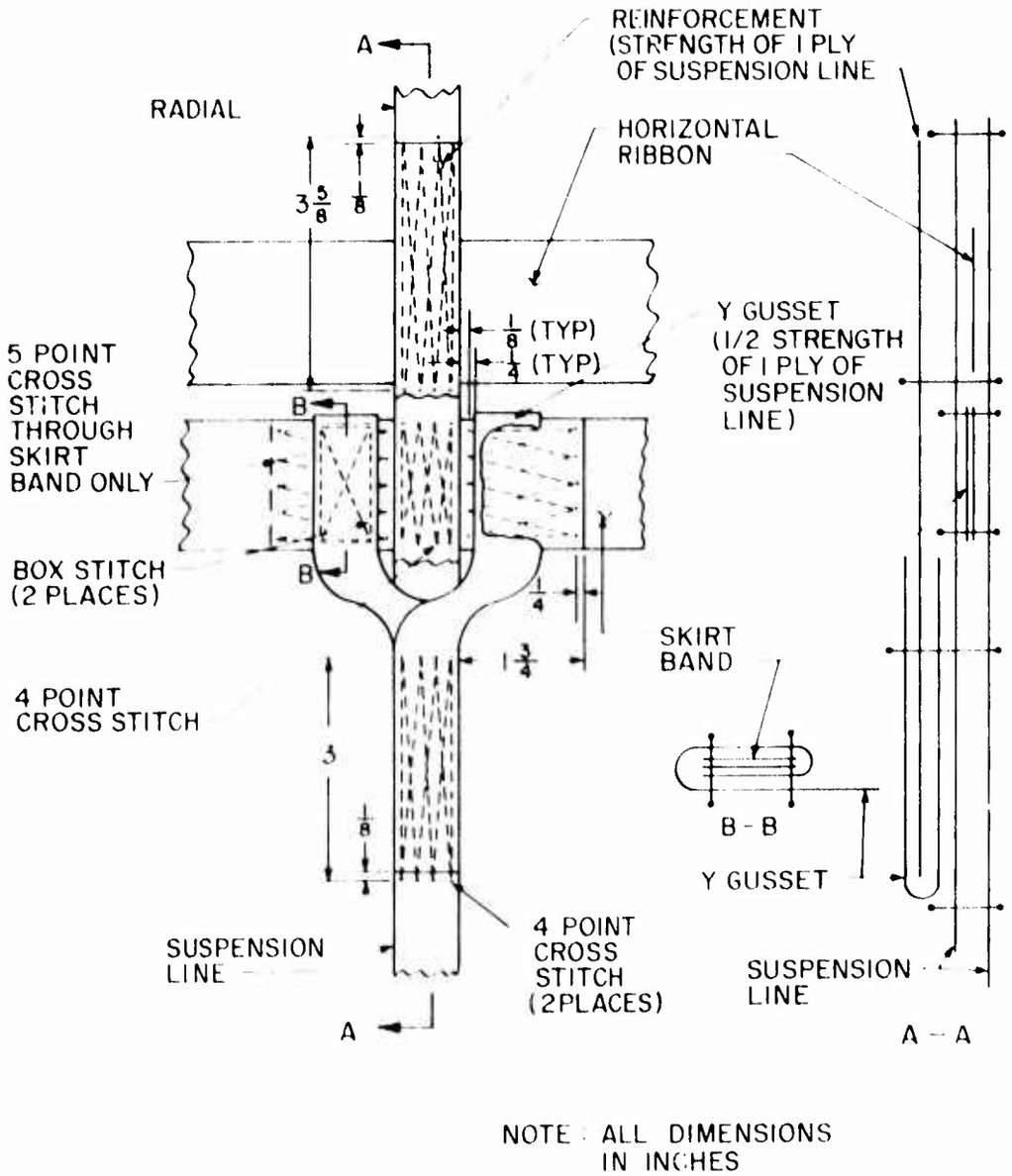

NOTE: ALL DIMENSIONS
IN INCHES

Figure B-6. Design Details for a Typical Skirt Band Splice and Suspension Line to Skirt Reinforcement Joint.

of the parachute except the canopy on the scale and supporting the canopy in the same manner as the rest of the parachute was supported in the first weighing. The weight determined from the second weighing was subtracted from the total parachute weight to give a second canopy weight. The average of the two canopy weights was used.

The total parachute and canopy weights established in this manner for each test parachute are tabulated in Tables 2 and 3 of Section II. The weights of the nylon parachutes ranged from 20.0 to 62.0 lb and the weights of comparable strength Kevlar parachutes ranged from 8.2 to 35.6 lb.

APPENDIX C
DESCRIPTION AND DESIGN OF THE PARACHUTE ATTACHMENT, DEPLOYMENT, AND RELEASE COMPONENTS

A number of components were used during this test program to provide for parachute attachment to, and deployment and release from, the Arrowhead and Tomahawk sleds. Photographs of the major components are presented in Figure C-1 and a sketch showing their sequence of operation is presented in Figure C-2.

1. PARACHUTE ATTACHMENT/DEPLOYMENT/RELEASE MECHANISMS

The parachute attachment/deployment/release mechanisms provided for: (1) attachment of the riser lines of the test parachute to the sled, through the drag force tensiometer; (2) initiation of the parachute deployment process; and, (3) release of the parachute after a test run. Two mechanisms were used during the test program; sketches of both are presented in Figures C-3 and C-4. Each mechanism consisted of: (1) a threaded adapter for fastening the tensiometer to the sled; (2) a tensiometer; (3) a shear pin to protect the tensiometer; (4) a parachute attachment/release fitting; and, (5) a drogue gun assembly for launching the deployment cone. Differences between the two mechanisms were in the design of the parachute attachment/release fitting. The first fitting used, Figure C-3, provided for the attachment of 12 parachute riser lines of widths up to 1 in. Parachute release was effected by cutting the riser lines with a linear shaped charge. The second fitting used, Figure C-4, provided for the attachment of 12 parachute riser lines of widths up to 1-1/8 in. Parachute release was effected by driving a release ring upstream with the explosive charge from four, 4 gram, S-68 squibs. The only malfunction of either mechanism occurred on test 6P-H5 when the reaction from

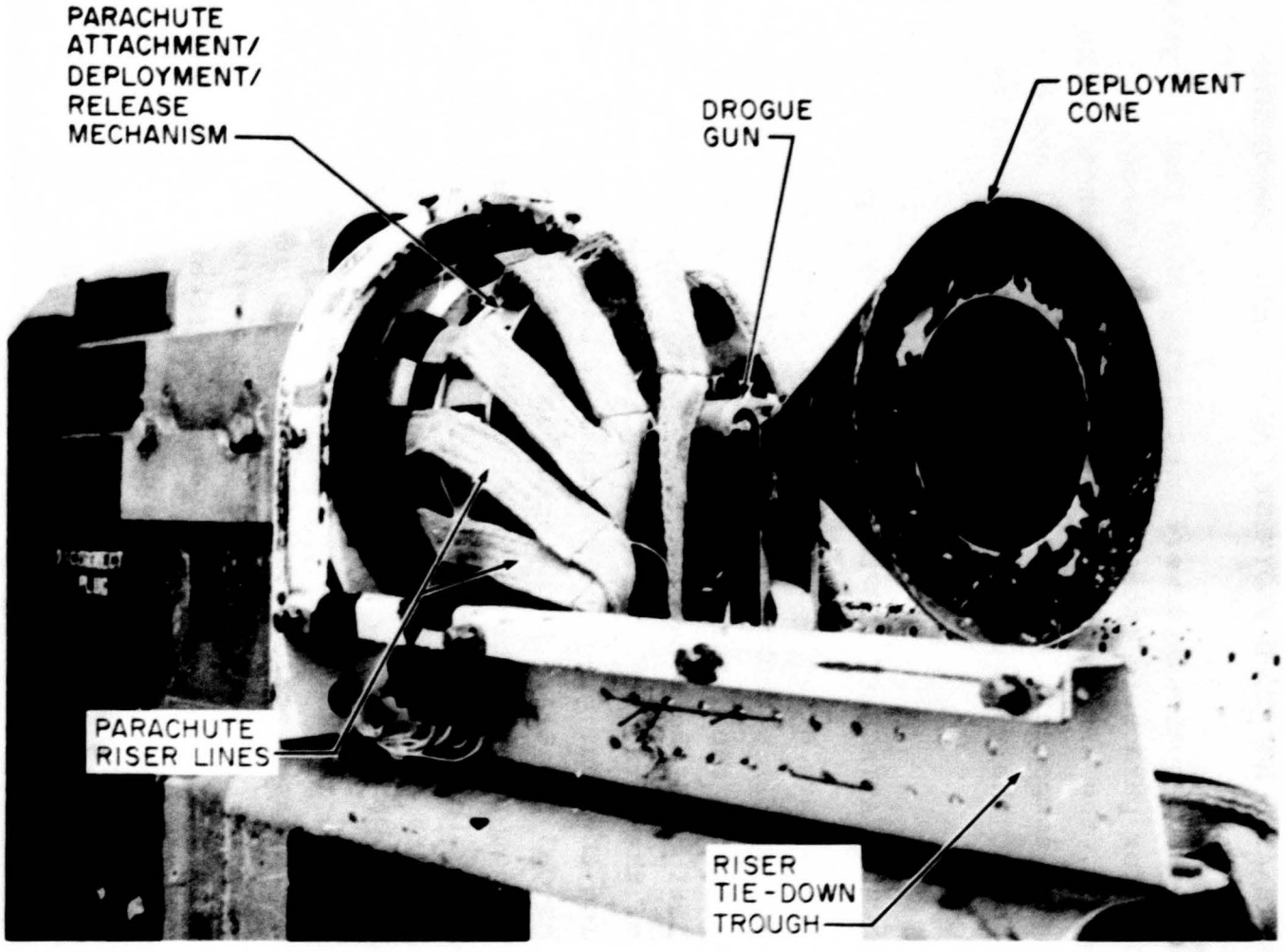

a. Top of Sled.

Figure C-1. Photographs Showing the Major Parachute Attachment, Deployment, and Release Components.

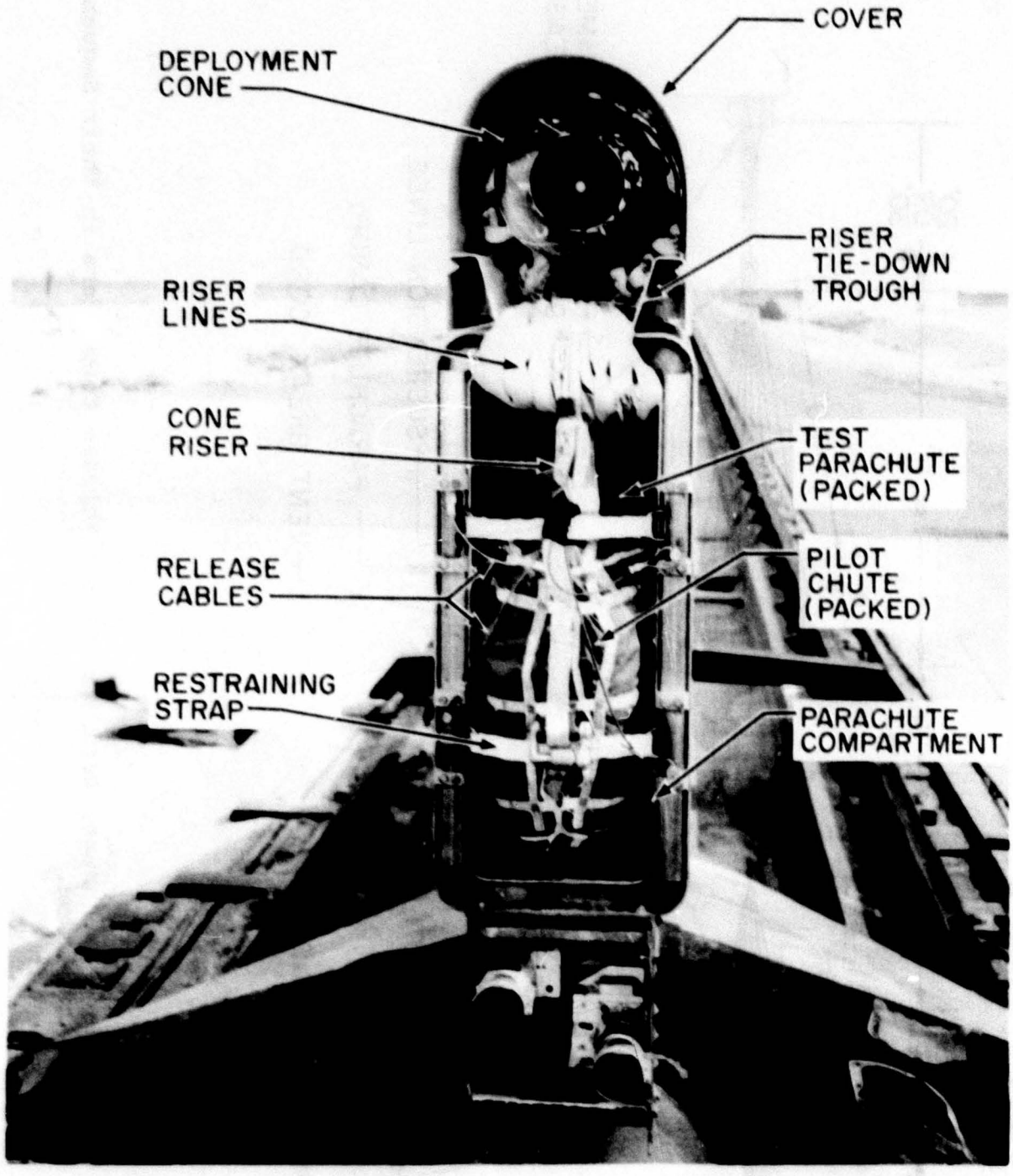

b. Parachute Compartment.

Figure C-1 (concluded). Photographs Showing the Major Parachute Attachment, Deployment, and Release Components.

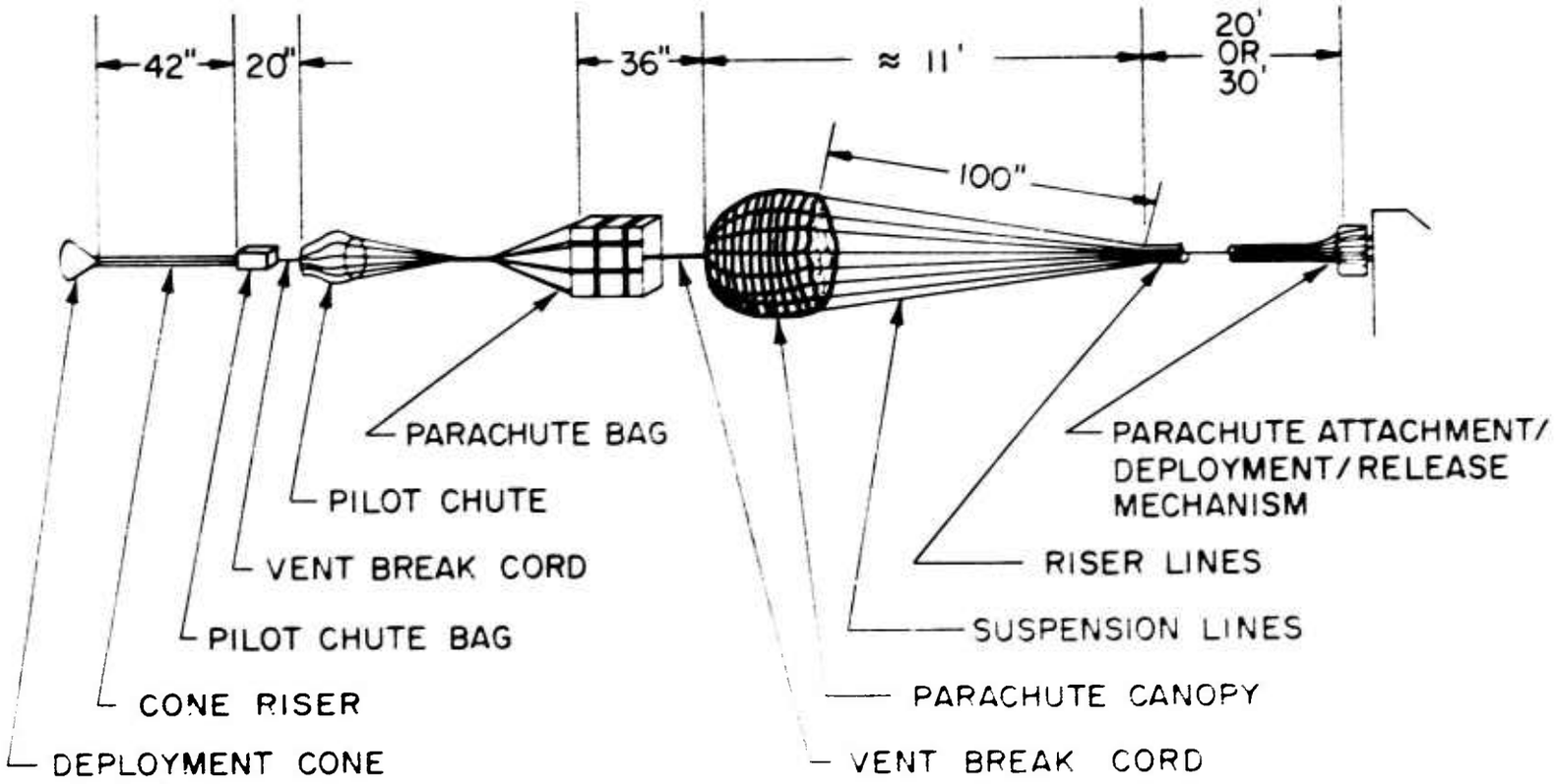

Figure C-2. Major Attachment, Deployment, and Release Components in Their Sequence of Operation.

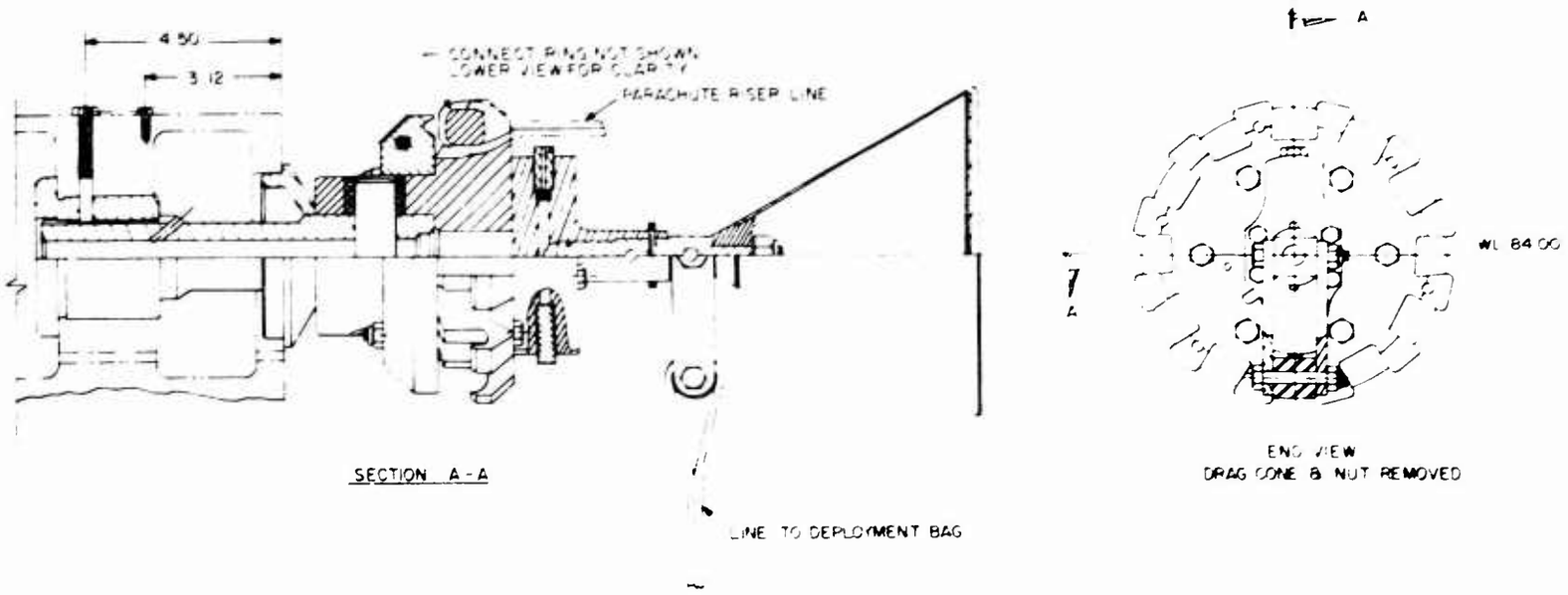

Figure C-3. Parachute Attachment/Deployment/Release Mechanism - Used on Tests 1 Through 11 (Those Prior to 1974).

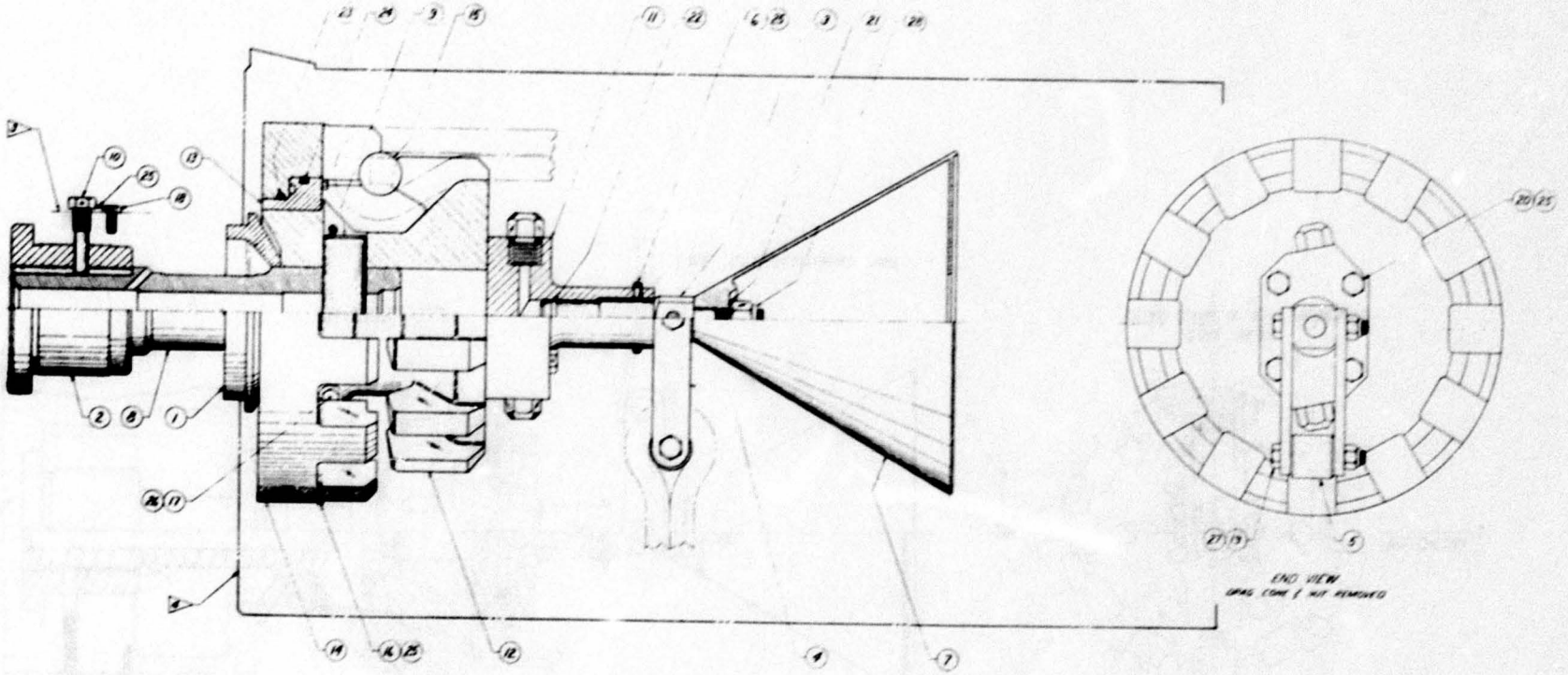

Figure C-4. Parachute Attachment/Deployment/Release Mechanism - Used on Tests 12 Through 20 (Those after 1973).

cone deployment sheared the pins in the release ring allowing the parachute to be released prematurely. The strengths of the shear pins were increased and no further malfunctions were experienced.

2. DEPLOYMENT CONE, CONE RISER, AND RELEASE CABLES

An 8 in. diameter, 60 deg included angle, aluminum deployment cone was used as the inertia slug and first stage drag device to initiate parachute deployment for all tests conducted under this program. Two M6 special (blasting) caps provided the energy in the drogue gun to drive the deployment cone mortar out of the gun with a muzzle velocity of approximately 85 ft/sec.

A cone riser was attached to the bucket handle type pin link of the deployment cone mortar. The riser transferred cone momentum and drag to the parachute restraining strap release cables and to the pilot chute bag. A sketch of the cone riser is presented in Figure C-5. The cone riser was basically a 40 in. long piece of 2 ply nylon webbing with attachment loops for connecting the riser to the deployment cone, pilot chute bag, release cables, and the ties in the riser tie-down trough.

The release cables consisted of 1/4 in. steel aircraft cable, copper nicro press fittings, and steel release pins. The length of cable between the pins was 24 in.

3. PILOT CHUTES

A number of different pilot chutes were used during this program; they are listed in Table C-1.

a. Early Sled Tests

Test parachute deployments for the first two runs conducted under this program were designed to be accomplished without the aid of a pilot chute. On the first test, 6P-E2,

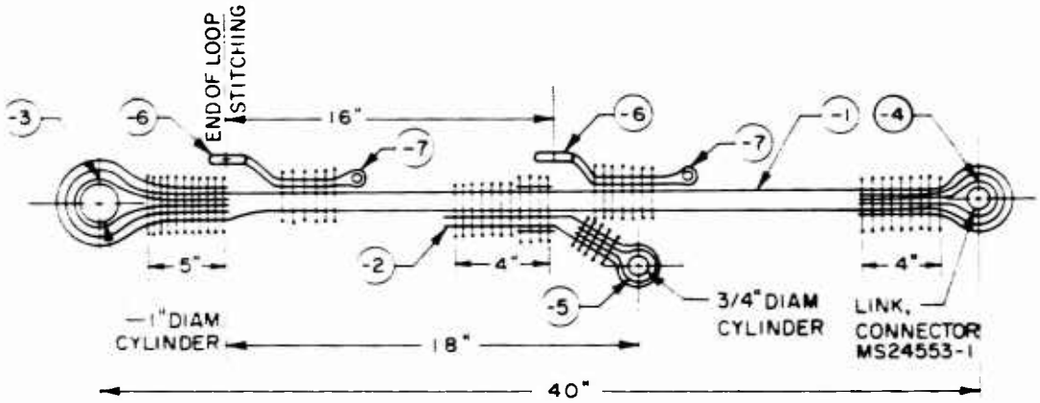

DASH NO	NOMENCLATURE	MATERIAL SPECIFICATIONS
-7	TIE-DOWN LOOP	MIL-W-5625, 1/2 in., 1000 lb
-6	CUT KNIFE	steel, 3/8 in. diameter hole
-5	RELEASE CABLE BUFFER	MIL-W-5665, TYPE XVII, 1 in., 1000 lb
-4	CONNECTOR LINK BUFFER	MIL-W-4088, TYPE XIX, $1\frac{3}{4}$ in., 10,000 lb
-3	CONE LINK BUFFER	MIL-W-4088, TYPE XVII, 1 in., 2500 lb
-2	RELEASE CABLE WEBBING	MIL-W-27657, TYPE III, 1 in., 6000 lb
-1	MAIN RISER WEBBING	MIL-W-27657, TYPE III, 1 in, 6000 lb

Figure C-5. Sketch of the Cone Riser.

TABLE C-1

PILOT CHUTES USED FOR THE TEST PROGRAM

Test Run	Test Run Designation	Pilot Chute	Test Run	Test Run Designation	Pilot Chute
1	6P-E2	None	11	6P-H1	13"D Supersonic-X-3
2	6P-E3	None	12	6P-H2	13"D Supersonic-X-3
3	6P-E4	18" Dp Hyperflo	13	6P-H3	13"D Supersonic-X-3
4	6P-F1	18" Dp Hyperflo	14	6P-E9	13"D Supersonic-X-3
5	6P-F2	18" D Supersonic-X-3	15	6P-E10	13"D Supersonic-X-3
6	6P-F3	18" D Supersonic-X-3	16	6P-G4	9.5"D Supersonic-X-3
7	6P-E6	18" D Supersonic-X-3	17	6P-G5	9.5"D Supersonic-X-3
8	6P-G1	13" D Supersonic-X-3	18	6P-H5	9.5"D Supersonic-X-3
9	6P-G2	13" D Supersonic-X-3	19	6P-H6	9.5"D Supersonic-X-3
10	6P-G3	13" D Supersonic-X-3	20	6P-H7	9.5"D Supersonic-X-3

the deployment cone deployed so late in the test run that it generated insufficient force to extract the test parachute from its compartment. On the second test, 6P-E3, the deployment cone deployed as programmed and extracted the parachute as desired. However, analysis of the trackside motion picture coverage showed that the test parachute hesitated on coming out of its compartment, indicating that the force transmitted from the deployment cone to the parachute bag may have been marginal. An existing 18 in. projected diameter, nomex, ribbon roof, Hyperflo type pilot chute was added to the deployment system for the third test, 6P-E4. The deployment cone failed to deploy on this test and the program was interrupted to establish a reliable deployment technique. The 18 in. diameter Hyperflo pilot chute was included in the first deployment system checkout test, 6P-F1, and it operated satisfactorily. All subsequent tests incorporated a pilot chute as a deployment aid.

b. Supersonic-X-3 Pilot Chute Design

The parachute type selected as the pilot chute for test runs 5 through 20 was the Supersonic-X-3 parachute as described in Reference 17. The Supersonic-X-3 parachute is one of a family of continuous surface of revolution parachutes designed for operation at supersonic and hypersonic speeds (Reference 18). The Supersonic-X parachute was selected because of its excellent performance characteristics at supersonic speeds (i.e., rapid inflation, excellent oscillatory stability,

---

(17) Galigher, L.L.: Aerodynamic Characteristics of Supersonic-X Parachutes at Mach Numbers of 2.1 and 4.0, Arnold Engineering Development Center Report AEDC-TR-69-8 (AD-846-695), January 1969.

(18) Babish, C.A. III: A Continuous Surface of Revolution Parachute for Supersonic/Hypersonic Speeds, AIAA Paper No. 70-1173, presented at the AIAA Aerodynamic Deceleration Systems Conference, September 1970.

average drag coefficient, and fair inflation stability) and because it is easily fabricated. Design details of the Supersonic-X-3 pilot chutes used on this program are given in Figure C-6.

c. Pilot Chute Bags

All pilot chutes were hand packed into their own split flap type deployment bags (see Figures C-11-g through C-11-i). The design shapes of the bags were parallelepipeds. Loops were sewn into the bags to accept vent break cords and pilot chute line break ties.

4. DEPLOYMENT CONTROL BREAK TIES

a. Deployment Problems at High Dynamic Pressures

Parachute deployment at high dynamic pressures introduces many critical constraints into the design of the deployment aids. This was especially evident during this test program.

Sufficient force had to be generated by a deployment aid to extract the test parachute from its compartment on-board the decelerating track sled. The deployment aid itself had to be deployed to a position behind the test parachute where it could generate the required force. These design constraints were not sufficiently satisfied during the first three tests on this program and the program was interrupted to develop a reliable deployment system. Modification to the cone deployment mechanism and the introduction of a pilot chute provided for satisfactory extraction of the test parachute.

The deployment aids were also required to separate the test parachute from the sled to a position downstream where parachute inflation was desired. For this program, the separation distance was as large as 40 ft. Parachute

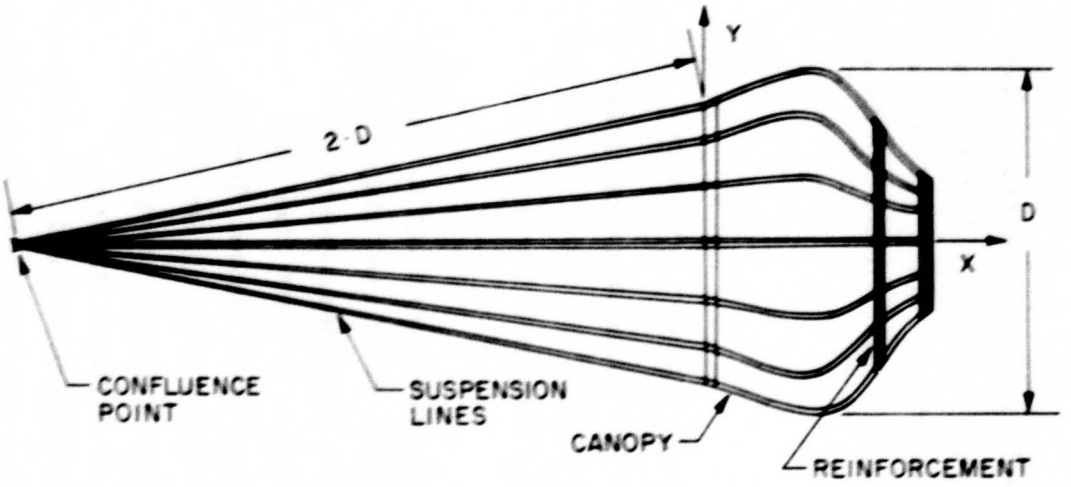

CANOPY PROFILE COORDINATES

X/D	Y/D	X/D	Y/D	X/D	Y/D
0.00	0.40	0.30	0.50	0.55	0.34
0.05	0.42	0.325	0.50	0.58*	0.28*
0.10	0.44	0.35	0.50	0.60	0.26
0.15	0.46	0.40	0.49	0.65	0.22
0.20	0.48	0.45	0.46	0.70	0.20
0.25	0.49	0.50	0.41	0.725	0.20

* LOCATION OF REINFORCEMENT

a. Parachute Profile.

Figure C-6. Design Details of the Supersonic-X-3 Pilot Chutes.

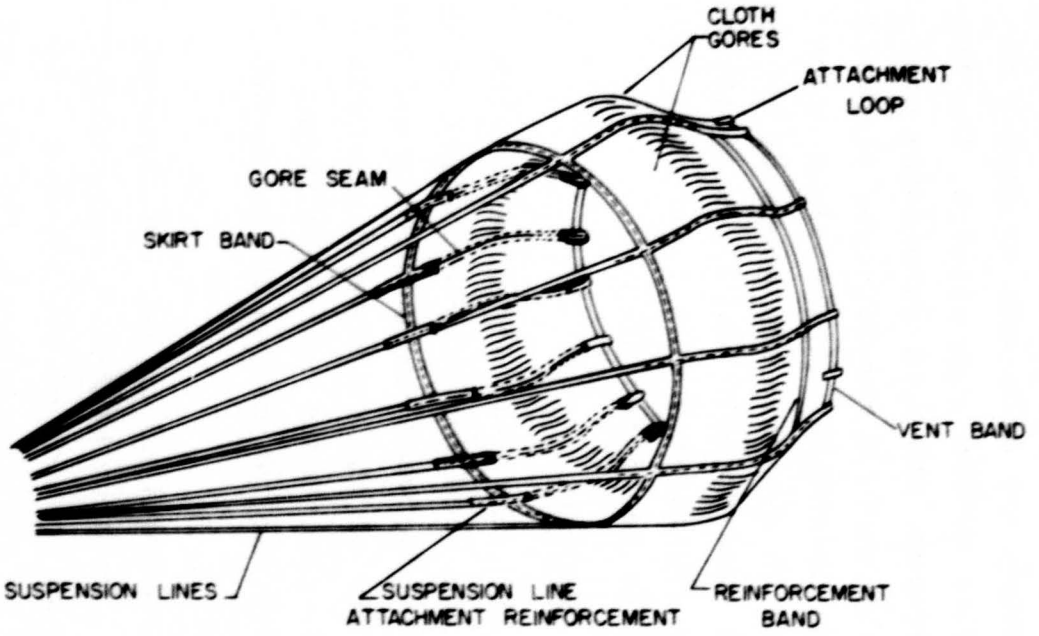

NOMENCLATURE	MATERIAL SPECIFICATIONS	18"D	13"D	9.5"D
		SUPERSONIC-X-3		
CLOTH CANOPY GORES	MIL-C-8021, TY. III, 14 oz/yd^2, 600 x 600 lb	x	x	x
SUSPENSION LINES	MIL-C-7515, TY. IX, 40001b	x	-	-
SUSPENSION LINES	MIL-C-7515, TY. VIII, 30001b	-	x	-
SUSPENSION LINES	MIL-C-7515, TY. VI, 20001b	-	-	x
SKIRT, VENT, & REINF. BANDS	MIL-W-27657, TY. V, 1 in., 90001b	x	-	-
SKIRT, VENT, & REINF. BANDS	MIL-W-27657, TY. III, 1 in., 60001b	-	x	-
SKIRT, VENT, & REINF. BANDS	MIL-W-5625, 1 in. tubular, 4000 lb	-	-	x

b. Construction and Materials.

Figure C-6 (Concluded). Design Details of the Supersonic-X-3 Pilot Chutes.

separation from the sled was to proceed orderly and parachute inflation was not to begin until all lines were stretched out. On the first two deployment system checkout tests, 6P-F1 and 6P-F2, the pilot chute extracted the test parachute from its compartment satisfactorily, but then proceeded to strip the bag from the parachute, leaving the parachute to deploy on its own and to begin inflation before line stretch. For the first five tests on this program, the test parachutes were constrained inside their bags using a more-or-less standard method for heavy duty ribbon parachutes. Three 33 lb nylon "quilting" ribbons were used to maintain the shape of the bag and from 10 to 17 ties were used to hold the lines to the bag; 2 ply, 90 lb nylon tape for the first 8 or 9 ties and 1 ply, 33 or 90 lb nylon tape for the remaining ties.

b. Break Tie Design Criteria

The results from the first two deployment system checkout tests pointed out the need for better control of the deployment process by the ties between the parachute and its bag. This need, and the nature of the deployment problems encountered during the first five tests on this program, established the criteria used for the design of the break ties for all subsequent tests.

The break ties were required to be of sufficient number and strength so that, without breaking prematurely, each tie would accelerate that portion of the parachute it was holding an amount equal to the acceleration the bag and parachute would have when acted upon by the maximum extraction force expected at any time during a test. Each break tie was also required to be broken by a steady pull of the minimum extraction force expected at that time during a test when the velocity of that portion of the parachute the tie was holding was brought up to the velocity of the sled.

c. Analytical Simulation of Deployment Dynamics

(1) Calculation Method

The locations and strengths of the break ties which would satisfy the design criteria were determined using a calculation method which provided analytical simulation of the behavior of the track sled and the components of the deployment system during the deployment process.

(2) Physical System

As shown in Figure C-2, components of the deployment system included the following:

deployment cone
cone riser
pilot chute bag
pilot chute
test parachute bag
test parachute

The period of interest for design of the break ties was during the time the extraction force acted on the component being deployed. For the case of break ties for the pilot chute, it was from the time of stretch of the cone riser until strip-off of the pilot chute bag; for the case of the break ties for the test parachute, it was from the time when the pilot chute opened until strip-off of the test parachute bag.

(3) Dynamic Model

One dynamic model was constructed which was applicable to both periods of interest. The physical system was separated into two point masses. One mass represented the track sled; the sled mass, m_s. The other mass was called the parachute mass, m_p, and was used to represent either: (1) the instantaneous mass of the pilot chute and

the test parachute bag and its contents, or (2) the instantaneous mass of the deployment cone, cone riser, and the pilot chute bag and its contents.

Each mass had only one degree of freedom, translation along the axis of deployment. The translations and forces considered in the analysis are defined in Figure C-7.

(4) Equations of Motion

The basic equations of motion for the sled and parachute masses were as follows:

$$\frac{d^2(x_s)}{dt^2} = -FS/m_s \qquad (C-1)$$

$$\frac{d^2(x_p)}{dt^2} = (R-D)/m_p \qquad (C-2)$$

where:

FS = Force resisting sled motion, taken as that value such that the ratio FS/m_s had the same value as the sled deceleration which was predicted for the time of deployment by the Holloman Track, and was assumed constant throughout the period of deployment, lb.

R = Resisting force of the parachute ties, lb. (Although included in the analytical simulation, this force was so small that it had negligible effect on system motions.)

D = Drag force of the pilot chute (or cone) and the parachute bag (or pilot chute bag), lb.

(5) Initial Conditions

Integration of the equations of motion provided velocities and displacements as functions of time.

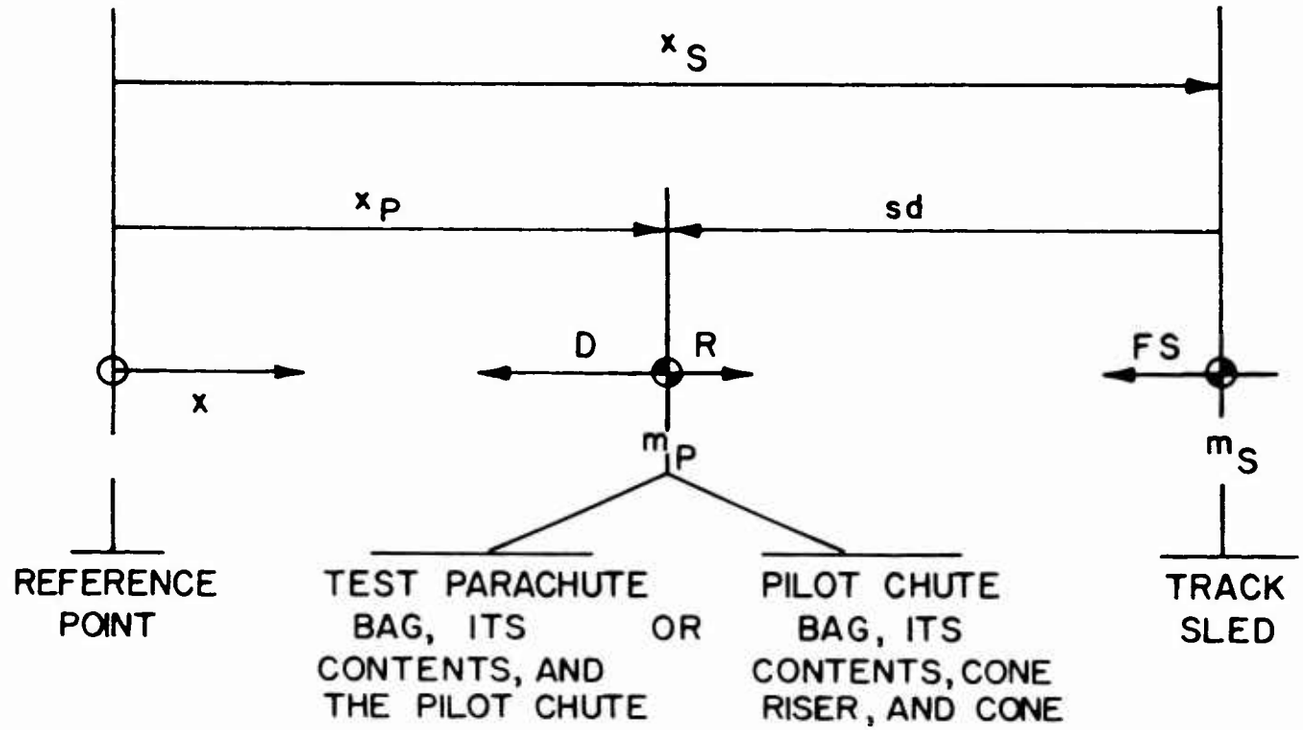

Figure C-7. Translations and Forces Used in the Model of Deployment Dynamics.

Evaluation of the constants of integration required values for the initial conditions. The displacements of the sled and parachute masses were taken as zero at the time of initiation of extraction of the parachute (or pilot chute) from the sled. The velocities of these two masses at this time were taken as the sled velocity which was predicted by the Holloman Track for the time of deployment initiation.

(6) Maximum Allowable Tie Strength

The design criteria for the maximum allowable break tie strength, $(TS)_{max}$, specified that the tie should break under the minimum expected drag force of the pilot chute and parachute bag. That is,

$$(TS)_{max} \leq (D)_{min} \qquad (C-3)$$

To ensure that the tie would break under the minimum expected drag force a design factor, DF1, was applied as follows:

$$(TS)_{max} = (D)_{min}/DF1 \qquad (C-4)$$

where,

$$DF1 = (SF)\ (KEF)\ (OF) \qquad (C-5)$$

and,

SF = Safety factor, 1.5
KEF = Knot efficiency factor, 0.75
OF = Overload factor, 1.5 (to account for the tie breaking at loads above its rated strength).

(7) Minimum Allowable Tie Strength

The design criteria for the minimum allowable break tie strength, $(TS)_{min}$, specified that the tie must accelerate the mass it was holding an amount equal to the acceleration the parachute mass would have when acted upon by the maximum expected drag force of the pilot chute and parachute bag. That is,

$$\frac{d^2(x_t)}{dt^2} = \frac{d^2(x_p)}{dt^2} \qquad (C-6)$$

where

$$\frac{d^2(x_p)}{dt^2} = [R - (D)_{max}]/m_p \qquad (C-7)$$

and

$$\frac{d^2(x_t)}{dt^2} = -(TS)_{min}/(DF2)m_t \qquad (C-8)$$

where

x_t = Translation of the mass that the tie was holding, ft

m_t = Mass that the tie was holding, slug,

and where the design factor, DF2, was

$$DF2 = (SF)/(KEF) \qquad (C-9)$$

Solving the above equations for the minimum allowable tie strength gave:

$$(TS)_{min} = (DF2)\ (m_t)\ [(D)_{max} - R]/m_p \qquad (C-10)$$

(8) Other Functional Relationships

Solving Equations C-4 and C-10 for the required tie strengths required functional relationships to be developed for the independent parameters of parachute mass, m_p, drag force, D, tie resistance, R, and tie mass, m_t, in terms of known quantities.

The parachute mass, m_p, as a function of separation distance, sd, was determined by weighing all appropriate components, such as lines, canopy, bag, pilot chute, cone riser, etc., and measuring appropriate parachute lengths before and after packing and installation on the sled.

Drag forces were calculated using the following general equation:

$$D = (C_D)\ (S)\ (0.5)\ (RHO)\ \left[\frac{d\ (x_p)}{dt}\right]^2 \qquad (C\text{-}11)$$

where

C_D = Drag coefficient,

S = Reference area, sq ft

RHO = Air Density at the Track, slug cu ft.

Expressions were assumed for the drag coefficients of the deployment cone, pilot chute bag, pilot chute, and parachute bag as functions of freestream Mach number and separation distance.

The resistance force of the parachute ties, R, was expressed as a function of separation distance to account for the number, location, and elongation of the ties, and as a function of the length, elongation at break, and the strength of the ties.

The mass that the ties was holding, m_t, was expressed in terms of the parachute mass distribution and the number and location of the ties.

(9) Computer Program

The analytical simulation of deployment dynamics was programmed for computer solution using the Air Force Aeronautical Systems Division MIMIC Computer Program (Reference 19) on the IBM 7090 (7094) computer and using the Control Data Corporation (CDC) MIMIC Digital Simulation Language (Reference 20) on the CDC 6600 and CYBER series computers. MIMIC provided digital solutions of the ordinary differential equations through an iteration process in accordance with the Runge-Kutta method.

Input values for a total of twenty quantities were required for each computer program run: the weight of the pilot chute and the weights of the parachute lines, canopy and bag; five lengths associated with the parachute before and after packing and installation; the percent of elongation at break of the ties; the lengths and number of bag, line, and canopy ties; the predicted velocity and acceleration of the track sled at deployment; and the reference areas for the pilot chute and parachute bag.

Computer program output was a listing of all program parameters as functions of time, including the

---

(19) Sanson, F.J. and Peterson, H.E., MIMIC Programming Manual, Air Force Aeronautical Systems Division Report, SEG-TR-67-31, July 1967.

(20) Anon., Control Data 6000 Computer Systems MIMIC Digital Simulation Language Reference Manual, Control Data Corporation Publication 44610400, January 1972.

maximum and minimum allowable break tie strengths and the translations, velocities, and accelerations of the point masses which represented the sled and the deployment system components.

(10) Band of Allowable Break Tie Strengths

Because the design criteria for the break ties required the use of both minimum and maximum expected drag forces, all computer program equations of motion and functional relationships appeared twice in the program; once accounting for all expected variations in parameters acting in the direction that would produce the minimum drag, and once acting to produce the maximum drag. This means, for example, that a maximum tie strength value output from the program specified the breaking strength of a tie that would break when the pilot chute was operating in the lowest expected wake dynamic pressure and acting on the parachute bag which was moving at the lowest expected absolute velocity (that which it would have if acted upon by a pilot chute with the maximum expected drag).

Figure C-8 presents typical plots of minimum and maximum allowable tie strengths as functions of separation distance. The upper curve (upper for the first 38 ft of separation distance) represents the maximum allowable tie strength. That is, the strengths of selected ties must be below this curve to ensure that they will break. The lower curve represents the minimum allowable tie strength, and the strengths of selected ties must be above this curve to ensure that they will be able to accelerate the mass of the parachute they are holding an amount equal to the acceleration of the parachute. The amount of separation of the two curves, in the proper manner (maximum allowable above the minimum allowable), was a function of the number and location of the ties which were input into the program and which were varied parametrically for each computer run.

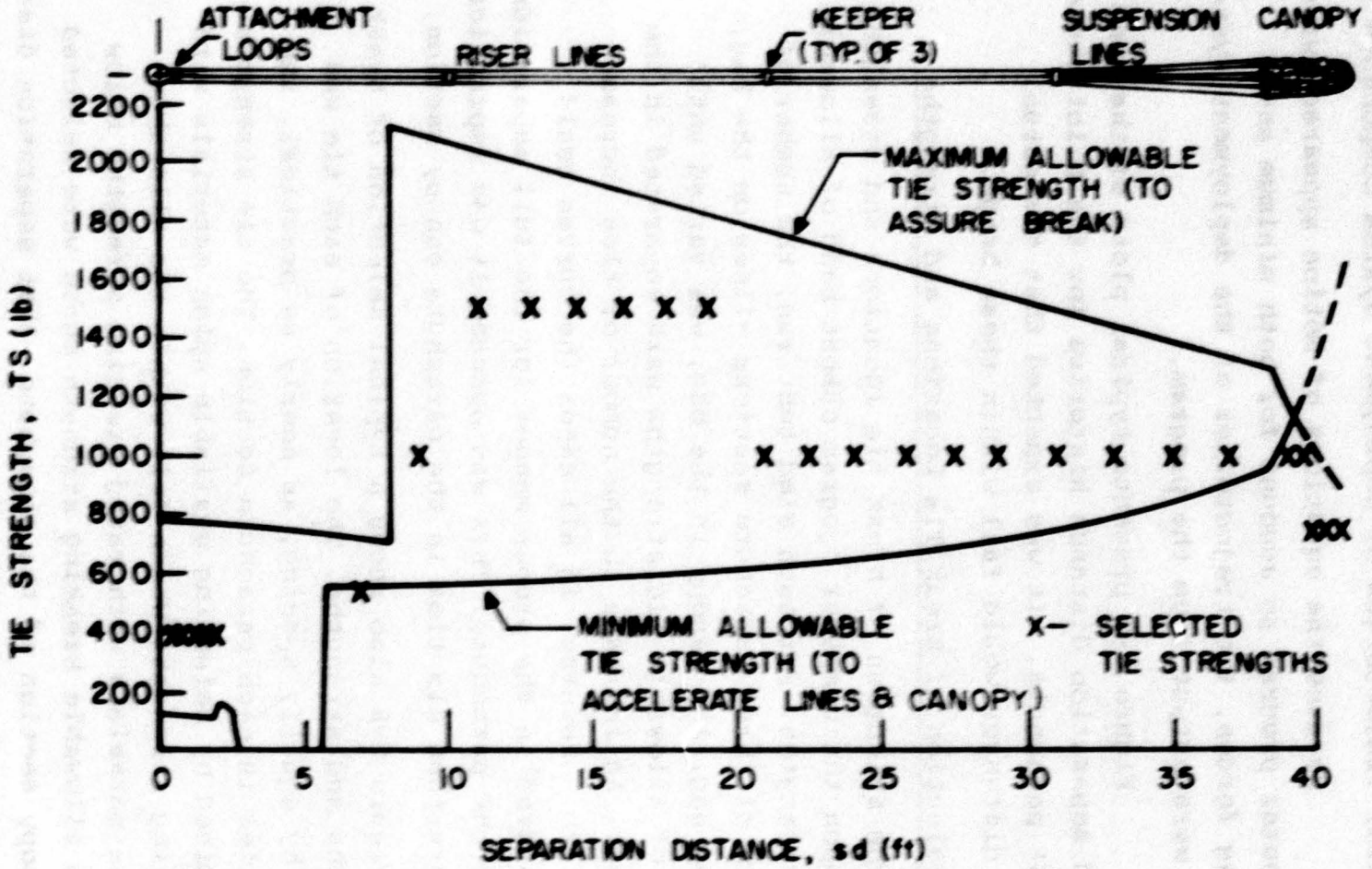

Figure C-8. Band of Allowable Tie Strengths - Test 6P-H7.

(11) Trajectories of Deployment System Components

Because the equations of motion appeared twice in the computer program to account for both minimum and maximum drag forces, two trajectories of the deployment system components were output from the program.

Figure C-9 presents typical plots of the band of expected separation distance histories for the pilot chute and the test parachute. It was expected that the actual separation distances would fall within these bands.

d. Selection of Break Tie Locations and Strengths

The selection of break tie locations and strengths was based upon the computer program output band of allowable break tie strengths. For each sled test run, the number of ties in each of three parachute sections -lines on the bag, lines in the bag, and canopy in the bag, was varied until the curves of allowable tie strengths were separated in the proper manner. An increase in the number of ties increased the band width. However, in all cases the curves could not be separated in the proper manner for the full separation distance of the parachute. This was because it was impractical to place more than six ties in the parachute canopy section.

Figure C-8 also shows a typical selection of break tie locations and strengths. The location of each tie was determined by equally spacing, as nearly as practical, the number of ties in each parachute section. The tie strengths were determined by selecting available nylon materials with rated breaking strengths which fell within the allowable band. Nylon materials with rated breaking strengths below the maximum allowable breaking strength curve were selected for the canopy section of the parachute -that separation distance where the allowable tie strength curves were improperly separated. This means, that although the canopy ties were

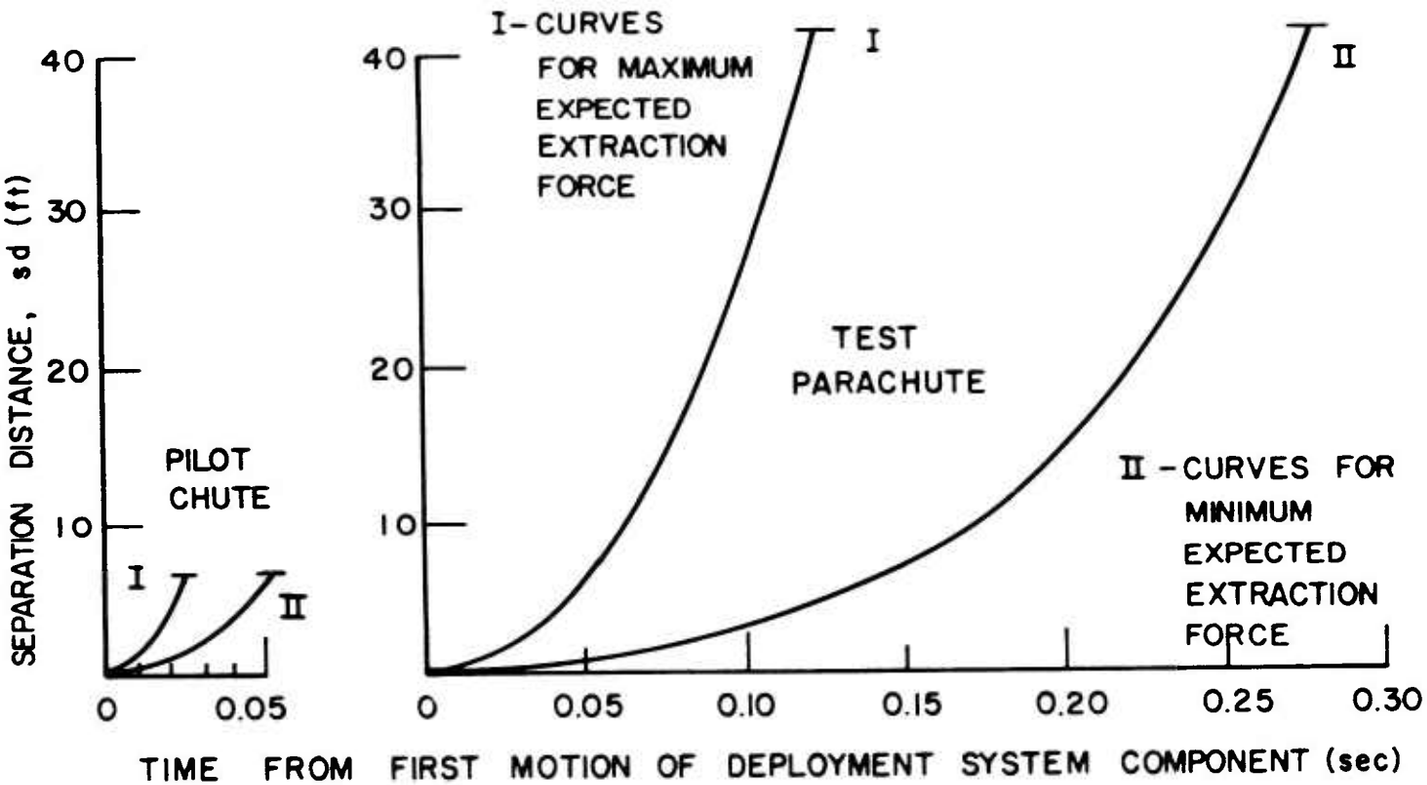

Figure C-9. Band of Separation Distance Histories for Deployment System Components-Test 6P-H7.

expected to break, they were not expected to provide sufficient force to accelerate the canopy an amount equal to the acceleration of the bag. That is, it was expected that the bag would be stripped from the canopy before the canopy was stretched out.

e. Design of the Break Ties

The analytical simulation method used to determine break tie strengths required that each tie hold a portion of the parachute mass, be of known length, and have a rated breaking strength. This requirement led to the development of a new design for the break ties.

The design of the break ties for the first five tests followed standard practices used for heavy duty ribbon parachutes. One end of a tie was fastened to a bag loop and the other end was passed around a "bight", or loop, in a group of lines and fastened to the same bag loop after pulling the bight tight. As the lines exited the bag, the bight tried to slip out of the break tie loop (and sometimes did) as it pulled on the tie. This break tie design was difficult to model in the computer program and estimations of the variations in the force at which a tie was expected to break were large and unreliable.

The design for the break ties used on this test program for the last 15 tests is illustrated in Figure C-10. Two line tie loops were sewn to opposing lines at each tie location. One end of each break tie was knotted to the first line tie loop. The other end was routed around the lines, through the second line tie loop, back through the first line tie loop, and finally tied to a bag loop. With this design: (1) the length of the tie was known; (2) the tie securely held its portion of the parachute - the more the lines pulled out of the bag, the more tightly the tie held the lines; (3) only a single ply of nylon material was required to break; and, (4) after the tie broke, the lines (or canopy) were free to deploy.

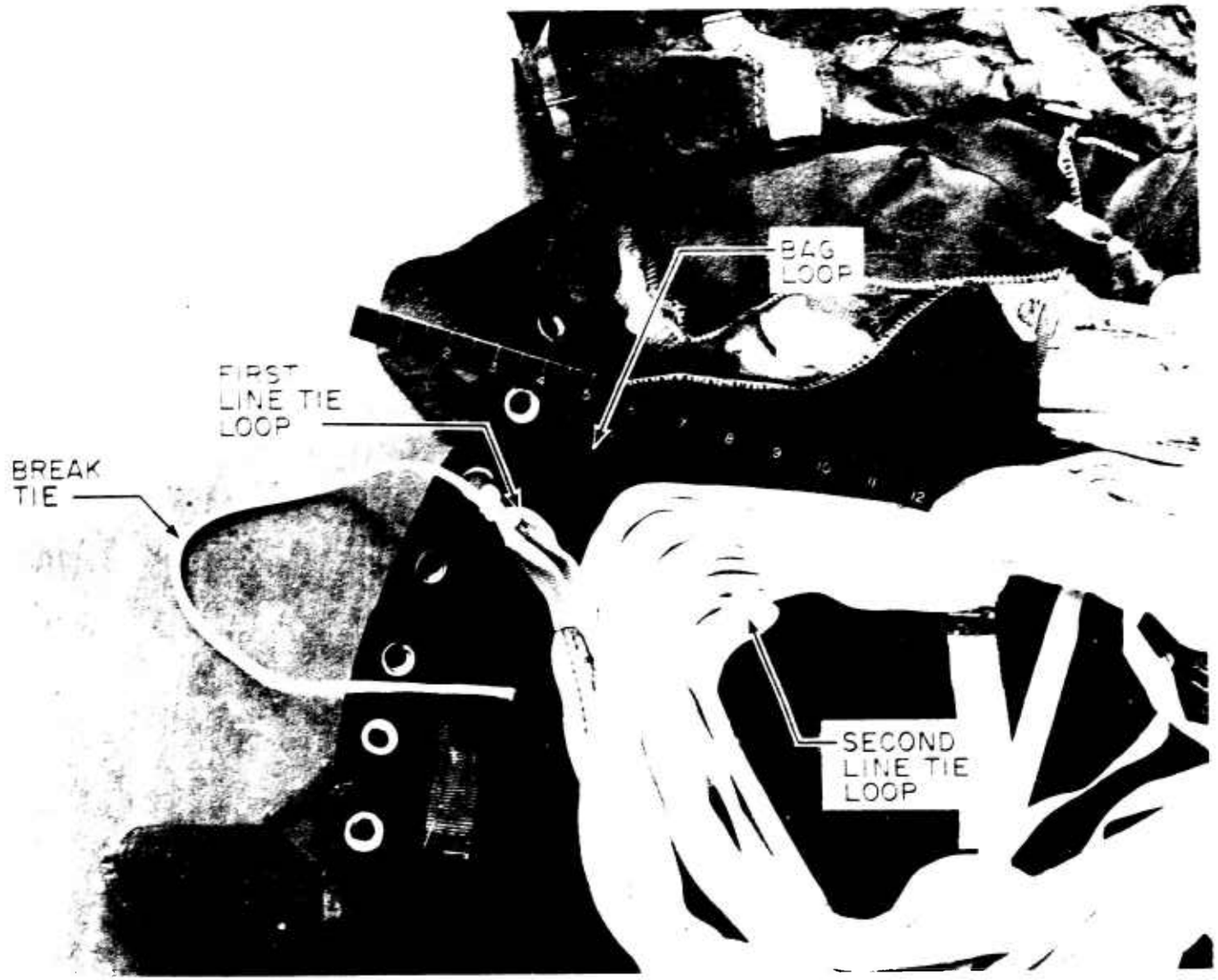

a. Step 1 - Break Tie Tied to First Loop.

Figure C-10. Design of the Deployment Control Break Ties.

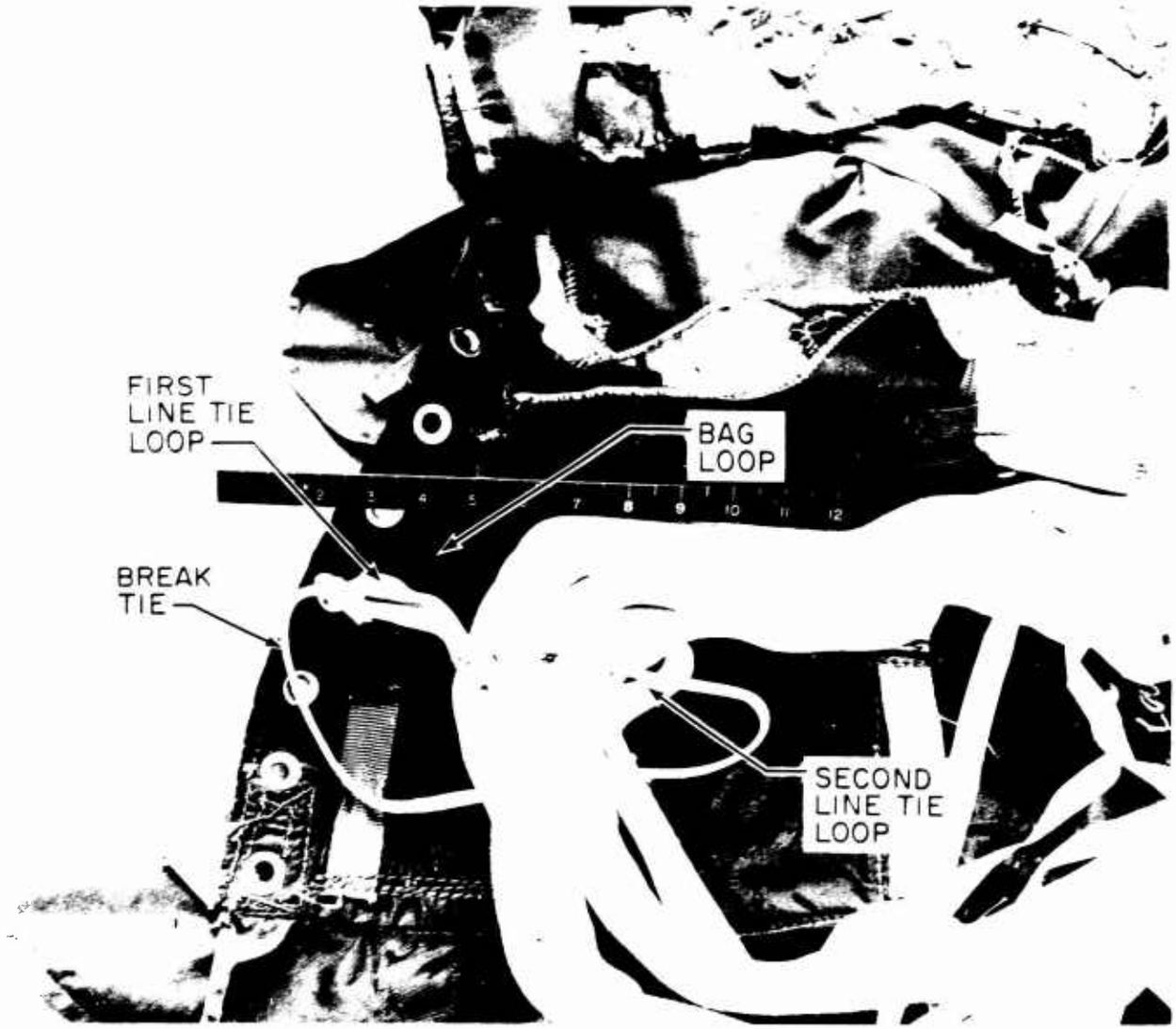

b. Step 2 - Break Tie Passed Through Second Loop.

Figure C-10 (Continued). Design of the Deployment Control Break Ties.

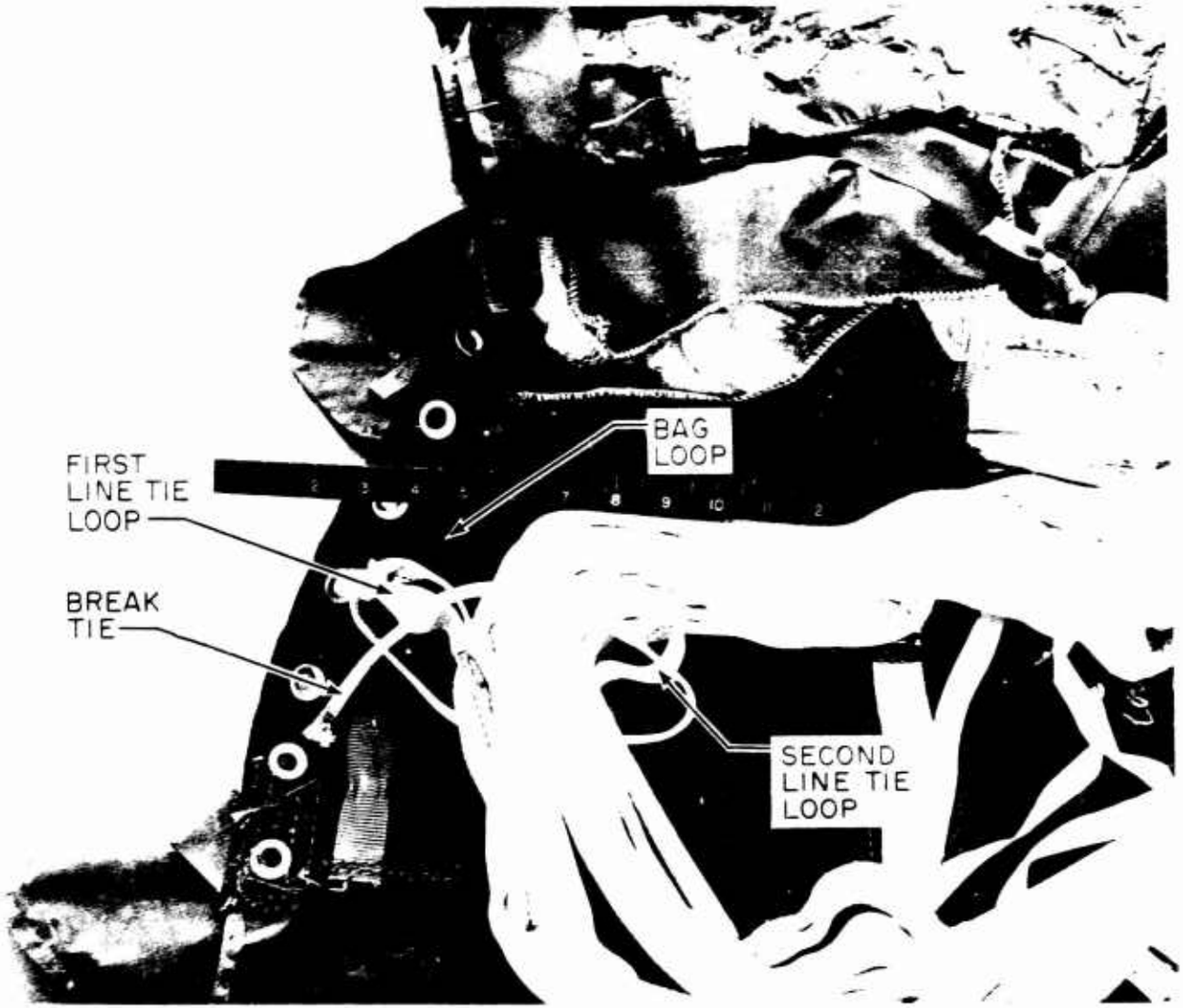

c. Step 3 - Break Tie Passed Back Through First Loop.

Figure C-10 (Continued). Design of the Deployment Control Break Ties.

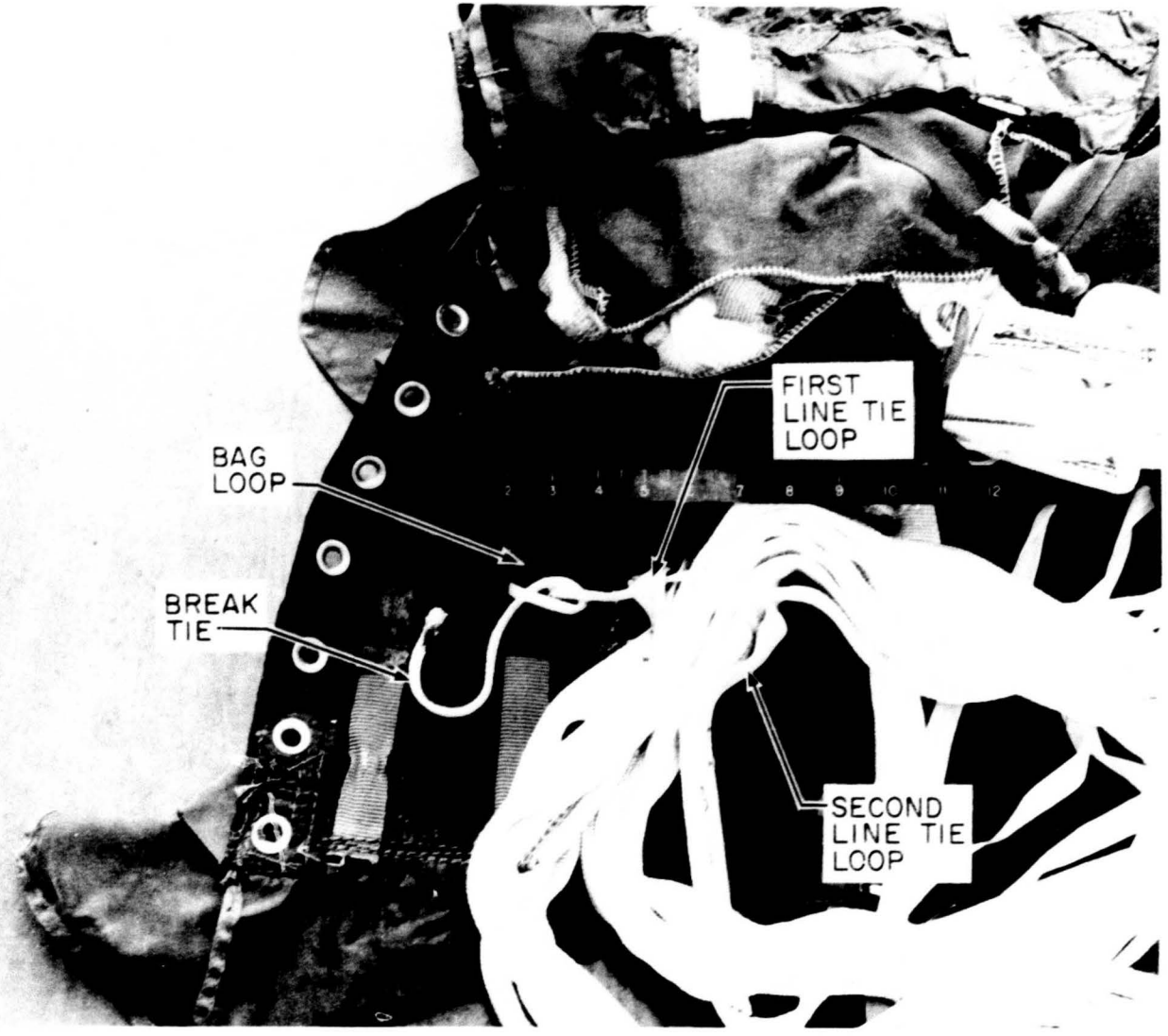

d. Step 4 - Break Tie Passed Through Bag Loop.

Figure C-10 (Continued). Design of the Deployment Control Break Ties.

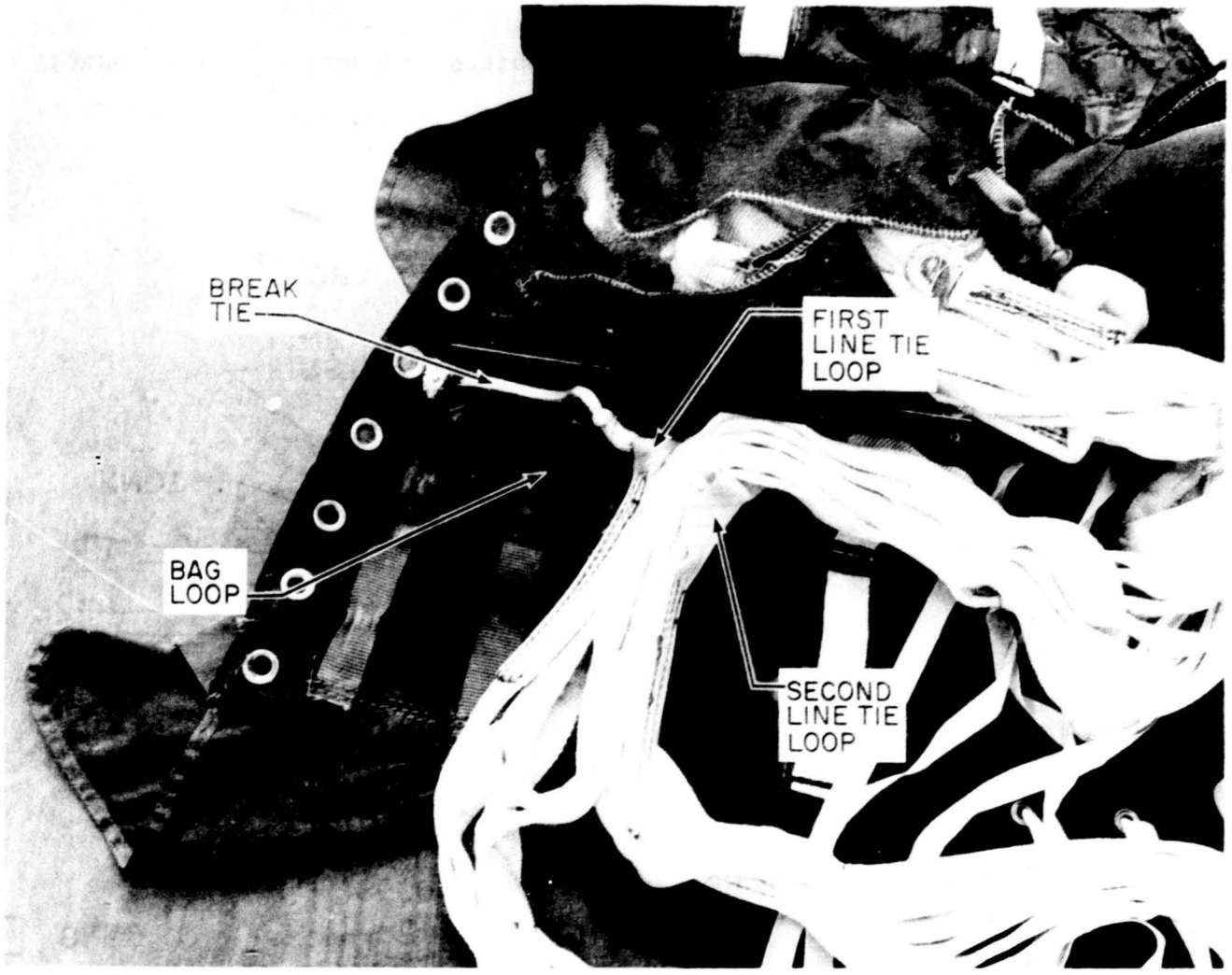

e. Step 5 - Break Tie Tied Tightly to Bag Loop.

Figure C-10 (Continued). Design of the Deployment Control Break Ties.

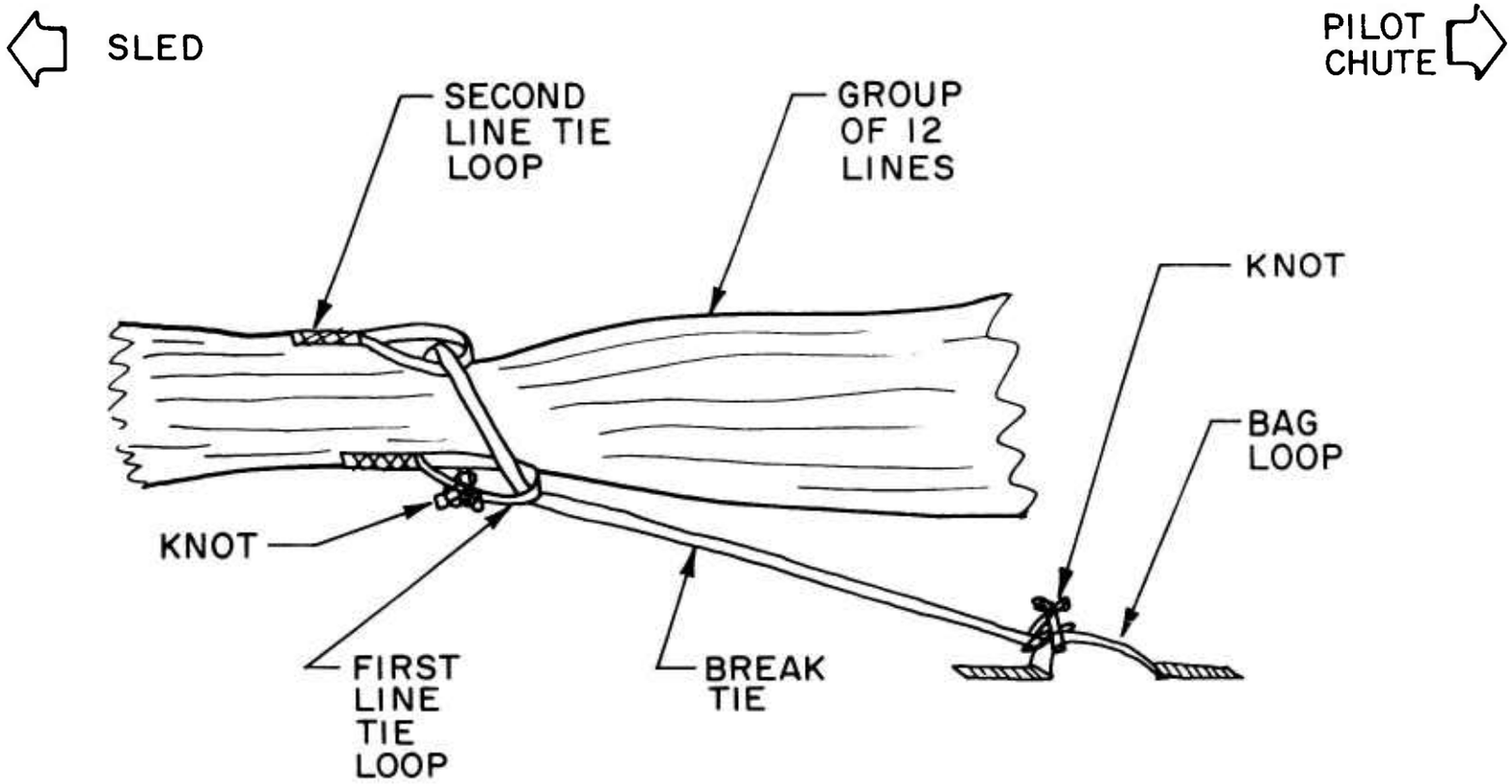

f. Sketch of a Break Tie Just Prior to Break.

Figure C-10 (Concluded). Design of the Deployment Control Break Ties.

f. Vent Break Cords

Two break cords connected the vents (apexes) of both the test parachute and the pilot chute to their bags. One cord was called the vent break cord and the other the "snubber." For the test parachute, the vent break cord was a single ply of nylon webbing with a free length of 30 in. The snubber was a single ply of nylon cord about 6 in. long. For the pilot chute, single ply nylon cord was used for both the vent break cord (12 in. long) and the snubber (about 4 in. long).

The required strength of the vent break cord, VBCS, was taken as the minimum expected drag force of the extraction devices at the time when the last of the parachute (or pilot chute) just exited the bag. That is,

$$VBCS = D_{min} \qquad \text{(C-12)}$$

where D_{min} was obtained from the computer program output.

The required strength of the snubber, SS, was taken as:

$$SS = (1/3)\ (VBCS) \qquad \text{(C-13)}$$

Available nylon materials with rated breaking strengths closest to the required strengths were selected for use as vent break cords and snubbers.

5. PARACHUTE PACKING

All parachutes were packed in a similar manner. Differences were in the design, number, locations, and strengths of the break ties and vent break cords. Photographs taken during a typical packing are presented in Figure C-11 and Table C-2 lists the materials used for the break ties and vent break cords for each test run.

a. Test Parachute Preparation

Prior to parachute packing, each test parachute was prepared to accept the packing aids. A 24 in. long vent line loop of 6000 lb webbing was placed around the vent lines to accept the vent break cords. Two cut knives were fastened 18 in. below the canopy skirt on suspension lines numbers 6 and 12 to accept and cut the canopy compartment closure tie. One cut knife was fastened 66 in. from the riser line attachment loop on suspension line number 12 to accept and cut the parachute bag closure tie. Loops of 1 in. wide webbing were sewn to the lines and canopy at those locations selected for placement of the deployment control break ties. Two loops were placed at each location on opposing lines, but not on the same two lines. For example, for test 6P-H7, 6 loops each were placed on lines 1 and 7, 9 and 3, and 11 and 5, and 5 loops each were placed on lines 2 and 8 and 10 and 4. Loops of 1/2 in. wide tape were sewn to one pilot chute line to accept the break ties.

All materials used to prepare the parachutes, with the exception of the steel knives, were of the same type as the parachute. That is, nylon thread, tape, and webbing were used with the nylon parachutes and Kevlar thread, tape, and webbing were used with the Kevlar parachutes.

b. Parachute Bags

All parachutes were hand packed into their own nylon, split flap type deployment bags (see Figure C-11-b through C-11-f). The design shapes of the bags were parallelepipeds. Loops were sewn into the bags to accept vent break cords and parachute line and canopy ties. Flaps were sewn to the outside of the bags to provide a storage compartment for the pilot chutes (see Figure C-11-i and C-11-j).

c. Packing Procedure

The following instructions were given for packing the parachute for test 6P-H7. Similar instructions were followed for the other tests (the designs of the break ties were different for the first five tests, see Paragraph 4.e above; the thread type underlined below was nylon for the nylon parachute and Kevlar for the Kevlar parachutes; and, when not specified, the packer could use any type knot).

1. (Refer to Figure C-11-a.) Stretch out the canopy and suspension and riser lines on the packing table. Arrange the lines in sequence, with line number 1 on top (in the middle). Tie a loop of nylon cord, MIL-C-5040, Type III, 550 lb, through the 12 riser line attachment loops so that the lines form a circle with all line numbers in sequence. Straighten the lines, arrange into one group, and hand tack with FF nylon or 3 cord cotton thread every 24 in. From the riser line attachment loops to the first cut knife, tack every 6 in.

2. (Refer to Figure C-11-b.) Lay out the test parachute bag and fit with nylon quilting ribbons, MIL-T-5608, Class B, 5/8 in, Type III, 70 lb, through the grommets. Tie the vent break cord to the vent and bag loops with a free length of 30 in. Tie a snubber to the vent and bag loops with a free length of approximately 6 in. Tack the vent loop with 3 cord Kevlar thread at the break cords and at the vent lines.

3. (Refer to Figure C-11-c.) Make an "S" fold in the canopy and bring the quilting ribbons from the first row of grommets through the canopy. Tie one end of the first canopy break tie to the first canopy tie loop with a bowline and locking knot. Route the other end of the first canopy break tie around the canopy, through the second canopy tie loop, and tie to a bag loop using three half-hitches and a

locking knot. (Sketches and photographs of this break tie design are presented in Figure C-10.) Tie the remaining canopy break ties.

4. (Refer to Figure C-11-d.) Loosely lace bag with nylon webbing, MIL-W-5625, 1/2 in., 1000 lb. Pass the quilting ribbons through the grommets in the canopy compartment and tie. Close and lock the canopy compartment with nylon webbing, MIL-W-5625, 1/2 in., 1000 lb, through the knives. (Maintain bag width - do not pull tight.) Safety tack each knife to the compartment closure webbing with two single turns of 3 cord nylon thread.

5. (Refer to Figure C-11-e.) Fold suspension and riser lines in an "S" curve and fasten the line break ties to the bag in the manner described above and shown in Figure C-10. Lace up the remainder of the bag and tie off the lacing. Tuck in the bag closure flaps and close the bag with nylon cord, MIL-C-5040, Type III, 550 lb, through one knife. Safety tack the knife with two single turns of 3 cord nylon thread. Hand tack the bag closure flaps with 3 cord nylon thread as required. Pull all quilting ribbons tight and tie.

6. (Refer to Figure C-11-f.) Tie the remaining riser lines to the outside bag loops using the bag break ties. Hand tack the riser lines to the outside of the bag with FF nylon or 3 cord cotton thread as required to prevent movement during handling and shipment. Hand sew two turns of 5 cord cotton thread through all twelve riser lines in 5 places. Leave 12 in. of thread free on each side and loosely tie the free ends. The first tie is 9 in. from the riser line attachment loop stitching and the remaining ties are spaced at 3 in. intervals. (These 5 cord cotton thread ties are shown in Figure C-12-d.)

7. (Refer to Figures C-11-g through C-11-j.) Pack the pilot chute. Stretch out the pilot chute on the packing table. Tie the vent break cord and snubber to the vent and bag loops with free lengths of 12 and 4 in. respectively. Tie the pilot chute lines to the bag using the pilot chute break ties. Fold the canopy over the lines. Close the bag over the lines just before the bridle with nylon cord, MIL-C-5040, Type II, 400 lb, through the 33 in. lanyard/knife. Safety tack the knife with three single turns of 3 cord nylon thread. Lace the bag with nylon cord, MIL-C-5040, Type III, 550 lb. Attach the pilot chute line bridle to the test parachute bag bridle with a connector link and safety tack the bridles to the link with 3 cord nylon thread. Fold the bag bridle, lanyard, and pilot chute line bridle into the pilot chute compartment and hand tack with single turns of 3 cord nylon thread as required. Arrange bridles such that the pilot chute bag opening is toward the bottom of the test parachute bag. Place the pilot chute in the compartment and hold in place with single turns of 3 cord nylon thread as required. Attach the cone riser to the pilot chute bag bridle with a connector link and safety tack the riser and bridle to the link with 3 cord nylon thread. Close the end flaps over the pilot chute and lock with a single turn of 3 cord nylon thread through the connector link. Close the outer flaps and lock with single turns of 5 cord nylon thread through the cone riser in three places.

8. (Refer to Figure C-11-k.) Tie nylon cord, MIL-C-5040, Type I, 100 lb, to each cut knife loop of the cone riser. Leave two free ends, one 6 in. and the other 24 in. long. Tie single turns of 3 cord cotton thread through two holes in each cone riser cut knife. Leave 24 in. free on each of the four ties. Wrap all cord and thread with masking tape for shipment.

6. PARACHUTE INSTALLATION ON THE SLEDS

The test parachute and the attachment, deployment, and release components were installed on the sleds in a manner which would ensure deployment of all items in the proper sequence and at the proper time. The packed test parachute and pilot chute were held in the parachute compartment by restraining straps. Those portions of the parachute riser lines and the cone riser which were not fastened to the parachute bag were tied to a trough on top of the sled. These lines and riser and the deployment cone were protected from windblast by a cover.

The following instructions were given for installing the parachutes on the sleds:

1. (Refer to Figure C-12-a.) Attach the parachute attachment/deployment/release mechanism to the sled and insert the tensiometer shear pin.

2. (Refer to Figure C-12-b.) Attach the parachute riser line loops to the parachute attachment/release fitting or to the release fitting lugs (depending upon which attachment/deployment/release mechanism was used).

3. (Refer to Figure C-12-c.) Insert the packed test parachute and pilot chute into the sled parachute compartment with the parachute riser lines on top and the pilot chute compartment facing aft. Lay the parachute riser lines in the tie-down trough and attach the parachute attachment/release fitting or lugs to the parachute attachment/deployment/release mechanism with parachute line number 1 on top. Split the parachute riser lines into two groups and tie off the groups with two turns of 5 cord cotton thread as required to allow for clear cone deployment and room for the cone riser to loop forward from the deployment cone link (see also Figure C-12-f).

4. (Refer to Figure C-12-d.) Route the free ends of the 5 cord cotton thread ties, which are on the parachute riser lines, through holes on either side of the tie-down trough, pull tight, and tie. Cut off excess thread.

5. (Refer to Figure C-12-e.) Route one end of each of the two 100 lb nylon cord ties, which are on the cone riser, from a riser loop, out through a hole in one side of the tie-down trough which is forward of the knife, back through another hole which is even with the knife, through the knife, out through a hole in the other side of the trough, back through another hole, and tie to the other end of the 100 lb cord tie after pulling the tie tight. Safety tack the knife by tying the two 3 cord cotton ties, which are on the knife, through holes in the tie-down trough which are forward of the knife and back through a third hole in the knife. Cut off all excess thread.

6. (Refer to Figure C-12-f.) Attach the cone riser to the pin link on the deployment cone mortar. Insert the deployment cone into the droque gun assembly of the parachute attachment/deployment/release mechanism. Insert and safety wire its shear pin. The stitching of the cone riser loop must be forward of the cone pin link.

7. (Refer to Figure C-12-g.) Route the parachute restraining strap release cable (or cables) through the loop in the cone riser. Place the parachute restraining strap between the cone riser and the pilot chute compartment. Hold the ends of the restraining strap in the cylinders located on the edge of the parachute compartment and insert the cable release pins into the cylinders. Safety wire the pins. Install the cover on top of the sled.

TABLE C-2

BREAKING STRENGTHS (lb) OF VENT BREAK CORDS AND BREAK TIES

Run No.	Sled Test Run	TEST PARACHUTE								PILOT CHUTE		
		Vent Break Cord	Vent Snubber	Deployment Control Break Ties					Bag Ties	Vent Break Cord	Vent Snubber	Line Break Ties
				Canopy Ties		Line Ties						
				First	Second	First	Second	Third				
1	6P-E2	250	---	---	---	180(9)	33(4)	---	---	N/A	N/A	N/A
2	6P-E3	250	---	---	---	180(9)	90(3)	---	---	N/A	N/A	N/A
3	6P-E4	1000	---	---	---	180(9)	90(1)	---	---	180	---	---
4	6P-F1	1000	---	---	---	180(9)	90(1)	---	100(1)	180	---	---
5	6P-F2	1000	---	---	---	180(8)	90(9)	---	100(1)	180	---	---
6	6P-F3	1500	550	400(3)	---	600(6)	525(8)	---	100(3)	550	100	---
7	6P-E6	2300	750	400(3)	---	1000(3)	750(10)	550(1)	200(4)	550	170	100(4)
8	6P-G1	2500	800	800(3)	1000(3)	1000(15)	800(1)	---	375(5)	550	200	100(4)
9	6P-G2	2500	800	550(4)	800(2)	1000(15)	800(1)	---	375(5)	550	200	100(4)
10	6P-G3	2500	750	750(3)	900(3)	1000(14)	750(2)	---	375(5)	550	200	100(4)
11	6P-H1	3500	1000	1000(5)	---	1500(18)	1000(2)	---	550(5)	750	200	120(4)
12	6P-H2	3500	1000	1000(5)	---	1500(18)	1000(2)	---	550(5)	750	200	120(4)
13	6P-H3	3500	1000	1000(4)	---	1500(18)	1000(2)	---	550(5)	750	200	120(4)
14	6P-E9	750	250	100(4)	---	250(14)	---	---	100(3)	400	100	70(4)
15	6P-E10	750	250	100(4)	---	250(14)	---	---	100(3)	400	100	70(4)
16	6P-G4	1000	400	250(5)	---	400(16)	250(2)	---	100(3)	550	200	100(4)
17	6P-G5	1000	400	400(5)	---	400(16)	250(2)	---	100(5)	550	200	100(4)
18	6P-H5	2250	750	750(5)	---	550(2)	550(2)	---	400(3)	750	250	100(4)
19	6P-H6	2500	750	750(3)	1000(2)	1000(11)	1500(6)	550(1)	400(5)	750	250	100(6)

Numbers in parentheses are the number of ties of a particular strength tie.

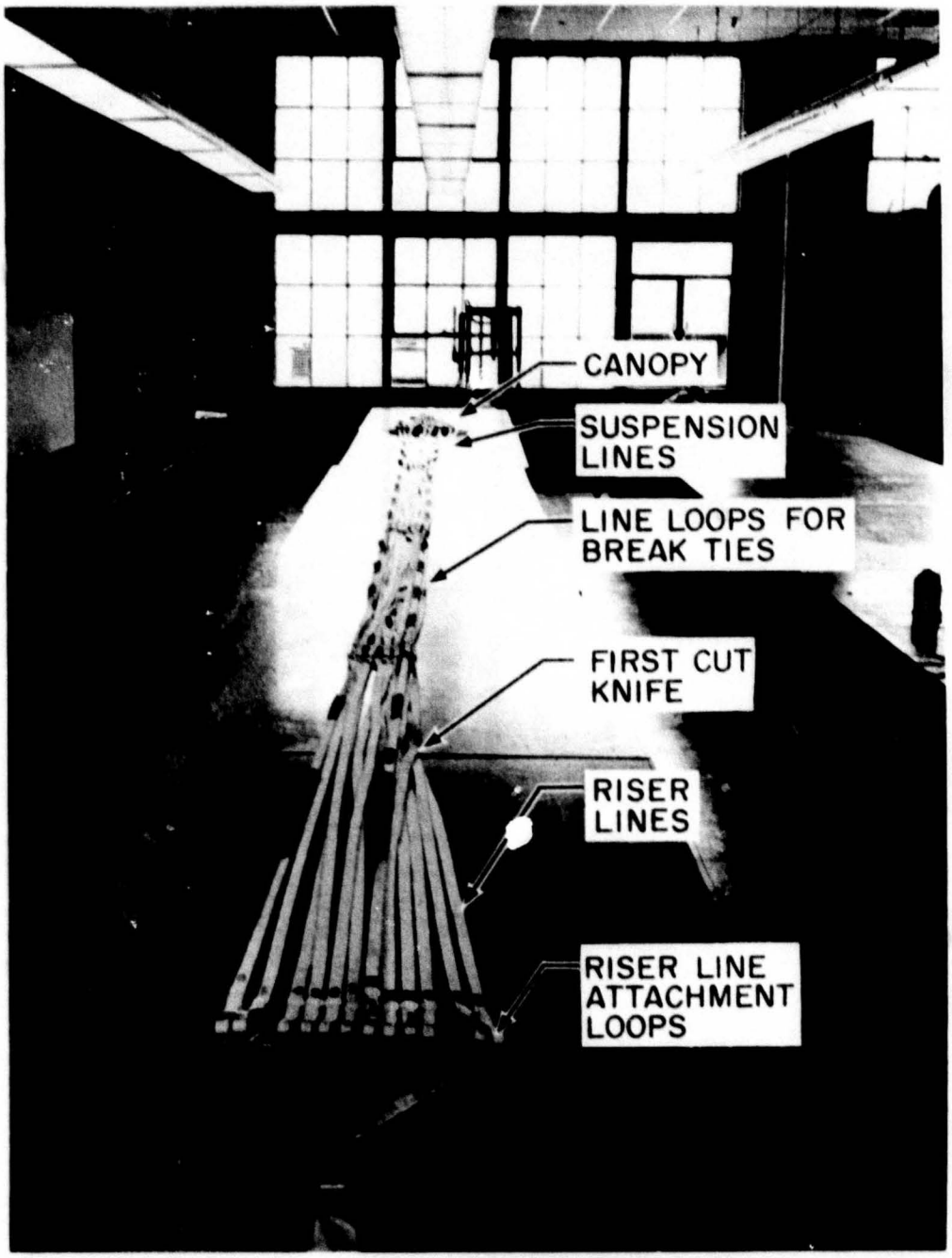

a. Packing Step 1.

Figure C-11. Photographs Taken During the Packing of the Parachute for Test 6P-G1.

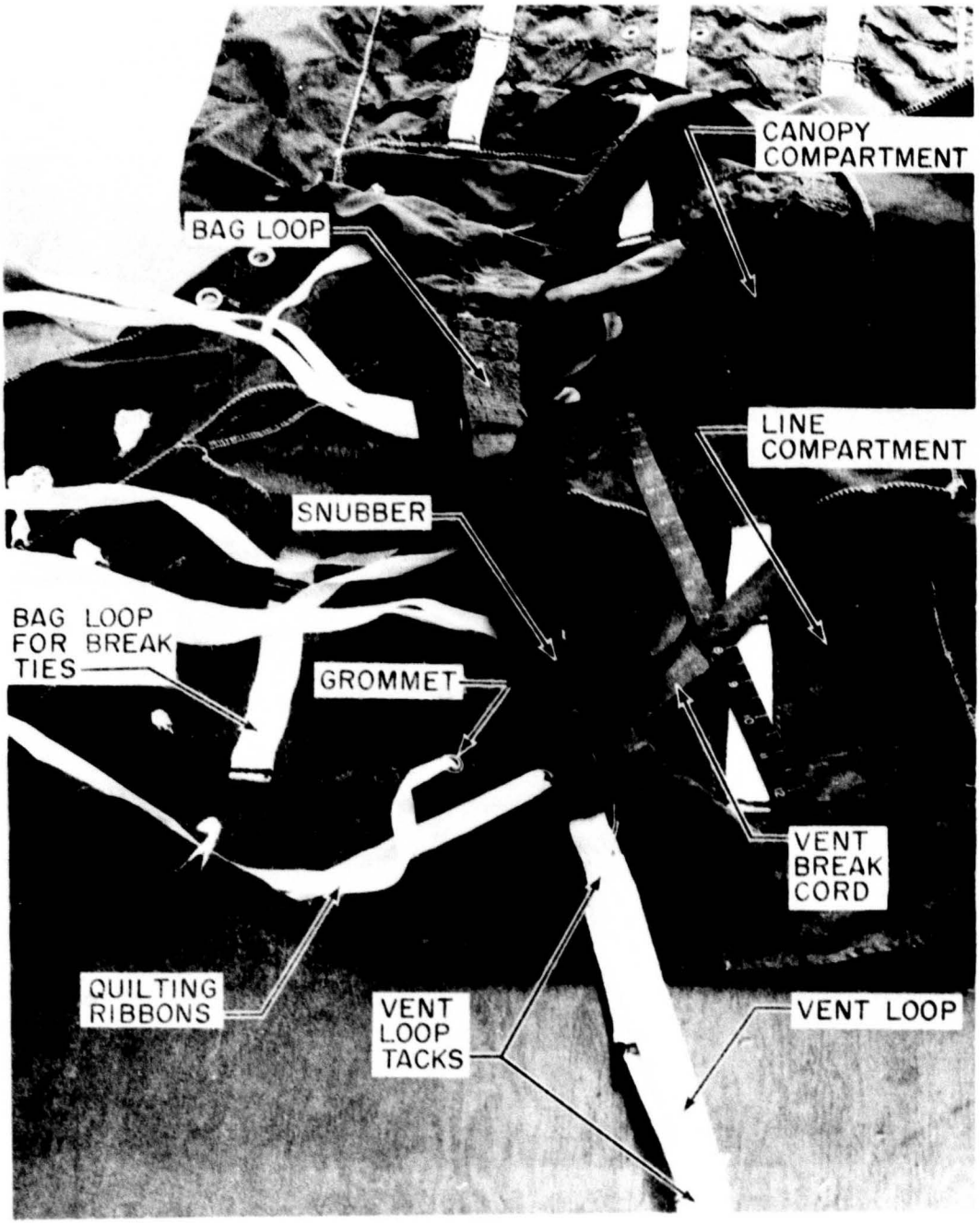

b. Packing Step 2.

Figure C-11 (Continued). Photographs Taken During the Packing of the Parachute for Test 6P-G1.

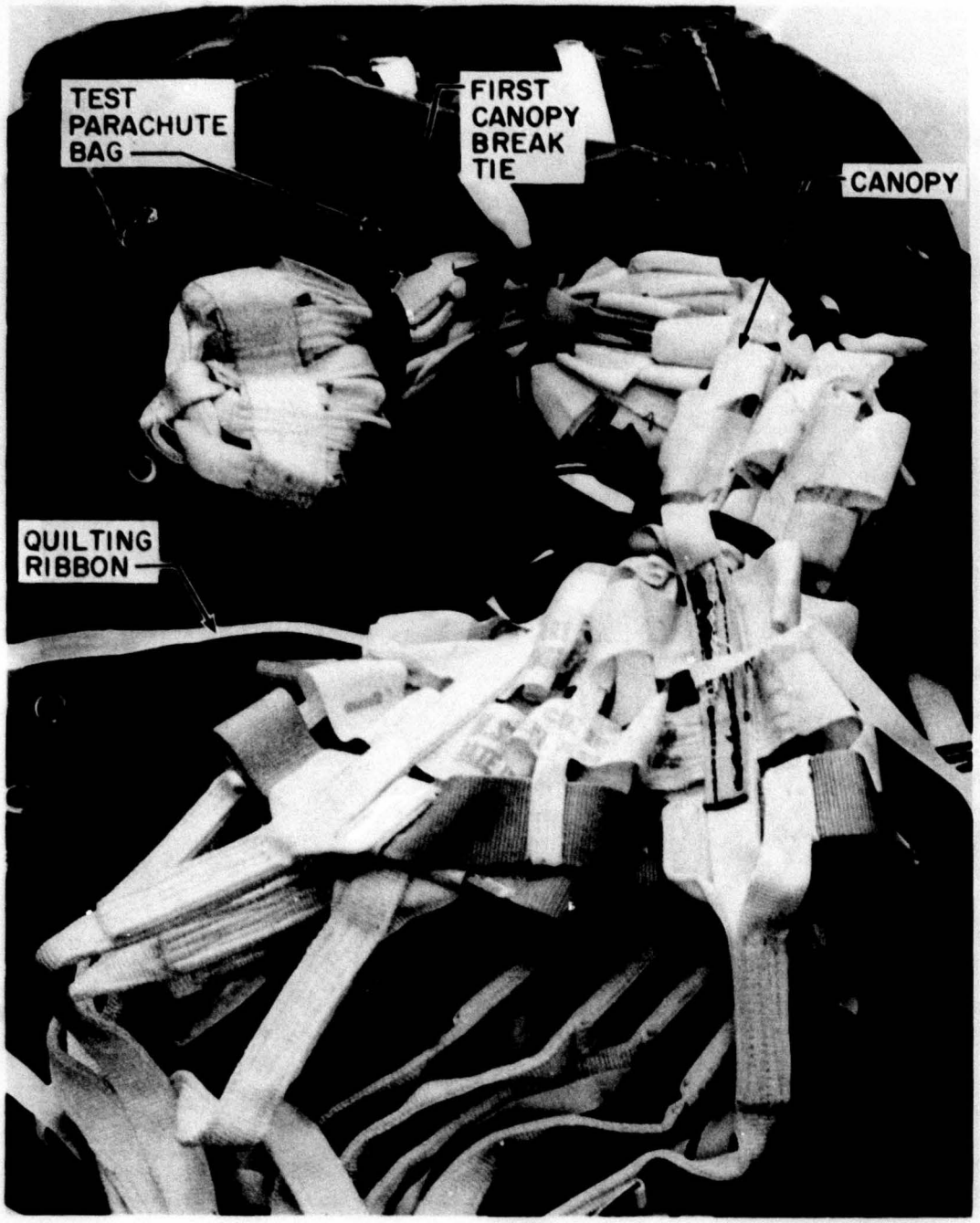

c. Packing Step 3.

Figure C-11 (Continued). Photographs Taken During the Packing of the Parachute for Test 6P-G1.

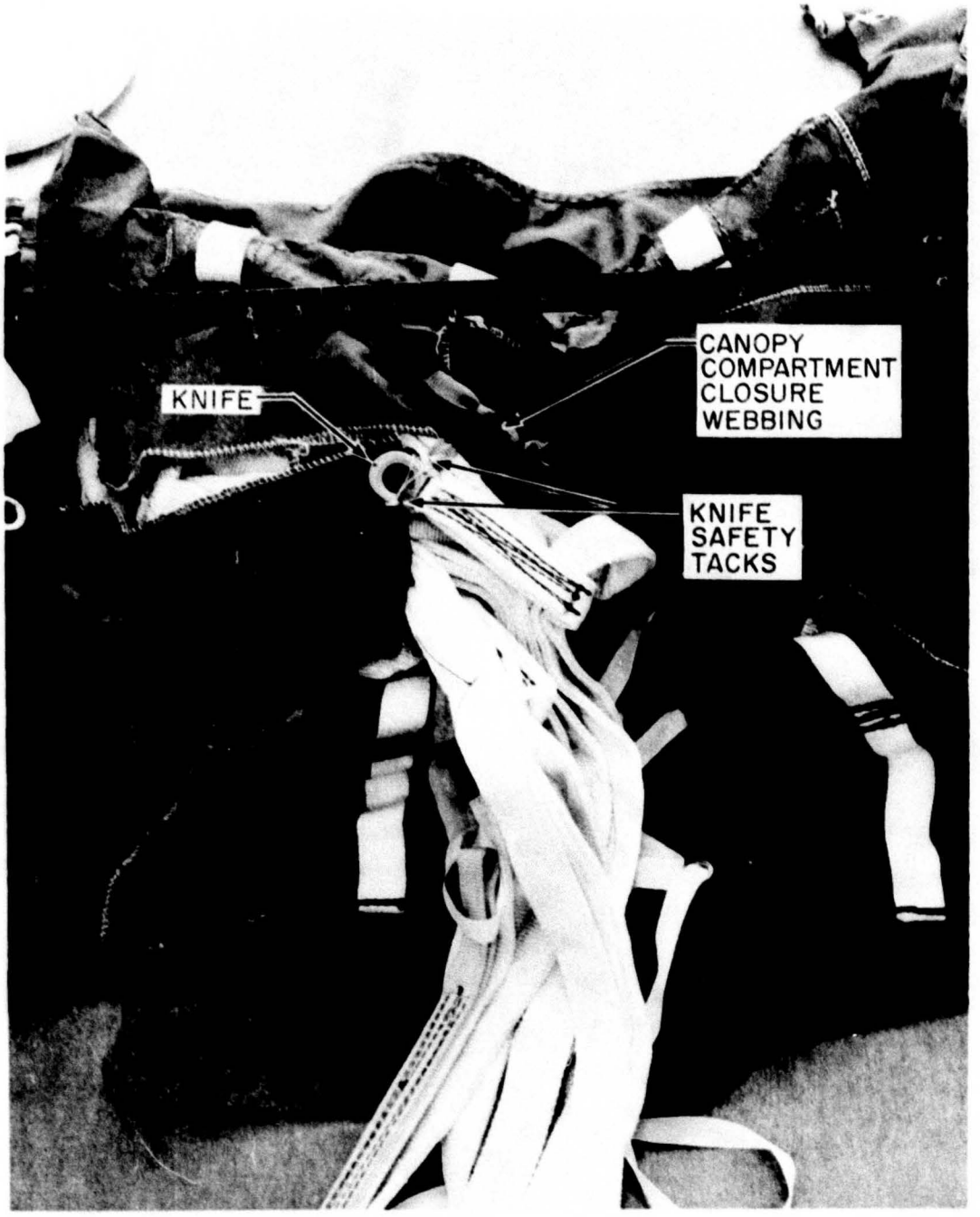

d. Packing Step 4.

Figure C-11 (Continued). Photographs Taken During the Packing of the Parachute for Test 6P-G1.

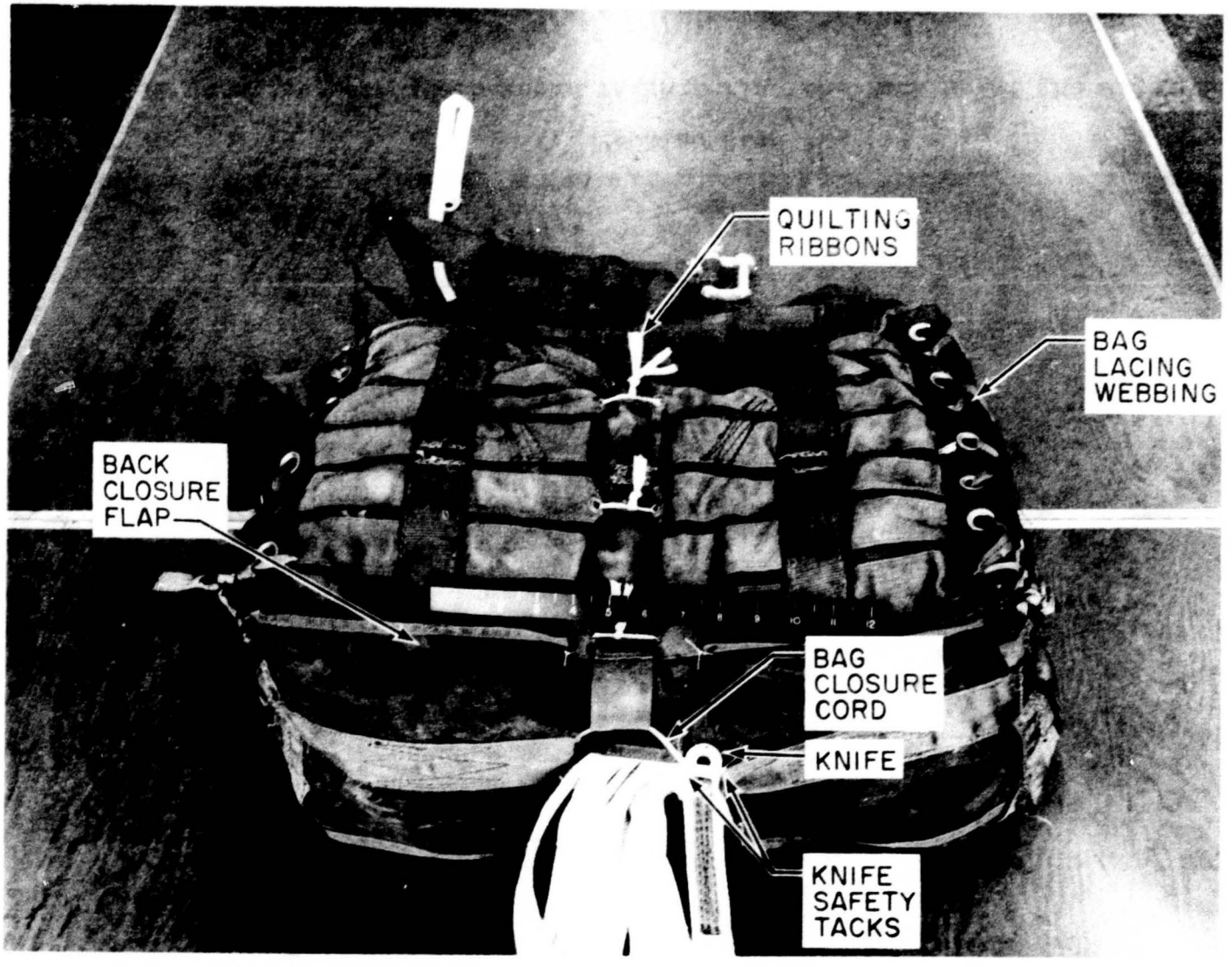

e. Packing Step 5.

Figure C-11 (Continued). Photographs Taken During the Packing of the Parachute for Test 6P-G1.

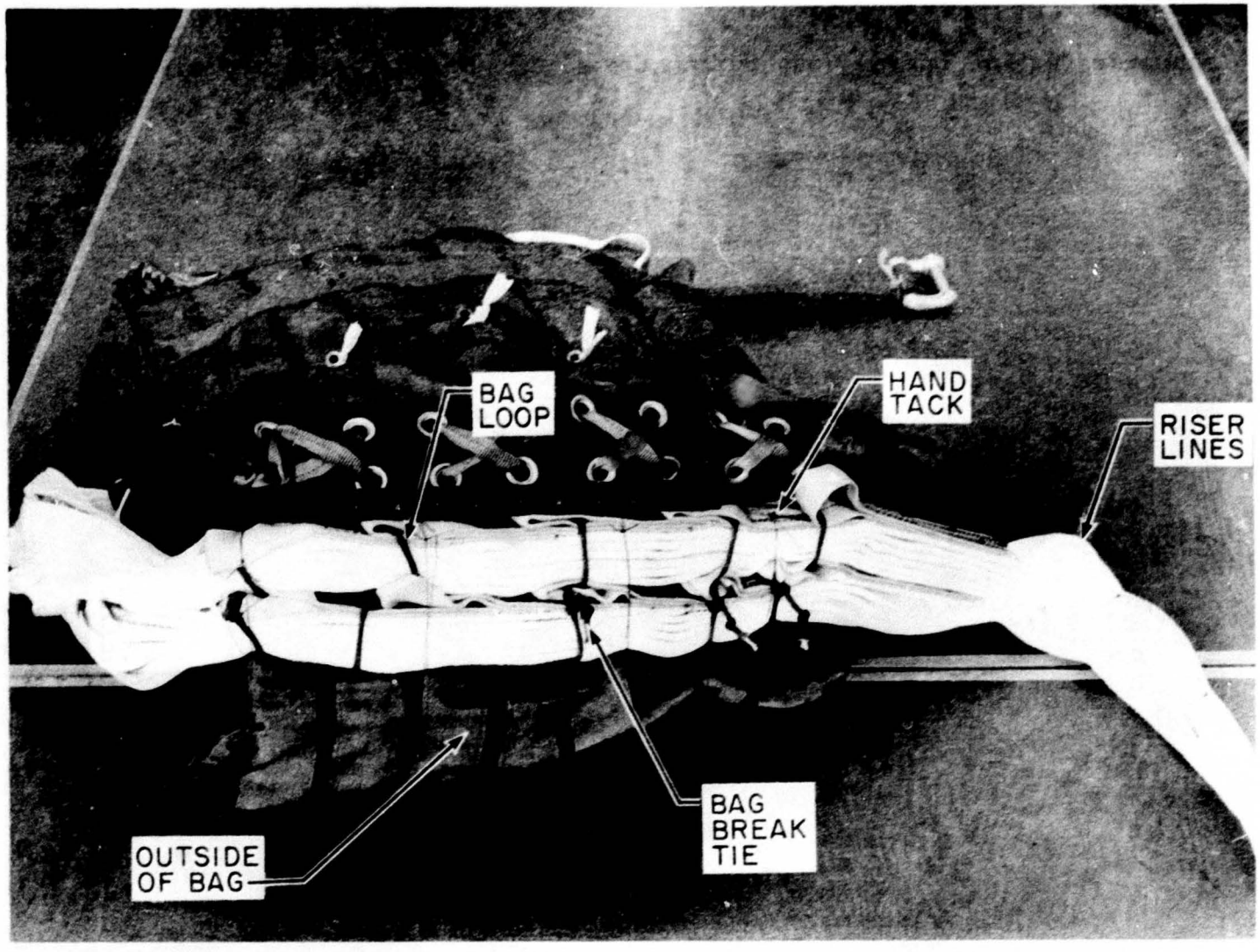

f. Packing Step 6.

Figure C-11 (Continued). Photographs Taken During the Packing of the Parachute for Test 6P-G1.

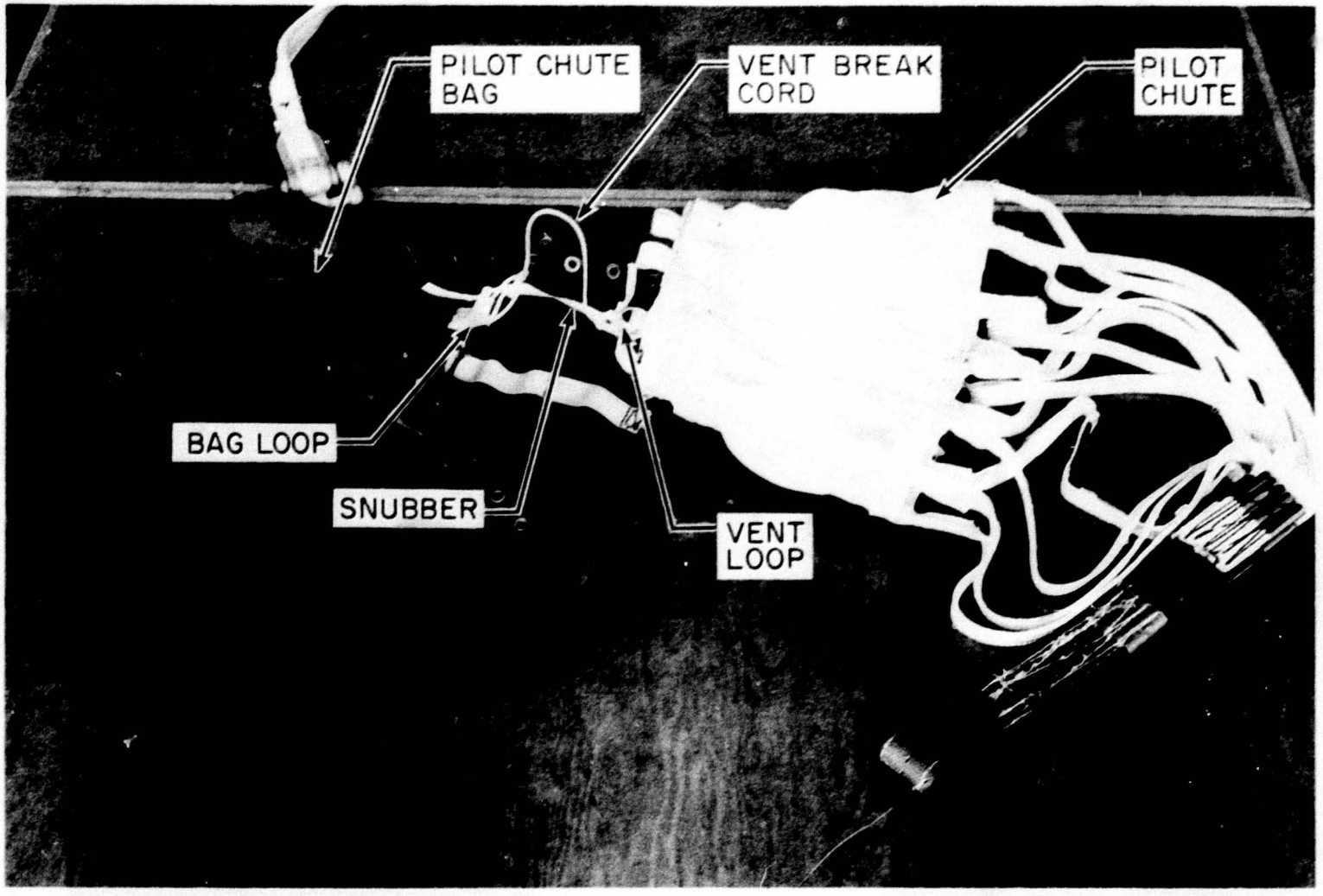

g. Packing Step 7 - Pilot Chute Vent Break Cords.

Figure C-11 (Continued). Photographs Taken During the Packing of the Parachute for Test 6P-G1.

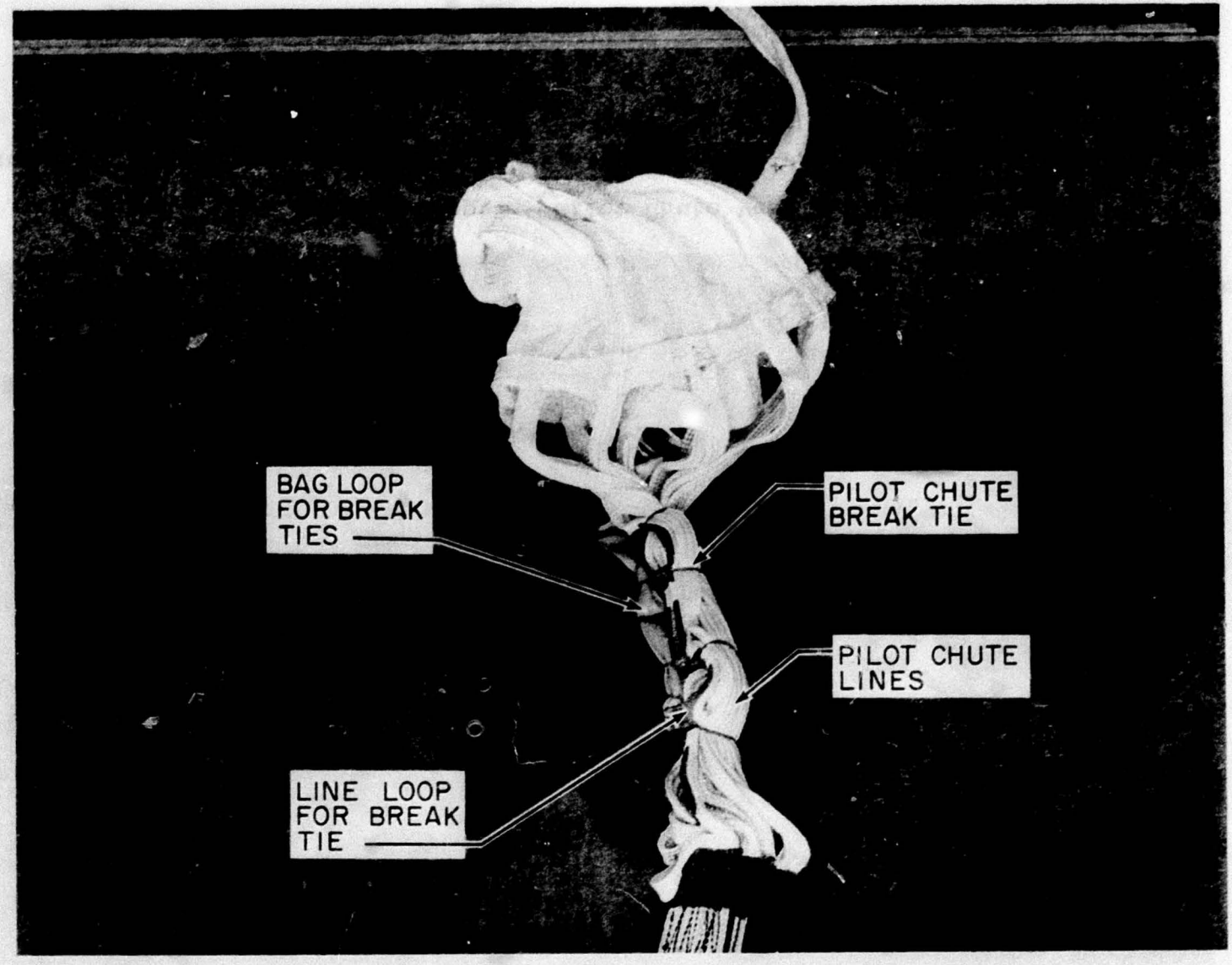

h. Packing Step 7 - Pilot Chute Break Ties.

Figure C-11 (Continued). Photographs Taken During the Packing of the Parachute for Test 6P-G1.

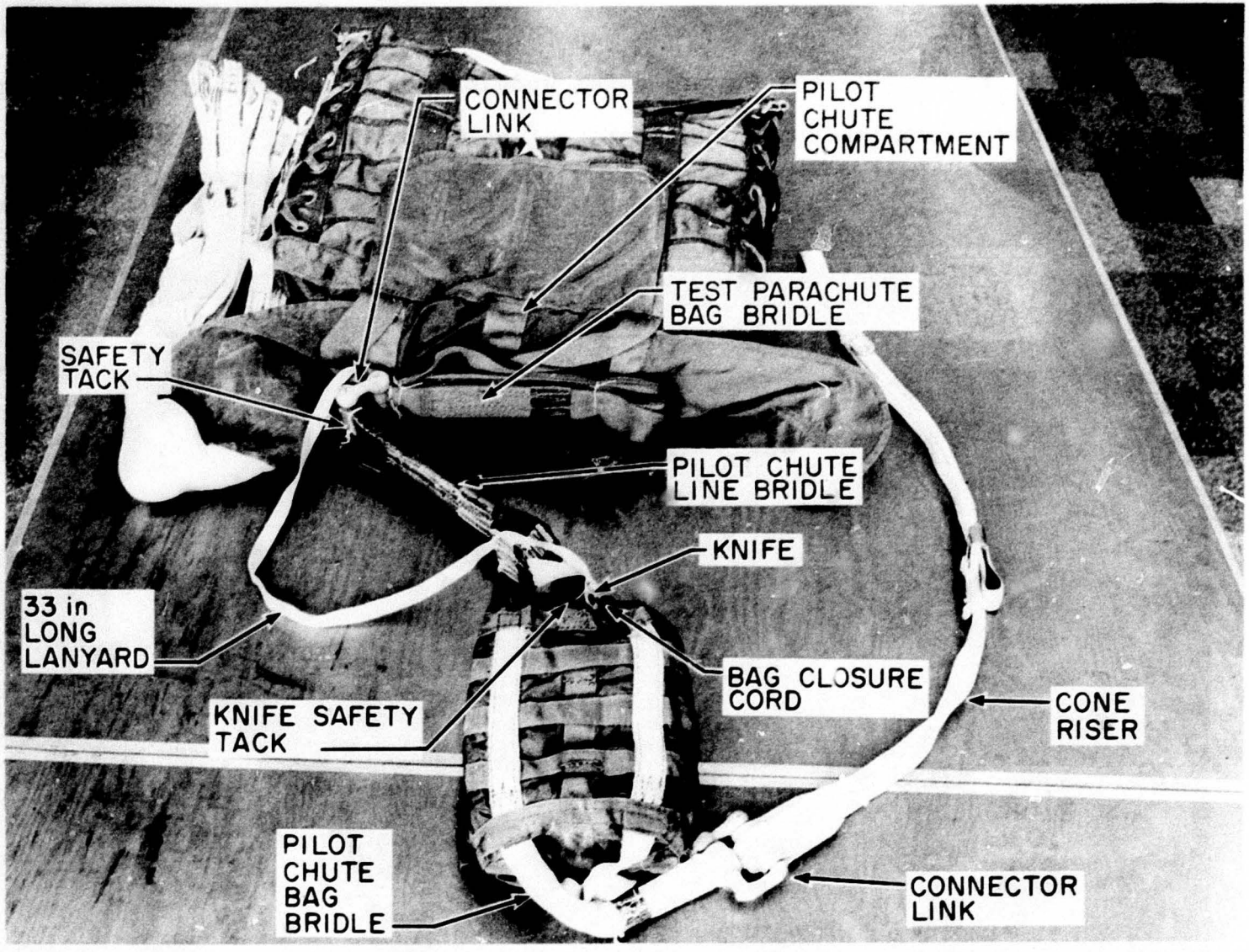

i. Packing Step 7 - Bridle Connections.

Figure C-11 (Continued). Photographs Taken During the Packing of the Parachute for Test 6P-G1.

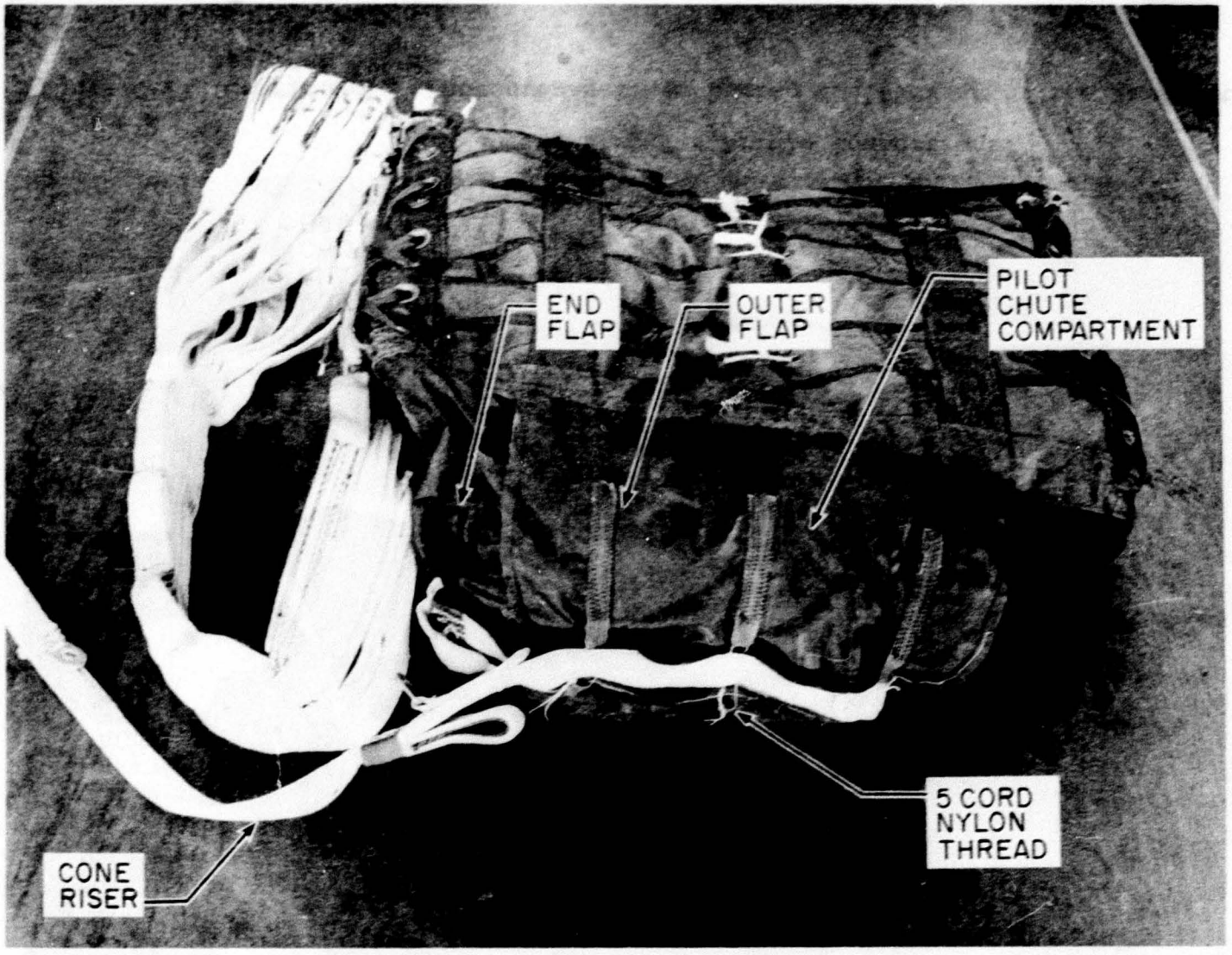

j. Packing Step 7 - Pilot Chute Compartment Closure.

Figure C-11 (Continued). Photographs Taken During the Packing of the Parachute for Test 6P-G1.

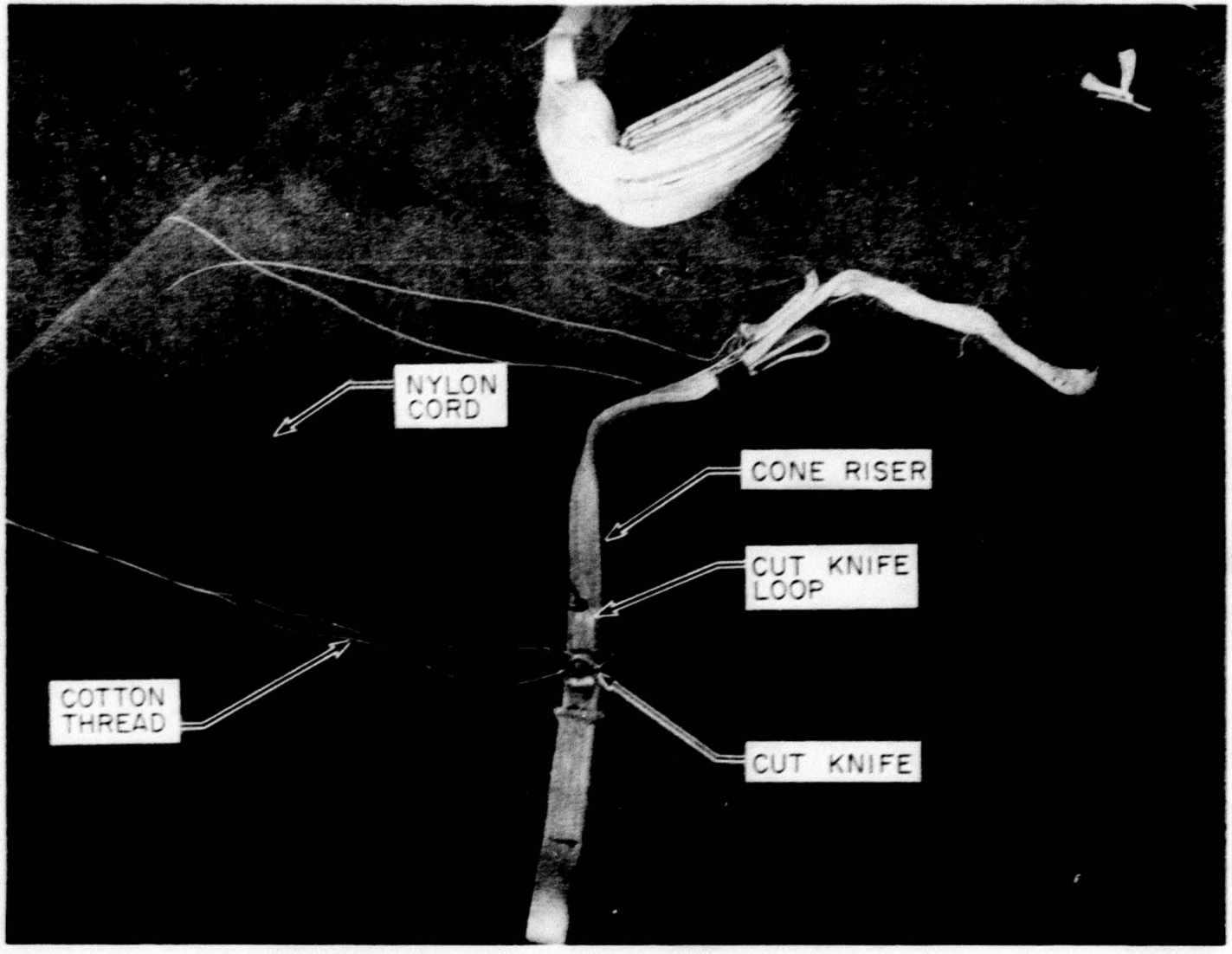

k. Packing Step 8.

Figure C-11 (Concluded). Photographs Taken During the Packing of the Parachute for Test 6P-G1.

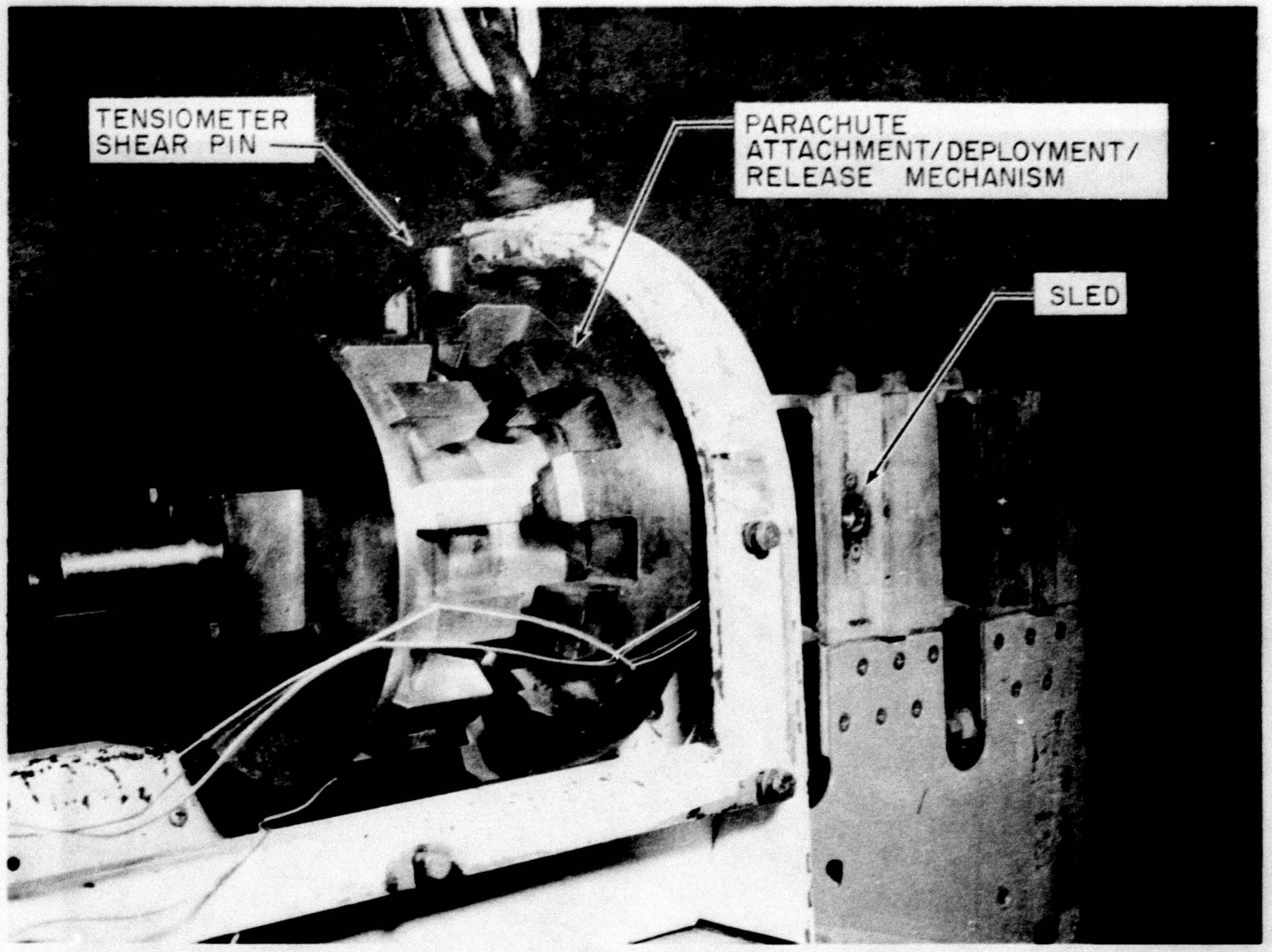

a. Installation Step 1.

Figure C-12-a. Photographs Taken During Parachute Installation on the Arrowhead Sled.

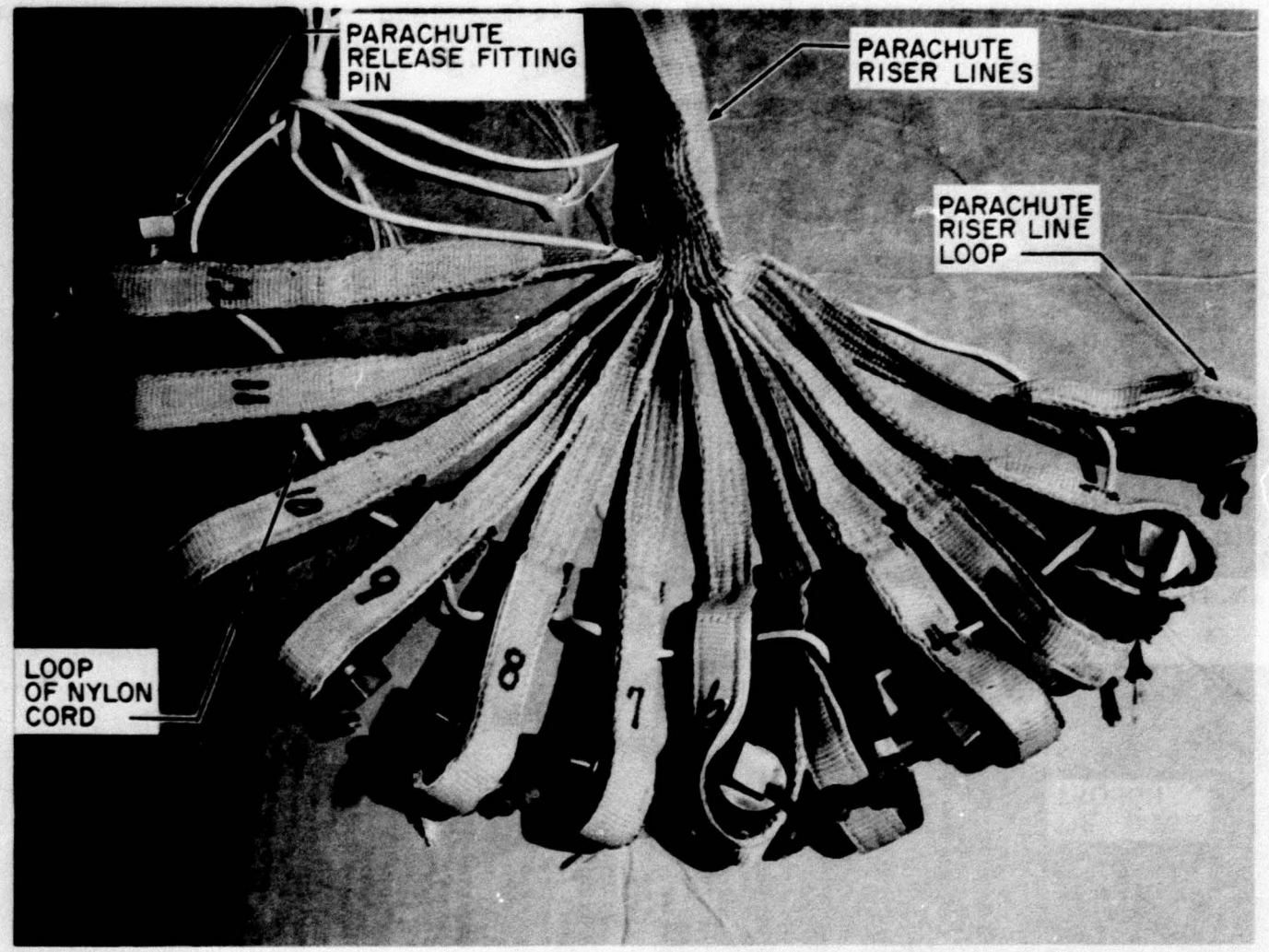

b. Installation Step 2.

Figure C-12 (Continued). Photographs Taken During Parachute Installation on the Arrowhead Sled.

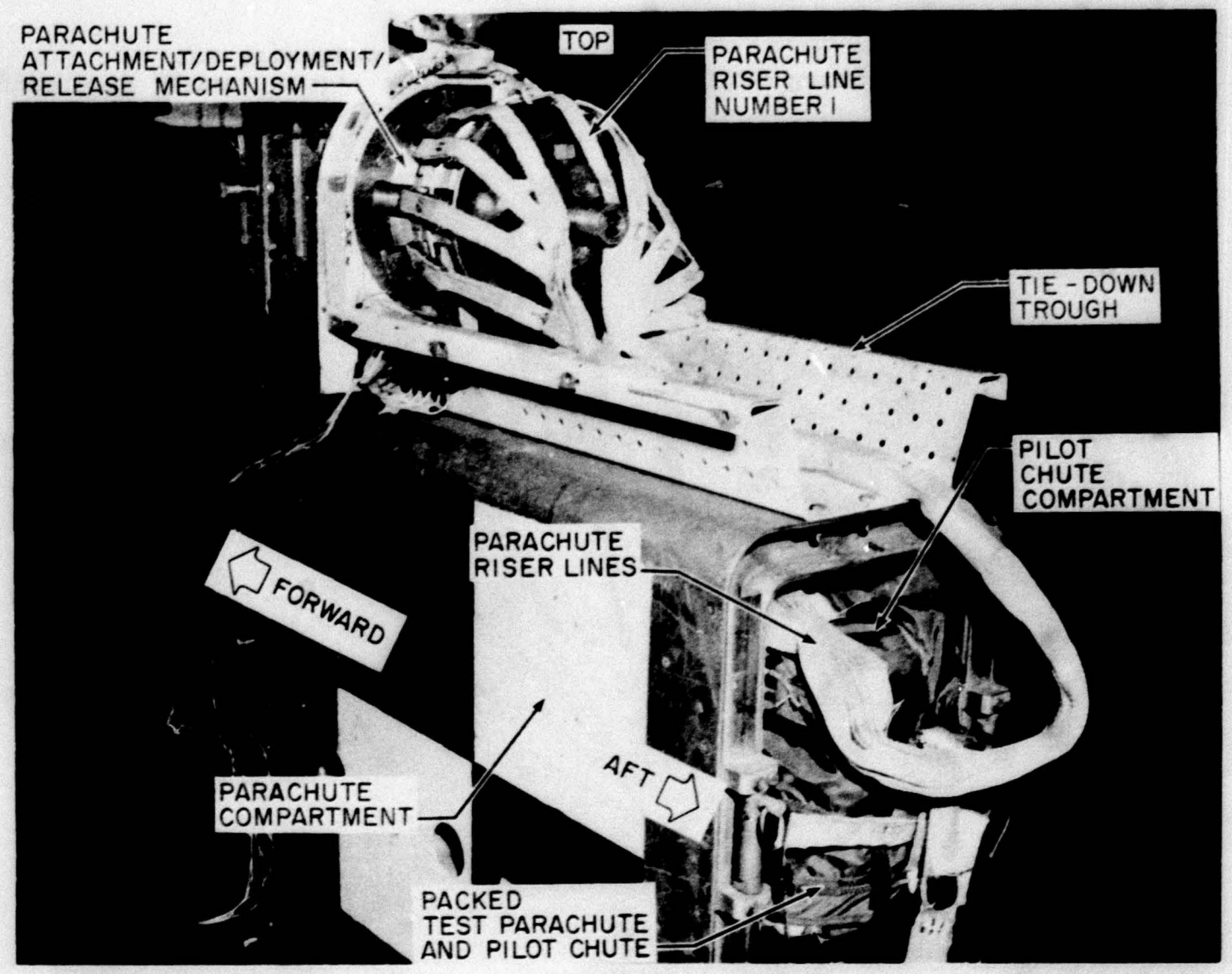

c. Installation Step 3.

Figure C-12 (Continued). Photographs Taken During Parachute Installation on the Arrowhead Sled.

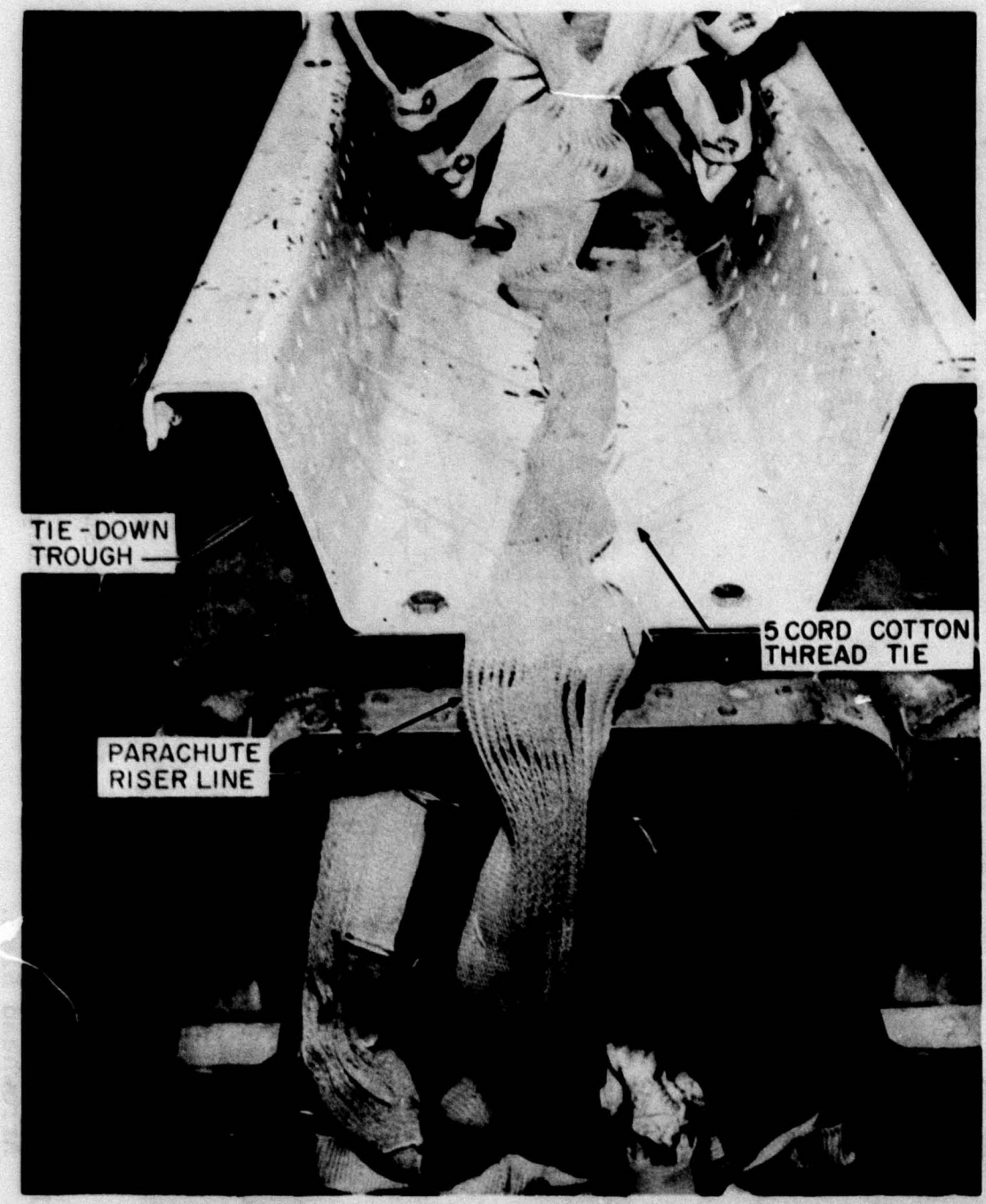

d. Installation Step 4.

Figure C-12 (Continued). Photographs Taken During Parachute Installation on the Arrowhead Sled.

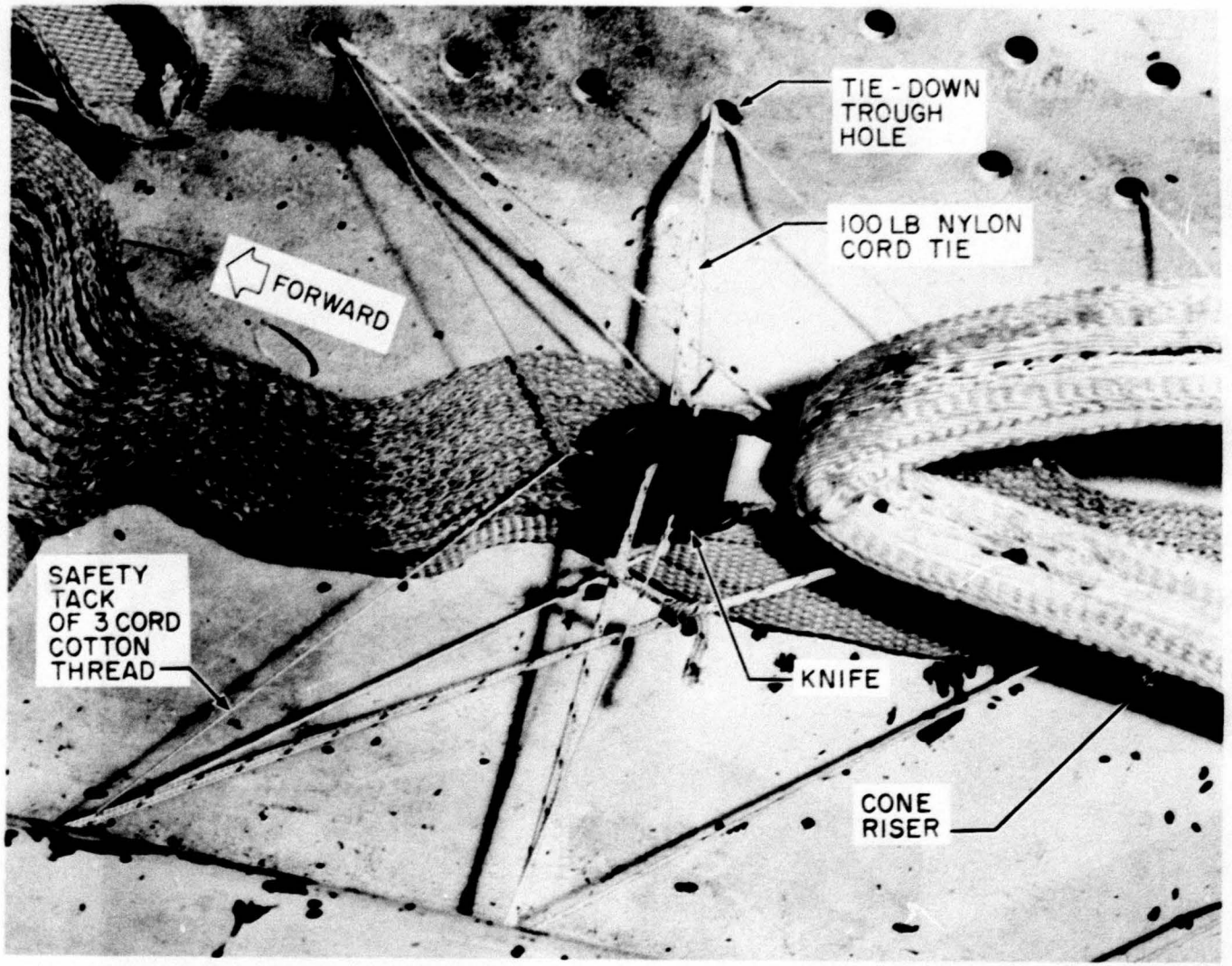

e. Installation Step 5.

Figure C-12 (Continued). Photographs Taken During Parachute Installation on the Arrowhead Sled.

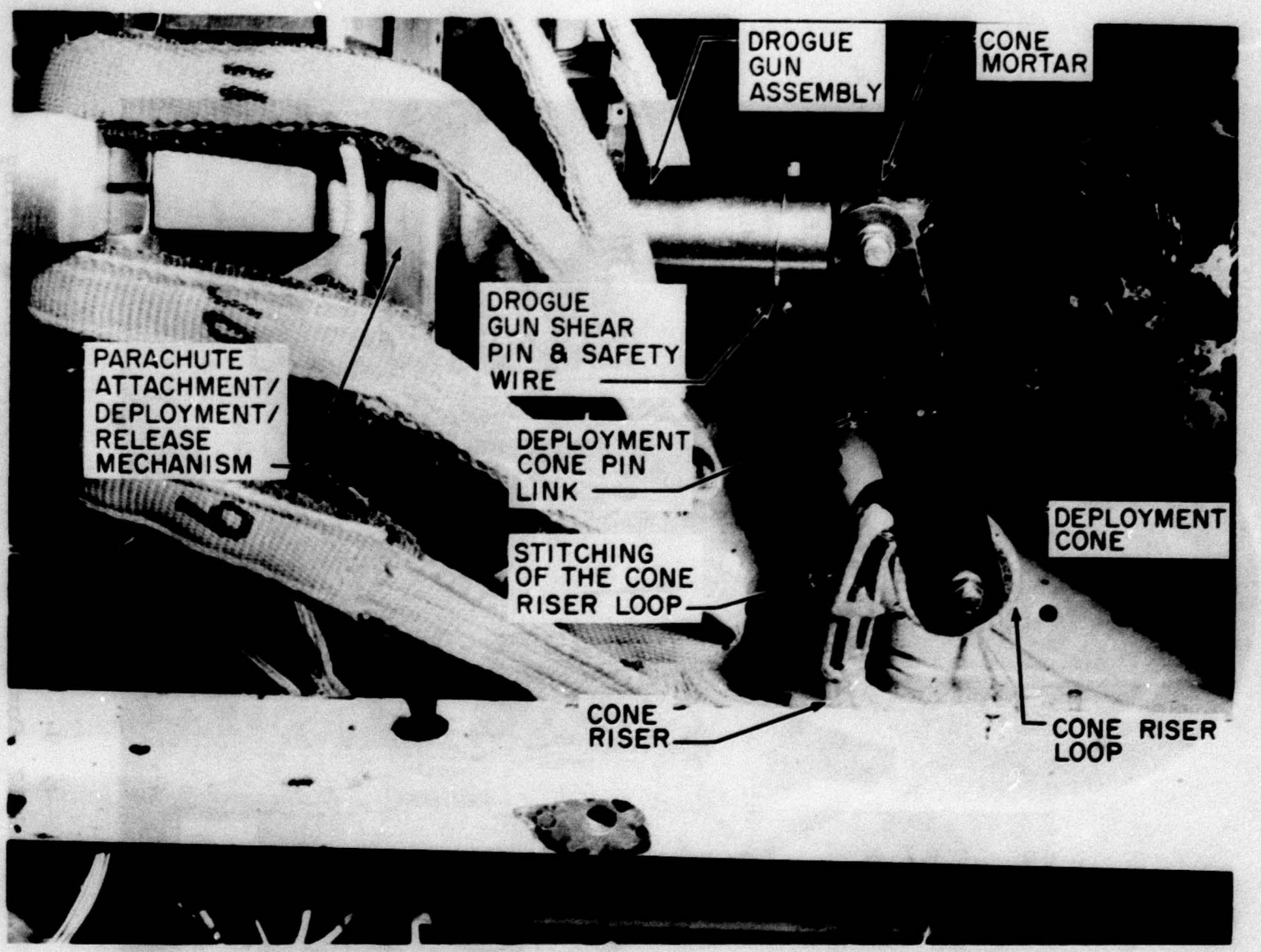

f. Installation Step 6.

Figure C-12 (Continued). Photographs Taken During Parachute Installation on the Arrowhead Sled.

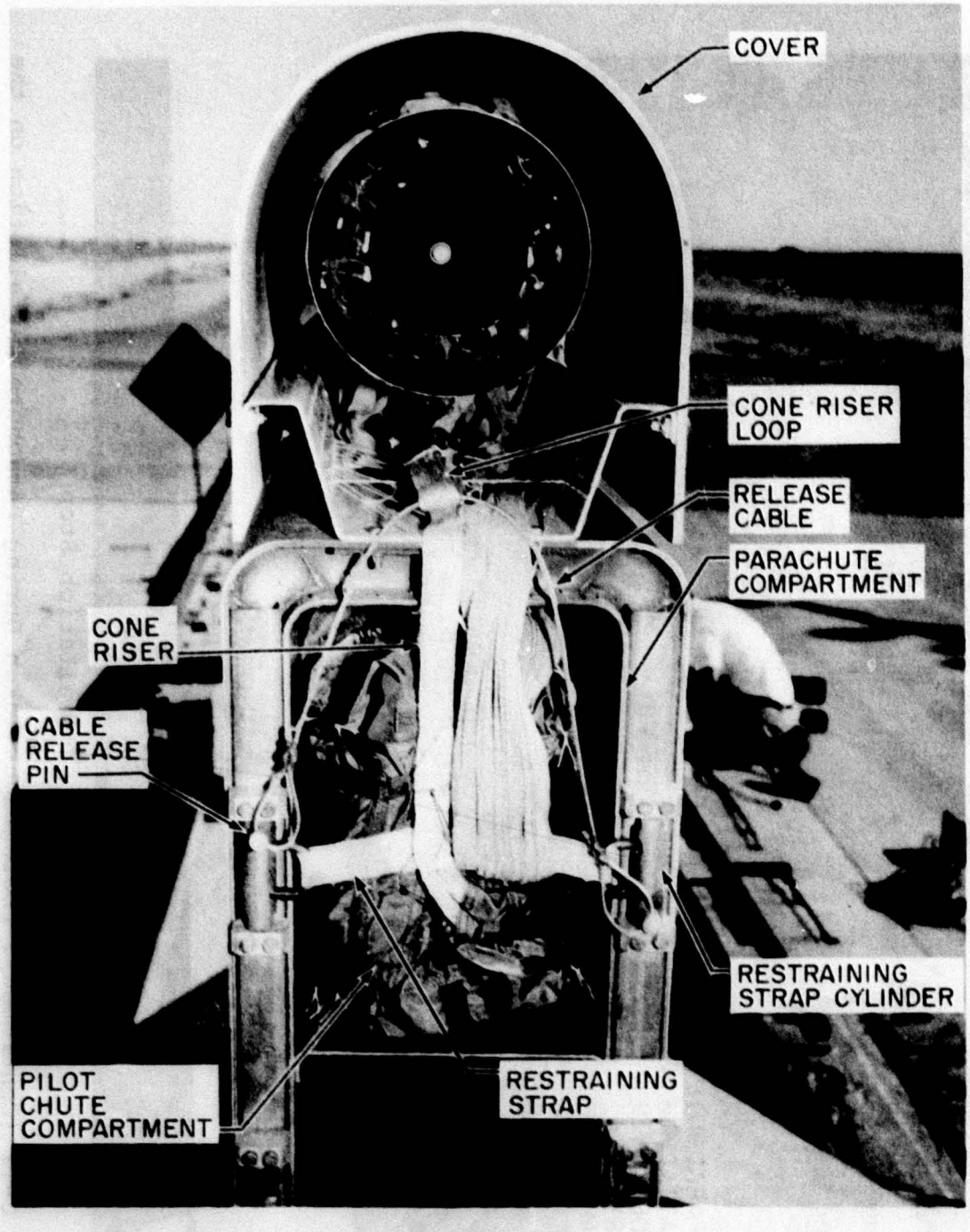

g. Installation Step 7.

Figure C-12 (Concluded). Photographs Taken During Parachute Installation on the Arrowhead Sled.

REFERENCES

1. Anon: The Holloman Track, Facilities and Capabilities, Air Force Special Weapon Center, 6585th Test Group, Track Test Division, Holloman Air Force Base, New Mexico Booklet, 1974.

2. Pederson, Paul E.: Study of Parachute Performance at Low Supersonic Deployment Speeds; Effects of Changing Scale and Clustering, Air Force Aeronautical Systems Division Technical Report 61-186, (AD 267 502), July 1961.

3. Pederson, P.E.: Study of Parachute Performance and Design Parameters for High Dynamic Pressure Operation, Air Force Flight Dynamics Laboratory Report FDL-TDR-64-66, (AD 607 036), May 1964.

4. Bloetscher, F.: Aerodynamic Deployable Decelerator Performance Evaluation Program, Phase II, Air Force Flight Dynamics Laboratory Report AFFDL-TR-67-25, (AD 819 915), April 1967.

5. Reichenau, D.E.A.: Aerodynamic Performance of Various Hyperflo and Hemisflo Parachutes at Mach Numbers from 1.8 to 3.0, Arnold Engineering Development Center Report AEDC-TR-65-57 (AD 358 325), March 1965.

6. Anon. (American Power Jet Co.): Performance of and Design Criteria for Deployable Aerodynamic Decelerators, Air Force Flight Dynamics Laboratory Technical Report ASD-TR-61-579, (AD 429 971), December 1963.

7. Beers, Yardley: Introduction to the Theory of Error, Addison-Wesley Publishing Company, Inc., Reading, Massachusetts, 1957.

8. Croxton, Frederick, E.: Elementary Statistics with Applications in Medicine and the Biological Sciences, Dover Publications, Inc., New York, 1959.

9. Broderick, Milan A.: Study, Design and Fabrication of a Supersonic Parachute Sled Test Vehicle, Contract No. AF 33(616)-7407, Cook Research Laboratories Design Analysis Report P-2019, November 1960, and Progress Reports P-2019, 1 through 5, August 1960 through April 1961.

10. Jenke, L.M.: Supersonic Wind Tunnel Tests of the IDS-6328 Parachute Test Sled, Arnold Engineering Development Center Report AEDC-TDR-64-38, (AD 431 849), March 1964.

11. Jenke, L.M. and Lucus, E.J.: Supersonic Wind Tunnel Tests of a Parachute Test Sled, Arnold Engineering Development Center Report AEDC-TDR-64-203, (AD 448 066), October 1964.

12. Lucus, E.J. and Jenke, L.M.: Supersonic Wind Tunnel Tests of an Outrigger Rocket Sled and Two Dual Rail Sleds, Arnold Engineering Development Center Report AEDC-TR-65-168, (AD 468 970), August 1965.

13. Babish, C.A.: Development and Evaluation of Kevlar 29 Materials for Air Force Weapon System Parachute Applications, paper presented at the Workshop on Super-strength Fiber Applications, Dayton, Ohio, April 20-21, 1977.

14. Abbott, N.J., et al.: Design of Parachute Component Materials from Kevlar 29 and 49, Air Force Materials Laboratory Report AFML-TR-74-65 Part IV, July 1976.

15. United States Air Force Draft Tentative Military Specifications for: Webbing, Textile, Kevlar; Tubular Webbing, Textile, Kevlar; Tape, Textile, Kevlar; Coreless Cord, Kevlar; and Thread, Kevlar, October 1976.

16. Military Specification: MIL-P-25716, Parachute System, Heavy Duty, General Specification For.

17. Galigher, L.L.: Aerodynamic Characteristics of Supersonic-X Parachutes at Mach Numbers of 2.1 and 4.0, Arnold Engineering Development Center Report AEDC-TR-69-8, (AD 846-695), January 1969.

18. Babish, C.A. III: A Continuous Surface of Revolution Parachute for Supersonic/Hypersonic Speeds, AIAA Paper No. 70-1173, presented at the AIAA Aerodynamic Deceleration Systems Conference, September 1970.

19. Sanson, F.J. and Peterson, H.E., MIMIC Programming Manual, Air Force Aeronautical Systems Division Report SEG-TR-67-31, July 1967.

20. Anon., Control Data 6000 Computer Systems MIMIC Digital Simulation Language Reference Manual, Control Data Corporation Publication 44610400, January 1972.

☆U.S.Government Printing Office: 1978 — 757-080/9